



UNIVERSIDADE D
COIMBRA

Joana Carrapiço Gonçalves

NOSE-TO-BRAIN DELIVERY OF LACOSAMIDE,
LEVETIRACETAM AND ZONISAMIDE AND
THE IMPACT OF BCRP EFFLUX: AN *IN*
VITRO/IN VIVO APPROACH

VOLUME I

Tese no âmbito do Doutoramento em Ciências Farmacêuticas, Especialidade de Farmacologia e Farmacoterapia, orientada pela Professora Doutora Ana Cristina Bairrada Fortuna e pelos Professores Doutores Amílcar Celta Falcão Ramos Ferreira e Gilberto Lourenço Alves, e apresentada à Faculdade de Farmácia da Universidade de Coimbra.

Maio de 2021

À minha Filha, Leonor

Ao João

Aos Meus Queridos Pais

AGRADECIMENTOS

À Professora Doutora Ana Bairrada Fortuna, minha orientadora,

uma palavra de agradecimento especial à minha orientadora, Professora Ana, pelo acolhimento, dedicação e oportunidade de desenvolver capacidades profissionais e pessoais. Acompanhou-me em cada passo deste longo processo, nunca me deixou divagar, demonstrando o rumo do sucesso. O apoio e demonstração de coragem, mesmo quando pensei que não seria possível, concretizou-se devido à sua determinação. Resta-me apenas agradecer e felicitar a excelente profissional que me encaminhou de forma exemplar.

Ao Professor Doutor Gilberto Lourenço Alves, meu coorientador,

agradeço a disponibilidade demonstrada ao longo da execução laboratorial, a sua contribuição científica foi sem dúvida de extrema importância. Agradeço ainda, todas as intervenções construtivas que permitiram melhorar a qualidade do trabalho desenvolvido.

Ao Professor Doutor Amílcar Falcão Ferreira, meu coorientador,

Deixo o meu agradecimento pela disponibilidade demonstrada, e o seu prestigiado contributo científico, que permitiram enriquecer o presente trabalho.

À Doutora Joana Bicker,

à Joana só tenho a agradecer a ajuda em todos os momentos de aflição. A sua transmissão de conhecimentos práticos, apoio e disponibilidade permitiram continuar mesmo quando aparentemente não fazia mais sentido. Reconheço a ajuda prestada, sacrificou a execução das suas tarefas pessoais e profissionais, e agradeço a sua cooperação. Sou grata pela sua amizade, que se revelou determinante em vários momentos, para além do apoio técnico.

Às minhas colegas e amigas de Laboratório,

Cristina Andrade e Filipa Silva,

um agradecimento muito sentido e nostálgico. Recordo a vossa chegada ao laboratório e da empatia imediata, que rapidamente se tornou em amizade. À Filipa aquele agradecimento por todo o apoio técnico e companheirismo. Cristina... foram tantos momentos difíceis que se tornaram tão mais simples na tua presença, com o teu apoio. Ficam as recordações e a amizade à distância de várias léguas apenas! Obrigada meninas.

Às minhas mais recentes colegas de laboratório,

Andreia Carona, Filipa Gouveia e Soraia Silva,

obrigada pela oportunidade de vos conhecer e partilhar convosco as aventuras da investigação. A todas vós que me ajudaram nas mais diversas situações, de forma prestável e cooperativa. Despenderam do vosso tempo na elaboração das tarefas necessárias a este projeto, e quanto a toda a vossa dedicação apenas me resta deixar o meu modesto agradecimento.

À Doutora Sandra de Jesus,

agradeço a partilha de sabedoria, técnica e empírica, da sua vasta experiência enquanto investigadora. Um verdadeiro exemplo de dedicação e tranquilidade necessários à investigação científica.

À Professora Doutora Carla Vitorino,

pela sua amabilidade em acompanhar e auxiliar a execução de ensaios de tecnologia farmacêutica. Agradeço a disponibilidade e cooperação.

À minha filha Leonor,

devo antes de mais um pedido de desculpa pela ausência em tantos momentos, quando o dever de dedicação ao trabalho se impunha. Pretendo transmitir à Leonor, através da realização do presente trabalho e tudo o que a sua concretização implicou, um exemplo

de dedicação e empenho, determinantes para alcançar o objetivo ambicionado. Obrigada por existires...

Ao João,

difícilmente conseguirei exprimir a importância não só do teu apoio e prestabilidade, mas principalmente da tua presença e preocupação permanentes. Não me permitiste desistir sempre que considere que teria de o fazer, sempre me mostraste que seria capaz de alcançar o objetivo a que me propus com a tua inteira concordância. Este projeto faz parte de nós, do nosso AMOR, também te pertence e tem muito de ti. Este representa a concretização de um sonho de entre tantos que trazemos connosco e certamente vamos realizar...

Aos meus Pais,

é um privilégio ser filha de pessoas tão grandiosas, que me conduziram ao longo da vida, e me prepararam para o Mundo. Não me privaram das dificuldades, mas sempre se revelaram disponíveis para mim, para me apoiar e mostrar que quaisquer que sejam as contrariedades vão estar sempre comigo. São um verdadeiro exemplo de trabalho árduo e determinação, valores que me foram transmitidos e me permitiram chegar aqui. Obrigada por TUDO!

TABLE OF CONTENTS

LIST OF ABBREVIATIONS	III
LIST OF FIGURES	VII
LIST OF TABLES	XIII
PUBLICATIONS	XXI
ABSTRACT	XXV
RESUMO	XXIX
CHAPTER I INTRODUCTION	1
I.1. EPILEPSY	3
I.1.1. HISTORICAL CONTEXTUALIZATION	3
I.1.2. EPIDEMIOLOGY OF EPILEPSY	4
I.1.3. SEIZURES CLASSIFICATION	5
I.1.4. ETIOLOGY OF EPILEPSY	10
I.2. PHARMACOTHERAPY OF EPILEPSY	13
I.2.1. ANTIEPILEPTIC DRUGS	14
I.2.2. PHARMACORESISTANT EPILEPSY	30
I.3. NOVEL PHARMACOLOGICAL STRATEGIES AGAINST EPILEPSY	34
I.3.1. NEW PHARMACOLOGICAL TARGETS	35
I.3.2. CIRCUMVENT THE BLOOD-BRAIN BARRIER	39
I.4. INTRANASAL ADMINISTRATION & NOSE-TO-BRAIN DRUG DELIVERY	43
I.4.1. ANATOMY AND HISTOLOGY OF THE NASAL CAVITY	44
I.4.2. NASAL PHYSIOLOGY	47
I.4.3. NOSE-TO-BRAIN DRUG DELIVERY	49
I.5. RELEVANCE OF BREAST CANCER RESISTANCE PROTEIN TO BRAIN DISTRIBUTION AND CENTRAL-ACTING DRUGS	52
I.5.1. BCRP: STRUCTURE AND LOCALIZATION	53

I.5.2. HOW TO INVESTIGATE BCRP RELEVANCE AND DRUG-BCRP INTERACTIONS?	56
I.5.3. BCRP IN DRUGS PHARMACOKINETICS AND BRAIN DISTRIBUTION	75
I.5.4. DRUGS-BCRP TRANSPORTER INTERACTION	78
I.5.4.1. BCRP Substrates	79
I.5.4.2. BCRP Inhibitors	82
I.5.4.3. BCRP Inducers	86
I.5.5. BCRP AND EPILEPSY	88
CHAPTER II OBJECTIVES	91
II.1. GENERAL OBJECTIVES	93
II.2. SPECIFIC OBJECTIVES	94
CHAPTER III ANALYTICAL DRUG QUANTIFICATION	97
III.1. INTRODUCTION	99
III.2. MATERIAL & METHODS	100
III.2.1. CHEMICALS & REAGENTS	100
III.2.2. PREPARATION OF SOLUTIONS	101
III.2.2.1. Stock & Working Sample Solutions	101
III.2.2.2. Calibration Standards & QC Samples	102
III.2.3. SAMPLE PREPARATION	102
III.2.4. CHROMATOGRAPHIC SYSTEM & CONDITIONS	103
III.2.5. METHOD VALIDATION	104
III.2.5.1. Selectivity	104
III.2.5.2. Linearity of the Calibration Curve	105
III.2.5.3. Precision & Accuracy	105
III.2.5.4. LLOQ & Limit of Detection	106
III.2.5.5. Sample Dilution	106
III.2.5.6. Recovery	107
III.2.5.7. Carry-over Effect	107


III.2.5.8. Stability	107
III.2.6. METHOD APPLICATION TO REAL SAMPLES FROM EPILEPTIC PATIENTS	108
III.3. RESULTS & DISCUSSION	109
III.3.1. METHOD DEVELOPMENT	109
III.3.1.1. Chromatographic Separation of the Analytes	109
III.3.1.2. Optimization of Sample Preparation	112
III.3.1.3. Optimization of Diode-Array Detection	113
III.3.2. METHOD VALIDATION	115
III.3.2.1. Selectivity & Sensitivity	115
III.3.2.2. Linearity, LLOQ & LOD	116
III.3.2.3. Precision & Accuracy	120
III.3.2.4. Recovery & Carry-Over Effect	120
III.3.2.5. Stability	121
III.3.3. METHOD APPLICATION TO CLINICAL SAMPLE ANALYSIS & INCURRED SAMPLE REANALYSIS	124
III.4 CONCLUSION & FUTURE PERSPECTIVE	127
CHAPTER IV NOSE-TO-BRAIN DELIVERY OF LEVETIRACETAM AFTER INTRANASAL ADMINISTRATION TO MICE	129
IV.1. INTRODUCTION	131
IV.2. MATERIAL & METHODS	134
IV.2.1. DRUGS & REAGENTS	134
IV.2.2. DEVELOPMENT AND CHARACTERIZATION OF THERMOREVERSIBLE GEL	134
IV.2.3. <i>IN VITRO</i> STUDIES	135
IV.2.4. <i>IN VIVO</i> STUDIES	136
IV.2.4.1. Animals and Ethics	136
IV.2.4.2. <i>In Vivo</i> Pharmacokinetic Single-Dose Study	137

IV.2.4.2.1. Quantification of Levetiracetam in Biological Samples	138
IV.2.4.2.2. Pharmacokinetic Analysis and Calculations	140
IV.2.5. STATISTICAL ANALYSIS	143
IV.3. RESULTS	144
IV.3.1. OPTIMIZATION AND CHARACTERIZATION OF THE INTRANASAL THERMOREVERSIBLE GEL	144
IV.3.2. <i>IN VITRO</i> CELLULAR VIABILITY OF RPMI-2650 AND CALU-3 CELLS	147
IV.3.3. PHARMACOKINETICS OF LEVETIRACETAM AFTER SINGLE-DOSE ADMINISTRATIONS	148
IV.3.4. HISTOLOGICAL EVALUATION OF LUNG TISSUE FROM <i>IN VIVO</i> MULTIPLE-DOSE STUDY	153
IV.4. DISCUSSION	153
IV.5. CONCLUSION	158
CHAPTER V PRE-CLINICAL ASSESSMENT OF THE NOSE-TO-BRAIN DELIVERY OF ZONISAMIDE AFTER INTRANASAL ADMINISTRATION	159
V.1. INTRODUCTION	161
V.2. MATERIAL & METHODS	164
V.2.1. CHEMICALS & REAGENTS	164
V.2.2. <i>IN VITRO</i> ASSAYS	164
V.2.2.1. Human Lung Adenocarcinoma Cell Line <i>In Vitro</i> Viability	164
V.2.2.2. Human Nasal Septum Cell Line <i>In Vitro</i> Viability	165
V.2.3. <i>IN VIVO</i> PRE-CLINICAL STUDIES	166
V.2.3.1. Ethical Considerations and Animals	166
V.2.3.2. Preparation of Zonisamide Formulations	167
V.2.3.3. <i>In vivo</i> pharmacokinetic study	167
V.2.3.4. Drug Analysis	169
V.2.4. <i>IN VIVO</i> PHARMACOKINETIC STUDIES	171
V.2.5. STATISTICAL ANALYSIS	173

V.3. RESULTS	174
V.3.1. <i>IN VITRO</i> CELL VIABILITY STUDIES	174
V.3.2. PHARMACOKINETICS OF ZONISAMIDE	175
V.4. DISCUSSION	183
CHAPTER VI IS INTRANASAL ADMINISTRATION AN OPPORTUNITY FOR DIRECT BRAIN DELIVERY OF LACOSAMIDE?	189
VI.1. INTRODUCTION	191
VI.2. MATERIAL & METHODS	193
VI.2.1. CHEMICALS & REAGENTS	193
VI.2.2. PREPARATION OF LACOSAMIDE FORMULATIONS	194
VI.2.3. <i>IN VITRO</i> CELL VIABILITY ASSAYS IN RPMI-2650 AND CALU-3 CELL LINES	194
VI.2.4. <i>IN VIVO</i> STUDIES	196
VI.2.4.1. Animals and ethics	196
VI.2.4.2. <i>In Vivo</i> Pharmacokinetic Study	197
VI.2.4.3. Quantification of Lacosamide in Biological Samples	197
VI.2.4.4. Pharmacokinetic and Statistical Analysis	199
VI.3. RESULTS	201
VI.3.1. CELL VIABILITY OF INTRANASAL THERMOREVERSIBLE GEL	201
VI.3.2. <i>IN VIVO</i> PHARMACOKINETIC ANALYSIS	203
VI.4. DISCUSSION	206
VI.5. CONCLUSION	209
CHAPTER VII A COMBO-STRATEGY TO IMPROVE BRAIN DELIVERY OF ANTIEPILEPTIC DRUGS: FOCUS ON BCRP AND INTRANASAL ADMINISTRATION	211
VII.1. INTRODUCTION	213
VII.2. MATERIAL & METHODS	214
VII.2.1. CHEMICALS & REAGENTS	214

VII.2.2. <i>IN VITRO</i> STUDIES	215
VII.2.2.1. Cell Culture	215
VII.2.2.2. Cell Viability Assays	216
VII.2.2.3. Intracellular Accumulation Assays	217
VII.2.2.4. Bidirectional Transport Studies: MDCK-II and MDCK-BCRP Cells	218
VII.2.2.5. RPMI-2650 Cell Permeability Studies	220
VII.2.3. PLASMA AND BRAIN DISPOSITION OF ZONISAMIDE IN MICE	220
VII.2.4. Statistical Data Analysis	223
VII.3. RESULTS	224
VII.3.1. CELLULAR VIABILITY OF MDCK-II, MDCK-BCRP AND RPMI-2650 CELLS	224
VII.3.2. <i>IN VITRO</i> IDENTIFICATION OF BCRP INHIBITORS	225
VII.3.3. <i>IN VITRO</i> IDENTIFICATION OF BCRP SUBSTRATES	226
VII.3.4. PERMEABILITY OF AEDs THROUGH RPMI-2650 CELLS	229
VII.3.5. <i>IN VIVO</i> PLASMA AND BRAIN DISPOSITION OF ZONISAMIDE	229
VII.4. DISCUSSION	233
VII.5. CONCLUSION	236
CHAPTER VIII GENERAL DISCUSSION	239
CHAPTER IX CONCLUSION	255
REFERENCES	261
APPENDIX A	321
APPENDIX B	325

**LIST OF
ABBREVIATIONS,
FIGURES, TABLES AND
EQUATIONS**



LIST OF ABBREVIATIONS

A

ABC	ATP-binding cassette
ADME	Absorption, distribution, metabolism, and excretion
AEDs	Antiepileptic drugs
AMPA	α -Amino-3-hydroxy-5-methyl-4-isoxazolepropionic acid
ATP	Adenosine triphosphate
AUC	Area under the curve
AUC _{extrap}	AUC extrapolated from t_{last} to infinity
AUC _{inf}	AUC from time zero to infinity
AUC _t	AUC from time zero to the time of the last quantifiable drug concentration

B

BBB	Blood-brain barrier
BCRP	Breast cancer resistance protein

C

Caco-2	Colorectal adenocarcinoma cell line
C _{last}	Last quantifiable drug concentration
CL/F	Apparent clearance
C _{max}	Maximum concentration
CNS	Central nervous system
COMT	Catechol- <i>O</i> -methyl transferase
CRMP2	Collapsin response mediator protein-2
CSF	Cerebrospinal fluid
CV	Coefficient of variation
CYP	Cytochrome P450

D

DAD	Diode array detection
DDI	Drug-drug interaction
DGAV	<i>Direção-Geral de Alimentação e Veterinária</i>
DMSO	Dimethyl sulfoxide
DTE	Drug targeting efficiency
DTP	Direct transport percentage

E

EEG	Electroencephalogram
EMA	European Medicines Agency
EPSP	Excitatory postsynaptic potential
ER	Efflux ratio
E3S	Estrone-3-sulfate

F	FDA	Food and Drug Administration
G	GABA	γ -Aminobutyric acid
	GABRG2	Gamma-Aminobutyric Acid Type A Receptor Subunit Gamma2
	GAT1	γ -Aminobutyric acid transporter 1
	GPR	G protein-coupled receptor
H	HIV	Human immunodeficiency virus
	HPLC	High pressure liquid chromatography
I	IC ₅₀	Half maximal inhibitory concentration
	ILAE	International League Against Epilepsy
	IN	Intranasal
	I _{NAP}	Persistent sodium current
	IS	Internal standard
	IV	Intravenous
K	k _{el}	Apparent elimination rate constant
	KCNT1	Potassium Sodium-Activated Channel Subfamily T Member 1
	KO	Knockout
L	LC-MS/MS	Liquid chromatography–mass spectrometry
	LLE	Liquid-liquid extraction
	LLOQ	Lower limit of quantification
	LOD	Limit of detection
	LogD	Octanol/water partition coefficient
M	MCC	Mucociliary clearance
	MDCK	Madin-Darby canine kidney
	MRP	Multidrug resistance-associated protein
	MRT	Mean residence time
	MS/MS	Tandem mass spectrometry
	mTOR	Mammalian target of rapamycin
N	Na-F	Sodium fluorescein
	NBD	Nucleotide-binding domain
	NCE	
	NMDA	<i>N</i> -methyl-D-aspartate
O	OATP	Organic anion transporting polypeptide

P	P _{app}	Apparent permeability
	PAF	Paraformaldehyde
	P-gp	P-glycoprotein
	PPI	Proton pump inhibitors
Q	QC	Quality control
R	r ²	Coefficient of determination
	RE	Relative error
	ROS	Reactive oxygen species
	RPMI	Human nasal septum cell line
	R&D	Research and Development
S	SCN1A	Sodium Voltage-Gated Channel Alpha Subunit 1
	SEM	Standard error of the mean
	SNP	Single nucleotide polymorphism
	SV2A	Synaptic vesicle glycoprotein 2
T	t _{1/2}	Elimination half-life
	TEER	Transepithelial electrical resistance
	TKO	Triple knockout
	t _{last}	Time of the last quantifiable drug concentration
	t _{max}	Time to achieve maximum concentration
	TMD	Transmembrane domain
	TSC	Tuberous sclerosis complex
U	UV	Ultraviolet
V	VGCC	Voltage-gated calcium channel
	VGSC	Voltage-gated sodium channel
W	WHO	World Health Organization
	WT	Wild type

LIST OF FIGURES

- Figure I.1** Classification of epileptic seizures **(A)** basic version and **(B)** expanded version, according to the International League Against Epilepsy [32]. 7
- Figure I.2** Classification of epilepsies: etiological factors, types of seizures and types of epilepsy, related to the onset of the epileptic seizures [34]. 10
- Figure I.3** Classification of marketed antiepileptic drugs into generations in accordance with their data of development. 16
- Figure I.4** Mechanisms of action proposed for antiepileptic drugs in **(A)** modulation of voltage-gated ion channels, **(B)** inhibitory synapse and **(C)** excitatory synapse. AMPA, *α -amino-3-hydroxy-5 methyl-4-isoxazole propionic acid*; GABA, *γ -aminobutyric acid*; GABA-T, *4-aminobutyrate aminotransferase*; GAD, *glutamic acid decarboxylase*; NMDA, *N-methyl-D-aspartate*; SV2A, *synaptic vesicle glycoprotein 2A* (Adapted from [607]). 18
- Figure I.5** New pharmacological strategies for epilepsy. 34
- Figure I.6** Schematic representation of the anatomy of the human nasal cavity. Scaly mucosa characterized by green outline. Lower, middle and upper turbinates are characterized by blue. Blue region depicts the nasal mucosa. The region outlined in yellow symbolizes the olfactory region (Adapted from [237]). CSF, *cerebrospinal fluid*. 45
- Figure I.7** Schematic representation of indirect and direct delivery of drugs to the brain after intranasal (IN) administration. 50
- Figure I.8** **(A)** Simplified distribution of efflux transporters across cerebral endothelial cells and **(B)** two-dimensional structural and topological models of P-glycoprotein (P- gp) and breast cancer resistance protein (BCRP). P-gp has six transmembrane domains (TMD) in two halves and two nucleotide binding domains (NBD), while Breast Cancer Resistant Protein (BCRP) has six transmembrane segments and only one efflux transporter nucleotide binding domain. 54

- Figure I.9** Schematic representation of **(A)** intracellular accumulation **(B)** and bidirectional transport assays. 56
- Figure III.1** UV and visible absorption spectrum of levetiracetam, zonisamide and lacosamide. Upper line: absorbance intensity of each AED in function of specific wavelengths; Lower line: complete UV-Vis absorption spectrum of each AED. 113
- Figure III.2** Typical HPLC-DAD chromatograms of extracted human plasma samples. Blank sample at 220 nm **(A)** and at 239 nm **(B)**, sample spiked at level of the lower limit of quantification at 220 nm **(C)** and at 239 nm **(D)**, and sample spiked at level of the upper limit of the calibration range at 220 nm **(E)** and at 239 nm **(F)**. DAD, *diode array detection*; IS, *internal standard*; LACO, *lacosamide*; LEV, *levetiracetam*; ZNS, *zonisamide*. 114
- Figure III.3** Representative chromatograms of plasma samples obtained from epileptic patients treated with different AEDs. **(A)** Levetiracetam (LEV) administered by intravenous route (dose of 1000 mg each 24 h); **(B)** orally administered zonisamide (ZNS) at the dose of 300 mg each 24 h; and **(C)** intravenous administration of lacosamide (LAC) at 600 mg each 24 h. The determined plasma concentrations correspond to those exposed in **Table III.8**. IS, *Internal standard*. 125
- Figure IV.1** Viability (%) of RPMI-2650 cells after incubation with levetiracetam for 24 h (50–400 μ M); empty Polycarbophil and Carbopol[®] thermoreversible gels; and thermoreversible gels loaded with levetiracetam at the same concentrations. Data represented as mean \pm standard deviation (9 replicates in three independent replicates). 147
- Figure IV.2** Viability (%) of Calu-3 cells after incubation with levetiracetam for 24 h (1, 5, 10, 25, 50 and 100 μ M). Data represented as mean \pm standard deviation (9 replicates, three independent replicates). 148
- Figure IV.3** Concentration-time profiles of levetiracetam up to 240 min post-dosing in plasma (A), brain (B), lung (C) and kidney (D) following

intranasal (IN) and intravenous (IV) administration (625 µg/animal) to mice. Symbols represent the mean values ± SEM of five determinations per time point (n = 5). * t(8) = 0.729, p = 0.033; ** t(8) = 4.36, p = 0.0024; # t(8) = 3.56, p = 0.0074; Y t(8) = 2.41, p = 0.0424; YY t(8) = 3.11, p = 0.014. 149

Figure IV.4 Tissue-to-plasma concentration ratios of levetiracetam at 5, 15, 30, 60, 90, 120 and 240 min after administration of the drug by intranasal (IN) or intravenous (IV) route. **(A)** represents the brain-to-plasma concentration ratios variation *versus* time; **(B)** represents the lung-to-plasma concentration ratios variation *versus* time and **(C)** represents the kidney-to plasma concentration ratios variation *versus* time. *t(8) = 0.024, p = 0.011. 151

Figure IV.5 Photomicrographs of hematoxylin-eosin stained lung mice sections of **(A)** control group and **(B)** treated group (magnification: 40x). 153

Figure V.1 Representative chromatograms achieved during validation of the analytical technique described in section 2.3.4 for mice plasma **(A)**, brain **(B)**, lung **(C)** and kidney **(D)** spiked at the lower limit of quantification (LLOQ) level and at the upper limit of quantification of the calibration ranges; the internal standard (IS, antypirine) was detected at 220 nm while zonisamide (ZNS) was at 239 nm. 170

Figure V.2 Viability (%) of Calu-3 and RPMI-2650 cells after incubation with zonisamide for 24 h (1, 5 10, 25, 50 and 100 µM). Data represented as mean ± standard deviation (n = 4, three independent replicates). 174

Figure V.3 Viability (%) of RPMI-2650 cells after incubation with zonisamide for 24 h (50–400 µM); empty Noveon® Polycarbophil and Carbopol® thermoreversible gels (0.02 % for both); and thermoreversible gels loaded with zonisamide at the same concentrations. Data represented as mean ± standard deviation (n = 4, three independent replicates). 175

Figure V.4 Concentration-time profiles of zonisamide up to 800 min post-dosing in plasma (A), brain (B), lung (C) and kidney (D) following intranasal (IN,

16.7 mg/kg), intravenous (IV, 16.7 mg/kg) or oral administration (80 mg/kg) to mice. The figure below each profile corresponds to the respective enlargement up to 250 min post-administration. Symbols represent the mean values \pm standard error of the mean (SEM) of five determinations per time point (n = 5).

176

Figure V.5 Dose-normalized concentration- time profiles of zonisamide up to 800 min post-dosing in plasma **(A)**, brain **(B)**, lung **(C)** and kidney **(D)** following intranasal (IN, 16.7 mg/kg), intravenous (IV, 16.7 mg/kg) or oral administration (80 mg/kg) to mice. The figure below each profile corresponds to the respective enlargement up to 60 min post administration. Symbols represent the mean values \pm standard error of the mean (SEM) of five determinations per time point (n = 5). Statistical differences are in relation to the IV administration route as follows: * $p < 0.05$, ** $p < 0.01$, *** $p < 0.001$ assessed by two-way ANOVA followed by Dunnett's multiple comparison test.

177

Figure V.6 Tissue-to-plasma concentration ratios of zonisamide at 5, 15, 30, 60, 120, 240, 360, 480 and 720 min after drug administration by intranasal (IN), intravenous (IV) or oral route. **(A)** represents the variation of brain-to-plasma concentration ratios versus time; **(B)** represents the variation of lung-to-plasma concentration ratios versus time and **(C)** represents the variation of kidney-to-plasma concentration ratios versus time. Statistical differences are in relation to the IV administration route as follows: * $p < 0.05$, ** $p < 0.01$, *** $p < 0.001$ assessed by two-way ANOVA followed by Dunnett's multiple comparison test.

182

Figure VI.1 Viability (%) of RPMI-2650 cells after incubation with lacosamide, empty Noveon® Polycarbophil and Carbopol® thermoreversible gels, and thermoreversible gels loaded with lacosamide at the same concentrations, for 24 h (50, 100, 150, 200, 250 and 400 μ M). Data represented as mean \pm standard deviation (n = 4, three independent replicates).

202

- Figure VI.2** Viability (%) of Calu-3 and RPMI-2650 cells after incubation with zonisamide for 24 h (1-100 μ M). Data represented as mean \pm standard deviation (n = 4, three independent replicates). 202
- Figure VI.3** Concentration-time profiles of lacosamide after intranasal (IN) and intravenous (IV) administration (8.33 mg/kg) in plasma **(A)**, brain **(B)**, lung **(C)** and kidney **(D)**. The symbols represent the mean \pm standard error of the mean values of five determinations per time point (n = 5). * $p < 0.05$. 205
- Figure VII.1** **(A)** Hoechst 33342 intracellular accumulation in MDCK-BCRP cells, in the presence and absence of 0.5 μ M Ko143 (positive control). **(B)** Intracellular accumulation of Hoechst 33342, after incubation with lacosamide (LAC), **(C)** levetiracetam (LEV) and **(D)** zonisamide (ZNS) for 30 min. Data compared with negative control cells (without inhibitor) and expressed as mean \pm standard deviation (n = 4). * $p < 0.05$, ** $p < 0.01$ and *** $p < 0.001$. 226
- Figure VII.2** Mean concentration-time profiles of zonisamide after its intranasal (IN) or intravenous (IV) administrations with and without the co-administration of elacridar (2.5 mg/kg, intravenous), depicted in plasma **(A)** and brain **(B)**. Each data point is presented as mean \pm standard error of the mean (SEM) (n = 4 animals per group) and significant differences between group concentrations at specific time-points were assessed by the two-way analysis of variance (ANOVA) with Dunnett's Multiple Comparison Test. * $p > 0.05$ In relation to vehicle after IV administration. 230
- Figure A.1** Accumulation of Hoechst 33342 in MDCK-BCRP cells. Demonstration of BCRP functionality after incubation with 0.5 μ M KO143. Intracellular uptake observed following an incubation period with test compounds at indicated concentrations (μ M). Data expressed as mean \pm SD (n = 9, 3 independent assays). $p < 0.01$ (**) and $p < 0.001$ (***) 324

Figure B.1 Tissue-to-plasma concentration ratios of levetiracetam at 5 and 15 min after administration of levetiracetam (625 $\mu\text{g}/\text{animal}$) with the micropipette and the polyurethane tube. **(A)** represents the brain-to-plasma concentration ratios variation *versus* time; **(B)** represents the lung-to-plasma concentration ratios variation *versus* time. Data is represented as mean \pm standard error of mean (SEM). 332

LIST OF TABLES

Table I.1	Description of the type of epileptic seizures, according to the International League Against Epilepsy 2017 Classification Seizure [32].	8
Table I.2	Antiepileptic drugs recommended for each type of seizure, and those that should be avoided in accordance with the National Institute of Excellence in Health and Care [79].	17
Table I.3	Classification of antiepileptic drugs according to their molecular targets, adapted from [56, 76].	19
Table I.4	Compounds under clinical investigation for therapeutic application in epileptic disorders.	38
Table I.5	Advantages, limitations and examples of formulations available for antiepileptic drugs (AEDs) administration.	41
Table I.6	Examples of BCRP substrates: evidence from <i>in vitro</i> and <i>in vivo</i> non-clinical studies.	58
Table I.7	Examples of BCRP inhibitors and their influence on the disposition of drugs: evidence from <i>in vitro</i> and <i>in vivo</i> non-clinical studies.	69
Table I.8	Example of drugs that demonstrated to be BCRP inducers. The principal experimental conditions and results are presented.	87
Table III.1	Chromatographic characteristics of the peaks corresponding to levetiracetam (LEV), zonisamide (ZNS) and lacosamide (LAC) under the chromatographic conditions tested during method development.	111
Table III.2	Retention time (initial-final) presented by some drugs potentially co-administered with levetiracetam, lacosamide and zonisamide, after submitted to plasma sample preparation and HPLC-DAD methodology herein developed.	115

Table III.3	Regression parameters of the calibration curve generated for each weighting factor (w_i) and the respective sum of the relative errors (\sum % RE) for the calibration standard data; n = 35.	117
Table III.4	Calibration curve parameters of levetiracetam, zonisamide and lacosamide, in human plasma. Regression equation and correlation coefficient (r) are expressed as the mean of five calibration curves (n = 5).	118
Table III.5	Intra-day and interday accuracy and precision data of levetiracetam, zonisamide and lacosamide employing the novel HPLC-diode array detection technique herein developed.	119
Table III.6	Absolute recovery from human plasma (%) of Levetiracetam, zonisamide and lacosamide employing the sample treatment and extraction procedures herein optimized. Low, medium and high-quality control samples were used (n = 5). The absolute recovery is also presented for the internal standard (n = 5).	121
Table III.7	Stability data for levetiracetam, zonisamide and lacosamide under several conditions of sample handling and storage (n = 5).	123
Table III.8	Characteristics regarding drug posology and co-administered antiepileptic drugs instituted to the epileptic patients and the corresponding plasma concentration of levetiracetam, zonisamide and lacosamide assessed after employing the method herein developed.	126
Table III.9	Incurred samples reanalysis (ISR) of plasma samples obtained from epileptic patients.	127
Table IV.1	Main parameters of the HPLC-DAD method validation employed to quantify levetiracetam in plasma, brain, lung and kidney matrices (n = 5).	140
Table IV.2	Mechanical properties of the several nasal gel formulations prepared to incorporate levetiracetam. Results are indicated as a mean of six replicates \pm standard deviation (n = 6).	146

Table IV.3	Pharmacokinetic parameters of levetiracetam in plasma, brain, lung and kidney tissues following its intranasal (IN) and intravenous (IV) administration (20.8 mg/kg) to mice.	150
Table V.1	Main parameters of the HPLC-DAD method validation employed to quantify zonisamide in plasma, brain, lung and kidney matrices (n = 5)	171.
Table V.2	Pharmacokinetic parameters of zonisamide in plasma, brain, lung and kidney tissues following its intranasal (IN, 16.7 mg/kg), intravenous (IV, 16.7 mg/kg) and oral (80 mg/kg) administration to mice.	178
Table V.3	Dose-normalized pharmacokinetic parameters of zonisamide in plasma, brain, lung and kidney tissues following its intranasal (IN, 16.7 mg/kg), intravenous (IV, 16.7 mg/kg) and oral (80 mg/kg) administration to mice.	179
Table VI.1	Validation parameters of the analytical method developed in high performance liquid chromatography (HPLC-DAD) for quantification of lacosamide in plasma and brain, lung and kidney homogenate (n = 5).	199
Table VI.2	Equations for determination of bioavailability and drug delivery parameters described in section VI.2.4.4.	200
Table VI.3	Pharmacokinetic parameters following administration of lacosamide (8.33 mg/kg) in plasma and tissue (brain, lung and kidney) of mice through intranasal thermoreversible gel (IN) and intravenous solution (IV).	204
Table VII.1	Chromatographic conditions and partial validation parameters obtained for the high performance liquid chromatography-diode array (HPLC-DAD) assays applied for the quantification of the antiepileptic drugs, lacosamide, levetiracetam and zonisamide, and the reference BCRP substrate (sulfasalazine) in <i>in vitro</i> samples.	221
Table VII.2	Bidirectional apparent permeability coefficient (P_{app}) from apical to basolateral (AP-BL) and basolateral to apical (BL-AP) compartments,	

efflux ratio (ER) and net flux ratio in MCDKII and MDCK-BCRP cells for lacosamide, levetiracetam, zonisamide. Sulfasalazine was used as reference BCRP substrate. P_{app} values are expressed as mean (standard deviation) (n = 3). 228

Table VII.3 Plasma and brain pharmacokinetic parameters after intranasal (IN) and intravenous (IV) administration of zonisamide (16.7 mg/kg) with vehicle (transcutol, 4 mL/kg, IV) or BCRP inhibitor, elacridar (2.5 mg/kg, IV). 231

Table VII.4 Brain/plasma ratios obtained after the intranasal (IN) or intravenous (IV) administration of zonisamide to mice (16.7 mg/kg) with vehicle (transcutol, 4 mL/kg, IV) or BCRP inhibitor, elacridar (2.5 mg/kg, IV) (n = 4). Statistical differences are reported in relation to the correspondent vehicle group. 232

Table VIII.1 Summary of in vitro and in vivo results. Apparent permeability (P_{app}) from apical to basolateral side (AP-BL) obtained across RPMI-2650 cell monolayers, drug targeting efficiency (DTE), direct transport percentage (DTP) and ratios between area under the curve (AUC) of tissues and plasma for the three investigated AEDs. 253

Table B.1 Concentrations of levetiracetam in plasma, brain and lung after its nasal administration with two distinct devices to mice (625 $\mu\text{g}/\text{animal}$). Data is represented as mean \pm standard deviation. 331

LIST OF EQUATIONS

Equation IV.1 - Cell viability	136
Equation IV.2 - Absolute bioavailability	141
Equation IV.3 - Drug targeting efficiency (DTE%)	141
Equation IV.4 - Direct transport percentage (DTP)	142
Equation IV.5 - Brain bioavailability	142
Equation V.1 - Cell viability	165
Equation V.2 - Absolute bioavailability	172
Equation V.3 - Relative bioavailability	172
Equation V.4 - Drug targeting efficiency (DTE%)	172
Equation V.5 - Direct transport percentage (DTP)	172
Equation V.6 - Brain bioavailability	173
Equation VI.1 - Cell viability	195
Equation VII.1 - Cell viability	217
Equation VII.2 - Mass balance	219
Equation VII.3 - Apparent permeability coefficient (P_{app})	219
Equation VII.4 - Drug targeting efficiency (DTE%)	223
Equation VII.5 - Direct transport percentage (DTP)	223

PUBLICATIONS



PUBLICATIONS

GONÇALVES, J.; SILVA, S.; GOUVEIA, F. *et al.* - A combo-strategy to improve brain delivery of antiepileptic drugs: Focus on BCRP and intranasal administration. *International Journal of Pharmaceutics*. 593 (2021) 120161. DOI: 10.1016/j.ijpharm.2020.120161

GONÇALVES, J.; ALVES, G.; FONSECA, C. *et al.* - Is intranasal administration an opportunity for direct brain delivery of lacosamide? *European Journal of Pharmaceutical Sciences*. 157 (2021) 105632. DOI: 10.1016/j.ejps.2020.105632

GONÇALVES, J.; ALVES, G.; CARONA, A. *et al.*- Pre-Clinical Assessment of the Nose-to-Brain Delivery of Zonisamide After Intranasal Administration. *Pharmaceutical Research*. 37:4 (2020) 74. DOI: 10.1007/s11095-020-02786-z

GONÇALVES, J.; BICKER, J.; GOUVEIA, F. *et al.* - Nose-to-brain delivery of levetiracetam after intranasal administration to mice. *International Journal of Pharmaceutics*. 564 (2019) 329–339. DOI: 10.1016/j.ijpharm.2019.04.047

GONÇALVES, J.; BICKER, J.; ALVES, G. *et al.*- Relevance of Breast Cancer Resistance Protein to Brain Distribution and Central Acting Drugs: A Pharmacokinetic Perspective. *Current Drug metabolism*. 19:12 (2018) 1021-1041. DOI: 10.2174/1389200219666180629121033

GONÇALVES, J.; ALVES, G.; BICKER, J. *et al.* - Development and full validation of an innovative HPLC-diode array detection technique to simultaneously quantify lacosamide, levetiracetam and zonisamide in human plasma. *Bioanalysis*. 10:8 (2018) 541–557. DOI: 10.4155/bio-2017-0199

ABSTRACT/ RESUMO



ABSTRACT

Epilepsy has a major negative impact on the quality of life of the patients and their families. With an increasing incidence, mortality and morbidity, epilepsy dictates the need for developing new safe and effective therapeutic strategies namely due to the significant percentage of patients who do not respond to the current marketed antiepileptic drugs (AEDs). The blood-brain barrier (BBB) and the efflux transporters therein expressed, including the Breast Cancer Resistance Protein (BCRP), are well-known barriers that must be overcome when an AED is administered by classic systemic routes. Furthermore, the overexpression of efflux transporters has already demonstrated to contribute to the development of pharmacoresistant epilepsy. The current scientific knowledge regarding BCRP interactions with AEDs remains scarce even though this information is extremely important to predict AEDs distribution into the central nervous system (CNS). Ideally, the administration of AEDs through alternative routes that would allow the direct access of the drug to the brain would be desirable.

In this context, the present PhD thesis was planned to investigate the potential of the intranasal (IN) route to directly deliver three AEDs of new generation into the CNS. Through neural and olfactory epithelial pathways, their direct nose-to-brain delivery is expected to occur, circumventing the BBB and efflux transporters. To attain this main objective, comparative pharmacokinetic studies were carried out for lacosamide, levetiracetam and zonisamide after their administration through IN, intravenous (IV) and oral routes to male CD-1 mice. Firstly, a high performance liquid chromatography (HPLC) with diode array detection (DAD) method was developed and validated to accurately quantify the AEDs in mouse plasma, brain, lung and kidney tissues collected from the *in vivo* pharmacokinetic studies. Furthermore, the interaction of the AEDs with the BCRP was assessed *in vitro* resorting to accumulation and bidirectional transport cell models.

Initially, the HPLC-DAD technique was developed and optimized in human plasma to reduce the number of animals required for method development and validation in mouse matrices. It consisted of a gradient elution, mainly made of water, carried on a reversed-phase C₁₈ HPLC column and setting the wavelength at 220 and 239 nm to

simultaneously detect the three AEDs and the internal standard (IS). The HPLC-DAD analysis was preceded by a double liquid-liquid extraction (LLE) with ethyl acetate to reproductively extract and concentrate lacosamide, levetiracetam and zonisamide. This technique was validated in accordance with the international guidelines and has been used in routine therapeutic drug monitoring. Minor adjustments were introduced to quantify the AEDs in mice samples.

In vitro cell-based models were used to identify BCRP inhibitors and/or substrates. Intracellular accumulation assays used Madin-Darby canine kidney (MDCK-II) cells overexpressing BCRP (MDCK-BCRP) and identified lacosamide and zonisamide as BCRP inhibitors. However, lacosamide demonstrated to be more potent, inhibiting the efflux transporter at therapeutic levels while zonisamide required concentrations considerably superior to those of its therapeutic window. On the other hand, the bidirectional permeability studies carried on MDCK-II and MDCK-BCRP demonstrated that zonisamide is a BCRP substrate. In addition, permeation through nasal mucosa was predicted *in vitro* through the Human nasal septum cell line (RPMI-2650), demonstrating to increase as the AED lipophilicity enhanced.

The *in vivo* pharmacokinetic profiles achieved for the three AEDs evidenced that all of them markedly attained the brain through nose-to-brain direct transport, even systemic pathways were also evident. Levetiracetam was the one with the highest values of drug targeting efficiency (DTE) and direct transport percentage (DTP) to the brain, which were 182.35 % and 46.38 %, respectively. In addition, it was also demonstrated that the apparent permeability through RPMI-2650 cells was correlated with *in vivo* brain/plasma ratios but not with DTE or DTP. Lastly, the co-administration of zonisamide (through IN or IV routes) with elacridar, a BCRP inhibitor, demonstrated that the brain concentrations increased after IV injection but remained almost unchanged after IN instillation. These results corroborate that zonisamide is a BCRP substrate and suggest that IN route is probable to reduce the effect of BCRP on drugs transport into the CNS.

Taking into account the herein obtained data, IN administration revealed to be a promising strategy to directly deliver AEDs into the brain and avoid the influence of BCRP at the BBB. In a broader application scope, it is hence expected to become a great

opportunity for the treatment of refractory epilepsy, reducing also the inter- and intra-individual variability associated to hepatic metabolism and drug-drug interactions (DDI) that are often observed with conventional administration routes.

RESUMO

A epilepsia tem um elevado impacto negativo na qualidade de vida dos doentes e dos seus familiares. Com uma incidência, mortalidade e morbilidade crescentes, a epilepsia impõe a necessidade de descobrir novas estratégias terapêuticas seguras e eficazes, particularmente quando considerada a percentagem significativa de doentes que não responde aos fármacos antiepiléticos (AEDs) atualmente disponíveis na prática clínica. A barreira hematoencefálica (BBB) e os transportadores de efluxo aí expressos, incluindo a *Breast Cancer Resistance Protein* (BCRP), são barreiras bem conhecidas que têm de ser superadas quando um AED é administrado pelas vias sistémicas clássicas. Além disso, a sobreexpressão de transportadores de efluxo já demonstrou contribuir para o desenvolvimento de epilepsia farmacorresistente. O conhecimento científico sobre a interação da BCRP com AEDs permanece atualmente escasso, apesar da sua relevância na distribuição de AEDs para o sistema nervoso central (CNS). Desta forma, a administração de AEDs por vias alternativas que permitissem o acesso direto do fármaco ao cérebro seria desejável e ideal.

Neste contexto, a presente tese de Doutoramento foi elaborada para investigar o potencial da via intranasal (IN) para permitir o acesso direto de três AEDs de nova geração ao cérebro. Através das vias neuronal e olfativa, espera-se que ocorra a passagem direta da cavidade nasal para o cérebro, contornando a BBB e os transportadores de efluxo aí expressos. Para atingir este objetivo, estudos farmacocinéticos foram realizados para a lacosamida, levetiracetam e zonisamida, após administração por via IN, intravenosa (IV) e oral a murganhos CD-1 machos. Primeiramente, desenvolveu-se e validou-se um método de cromatografia líquida de elevada eficiência com deteção de díodos para quantificar com precisão e exatidão os AEDs em plasma, cérebro, pulmão e rim de murganho, obtidos dos estudos *in vivo* realizados. Para além disso, a interação dos AEDs com a BCRP foi avaliada *in vitro* com recurso a modelos celulares de acumulação e de transporte bidirecional.

Inicialmente, a técnica bioanalítica foi desenvolvida e otimizada em plasma humano para reduzir o número de animais necessário para o desenvolvimento do método e validação em matrizes de murganho. Um único método cromatográfico permitiu a

separação dos três AEDs e do padrão interno (IS) numa coluna de HPLC de fase reversa (C₁₈), com recurso a eluição por gradiente e fase móvel constituída maioritariamente por água, com deteção a 220 e 239 nm. A bioanálise foi precedida por uma dupla extração líquido-líquido (LLE), com acetato de etilo, para extrair e concentrar reproduzivelmente a lacosamida, o levetiracetam e a zonisamida. Esta técnica foi validada de acordo com as *guidelines* internacionais e tem sido utilizada na monitorização dos fármacos referidos. Alguns pequenos ajustes foram introduzidos para quantificar os AEDs em amostras de murganho.

Modelos celulares *in vitro* foram usados para identificar inibidores e/ou substratos da BCRP, recorrendo às linhas celulares de *Madin-Darby* de rim de cão (MDCK-II) e que sobreexpressam BCRP (MDCK-BCRP). Os ensaios de acumulação permitiram identificar a lacosamida e a zonisamida como inibidores da BCRP. No entanto, a lacosamida demonstrou ser mais potente, inibindo o transportador de efluxo em níveis terapêuticos, enquanto a zonisamida exigiu concentrações consideravelmente superiores à sua margem terapêutica. Por outro lado, os estudos de permeabilidade bidirecional realizados em MDCK-II e MDCK-BCRP revelaram a zonisamida como substrato da BCRP. Além disso, a permeabilidade através da mucosa nasal foi predita *in vitro* através de células RPMI-2650, demonstrando ser tanto maior quanto maior a lipofilia do AED.

Os perfis farmacocinéticos obtidos *in vivo* evidenciaram o transporte direto dos AEDs ao cérebro, assim como também revelaram que a via sistémica está presente. O levetiracetam foi o AED com maiores valores *drug targeting efficiency* (DTE) e da percentagem de fármaco diretamente transportado (DTP) para o cérebro (182,35 % e 46,38 %, respetivamente). Além disso, também foi demonstrado que a permeabilidade aparente através das células RPMI-2650 se correlaciona com os rácios cérebro/plasma observados *in vivo*, mas não com o DTE ou o DTP. Por último, a coadministração de zonisamida (IN ou IV) com elacridar, um inibidor da BCRP, demonstrou que as concentrações cerebrais aumentaram após a injeção IV, mas permaneceram quase inalteradas após a instilação IN. Os resultados identificaram que a zonisamida é substrato BCRP e sugerem que o efeito da BCRP no transporte de fármacos para o SNC pode ser reduzido pela administração IN.

Considerando os resultados obtidos durante a presente tese de Doutorado, a administração IN revelou-se uma estratégia promissora para permitir o acesso direto da lacosamide, levetiracetam e zonisamida ao cérebro e evitar a influência da BCRP na BBB. Assim, espera-se que a via IN represente uma oportunidade não só para o tratamento da epilepsia refratária, mas também para reduzir a variabilidade inter e intra-individual associada ao metabolismo hepático e às interações farmacológicas, frequentemente observadas pelas vias de administração convencionais.

CHAPTER I

INTRODUCTION



I.1. EPILEPSY

Epilepsy is a progressive chronic brain disorder, characterized by spontaneous and recurrent seizures. Throughout the evolutionary history of science, concepts have been clarified and the distinction between epilepsy and seizure has been established by the International League Against Epilepsy (ILAE). Accordingly, a seizure is defined as “a transient occurrence of signs and/or symptoms due to abnormal excessive or synchronous neuronal activity in the brain” [1] while epilepsy is a disease of the brain defined by any of the following conditions: “(1) At least two unprovoked (or reflex) seizures occurring >24 h apart; (2) One unprovoked (or reflex) seizure and a probability of further seizures similar to the general recurrence risk (at least 60 %) after two unprovoked seizures, occurring over the next 10 years; (3) Diagnosis of an epilepsy syndrome” [2]. More than a decade ago, epilepsy was the disease while seizure was a symptom [3]. However, convulsive seizures do not necessarily represent epilepsy, which may be of idiopathic etiology, underlying an acute or chronic pathology [4, 5]. The definition of epilepsy has also undergone major changes over time, according to the knowledge that has been acquired about the disease. The aforementioned definition is the most currently used, particularly due to its clarity and objectivity [2].

I.1.1. HISTORICAL CONTEXTUALIZATION

Dating at least 1000 years B.C., the remote Babylonian Medicine book is the oldest detailed document regarding epilepsy, identifying different types of seizures [6]. Nevertheless, at that time, epilepsy was considered a condition of supernatural causes, and each seizure type was associated with an evil spirit or God. Consequently, treatment was not medicinal but spiritual. This theory was changed by Hippocrates, who assertively identified the brain as the focus of organic disorders, discarding the divine theory as the etiology of epilepsy. This concept was not accepted, and in the middle ages, supernatural causes gained followers, also fueled by the acceptance of

Christianity, where religion was sovereign over all subjects. In the Renaissance, several scientific attempts were made to support epilepsy as a physical condition without divine influence, although without great success [7–9]. The crucial anatomical, pathological, pharmaceutical and physiological chemical discoveries that occurred in the Age of Enlightenment brought evidence that seizures were caused by neurological mechanisms [10], establishing epilepsy as a brain disorder. This idea was corroborated by the control of convulsive episodes by bromides in the late 19th century and barbiturates at the beginning of the 20th century, when the relationship between uncontrolled neuronal electrical discharges and seizures was finally identified [11].

In the 20th century, technological, scientific and medicinal advances, coupled to the implementation of novel complementary diagnostic methods (e.g. electroencephalogram, EEG), increased the knowledge about the pathophysiological mechanisms underlying epilepsy [12]. However, these mechanisms are not yet fully understood, despite efforts to conduct studies in that direction. Several molecules have been developed and proved to be effective, but they mainly act on ictogenesis, instead of also inhibiting neurobiological changes that occur during epileptogenesis [13–15].

I.1.2. EPIDEMIOLOGY OF EPILEPSY

Nowadays, epilepsy affects approximately 70 million people [16, 17], corresponding to 0.9 % of the world population [18]. It represents one of the most common neurological disorders, regardless of gender, age, geographic location, race and social class. However, its etiology depends on sociodemographic characteristics, clinical diagnostic capacity and genetic predisposition combined with risk factors [5] such as congenital malformations, infections at the central nervous system (CNS), brain neoplasm, Alzheimer's, head trauma and alcoholism [19]. It is more prevalent in men than women and at the extremes of age pyramid [5]. Epidemiological studies suggest that 102.4 per 100,000 children up to 12 months of age develop epilepsy [20].

In adults, an increase in the development of the disease is less, with a high incidence in people over the age of 70 years [21]. In children, the etiology has been correlated with the age of seizures onset, where 28 % of the cases were due to structural/metabolic causes up to 1 year of age and 22 % related to genetic changes, with symptoms manifested in older age [20]. Regarding the type of seizures, there is a greater occurrence of focal seizures, regardless of age [22], and the most serious condition of the disease, *status epilepticus*, has an incidence of 9.9 to 41 per 100,000 people per year [23].

The ILAE Epidemiology Committee recommends that a different and less specific concept of epilepsy should be considered for epidemiological studies. Accordingly, epilepsy should be considered when 2 or more spontaneous seizures occur in an interval of at least 24 hours, not requiring the fulfillment of the other criteria that are mandatory for disease diagnosis [24]. It is estimated that about 80 % of epileptic patients live in low and middle-income countries [16], with a greater annual incidence in underdeveloped countries (139 per 100,000 inhabitants) compared to developed countries (48.9 per 100,000 inhabitants) [25]. Several justifications are possible and plausible for such a discrepancy starting with neonatal care and a higher probability of contracting CNS infections that may lead to epilepsy [26].

Immediate causes responsible for deaths directly attributable to epilepsy and seizures include *status epilepticus*, sudden death, injuries from falls and suicide. Nevertheless, it is noteworthy that comorbidities and an impaired quality of life of patients have a greater impact on the disease [27].

I.1.3. SEIZURES CLASSIFICATION

In 1969, Henri Gastaut developed the first epileptic seizure classification system published by the ILAE [28], accompanied by the development of diagnostic methods, including the video display of epileptic seizures on magnetic tape, the simultaneous recording of the EEG using hard-wired recording techniques and radiotelemetry with split screen display and instant replay [29]. Altogether, they allowed the definition of

patterns of specific epilepsy syndromes and the collection of knowledge about the semiology of epileptic seizures that was still unclear [30, 31]. Therefore, the concepts of partial and generalized seizures, simple and complex partial seizures and generalized seizures were established for the first time in 1981 by the ILAE [29]. Despite remoting to more than two decades, this conceptualization allowed the establishment of an essential taxonomic base for the universal understanding of clinicians and researchers and it makes part of the terminology used in lastly published review of the ILAE [32]. Accordingly, there are two classifications, the basic and the expanded classification as detailed in **(Figure I.1)**. The basic classification is intended for non-specialized clinicians, while the expanded classification is for physicians experienced in the diagnosis and treatment of the disease [32]. Their main characteristics are summarized in **Table I.1**.

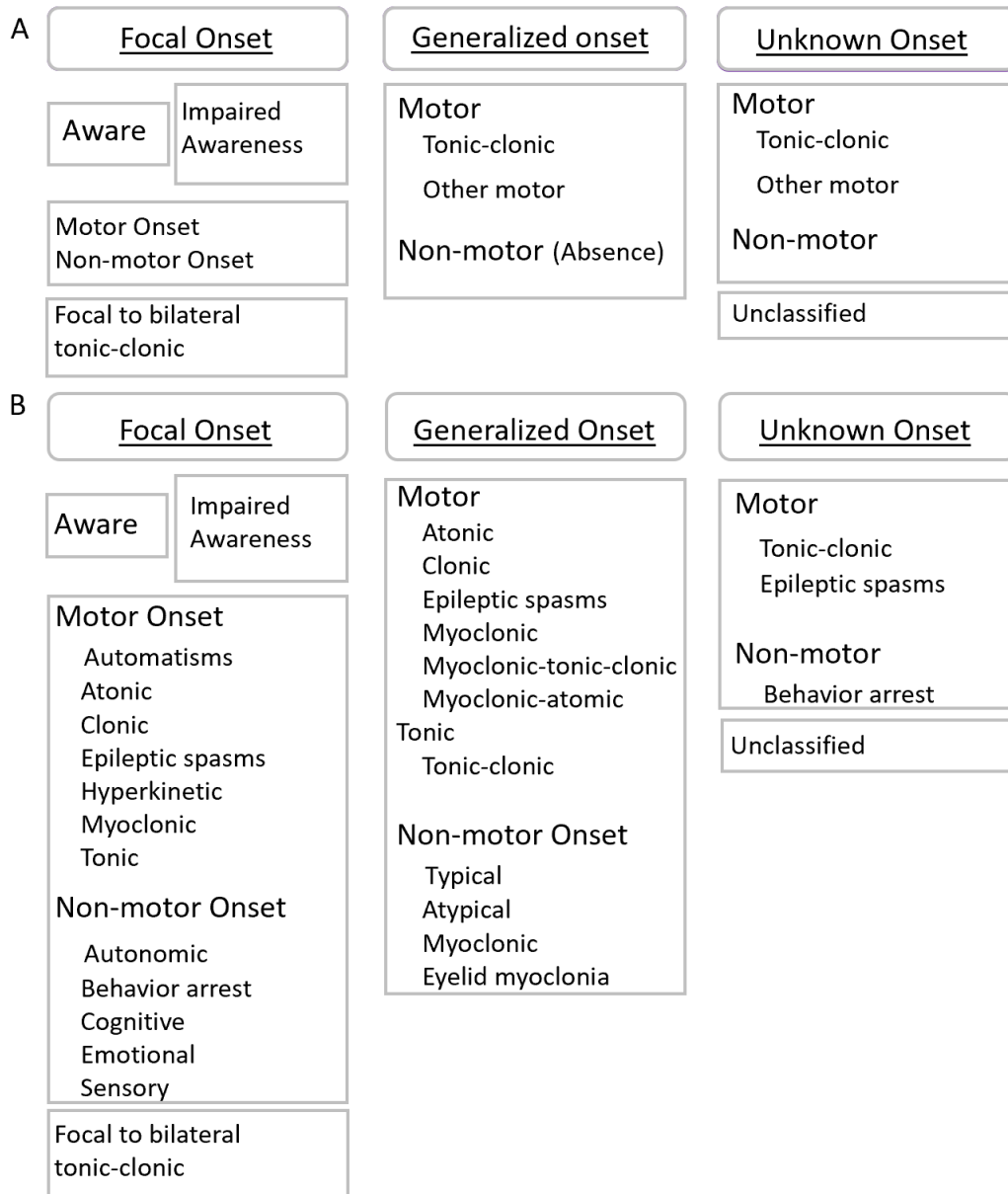


Figure I.1 Classification of epileptic seizures **(A)** basic version and **(B)** expanded version, according to the International League Against Epilepsy [32].

Table I.1 Description of the type of epileptic seizures, according to the International League Against Epilepsy 2017 Classification Seizure [32].

Epileptic Seizure Description
<p>Focal onset seizures:</p> <ul style="list-style-type: none"> • Focal automatisms seizure: A seizure with automatic fumbling behavior, such as lip-smacking, hand-rubbing, picking at objects, walking in circles, repeating meaningless phrases, or undressing. • Focal atonic seizure: Focal, for example in one arm or leg, sudden loss of muscle tone and strength, resulting in a transiently limp limb. • Focal clonic seizure: Sustained rhythmical jerking of one part of the body or face. • Focal epileptic spasms: Sudden flexion or bending of the trunk with flexion or extension of the limbs lasting less than a few seconds. These often occur in clusters. The term infantile spasms apply to epileptic spasms occurring during infancy. Video-EEG monitoring and a brain MRI ma. be needed to determine whether onset of epileptic spasms is focal or generalized. • Hyperkinetic seizure: A seizure with vigorous thrashing or pedaling movements. Even though both sides of the body are usually involved with these seizures, the EEG often shows a focal and frontal lobe origin. Some people used to call these hypermotor seizures. • Focal myoclonic seizure: Irregular and brief lightning jerks of limbs or face on one side of the body. • Focal tonic seizure: Stiffening of arm, leg, or neck producing a forced posture during the seizure. • Focal autonomic seizure: A seizure whose primary effect is on autonomic nervous system functions, such as heart rate, blood pressure, sweating, skin color, piloerection, and gastrointestinal sensations. • Focal behavior arrest seizure: In this seizure type, movement stops, sometimes called a freeze or a pause. A seizure should only be classified as a focal behavior arrest seizure if the behavior arrest is the main feature through the entire seizure. • Focal cognitive seizure: This type of seizure refers to impaired cognition during a seizure. The impairment might affect language, spatial perception, ability to calculate math, or other cognitive functions. Do not count loss of awareness or memory (unless only memory is impaired) as a focal cognitive seizure, because awareness is used to describe other seizure types. • Focal emotional seizure: This seizure type begins with spontaneous fear, anxiety, or less often joy. There may be involuntary laughing or crying, each of which might or might not be accompanied by a subjective emotion. Gelastic and dacrystic seizures would fit into this group. • Focal sensory seizure: Sensory seizures can consist of tingling or numbness, visual symptoms, sounds, smells, tastes, tilting or vertigo, and hot-cold feelings.
<p>Generalized onset seizures</p> <ul style="list-style-type: none"> • Generalized tonic-clonic: Immediate loss of awareness, with stiffening of all limbs (tonic phase), followed by sustained rhythmic jerking of limbs and face (clonic phase). Duration is typically 1 to 3 min. The seizure may produce a cry at the start, falling, tongue biting, and incontinence. • Generalized clonic: Rhythmical sustained jerking of limbs and/or head with no tonic stiffening phase. These seizures most often occur in young children. • Generalized tonic: Stiffening of all limbs, without clonic jerking. • Generalized myoclonic: Irregular, unsustained jerking of limbs, face, eyes, or eyelids. The jerking of generalized myoclonus may not always be left-right synchronous, but it occurs on both sides. Myoclonus may be part of a seizure or a non-epileptic motor disorder. • Generalized myoclonic-tonic-clonic: This seizure is like a tonic-clonic seizure, but it is preceded by a few myoclonic jerks on both sides of the body. Such seizures are commonly seen in people with the syndrome of juvenile myoclonic epilepsy. • Generalized myoclonic-atonic: This seizure presents with a few myoclonic jerks, followed by a limp drop. These seizures may be seen in children with Doose syndrome. • Generalized atonic: This is an epileptic drop attack, with sudden loss of muscle tone and strength and a fall to the ground or a slump in a chair. Atonic seizures usually last only seconds. • Generalized epileptic spasms: Brief seizures with flexion at the trunk and flexion or extension of the limbs. Video-EEG recording may be required to determine focal versus generalized onset. • Generalized typical absence: Sudden cessation of activity with a brief pause and staring, sometimes with eye fluttering and head nodding or other automatic behaviors. In the more severe

seizures, awareness and memory are impaired. Recovery is immediate. The EEG during these seizures always shows generalized spike-waves.

- **Generalized atypical absence:** Like typical absence seizures but may have slower onset and recovery and more pronounced changes in tone. Atypical absence seizures can be difficult to distinguish from focal impaired awareness seizures, but absence seizures usually recover more quickly, and the EEG patterns are different.
 - **Generalized myoclonic absence:** A seizure with a few jerks and then an absence seizure.
 - **Generalized eyelid myoclonia:** Eyelid myoclonia represents jerks of the eyelids and upward deviation of the eyes, often precipitated by closing the eyes or by light. These may be associated with absence seizures in people with Jeavons's syndrome.
-

Unknown onset seizures

- Clinicians using the classification will identify a seizure as focal or generalized onset if there is at least an 80 % confidence level about the type of onset.
 - The most important seizures of unknown onset are tonic-clonic, epileptic spasm, and behavior arrest (which could be either a focal impaired awareness or absence seizure). If a seizure onset becomes clarified at a later date, the type will change.
-

The type of seizure is the primary aspect to consider when assigning the classification of epilepsy. It may be focal, generalized or unknown, depending on the region of the brain that is affected, but often involves sudden uncontrollable spasms and even unconsciousness. Focal seizure was originally named partial seizure, but this changed as it refers to an anatomical region where the neurological dysfunction occurs [1]. Generalized seizures have bilateral origin in opposition to focal seizures that result from a specific structure. It is important to note that a seizure of focal origin can evolve to a generalized seizure if it affects bilateral neural networks. A seizure is called “unknown” when the diagnosis of epilepsy is unequivocal, but it is not possible for the clinician to determine whether the seizure is local or generalized [34]. This category is reserved to classify seizures for which the clinician has less than 80 % confidence regarding the initial nature of the seizures [32].

Any seizure, regardless of the type, can progress to *status epilepticus*, which is characterized by prolonged or repeated epileptic seizures in brief intervals of time, resulting in a lasting condition. This epileptic state generally has irreversible consequences related to the duration of the seizure, such as injury, alteration of the neural networks or death [35]. However, it has been suggested to be induced by seizures, where cardiorespiratory alterations are the most appropriate explanation for its occurrence [5].

It should be noted that the classification of epilepsies or epileptic syndromes does not take into account only the type of seizures, but also the etiology (described

in **Section I.1.4**), comorbidities and the entire clinical condition of the patient. This multivalent diagnostic classification is based on three levels: type of seizure categorized according to the ILAE operational classification, type of epilepsy (generalized, focal, combined or unknown) and epilepsy syndrome. **Figure I.2** contemplates the recent understanding of epilepsies and their underlying mechanisms [34].

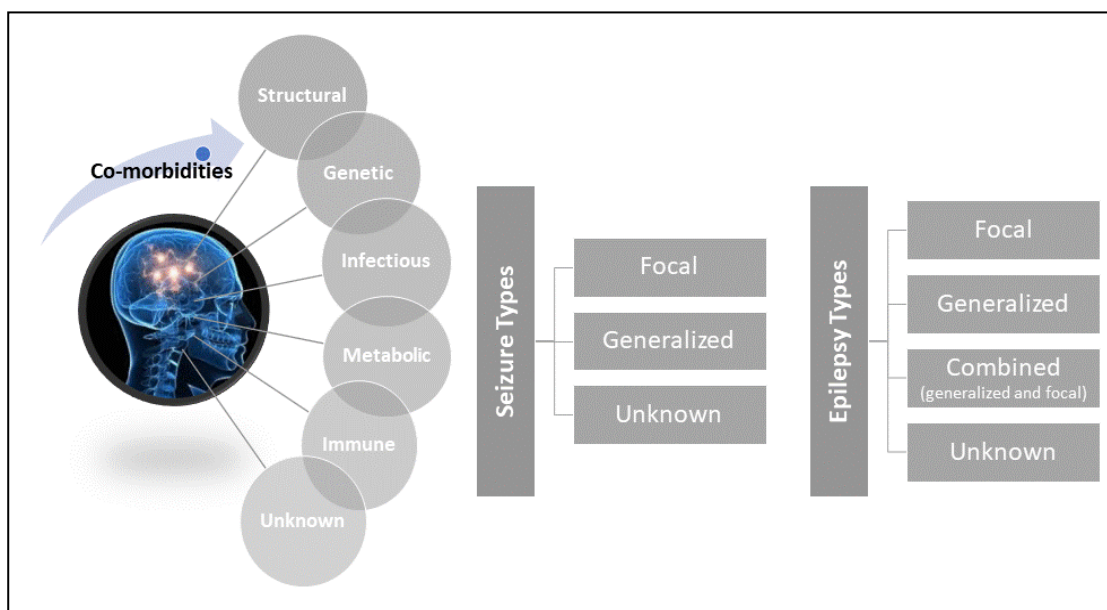


Figure I.2 Classification of epilepsies: etiological factors, types of seizures and types of epilepsy, related to the onset of the epileptic seizures [34].

I.1.4. ETIOLOGY OF EPILEPSY

The biochemical, cellular and neuronal mechanisms underlying epilepsy are not yet fully understood, but several pathways have properly been identified, supporting that a multidisciplinary etiology underlies epilepsy development in a specific patient at a specific time [36]. In general, the etiology is based on structural, functional, metabolic and genetic hypotheses [37]. The ILAE classification from 2017 comprises six etiological groups (**Figure I.2**). The *structural group* may be congenital due to malformations during cortical development or acquired as a consequence of other pathologies [37] while the *genetic group* results from well-known mutations [17, 38]. For example, mutations at *SCN1A* gene that encodes voltage-gated sodium channels (VGSCs) [39], the variation N79S of the GABA_A receptor γ 2 subunit gene (*GABRG2*)

that encodes the major isoforms of GABA_A receptor ($\gamma 2$ subunit) in the brain [40]. *Infectious* causes are the most common worldwide and result from bacterial or viral infections in the CNS [19, 41]. On the other hand, the *metabolic group* is characterized by changes in patient's metabolism that culminate in recurrent seizures [40]. For example, the metabolic imbalance of neurotransmitters such as GABA, in premature infants with immaturity of the chloride cation co-transporter, causes unregulated excitability and consequently promotes the development of epileptogenesis [40, 41]. Immunosuppressed people are often infected with microorganisms clinically associated with convulsive conditions, such as toxoplasma in latent children, human *herpesvirus* or Creutzfeldt–Jakob disease in the elderly [19, 42]. When the causes are not identified the group is named *unknown*.

The complexity underlying the etiology and physiopathology of epilepsy has been a constant challenge for scientists, not only because of the wide variety of seizures and symptoms but also because of the distinct responses to the current marketed antiepileptic drugs (AEDs) throughout disease evolution. Indeed, approximately one third of epileptic patients develop resistance to AEDs, suggesting the occurrence of structural, biological and biochemical changes over time [43].

Briefly, epilepsy is characterized by recurrent, abnormal and spontaneous electrical discharges (convulsions) that cause changes in perception, consciousness and motor activity, through a process called epileptogenesis, where a brain changes its normal physiological condition to an epileptic condition [44]. Currently, there are several viable and scientifically accepted theories that justify the brain hyperexcitability: (1) changes regarding the distribution, number, structure and intrinsic activity of ion channels expressed in neuronal membranes which may compromise the intra and extracellular ion concentrations involved in generation of potentials of action; (2) biochemical changes in receptors and consequently their binding to neurotransmitters; (3) changes in neurotransmitter release and uptake with consequent local neurotransmitter imbalance [e.g., glutamate, γ -aminobutyric acid (GABA), acetylcholine, norepinephrine, and serotonin]; (4) modulation of second messenger systems and gene expression; (5) changes in metabolism of glia cells; and (6) modification in the function of inhibitory circuits [45]. These premises refer to a

process called ictogenesis, which has been the main pharmacological target of interest to develop AEDs [46, 47]. Neuromodulators, acetylcholine, norepinephrine, serotonin and histamine are involved in the transient imbalance of excitatory (glutamate) and inhibitory (GABA) neurotransmitters [37, 45], actively participating in the induction of seizures. Glutamate, as the main excitatory neurotransmitter of mammal CNS, is found in altered levels in the epileptic brain [48, 49]. A study conducted by Çavuş *et al.* demonstrated that cortical epileptogenic foci had higher levels of glutamate when compared to the non-epileptogenic cortex [50]. While the excitatory system can be considered as hyper-activated in epilepsy, the GABAergic system, responsible for brain inhibitory modulation, loses its activity due to damage of GABA-producing cells. This clearly interrupts the physiological balance of excitation/inhibition, promoting, subsequently, new cell lesions followed by apoptosis [51]. Thus, glutamate receptors constitute a therapeutic target in order to develop antagonists that will decrease their excitatory activity and consequently the development of epileptic seizures. In opposition, GABA agonists act on the GABAergic receptors and potentiate their inhibitory activity [52].

Neuroinflammation has been also associated to epilepsy. It is characterized by the transient release of pro- and anti-inflammatory mediators, namely cytokines, with additional activation and recruitment of innate immune cells, astrocytes and microglia. Thus, epileptogenesis process evolves neuroinflammation, as an inflammatory response to brain damage by activation of innate immunity [53, 54]. On the other hand, scientific evidence shows the contribution of neuroinflammation to ictogenesis, by establishing the causal relationship of inflammation to seizure activity [53]. Furthermore, the healthy blood-brain barrier (BBB) is impermeable to macromolecules and immune cells of the innate system, however after an epileptogenic episode, the permeability of the BBB increases, allowing proteins, high molecular weight molecules and immunologic cells to attain the CNS [55].

I.2. PHARMACOTHERAPY OF EPILEPSY

Pharmacological treatment of epilepsy aims at attaining a complete control of seizures, with tolerable or no adverse effects, affording quality of life to patients and reducing the associated mortality. Pharmacotherapy is, until now, the mainstream treatment for epilepsy. Nevertheless, non-pharmacological therapies, such as surgery for removal of the epileptogenic focus, *vagus* nerve stimulation and ketogenic diet, may be applied in patients with very specific characteristics [56–58].

The wide panoply of AEDs available and its extensive use undeniably support drugs efficiency and low risk-benefit ratio. However, one in every three patients does not respond to the AED or have a high incidence of serious or intolerable adverse effects that hamper the adherence to therapy [59]. This condition is named refractory epilepsy, pharmaco-resistant epilepsy, intractable epilepsy or drug-resistant epilepsy, as it will be explained in the next section [60].

Most of the AEDs used in clinical practice does not inhibit or slows down epileptogenesis. Indeed, the drugs currently available mainly act on the symptoms and ictogenesis than in treating epileptogenesis. Thus, the terminology of "anticonvulsant drug" has been adopted for this pharmacological class in place of the term "antiepileptic drug" [61]. However, and considering that the term antiepileptic is more commonly used among the scientific community, it will be applied throughout this thesis.

Monotherapy is preferable when starting the treatment of epilepsy [62]. Indeed, polytherapy is not necessarily associated with a better seizure control [63] and it may involve several disadvantages: higher incidence of adverse effects and eventually toxicity; drug-drug interactions (DDIs); decrease of drug compliance and higher economical costs. Hence, polytherapy is the alternative when a single drug does not control the occurrence of seizures. Since there are more than 20 molecules currently available in clinical practice with different and complementary mechanisms of action [45, 64], administration of adjuvant therapies tends to maximize drug efficacy. The AEDs should interact on different therapeutic targets, promoting synergistic effects

and minimizing the occurrence of cumulative adverse effects that may occur when two AEDs with the same mechanism of action are used [64]. Importantly, it must be herein emphasized that some AEDs have multi-targeting activities, a pharmacological property named "polypharmacology" [65]. An example of this phenomenon is cenobamate, which has combined effects on persistent sodium streams and GABA_A receptors [66]. Furthermore, lacosamide has a wide range of clinical indications probably due to its interaction with distinct pharmacological targets: its slow inactivation of VGSC confers drug anticonvulsant effect [67], while its neuroprotective action is related to the lacosamide interaction with the collapsin response mediator protein type 2 (CRMP2) [68].

The selection of the appropriate drug represents one of the greatest challenges, and several parameters must be considered, assuming that the diagnosis and classification of the type of seizure and epilepsy is correct. Indeed, the mechanism of action of the drug must involve at least one specific target underlying the type of seizure that was diagnosed. Furthermore, patients characteristics and their comorbidities, as well as the pharmacological properties of the drug must be appreciated [69, 70].

I.2.1. ANTIEPILEPTIC DRUGS

The development of the AEDs and their introduction into the market go back to 19th century, encompassing almost two dozens of drugs nowadays (**Figure I.3**). The treatment of epilepsy initiated occasionally in 1857 with the administration of potassium bromide and, in 1912, with phenobarbital, even though without any randomized clinical trial demonstrating evidence of efficacy and tolerability in epileptic patients [71, 72]. The "modern" era of antiepileptic pharmacotherapy began in 1938 with the introduction of phenytoin [73]. Its anticonvulsant properties were indeed revolutionary, constituting an innovative landmark for the treatment of epilepsy. Surprisingly, phenytoin proved to be more toxic than bromides and hypnotics, and it was indicated only for patients resistant to these drugs [72].

The 70s and 80s were marked by the development of pathophysiological and pharmacological investigations within the scope of epilepsy, leading to crucial and accurate information about the pathology and possible molecular targets that made possible the revolutionary posterior introduction of multiple AEDs in the market. In this context, carbamazepine, valproic acid and benzodiazepines appeared in a balanced way, together with barbiturates and phenytoin, constituting the classic generation of AEDs, also named 1st generation. Despite the unquestionable success achieved with the discovery of these pioneering AEDs, clinical practice demonstrated that they easily trigger toxic side effects, present high intra- and inter-variability and hence unpredictable pharmacokinetics, narrow therapeutic window and high potential to develop DDIs [74]. These facts, linked to the increasing knowledge regarding the pathophysiology of epilepsy, allowed the research and development of new AEDs.

The wave of new AEDs started in 1988, as well as the establishment of new terminology guidelines and classification of epileptic seizures. The structural variety of currently commercialized molecules is immense, with different mechanisms of action, improved pharmacokinetic profiles, less potential for the development of DDIs, lower adverse effects, better tolerability and wider therapeutic range [75]. AEDs are currently classified into three generations (**Figure I.3**): 1st generation that refers to the drugs approved until 1993, 2nd generation that include the AEDs approved between 1993 and 2007, and the 3rd generation that represents the most recent drugs approved since 2008 until today [76]. Their anti-seizure effectiveness is undeniable, but pharmacological treatment directed to the epileptogenic mechanisms remains an unmet clinical need [77].

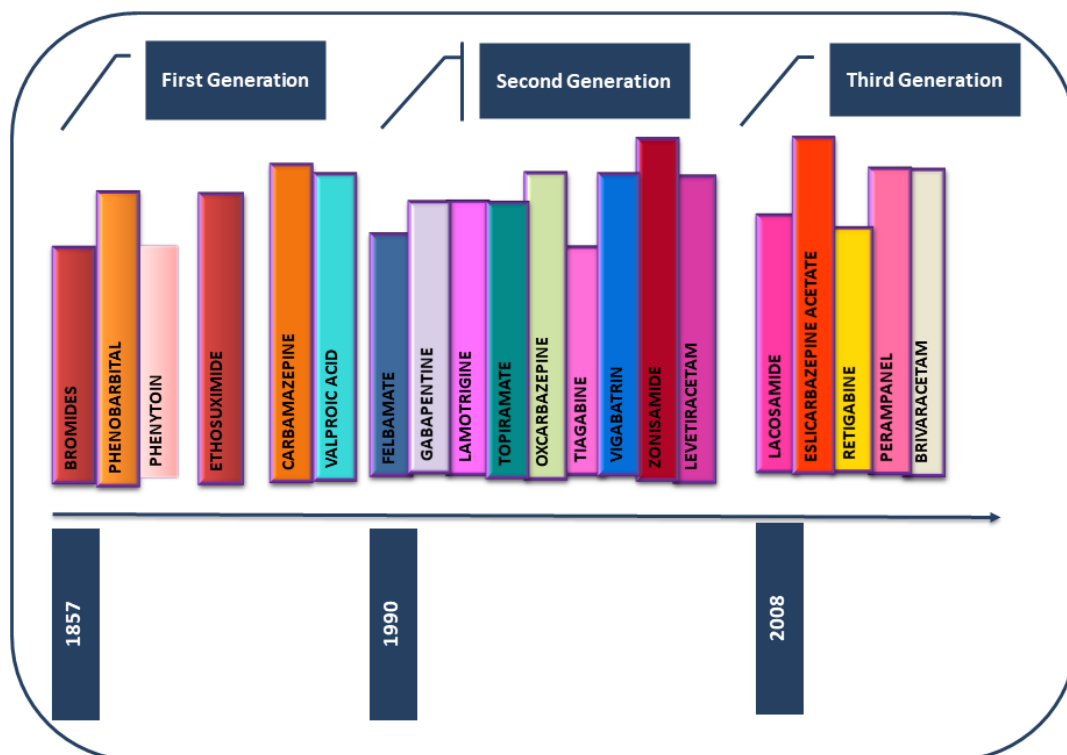


Figure I.3 Classification of marketed antiepileptic drugs into generations in accordance with their data of development.

Among such a variety of AEDs, it is important to establish which are indicated for each type of epileptic seizure, taking advantage of the specificity of each molecule and decreasing the probability of ineffective treatment or worsening the patient's clinical condition [78]. Thus, there was a need to create a quick and noticeable consultation system summarizing the drugs indicated for each type of seizure. The National Institute of Excellence in Health and Care [79] established guidelines that identify the first-line drugs recommended for each type of seizure and epileptic syndrome, and the alternative drugs that should be used when first-line drugs are ineffective or intolerable (**Table I.2**).

Table I.2 Antiepileptic drugs recommended for each type of seizure, and those that should be avoided in accordance with the National Institute of Excellence in Health and Care [79].

Type of seizure	Monotherapy	Adjuvant therapy	Avoid
Focal seizure	<u>1st line:</u> Carbamazepine Lamotrigine	Carbamazepine Clobazam Eslicarbazepine acetate Gabapentin Lacosamide Lamotrigine Levetiracetam Oxcarbazepine Topiramate Valproic acid	Brivaracetam Perampanel Pregabalin Phenobarbital Phenytoin Retigabine Tiagabine Vigabatrin Zonisamide
	<u>2nd line:</u> Levetiracetam Oxcarbazepine Valproic acid		Not reported
Absence seizures	<u>1st line:</u> Ethosuximide Valproic acid	Clobazam Clonazepam Ethosuximide Lamotrigine Levetiracetam	Carbamazepine Gabapentin Oxcarbazepine Phenytoin Pregabalin
	<u>2nd line:</u> Lamotrigine	Topiramate Valproic acid Zonisamide	Tiagabine Vigabatrin
Generalized tonic-clonic seizures	<u>1st line:</u> Valproic acid	Clobazam	Carbamazepine Gabapentin
	<u>2nd line:</u> Lamotrigine	Lamotrigine Levetiracetam Topiramate Valproic acid	Oxcarbazepine Phenytoin Pregabalin
	<u>3rd line:</u> Carbamazepine Oxcarbazepine		Tiagabine Vigabatrin
Myoclonic seizures	<u>1st line:</u> Valproic acid	Clobazam Clonazepam Levetiracetam Topiramate	Carbamazepine Gabapentin Oxcarbazepine Phenytoin
	<u>2nd line:</u> Levetiracetam Topiramate	Zonisamide Valproic acid	Pregabalin Tiagabine Vigabatrin
Tonic or atonic seizures		Lamotrigine	Carbamazepine Gabapentin
	Valproic acid	Rufinamide Topiramate	Oxcarbazepine Pregabalin Tiagabine Vigabatrin

AEDs are generally known for one or more mechanisms of action, although, sometimes, not fully understood. With their wide use in clinical practice, other pharmacological have been identified, and, therefore, their mechanisms of action are constantly being updated. Thus, AEDs may act through four principal mechanisms (**Figure I.4**) (1) modulation of voltage-gated ion channels; (2) enhancement of GABA inhibitory activity; (3) reduction of the glutamatergic excitatory system; and (4) modulation of neurotransmitters. Very recently, a fifth mechanism has been postulated and it regards the inhibition of the mammalian target of rapamycin (mTOR) signaling pathway; AEDs with this mechanism of action are strictly administered in focal seizures resulting from tuberous sclerosis complex (TSC), which is due to heterozygous mutations in either *TSC1* or *TSC2* genes [61, 80]. **Table I.3** describes the classification of the AEDs according to their molecular targets.

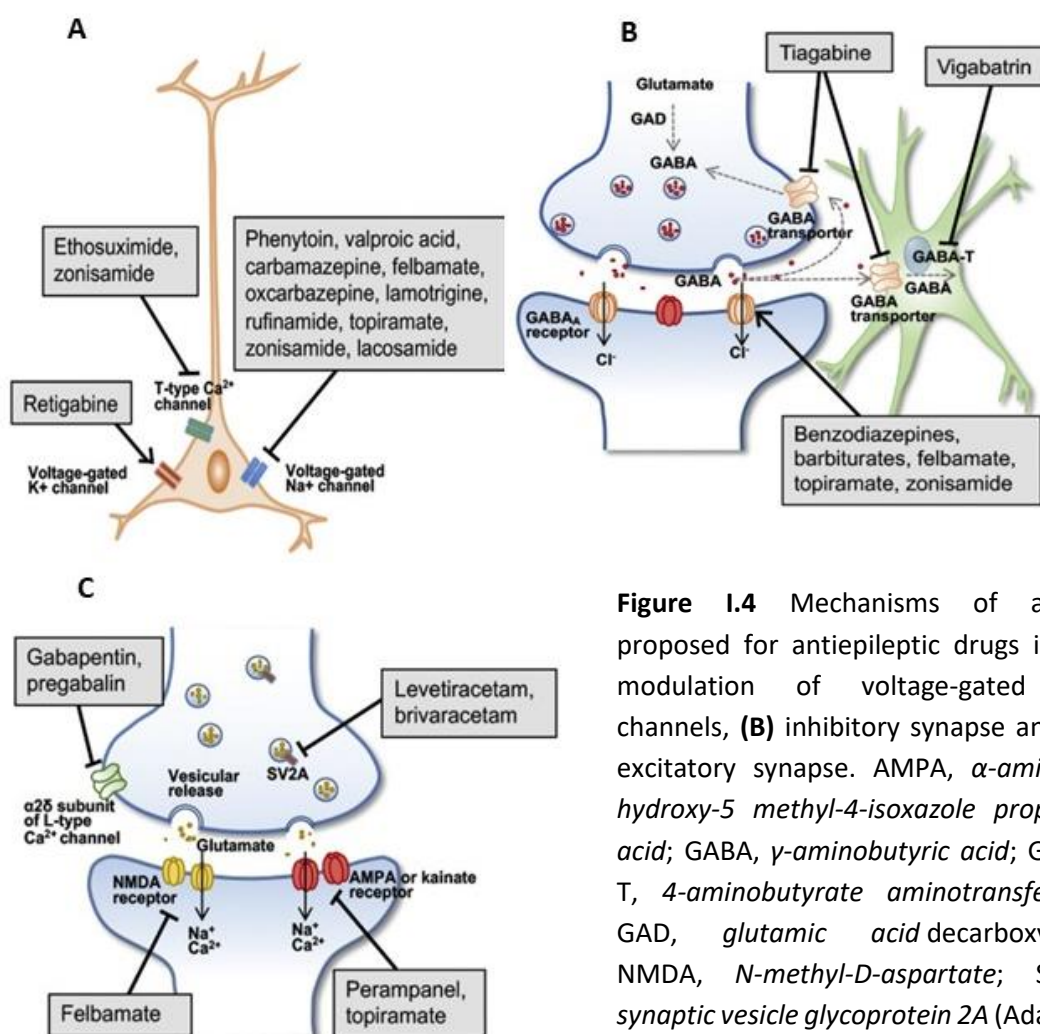


Figure I.4 Mechanisms of action proposed for antiepileptic drugs in **(A)** modulation of voltage-gated ion channels, **(B)** inhibitory synapse and **(C)** excitatory synapse. AMPA, α -amino-3-hydroxy-5-methyl-4-isoxazole propionic acid; GABA, γ -aminobutyric acid; GABA-T, 4-aminobutyrate aminotransferase; GAD, glutamic acid decarboxylase; NMDA, *N*-methyl-*D*-aspartate; SV2A, synaptic vesicle glycoprotein 2A (Adapted from [607]).

Table 1.3 Classification of antiepileptic drugs according to their molecular targets, adapted from [56, 76].

Molecular Target	Antiepileptic Drugs
Voltage-gated ion channels:	
Voltage-gated Na ⁺ channels	Carbamazepine, Cenobamate, Eslicarbazepine acetate, Phenytoin, Lacosamide, Lamotrigine, Oxcarbazepine, Phenytoin <u>Possibly:</u> Rufinamide, Topiramate, Zonisamide
Voltage-gated Ca ²⁺ channels	Ethosuximide
Voltage-gated K ⁺ channels	Retigabine
GABA-mediated inhibition:	
GABA _A receptors	Benzodiazepines (Diazepam, Lorazepam, Clonazepam, Midazolam, Clobazam), Phenobarbital, Primidone, Stiripentol <u>Possibly:</u> Cenobamate, Felbamate, Retigabine, Topiramate
GAT1 GABA transporter	Tiagabine
GABA transaminase	Vigabatrin
Carbonic anhydrase	Acetazolamide, Topiramate, Zonisamide <u>Possibly:</u> Lacosamide
Synaptic release machinery:	
SV2A	Levetiracetam, Brivaracetam
α2δ subunit of VGCC	Gabapentin, Pregabalin
Ionotropic glutamate receptors:	
AMPA receptor	Perampanel
Disease specific:	
mTORC1 signaling	Everolimus
Lysosomal enzyme replacement	Cerliponase alfa (recombinant tripeptidyl peptidase)
Mixed/unknown	Valproic acid, Felbamate, Cenobamate, Topiramate, Zonisamide, Rufinamide, Adrenocorticotrophin, Cannabidiol

AMPA, *α-amino-3-hydroxy-5-methyl-4-isoxazolepropionic acid*; Ca²⁺, *calcium ion*; GABA, *γ-Aminobutyric acid*; GABA_A, *γ-aminobutyric acid receptor type A*; GAT1, *γ-aminobutyric acid transporter 1*; mTORC1, *mammalian target of rapamycin complex 1*; SV2A, *synaptic vesicle glycoprotein 2A*; VGCC, *voltage-gated calcium channel*.

(1) Modulation of voltage-dependent ion channels

VGSC are multimeric protein complexes constituted by α-subunits, which surround a pore that is semi-permeable to sodium, and β-subunits that modulate the biophysical properties (kinetics and trafficking) of the channel. Amongst the nine genes encoding the pore-forming α-subunits, those most expressively found in the CNS are Nav1.1 (*SCN1A*), Nav1.2 (*SCN2A*), Nav1.3 (*SCN3A*), and Nav1.6 (*SCN8A*) and they are the responsible for initiation and propagation of action potentials in neurons. The physiological function of VGSCs is mediated by voltage changes and the

channel may exist in three different stages: closed, open or inactivated. At the resting potential membrane, VGSC is closed, hampering sodium passage through the pore [82]. When neuronal membrane depolarizes through the activation of synaptic glutamate receptors, the sodium channel opens and enables the influx of sodium following its electrochemical gradient [83]. This process, named activation, occurs in few milliseconds, and generates the action potential in neurons. Simultaneously, the same depolarization also induces conformational changes in the intracellular protein portion of the VGSC (named ball and chain), which is attracted to the pore, blocking it. The open channel is, hence, converted to a non-conducting inactivated state by the fast inactivation process. Even if depolarization takes more time, a slow inactivation process occurs mediated by the VGCS extracellular portion that is displaced by the depolarization but with slower kinetics. Therefore, channels may be at two non-conducting inactive states which are biophysically different from the closed state. The intra and extracellular protein portions responsible for fast and slow inactivation are removed during hyperpolarization, allowing the re-opening of the channel [84].

In 1 % of the neurons, the inactivation of the sodium current is not complete, resulting in a small persistent sodium current (I_{NaP}), with kinetics of inactivation during tens of seconds [85]. I_{NaP} reduces the threshold for action potential generation, promoting epileptic burst firing, sustained repetitive firing and augmentation of depolarizing synaptic currents. Consequently, larger than normal I_{NaP} amplitudes contribute to hyperexcitability and cytoplasmic sodium concentrations and lead to epilepsy and other disorders [86]. Indeed, models of temporal lobe epilepsy and neurons from resected temporal lobe of patients with epilepsy revealed I_{NaP} amplitudes 2 to 5-fold of those observed in healthy individuals. Phenytoin inhibits I_{NaP} , preventing the process of repetitive electrical discharge [86]. Moreover, several VGSC mutations have been identified in α -subunits Nav1.1, Nav1.2, Nav1.3 and Nav1.6, and β -subunits in rodents and humans and associated to distinct types of epilepsy [80]. These mutations lead to differences in channel functions that seem to be involved in the process of epileptogenesis and maintenance of the epileptic state.

Besides phenytoin, many other sodium channel blockers are currently used in the treatment of focal and primary generalized tonic–clonic seizures. They include carbamazepine, oxcarbazepine, eslicarbazepine (the active metabolite of oxcarbazepine and eslicarbazepine acetate), lamotrigine, lacosamide, rufinamide and topiramate. All of them interact with the VGSC at the binding site of sodium that is located in the inner part of the pore. They are considered voltage dependent as they bind preferentially when the channel is in the inactive state (depolarized state instead of resting membrane potential) and maintain the channel inactive while the drug is bound. Therefore, during depolarization and quick firing, the VGSC remains more time in the inactivated state, enrolling the drug in this configuration. VGSC blockers are also use-dependent, because they reduce high-frequency trains of action potentials much more potently than they attenuate individual action potentials or firing at low frequencies [87–89].

All VGSC blockers act on fast and slow inactivation processes, with exception of lacosamide, which is the only AED that facilitates slow inactivation without altering the fast component probably because it binds more slowly to fast-inactivated sodium channels [80]. Thus, classic AEDs, such as phenytoin and carbamazepine, inhibit the triggering of the action potential in hundreds of milliseconds, while lacosamide takes 1-2 seconds [80]. More recently, the same mechanism has been attributed to eslicarbazepine: a very slow connection to the channel, with a consequent increase in the time required for inhibition of the generation of the action potential [90]. It has been proposed that this slower binding to fast-inactivated sodium channels may be related to greater efficacy and tolerability [91].

Interestingly, topiramate is also a VGSC blocker that, at low concentrations, binds to sodium channels through phosphorylation, while its mechanism of action is identical to that aforementioned for the other AEDs at higher concentrations [92].

Importantly, the VGSC not only control excitability in the CNS, but also in the peripheral autonomic nervous system, cardiovascular system and digestive system. Therefore, the successful development of AEDs demands drug selectivity to brain VGSC [93].

Voltage-gated calcium channels (VGCCs) are ubiquitously expressed in the CNS, developing a widespread effect on neuronal excitability, synaptic transmission, neurotransmitter release, gene expression, neuro-architectural development and intracellular signal propagation. Different subtypes of VGCCs are, hence, expressed to attain these functions, all of them are multimeric membrane complexes composed of α_1 , β_1 , γ , and $\alpha_2\delta$ subunits. The $\alpha_2\delta$ proteins ($\alpha_2\delta-1$, $\alpha_2\delta-1$ and $\alpha_2\delta-2$) are accessory subunits of VGCC subunits, enhancing calcium channel trafficking and insertion in the plasma membrane, and influencing the biophysical properties of the channels. Gabapentinoid drugs (namely gabapentin and pregabalin) are used in the therapy of certain forms of epilepsy and are also effective in alleviating neuropathic pain. When chronically administered, they bind and inhibit the $\alpha_2\delta$ subunits, impairing their trafficking and decreasing synaptic neurotransmission [94]. Since $\alpha_2\delta$ proteins are mainly expressed in the hippocampus, cortex and amygdala, while nonexistent in the thalamus [95], gabapentinoids are not indicated in absence seizures localized in the thalamus [96]. The interaction between gabapentinoids and the $\alpha_2\delta-1$, $\alpha_2\delta-1$ and $\alpha_2\delta-2$ subunits is not yet completely understood, since they have weak activity in VGCCs or in the consequent release of neurotransmitters [97]. The currently proposed mechanism underlies the fact that the activity of N-methyl-D-aspartate (NMDA) receptors is increased by epileptic seizures [98] and the interaction of gabapentinoids with C-terminal $\alpha_2\delta-1$ promotes the normalization of NMDA receptors in the synaptic cleft, reducing their activity [96].

Broadly, VGCCs are classified into low (T-type) or high (L-type) threshold in accordance with the membrane potential at which they are activated.

The T-type calcium channels are predominantly expressed in the intrinsic thalamocortical relay neurons, playing a major role in the generation of the rhythmic 3-Hz spike-and-wave discharge characteristic of the generalized absence seizures [99, 100]. Activation of T-type VGCCs occurs at negative membrane potentials and shows a fast voltage-dependent inactivation with respect to other VGCCs contributing to the generation of pathological oscillations underlying spike-and-wave discharge. Owing to these properties, the three types of T channels (Cav3.1, Cav3.2, and Cav3.3) have demonstrated to be involved in the generation of repetitive firing in the thalamocortical network. Importantly, GABAergic neurons of the thalamic reticular

nucleus hyperpolarize thalamic relay neurons, which de-inactivate T-type calcium channels, allowing the channels to generate burst firing and the propagation of spike-and-wave discharge in the thalamocortical circuit, leading to absence seizures [96]. Corroborating the involvement of T-type VGCCs in absence seizures are human and preclinical trials, demonstrating that mutations at the T-type calcium channel gene are associated with and have been described in other epilepsy phenotypes [101]. Ethosuximide is the only drug that is indicated for the treatment of absence seizures, specifically because it inhibits all the three types of T-type VGCCs in the thalamocortical circuit [80, 96, 102]. It has been also proposed that zonisamide, besides acting on VGSC, also inhibits T-type VGCC as it is slightly effective in controlling absence seizures [103], as well as valproate [104].

Regarding high threshold calcium channels (L-type), they are subclassified by their pharmacological properties into N, P/Q and R channels, which are distributed throughout dendrites, cell bodies and nerve terminals. The N and P/Q (Cav2.1) type channels are the most important in regulating neurotransmission, however the former is prominently expressed in peripheral nerve terminals while the last is mainly expressed in CNS, particularly in Purkinje cells and cerebellum granule cells. P/Q type channels promote calcium influx and activation of α -amino-3-hydroxy-5-methyl-4-isoxazolepropionic acid (AMPA) receptors and therefore they are critically involved and with great influence on neuronal excitability and cerebellar plasticity. Interestingly, mutations in the Cav2.1 channel are associated with a predisposition to seizure disorders [101].

Potassium channels play an important role in the CNS, because their opening allows the efflux of potassium, causing a hyperpolarization by decreasing the positive intracellular charge and a generalized reduction in excitability. Retigabine, also named ezogabine, was the first AED developed as an activator of neuronal potassium channels, keeping them opened to stabilize neuronal membranes during repetitive firing [105]. However, it was recently withdrawn from the European market. Interestingly, mutations in the *KCNT1* gene that encodes the potassium channel have been identified in epileptic patients. In these cases, the antiarrhythmic quinidine

seems to be effective in inhibiting potassium channels as it is a partial KCNT1 antagonist [106].

(2) Increase of GABAergic activity

Besides reducing the probability of seizure occurrence by decreasing the capacity of neurons to fire action potentials at high rate to adjacent and distant brain sites, several AEDs also act as enhancers of GABA inhibitory activity. This strengthening of inhibition surrounding is attained by promoting GABA release to the synaptic cleft and its action on GABA_A receptors. AEDs have no effect on the GABA_B receptor that is coupled to the potassium pore [107].

The ionotropic GABA_A receptor is a Cys-loop-type ligand-gated chloride channels expressed in the post-synaptic [108] membrane of inhibitory synapses at the proportion of 1:4. This means that only about one in five cortical neurons is GABAergic. Nevertheless, their function is essential for the control of the firing rate and timing of excitatory neurons, restraining the generation of abnormal epileptic behavior [109].

Hence, to avoid the occurrence of seizure episodes, it is necessary to increase the concentration of the GABA neurotransmitter (**Figure I.4**). GABA cannot be administered, since it does not cross the BBB, requiring at least one of the following mechanisms: agonist effect on GABA_A receptors, inhibition of GABA transaminase that metabolizes the neurotransmitter in synaptic cleft or inhibition of GABA transporter 1 (GAT1) expressed in the pre-synaptic membrane [107]. Benzodiazepines act on the $\gamma 2$ subunit of GABA_A receptors as positive allosteric modulators, promoting GABA binding to the receptor and consequently increasing the chloride channel-opening frequency. Chloride influx into the postsynaptic neuron leads to cell hyperpolarization and increase of the membrane excitability threshold, conferring broad-spectrum anti-seizure action [110]. Benzodiazepines also affect $\alpha 3$ -containing GABA_A receptors expressed in the thalamic reticular nucleus,

desynchronizing the thalamocortical oscillations underlying generalized spike-and-wave discharge in absence seizures [111].

Barbiturates are also positive allosteric modulators at low doses but they can act as GABA agonists at higher doses, directly activating GABA_A receptors without the presence of the neurotransmitter [112]. In opposition to benzodiazepines, barbiturates such as phenobarbital increase the opening time of the chloride channel and are not indicated in absence seizures because they are not specific for $\alpha 3$ -containing GABA_A receptors. Nevertheless, they are also involved in the modulation of sodium and calcium channels [80]. Topiramate preferentially modulates a specific subset of GABA_A receptor which may contribute to its wide spectrum activity [80, 113].

The AED tiagabine increases GABA activity through the inhibition of a transporter that uptakes GABA into the neurons and glial cells, GAT1 (encoded by *SLC6A1* gene and mainly expressed in forebrain). Therefore, tiagabine suppresses the translocation of extracellular GABA into the intracellular compartment, rising extracellular neurotransmitter levels that will lead to the activation of extrasynaptic GABA receptors. On the other hand, vigabatrin inhibits GABA transaminase, which is responsible for GABA conversion into succinic semi-aldehyde and glutamate. Similarly to tiagabine, vigabatrin will also increase the concentration of the neurotransmitter in the synaptic cleft, promoting its inhibitory action [114].

(3) Decrease of glutamatergic activity

Glutamate is the main excitatory neurotransmitter and 80-90 % of neuronal synapses are excitatory. Between the presynaptic terminal of an excitatory neuron and a dendritic spine of the postsynaptic neuron, glutamate is released and diffuses from the synaptic cleft to interact with ionotropic or metabotropic glutamate receptors. Ionotropic glutamate receptors include AMPA receptors and kainate receptors. Both mediate a fast depolarization named excitatory postsynaptic potential that occurs within milliseconds. On the other hand, N-methyl-D-aspartate (NMDA) receptors are metabotropic and, even though they were expected to

contribute to epileptiform activity, their blockade is not sufficient to abolish epileptiform discharges and they are not validated as a therapeutic target for epilepsy. Notwithstanding, felbamate seems to inhibit the NMDA receptor, but its antiepileptic activity is mainly ascribed to its agonist effect on GABA_A receptor. However, genomic studies identified a mutation of the *GRIN2A* gene that encodes the NMDA receptor. In these circumstances, memantine can reduce the number of epileptic seizures, since it decreases the chronic over-stimulation of the NMDA receptor [106].

AMPA receptors, in opposition to kainate and NMDA receptors [115], are well-known for their direct involvement in epilepsy. AMPA receptor blockade avoids epileptic synchronization and it is the therapeutic target of perampanel [116], which is the only AED currently available as selective and non-competitive antagonist of the post-synaptic glutamatergic AMPA inotropic receptor (**Figure I.4**). Perampanel, approved as adjuvant treatment of focal and generalized seizures in drug-resistant patients, is very potent, requiring low plasma and brain concentrations to be effective [117]. Recent non-clinical studies have shown that perampanel also modulates inflammatory epileptogenic processes [118]. Topiramate is also an antagonist of AMPA receptors, however only after prolonged exposure [119, 120].

(4) Modulation of neurotransmitter release by presynaptic action

The modulation of the release of neurotransmitters contained in vesicles inside presynaptic neurons is the target of some AEDs. Levetiracetam and its analogs do not have their mechanism of action fully understood. However, scientific reports evidence that their pharmacological target is the synaptic vesicle glycoprotein 2A (SV2A), even though at distinct degrees of selectivity (**Figure I.4**). SV2A is a membrane glycoprotein expressed in the secretory vesicles of neurons and, even though its physiological function is not yet described, it seems to regulate calcium-dependent exocytosis and neurotransmitter loading/retention in synaptic vesicles [121].

Importantly, knockout animals that do not express SV2A develop lethal seizure

phenotype, demonstrating that SV2A restrains seizure activity [80]. Studies performed with SV2A^{+/-} mice, which have one copy of SV2A disrupted by gene targeting, revealed that the anticonvulsant efficacy of levetiracetam was compromised, in opposition to valproate, which mechanism of action is not mediated by SV2A [122]. Indeed, levetiracetam interacts with SV2A in a subtle way, without changing its configuration or locking a specific configuration as it would be expected if it was an inhibitor. It has been proposed that levetiracetam had no effect on synaptic physiology with low frequency activation, but it reduces the synaptic release of glutamate and GABA during high-frequency activation [121]. This frequency dependence is compatible with levetiracetam selective seizure protection as it requires high-frequency activation for prolonged periods. Additional targets have been hypothesized for levetiracetam, such as ion channels or inhibition of neurotransmission through interaction with receptors [123].

In turn, brivaracetam has 15 to 30 times higher affinity to SV2A and greater potency when compared to levetiracetam [124, 125]. In addition, brivaracetam demonstrated more significant anticonvulsant and antiepileptogenic properties than levetiracetam. In fact, at high doses, brivaracetam was also effective in normal animals against seizure-induced by maximal electroshock and several chemoconvulsants, for which levetiracetam had no seizure protection [126, 127].

(5) Inhibition of the mTOR pathway

The mTOR is ubiquitously expressed in mammalian tissues and regulates cell proliferation, autophagy and apoptosis by participating in multiple signaling pathways. In the brain, mTORC1 and mTORC2 pathways regulate dendritic growth and morphology, synaptic transmission and plasticity, neurogenesis and neural network activity. This guarantees normal cortical brain development, as well as the maintenance of neuronal cells and neurotransmission across the lifespan. Genetic abnormalities at *TSC1* and *TSC2* genes have been associated to multiple pathophysiological mechanisms that may cause epilepsy, namely TSC and focal cortical dysplasia [128]. Moreover, hyperactivation of the mTOR pathway is implied

in clinical syndromes associated with cortical developmental malformations and drug-resistant epilepsy [129]. Importantly, neuronal mTOR hyperactivity levels correlate with the severity of epilepsy and associated neuropathology [128].

As a common pathway by which numerous sporadic and familial mutations cause epilepsy, mTOR is starting to represent a novel therapeutic target for anticonvulsant drugs, exhibiting a high potential as a disease-modifying epilepsy therapy. Scientific reports indicate that the inhibition of mTOR by rapamycin and analogues is an important therapeutic intervention, since seizure activity is reduced, prevented and/or delayed, suggesting promising antiepileptogenic effects [59, 61]. Moreover, clinical studies demonstrated that the mTOR inhibitors, everolimus and sirolimus, have anti-seizure effects in patients with TSC and other epilepsies caused by mTOR dysregulation [129, 130].

(6) Cannabinoids

Very recently, the Food and Drug Administration (FDA) approved cannabidiol for the treatment of seizures associated with encephalopathies, such as Dravet syndrome and Lennox-Gastaut syndrome, in patients 2 years of age and older, based on results from adjuvant therapy placebo-controlled trials [131, 132]. Preliminary data from another recently completed placebo-controlled trial indicate that cannabidiol is also effective in the adjuvant therapy of seizures associated with TSC [133].

In spite of its wide spectrum of action, cannabidiol is not very potent, requiring high doses to achieve the desired effect [15, 134]. Interestingly, cannabidiol and other cannabinoids do not seem to interact with cannabinoid receptors (cannabinoid 1 and 2), despite the structural similarity confirmed by several preclinical trials. These facts prompted researchers to decode cannabidiol mechanism of action and, hence potential targets underlying epilepsy. Some hypotheses have already been proposed [135]. Accordingly, cannabidiol is neuroprotective, antioxidant and anti-inflammatory [136], as well as an agonist of transient receptor potential channels,

which are involved in the mediation of pain, temperature regulation and vision [137]. Cannabinoids are also agonists of serotonergic receptors and inhibit the reuptake of adenosine in VGSC and potassium channels [138]. The cannabinoids have considerable antagonistic effect it is on G protein-coupled receptor 55, expressed in excitatory and inhibitory synapses, modulating excitability and synaptic plasticity underlying ictogenesis and epileptogenesis [139, 140].

Despite the several reports suggesting the wide spectrum of efficacy against distinct seizure types and syndromes, current data only proved the clinical benefit of cannabidiol against tonic-clonic, tonic, clonic, and atonic seizures in patients with Dravet syndrome, and drop seizures in patients with Lennox-Gastaut syndrome [133]. Presently, the use of cannabidiol in the management of other seizure types should be considered investigational. Importantly, cannabidiol has revealed to be safe to be administered with AEDs that are first-line in the aforementioned syndromes, however its co-administration with valproic acid is not advisable due to the risk of transaminase elevations [133]. Today, well-designed studies are required to investigate potential predictors of therapeutic response, risk factors for adverse effects, DDIs, and the long-term overall safety of cannabinoids.

Bearing the aforementioned mechanisms of action in mind, it becomes evident that several AEDs exhibit a multi-target mechanism of action, which may contribute to widespread therapeutic indications. For instance, valproate is effective in several seizure types probably because it is a VGSC and T-type VGCC blocker and it increases synaptic or extrasynaptic GABA turnover [141, 142]. Felbamate inhibits NMDA receptor and it is a GABA_A agonist, thus acting on the imbalance of the main neurotransmitters underlying ictogenesis [143]. The broad spectrum of action of topiramate mainly results from its activity as a sodium channels blocker and GABA_A receptor agonist, even though it has also been ascribed as a AMPA antagonist [80].

I.2.2. PHARMACORESISTANT EPILEPSY

The high expectations regarding the marketed panoply of AEDs with increasing efficiency were suppressed by their clinical failure even when adequately prescribed. In fact, 30-40 % of patients do not respond to AEDs, developing pharmacoresistant epilepsy, also named “refractory epilepsy”, “drug-resistant epilepsy” or “intractable epilepsy” [60]. According to the ILAE, drug-resistant epilepsy is defined as “as failure of adequate trials of two tolerated and appropriately chosen and used AED schedules (whether as monotherapies or in combination) to achieve sustained seizure freedom” [144]. The progression of an epileptic disease should be considered a dynamic but not constant process [145]. This means that the identification of an epileptic patient as pharmacoresistant is only valid at the time of its assessment, and this situation can be changed further by the AEDs, demonstrating that a given treatment was not effective at any given time due to the pathophysiology of the underlying disorder [146]. However, it is recognized that the probability of success of alternative AEDs, after a therapeutic regimen with two AEDs, is reduced [147, 148]. Indeed, after developing resistance to a first AED, the probability of success with another AED in monotherapy is only about 10 %, albeit with a different mechanism of action [144].

Before the diagnosis of drug-resistant epilepsy, DDIs must be questioned, either by co-administration with other AEDs or other pharmacotherapeutic classes, because these patients generally suffer from multiple pathologies. The lack of compliance to therapy is another cause for the development of false drug resistance phenotypes [7].

Inter-individual variability is significant for several AEDs and influences treatment response, which may be sub-therapeutic or toxic. This contributes to an increase of mortality and morbidity (e.g. high risk of cognitive impairment, personal injury), and reduces the quality of life, with a parallel negative impact for health systems [89]. Therefore, the early identification of the underlying causes of drug resistance is essential to prevent the chronic manifestation of this highly complex disease. A few therapies can be considered for the refractory population, such as surgery or stimulation of the *vagus* nerve [149], but a vast number of patients are not eligible

for the previous interventions [63]. Under these circumstances, commercially available drugs with a wide therapeutic spectrum have proved to be useful [78].

The limited effectiveness of AEDs has been the focus of continuous research in order to understand the mechanisms underlying drug resistance and refractory epilepsy. This will be the basis of the implementation of new therapeutic strategies and/or development of molecules that not only increase drug efficacy in seizure control, but also treat and prevent the progress of epileptogenesis. Therapy failure involves complex and multifactorial mechanisms for which several hypotheses have been suggested: (1) the *target hypothesis*; (2) the *transporter hypothesis*; (3) the *pharmacokinetic hypothesis*; (4) the *neural network hypothesis*; (5) the *intrinsic severity hypothesis*; (6) and the *genetic hypothesis* [150].

With more than two decades, the target and transporter hypotheses are the prevailing and better scientifically supported theories [151]. The *target hypothesis* proposes that pharmaco-resistant epilepsy is due to structural, functional and biochemical changes that occur in the target-sites of AEDs, with consequent loss of drug affinity and effectiveness. For instance, alterations in function and configuration of VGSCs and GABA_A receptor were identified in animal models and refractory patients, supporting the loss of carbamazepine and benzodiazepine sensitivity to VGSCs and GABA_A receptor, respectively [152]. However, the multiple targets of AEDs compromise this hypothesis because alterations in all targets are unlikely to occur. On the other hand, the *transporter theory* postulates that ATP-binding cassette (ABC) efflux proteins, namely P-glycoprotein (P-gp, encoded by *ABCB1*) and multidrug resistance-associated proteins (MRPs), are overexpressed at the BBB, particularly at the endothelial cells and astrocytes of refractory epileptic patients compared to those who are seizure-free [153–155]. Histopathological analysis of brain tissue samples, collected during surgical intervention to remove the epileptogenic focus, revealed an overexpression of *ABCB1* gene in epileptic patients [156]. Several studies corroborate this discovery [150], however, in light of current knowledge, it is not possible to infer whether the greater *ABCB1* gene expression is intrinsic to the pathology (constitutive) and/or if it is acquired as a consequence of neural neurodegeneration caused by seizures (induced) [157]. Moreover, research results

are contradictory. On one hand, an overexpression of *ABCB1* in epileptogenic tissue was found, together with normal P-gp levels in tissue samples collected from the same patient [158]. On the other hand, P-gp overexpression in brain endothelium and glia has also been found in refractory patients comparatively to patients responsive to therapy [159].

Since several AEDs are substrates of ABC transporters, their access to the biophase is limited and drug concentrations in the brain may not attain the minimal effective level required for development of an anticonvulsant effect. This is strongly connected with the *pharmacokinetics hypothesis*, because ABC transporters are also overexpressed in peripheral blood vessels of patients with refractory epilepsy, as well as in other tissues such as small intestine [160]. This may compromise the systemic biodisposition of the AED and its brain concentration. Some examples of AEDs that are P-gp substrates include phenytoin, topiramate, carbamazepine, phenobarbital, lamotrigine, felbamate and gabapentin [161]. Nonetheless, there are AEDs that are not P-gp substrates, such as brivaracetam [162] and perampanel [163], and, hence, other mechanisms must be involved in their pharmacoresistance [150]. For instance, the Breast Cancer Resistance Protein (BCRP) is an ABC transporter that was more recently discovered and it is also expressed in BBB and overexpressed in epileptic brain [155]. However, few information exists regarding the AEDs that are BCRP substrates and therefore this was one of the focuses of the present thesis.

In addition, *neuronal network hypothesis* has been outlined. Under the influence of genes and microenvironment, the recurrent episodes of excessive neuronal activity that characterizes epilepsy can induce alterations in brain plasticity, neuronal degeneration, necrosis, gliosis, synaptic reorganization and remodeling of the neuronal network [164]. At this point, it is noteworthy that the neuronal network is not only altered in pharmacoresistant epilepsy but also in other pathologies that are treated with AEDs. Therefore, it is questionable whether there are intrinsic molecular or genetic mechanisms involved in plastic alterations that generate pharmacoresistant epilepsy in some patients, while others can achieve disease control with medication. The *intrinsic severity* and *genetic hypotheses* tried to answer these questions. The former states that pharmacoresistance is an inherent property

of epilepsy related to its severity and high seizure frequency before onset of AED therapy. This is the single most important factor associated with a low chance of attaining seizure remission with AEDs [116]. Complementarily, the *genetic hypothesis* is gaining force because several genetic mutations have been identified in pharmacodynamic and pharmacokinetic targets of the AEDs and in patients considered pharmacologically resistant to treatment [89]. Variations in the number of gene copies, characterized by recurrent microdeletions and microduplications, have been associated with drug resistance in epileptic patients and other neurodevelopmental and psychiatric disorders [165–167]. For instance, mutations in the *GLUT1* gene that encodes glucose transporter 1 (Glut1), responsible for the transport of glucose through the BBB, disturbs the functional activity of the CNS. This manifests itself phenotypically due to the conditioned access of the necessary energy source to the brain, causing disturbances in the CNS. The identification of this mutation allows treatment establishment, the control of epileptic seizures and the obtainment of alternative sources of energy to the brain such as the ketogenic diet [168]. On the other hand, the *genetic hypothesis* is supported by the several mutations/polymorphisms that alter the expression of ABC transporters and cytochrome P450 (CYP) enzymes, compromising drug concentrations in plasma and brain, and consequently therapeutic and toxic effects [150, 169–173].

I.3. NOVEL PHARMACOLOGICAL STRATEGIES AGAINST EPILEPSY

Pharmacological therapy is indispensable for the control of epileptic conditions. Even after surgical procedures to remove the epileptic focus, anticonvulsant treatment requires continuity to prevent relapses [174, 175]. Notable pharmacological advances have been made, with more than twenty AEDs currently available for clinical use. Nevertheless, their performance is still unsatisfactory, mainly because they consist of a symptomatic treatment with ineffectiveness in a considerable number of epileptic patients. In addition, AEDs have limited safety features, conditioned tolerability and clinically relevant DDIs, which demonstrate the emerging need to develop new molecules, validate new therapeutic targets or adopt strategies that improve the safety profile and decrease the rates of prevalence of refractory epilepsy [176].

In view of these facts, the expanded knowledge regarding epileptogenic, ictogenic and pharmacoresistant mechanisms is contributing to the development of new pharmacological strategies for epilepsy (**Figure I.5**). On one hand, the drugs may act on novel pharmacological targets that may underlie epileptogenesis, neuroinflammation and the neuroimmunological state. On the other hand, new pharmacological strategies can be developed/optimized to increase the cerebral exposure of AEDs in detriment of systemic exposure, thereby promoting drug effectiveness and reducing their side effects [177].

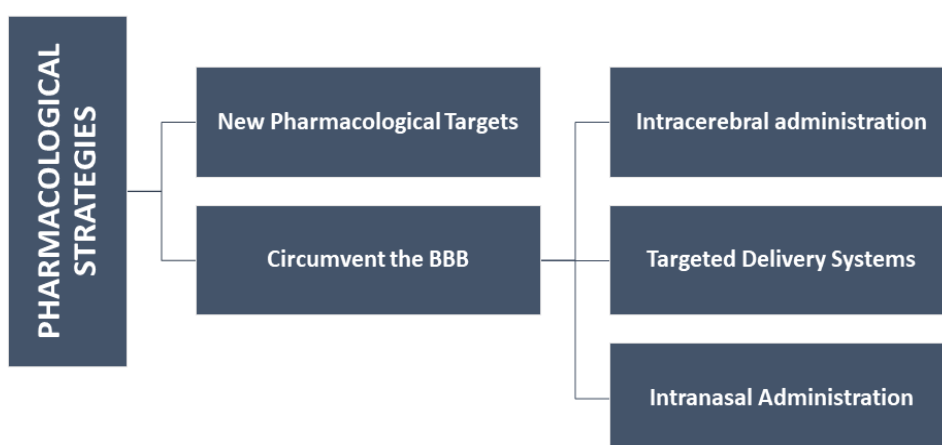


Figure I.5 New pharmacological strategies for epilepsy.

I.3.1. NEW PHARMACOLOGICAL TARGETS

Up to now, several Research and Development (R&D) programs of AEDs consisted on modifying the currently marketed AEDs to obtain new structurally-related compounds with the same mechanism of action of the original drug but optimized pharmacokinetics and clinical features [178]. For instance, carbamazepine, a 1st generation AED is the progenitor of oxcarbazepine (2nd generation), which in turn prompted the development of eslicarbazepine acetate (3rd generation). All are commercially available but the 2nd and 3rd generations are safer and have a CYP-independent metabolism that decreases their potential to develop DDIs [179]. Pregabalin, with wide application in neuropathic pain, is a derivative of gabapentin [180], while brivaracetam is a derivative of levetiracetam [181]. This rational is very attractive and useful, since it begins with a molecular structure with known pharmacological effect and to which changes in functional groups are introduced, maintaining the mechanism of action but optimizing less favorable characteristics of the original AED. Alternatively, the advances of combinatorial chemistry and the well-known structure of the targets, have promoted the rational and successful development of new molecules with different structures.

However, both R&D designs have two major drawbacks: the molecules are not being designed against epileptogenesis and are ineffective in refractory epilepsy. Still, it is interesting to highlight that levetiracetam revealed antiepileptogenic effects in a pilot phase II study in patients with traumatic brain injury at high risk of developing post-traumatic epilepsy [182]. The dose of 55 mg/kg/day administered up to 8 h after the occurrence of the traumatic injury during 30 days prevented the evolution of the clinical condition to convulsive episodes, triggered by epileptogenic processes. The dose was well-tolerated and considered safe, but more studies must be developed to support this hypothesis [183]. Similarly, eslicarbazepine acetate also showed antiepileptogenic activity. Its mechanism of action is essentially based on the inhibition of slow T-type calcium channels, apparently essential mediators in epileptogenesis. Doeser *et al.* demonstrated that the administration of 150 mg/kg of eslicarbazepine acetate to mice decreased neural loss. There was a prolonged

anticonvulsive protective effect up to 8 weeks after treatment with 150 and 300 mg/kg with eslicarbazepine acetate for 6 weeks [184]. More recently, a pilot study described the anti-epileptogenic and neuroprotective effect of lacosamide [68]. Mossy fiber sprouting and neural loss are considered relevant characteristics in the epileptogenic process and they are directly related to the recurrence of spontaneous seizures. Although this mechanism is a mystery to science, it is believed to be associated with the CRMP2. This cytosolic protein, involved in axonal growth and neural polarity, is highly expressed in the developing CNS. This function is provided by the phosphorylation state of CRMP2, mediated by several protein kinases, namely glycogen synthase kinase-3 β , inactivated after epileptic seizures, and a probable decrease in phosphorylated GSK3 β CRMP2, with consequent uncontrolled axonal growth [185–188]. Inhibition of lacosamide on CRMP2-mediated neurite growth, increased levels of phosphorylated GSK3 β CRMP2, and imposes an anti-epileptogenic effect, by reducing the mossy fiber sprouting and neural loss, in addition to suppressing recurrent spontaneous seizures. Thus, lacosamide may be a prophylactic alternative to epilepsy, with a neuroprotective effect and anticonvulsive efficacy [68].

The high attrition rate of R&D programs of AEDs has also been associated to the animal models applied for drug screening. Until the discovery of levetiracetam, maximal electroshock seizure (MES) and pentylenetetrazole (PTZ) models were used. Levetiracetam did not protect the animals in these models, but protected mice against 6-Hz seizure model. These findings made the 6-Hz mice model mandatory during the identification of new compounds with antiepileptic activity [189]. The heterogeneity of the observed clinical response is apparently a demotivating factor for investment by the pharmaceutical industry, since it is only intended for a limited number of patients and/or for very specific epileptic conditions, called orphan diseases. Even so, several molecules are currently under clinical investigation (**Table I.4**). The majority of the compounds are repurposed drugs, while only two have novel targets, i.e. beprodone and huperzine A, which are an agonist of melatonin type 3 receptor and an inhibitor of acetylcholinesterase, respectively [177].

Notwithstanding, it should be mentioned that oxidative stress and mitochondrial dysfunction also seem to contribute to refractoriness through the generation of

reactive oxygen species (ROS) and reactive nitrogen species, which cause cellular damage. Oxidative stress parameters were determined in the plasma of epileptic patients. Plasma concentrations of vitamin A, C and E (antioxidant agents) were higher in the control group, whereas lipid peroxidation was more accentuated in the plasma of epileptic patients. Phenobarbital improves the antioxidant levels of the patients, suggesting the implication of free radicals in epilepsy [190]. These mechanisms can become new targets and antioxidants are expected to be useful if administered in epilepsy. For instance, resveratrol, melatonin, tocopherol (vitamin E), selenium and allopurinol revealed to decrease levels of ROS preventing oxidative cell damage. In addition, it is known that the immune system plays a fundamental role in the development of epileptogenic foci, as well as neurodegeneration and inflammation. Neuroinflammation results from the activation of microglia, astrocytes, brain endothelial cells and peripheral immune cells; therefore, all can be ascribed as therapeutic targets for epilepsy [191]. Indeed, anti-inflammatory treatments, such as steroids, exhibited anticonvulsant activity, including in some drug-resistant epilepsy syndromes. Immunosuppressant drugs have also been considered to be used in epilepsy [192].

Table I.4 Compounds under clinical investigation for therapeutic application in epileptic disorders.

	Compound	Mechanism of action	Phase of development	References
Mechanisms of action similar to those of marketed AEDs	Ganaxolone	GABA receptor modulator	Phase I and II	[193]
	Selurampanel (BGG492)	Competitive antagonist for AMPA and kainate receptors	Phase II	[194]
	ICA-105665	Selective opener of neuronal Kv7 potassium channels	Phase II	[195]
	YKP3089 (cenobamate)	Selective blocker for the inactivated state of the sodium channel, facilitates presynaptic GABA release	Phase II and III	[196]
Novel mechanisms of action	Beprodone	Agonist of the melatonin type 3 receptor	Phase II	[197]
	Huperzine A	Inhibitor of AChE	Phase I	[197]
Repurposed compounds which were initially developed for the treatment of other diseases	Everolimus	Selective inhibitor of mTOR pathway	Phase III	[198]
	Fenfluramine	Serotonin reuptake inhibitor	Phase III	[196]
	Nalutozan	Nonazapirone 5-HT _{1A} partial agonist	Phase II	[199]
	Pitolisant	Histamine 3 receptor antagonist	Phase II	[197]
	Quinidine	Partial antagonist of KCNT1	—	[200]
	Valnoctamide	GABA _A receptor agonist	Phase II	[201]
Unknown mechanisms of action	JNJ-26489112	Multiple, unknown	Phase II	[202]
	Cannabidiol	Multiple, unknown (Agonist of Melatonin 3 receptor is a known mechanism)	Phase I, II and III	[203]

AChE, *acetylcholinesterase*

I.3.2. CIRCUMVENT THE BLOOD-BRAIN BARRIER

The BBB is a highly dynamic biological interface between the blood and the brain parenchyma. It restricts the entry of pathogens, toxic chemicals, and xenobiotics (including drugs) into neuronal tissue, in order to maintain its integrity. The dynamic but restrictive nature of the BBB has been a major challenge for drug delivery into neuronal tissue for the management of epilepsy and avoidance of refractoriness. As already explained, the *transporter hypothesis* claims that the expression of ABC efflux proteins increases as the disease advances, enhancing the impermeability of the BBB and consequently hampering drug access into the brain [204].

Therefore, the optimization of delivery systems of the marketed AEDs and the use of alternative routes of administration that do not require the passage through the BBB can be promising strategies. Alternative administration routes that make use of drug transport mechanisms independent of BBB passage are expected to avoid efflux proteins that are overexpressed in intestine and BBB and to attain a faster onset of action. This type of research, named as New Drug Application, has a high potential of success and it is faster and less expensive compared to the synthesis of new compounds, namely from a regulatory point of view [205].

Currently, the chronic treatment of epilepsy is achieved through oral drug administration, making use of a wide variety of formulations prescribed in accordance with the characteristics of each patient. For instance, solutions and suspensions are very useful in pediatrics and patients with dysphagia [206]. Prolonged-release capsules are preferred to immediate-release tablets, as dosing regimens are simplified and plasma drug fluctuations decrease. Furthermore, these formulations promote adherence to therapy. It is noteworthy that the same drug can be available in several formulations, which does not necessarily imply bioequivalence, since each pharmaceutical form presents its own incorporation, disposition and posology [207]. For instance, valproate in prolonged-release capsules, administered 1 or 2 times a day, is equivalent to 2 to 4 administrations of syrup or other form of immediate release [208]. Oral route is the route of choice for AED administration, due to the possibility of self-administration and to the ease of production of solid formulations with long life

and sustained delivery [209]. Nevertheless, several factors can compromise and/or alter drug bioavailability, such as intestinal absorption, which can be modified by enterogastric motility, intestinal pH, gastric emptying and DDIs, and also hepatic first-pass effect [210]. Importantly, this route cannot be used in emerging situations since the lag time is at least 1 h and steady-state must be attained [206]. In this situation, the intravenous (IV) route is preferable. Brivaracetam, levetiracetam, lacosamide, valproic acid, phenytoin, lorazepam, diazepam and phenobarbital are currently available as IV formulations, while others (lamotrigine, carbamazepine and topiramate) are under investigation/development. Although lacosamide has extensive intestinal absorption and bioavailability close to 100 %, it takes 0.5-4 h to reach the maximum plasma concentration, so parental route seems to be, currently, the most viable option for seizures [211]. With oral availability greater than 90 %, zonisamide has a favorable intestinal absorption, but also some drawbacks such as extensive hepatic metabolism and DDI [212]. In spite of the almost immediate onset of action and a bioavailability of 100 % when intravenously administered [213], the reality is that seizures mainly occur in ambulatory, outside medical facilities, where IV access, which implies a qualified professional, is not available [214]. In addition, in refractory patients, drug concentrations in the brain are conditioned by efflux transporters expressed in the BBB, and hence the IV route may not be the ideal solution [215].

In this context, the interest of exploring new alternative routes of administration gains relevance particularly if the BBB can be circumvented [214]. Additionally, it is important to minimize inter and intra-individual variability [216]. Several routes of administration have been tested (**Table I.5**), however the majority require the drug passage through the BBB, not allowing its direct delivery into the brain. Intracerebral and interventricular administrations have been successful, through targeted pharmacological suppression, with preservation of cellular and vascular structures. However, these techniques are invasive and their applicability to daily administration is impracticable [217]. At this point, intranasal (IN) route arises as a new hope for the administration of AEDs due to its non-invasive nose-to-brain delivery [218].

Table I.5 Advantages, limitations and examples of formulations available for antiepileptic drugs (AEDs) administration.

Delivery Route	Advantages	Limitations	AEDs Formulations	Ref.
Oral	Convenient Practical Painless Allows self-administration Ease of production: solid formulations with long life and modified delivery	Floating bioavailability Erratic and complex absorption First pass effect Heterogeneous response according to genetic factors Delay in the start of the action Requires patient cooperation is not suitable for emergencies	Carbamazepine: Suspension, syrup, tablet, chewable, tablet, SR, tablet, ER tablet, ER capsule Gabapentin: Solution, tablet, capsule Lacosamide: Solution, tablet Zonisamide: Capsules	[206, 210]
Intravenous	Ideal in acute situations Broad spectrum of action Rapid effect Secure administration Low inter and intra-individual variability Pediatric and geriatric application Precise dosing High bioavailability (100 %)	Sterile preparation is dispensable Eligible physical and chemical characteristics of molecules Harmonization in physiologically compatible vehicles Qualified professional for administration Efflux by proteins expressed in BBB Painful Invasive	Sterile Preparation: Diazepam Levetiracetam Midazolam Lorazepam Clonazepam Lacosamide Phenobarbital Valproate Phenytoin	[213–216, 219, 220]
Buccal/ Sublingual	Considerable volume management High vascularity and rapid absorption High surface area for absorption Not subject to first pass effect	Patient collaboration (not possible during a seizure) Swallowing part of the formulation	IV solution: Midazolam	[221, 222]
Intramuscular	Safe and effective Rapid administration	Slow and variable absorption rate Risk of erroneous injection Adjusting the needle to the patient's characteristics Local reaction	Sterile Preparation: Diazepam Levetiracetam Midazolam Lorazepam	[223–227]

		Absorption is influenced by the degree of vascularization of the injection site Painful Invasive		
Rectal	Convenient in the pediatric population Rapid onset of application in the correct location Applicable in emergencies	Uncomfortable and invasive in older children and adults Erratic absorption Difficulty predicting absorption site	Suppository: Diazepam	[206, 213]
Intrapulmonary	Quick onset of action High surface area	Difficult to predict the absorbed drug quantity Characteristics of aerosol drug particles Quality control tests for particles Deposition of particles in the mouth and gastrointestinal tract	—	[228, 229]
Intranasal	Quick onset of action Prevents first-pass metabolism Convenient Practical Non-invasive Useful for chronic treatment and seizures Self-administration	Low mean residence time Mucociliary clearance Enzymatic degradation Low volume to be instilled Administration head position	Nasal spray: Midazolam	[230, 231]
Subcutaneous Transdermal	Convenient for sick Large surface area for absorption Extended release Systemic effect	Systemic effect	—	[214]

With the expectation of circumvent, at least in part, systemic drug passage through the BBB and its efflux transporters, the IN administration route was herein selected to administer the AEDs under investigation. Since BCRP is involved in drug resistant epilepsy, avoiding this transporter can also be a promising strategy. Notwithstanding, little is known about the interaction of AEDs and BCRP and whether the IN route can decrease the impact of this ABC efflux transporter in nasal drug pharmacokinetics. **Sections I.4** and **I.5** will focus on the IN administration route and BCRP, which will be herein exploited as a combined strategy to increase the brain exposure of lacosamide, levetiracetam and zonisamide.

I.4. INTRANASAL ADMINISTRATION & NOSE-TO-BRAIN DRUG DELIVERY

As aforementioned, there is an extensive variety of administration routes, among which the oral one stands out for systemic effects, especially due to its good compliance and ease of self-administration. Nevertheless, delivery of drugs to the brain in sufficient quantities to achieve therapeutic levels is required for the treatment of epilepsy, implying the passage through intestinal membrane and the BBB. IV administration attains the therapeutic effect in a shorter period since absorption does not occur and the first pass mechanisms are negligible. However, it is health-professional dependent and invasive method with conditioned applicability [232].

In this context, efforts were herein made in order to investigate whether the IN administration of lacosamide, levetiracetam and zonisamide directly deliver the drug into the brain, overpassing the BBB and the BCRP efflux transporters therein expressed. In 1989, W. H. Frey II targeted insulin or insulin-like growth factor into the brain after IN delivery [233], as well as other high molecular weight substances such as proteins, and peptide. Nasal administration is suitable for lipophilic and hydrophilic molecules, since several transport mechanisms can be used [234]. However, it is known that the nasal epithelium is less permeable to polar substances, requiring the addition of permeation enhancers, which sometimes may cause mucosal irritation when they are in excess in the formulation [230].

The nasal cavity, namely olfactory epithelium, is recognized as a promising region for direct brain drug delivery as it allows the unique contact between the external environment and the brain. The anatomical location, histological constitution and physiological mechanisms inherent to the respiratory and olfactory mucosa give to nasal cavity a versatility to attain drug systemic or central pharmacological effects. This has been an area of increasing exploration for the development of pharmacological treatments for neurological, psychiatric and neurodegenerative diseases [218, 235].

I.4.1. ANATOMY AND HISTOLOGY OF THE NASAL CAVITY

The delivery of drugs from the nasal cavity has high potential due to its unique morphological and physiological characteristics.

Human nose is the organ responsible for the smell and exchange of air between the organism and the outside environment. It is a prominent structure on the face, separated from the oral cavity by the palatal bone and symmetrically divided into two cavities by the cartilaginous and partially bony nasal septum. Each cavity has a surface area of approximately 75 cm² and a volume of approximately 7.5 mL. The nasal cavity extends from the nostrils to the nasopharynx and can be broken down into three regions: nasal vestibule, respiratory and olfactory regions (**Figure I.6**) [236].

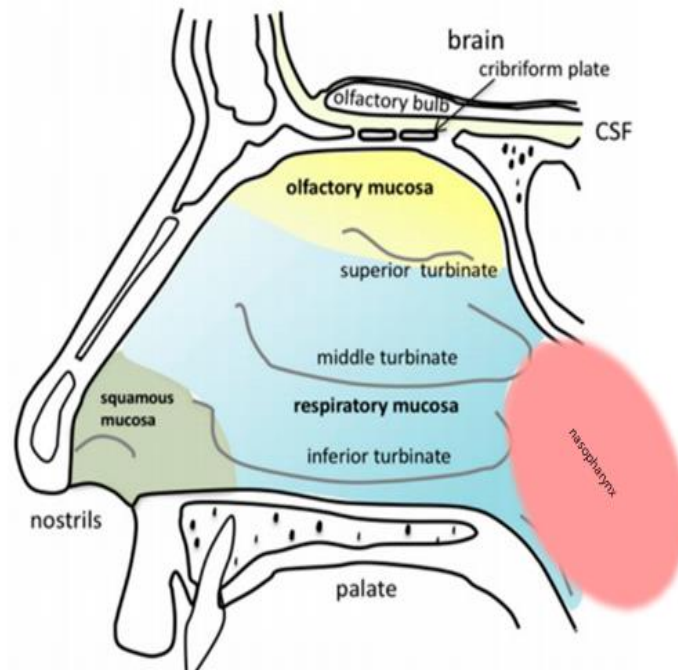


Figure 1.6 Schematic representation of the anatomy of the human nasal cavity. Scaly mucosa characterized by green outline. Lower, middle and upper turbinates are characterized by blue. Blue region depicts the nasal mucosa. The region outlined in yellow symbolizes the olfactory region (Adapted from [237]). CSF, cerebrospinal fluid.

The nasal vestibule occupies the most anterior position of the nasal cavity and opens in the face through the nostrils. The anterior portion is histologically similar to the skin, consisting of squamous and keratinized stratified epithelium, with hair follicles, sweat and sebaceous ganglia. This is the first defensive barrier against external agents. It has a surface area of only 0.6 cm^2 with little vascularization, where the absorption of local substances is irrelevant [238].

The respiratory region respects the lateral coverage of the nasal cavities, and it is differentiated into three turbinates or conchae, named as inferior, middle and superior turbinates; all together they have the important functions of filtering, humidifying and heating the inhaled air. Respiratory mucosa is constituted of a pseudo-stratified columnar epithelium that lies on basement membrane and *lamina propria*. The principal cell types of respiratory mucosa include the goblet cells that are responsible for nasal mucus secretion; the basal cells that maintain the cells together and guarantee the individual cell replacement; and the ciliated and non-ciliated columnar cells that are covered by numerous microvilli which considerably increase the

respiratory mucosa surface area to approximately 130 cm² [239, 240]. The ciliated columnar cells also display cytoplasmic mobile projections named cilia, which are essential to propel the mucus from nasal cavity to nasopharynx. Its high surface area, combined with its high vascularity, makes respiratory mucosa the major site for drug systemic absorption. Under these conditions, drugs administered by IN route are not subject to a hepatic first-pass effect, as, once absorbed into the bloodstream, they are directly sent to the superior vena cava, via the subclavian vein and the internal jugular vein, through the ophthalmic, sphenopalatine and facial veins that surround the respiratory epithelium [241]. On the other hand, the innervation of the respiratory region is mainly performed by maxillary and ophthalmic branches of the trigeminal nerve. However, the respiratory mucosa is only innervated laterally by the maxillary neural extension at the dorsal level while the anterior portion is innervated by ophthalmic ramification of the trigeminal nerve [242]. The trigeminal nerve is extensively involved in the sensory and motor functions and have peripheral branches up to the mandible, maxilla and eyeball [242]. These three peripheral trigeminal branches concentrate at the trigeminal ganglion, forming a single incoming nerve that ends in the brainstem, pons and then to the rest of the hindbrain [243]. The portion of the trigeminal nerve that passes through the cribriform plate may also contribute to delivery of drug from the nasal mucosa to the forebrain [244]. These innervations have been associated with the direct transport of drugs from the nasal cavity to the CNS as it will be explored in **Section I.4.3** [245].

The olfactory mucosa is located in the upper portion of the nasal cavities, on the lower surface of the ethmoid bone. Its surface area is reduced and varies according to the species. In humans, olfactory epithelium represents 10 % of nasal epithelium, approximately 10 cm², while in rodents it can reach 50 % of the total area [246, 247]. Human olfactory mucosa is composed of a pseudostratified olfactory epithelium based on basement membrane and *lamina propria*. The epithelium consists of basal cells, which are capable of differentiating into specialized cells, supporting cells and olfactory receptor cells [234, 248]. The columnar supporting cells contact only with the basement membrane, projecting microvilli from their luminal surface. They surround the olfactory nerve cells and are responsible for their regeneration along life span.

Moreover, supporting cells express several CYP enzymes, constituting a protective mechanism with additional phagocytic function, and maintain the extracellular potassium levels required for neuronal activity [249].

The olfactory receptor cells are bipolar neurons that project single dendrites to the olfactory neuroepithelium and a single unmyelinated axon into the olfactory bulb. These axons gather together with other olfactory axons, cross the *lamina propria* and the cribriform plate to attain the olfactory bulb, where they synapse with mitral cells. These sets of nerves are named as *fila olfactoria* and are enclosed in glial cells that allows the transition of the axons from the olfactory epithelium directly to the brain. This constitutes a mechanism for direct transport to the brain of substances administered in the olfactory region [250].

I.4.2. NASAL PHYSIOLOGY

Nasal mucosa is the physical barrier of the nasal cavity that protects the lower respiratory tree and the brain against exogenous substances, including pathogens, particles, drugs and other xenobiotics. The nasal mucosa lines the respiratory epithelium of the nasal cavity, where 1.5-2 L of mucus are daily secreted by the goblet cells [251, 252]. Composed mostly of water, nasal mucous is rich in various proteins (mucin, albumin, immunoglobulins, lysozyme, lactoferrin), inorganic salts and lipids [253]. It entraps inhaled particles and foreign pathogens and is renewed every 15-20 minutes by ciliary beating mediated by the ciliated epithelial cells [254, 255]. The coordinated interaction of these components results in mucociliary clearance (MCC) that removes particles deposited in the nasal mucosa in the form of expectoration or along the nasopharynx to the gastrointestinal tract. Despite its evident and crucial physiological protective mechanism, MCC is responsible for the short residence time of nasal formulations, constituting an inherent limitation of IN route. To overcome this condition, several technological formulations have been developed to increase the residence of nasal formulations [256–258]. Importantly, nasal mucosa also expresses metabolic enzymes even though in less extent than other metabolic organs such as the

liver. Nonetheless, nasal metabolism (and first pass effect) should not be ignored, as it has already demonstrated to decrease the bioavailability of therapeutic agents instilled in the nasal cavity [249]. More susceptible molecules, such as proteins and peptides, are often cleaved, with consequent alteration of their structure and therapeutic effects [259, 260].

On the other hand, transporters have also been found in nasal cavity. Located in plasma membranes, influx and efflux transporters mediate the entry and exit of substances from the cells, respectively. Two main superfamilies of transmembrane proteins are distinguished: ATP-binding cassette (ABC) that pump out substances from the cells by an ATP-dependent mechanism, and the solute carrier (SLC) that control the transport of ions through efflux or influx mechanisms [261, 262]. Although the expression of transporters in the nasal cavity is not yet sufficiently explored, some studies have identified them in the apical membrane of ciliated cells and nasal epithelial cells [263]. P-gp, encoded by the *ABCB1* gene, was found in the human nasal respiratory epithelium, it is also expressed in the apical membrane of endothelial BBB cells, liver, intestine, kidney and placenta [264, 265]. However, *in vitro* studies with nasal human respiratory epithelium revealed that the levels of P-gp expression are substantially lower in relation to other tissues; for example, in the liver the levels of transporter are about 250 times higher [266]. P-gp expression at the level of the nasal epithelium and nasal mucosa suggests that IN administration of P-gp substrates may be subject to efflux mechanisms [236, 265, 267–269]. Indeed, some studies have evidenced a reduction of the transport of P-gp substrates to the brain after their IN delivery [270].

More recently, Al-Ghabeish *et al.* researched the expression of BCRP in nasal tissues collected from humans and various animal species, revealing its lower expression in humans than in rat, mouse and cow [271]. The microarray determination revealed low levels of *ABCG2* in the human nasal mucosa, with no evidence of reported expression, and therefore the results were not conclusive regarding the expression of BCRP. The MucilAir™ nasal model exhibits low expression of BCRP, contrary to what was observed for P-gp, a qualified and continuous expression, through proteomic

determination. Similar results were verified for the cell model Calu-3, of the lung parenchyma [272].

MRP transporters, encoded by the *ABCC* gene, are distinguished into 9 subtypes, ABCC 1-9. MRP1 is considered the most abundant MRP isoform expressed in the human nasal respiratory mucosa [253] and adult rat [274]. It is predominantly expressed in the apical membrane of the ciliated cells of the respiratory epithelium. Although to a lesser extent than MDR1, high levels of MRP3, MRP4, MRP5 and MRP10 were observed, while MRP6 was identified at moderate levels [257, 271].

I.4.3. NOSE-TO-BRAIN DRUG DELIVERY

Once administered in nasal cavity, and surviving to MCC and enzymatic degradation, drugs can attain the brain by means of two major transport types (**Figure I.7**): the *indirect vascular transport* that requires systemic absorption followed by BBB crossing and the *direct transport* that encompasses neuronal and olfactory epithelial pathways [275].

When deposition of drug formulations occurs in the most extended part of nasal mucosa (i.e., in the respiratory region), the drug can be systemically absorbed or reach the trigeminal nerve in high quantities. Through paracellular or transcellular mechanisms, drugs can cross respiratory epithelium, attaining the basement membrane and then the systemic circulation. Once there, the drug cross the BBB and reach the brain indirectly [234, 276]. Larger and electrically charged particles naturally have a greater resistance to crossing the mucus layer in opposition to the small neutral charged particles and, therefore, their transport can be hampered [259, 260].

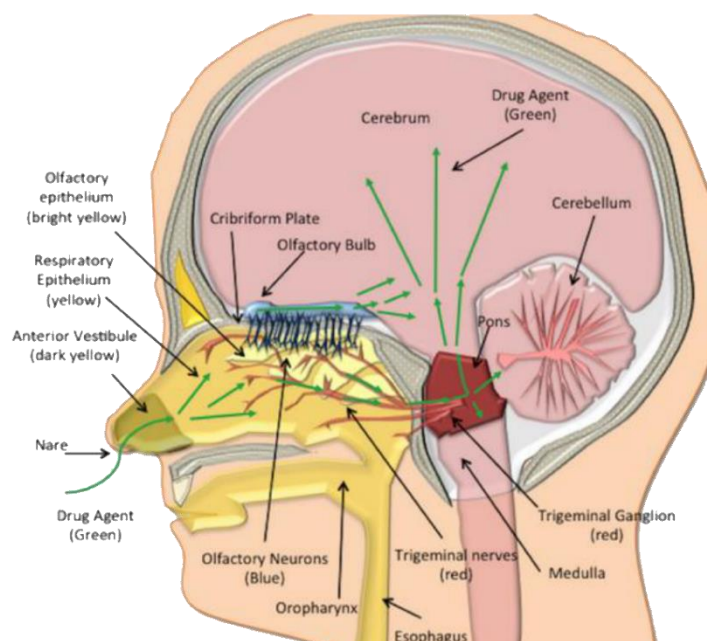


Figure I.7 Schematic representation of indirect and direct delivery of drugs to the brain after intranasal administration.

On the other hand, as explained in **Section I.4.1.**, the innervation of the respiratory region is mainly performed by the maxillary and ophthalmic branches of the trigeminal nerve which culminate in two different sites of the brain – near the pons and near the olfactory bulb – allowing drug delivery to both caudal and rostral brain areas. This bilateral entry of the trigeminal nerve into the brain addresses various regions such as thalamus, hypothalamus, amygdala, locus coeruleus, raphe nuclei, reticular activating system, limbic forebrain, anterior cingulate, and insula, enabling the wide distribution of the therapeutic compound [277]. Due to these anatomic characteristics, the involvement of trigeminal nerve in direct nose-to-brain drug delivery was questioned and, hence, demonstrated for the first time in 2004 [278]. After radiolabeled insulin IN administration to rats, the highest levels of radioactivity were found in trigeminal branches, ganglia and pons. Moreover insulin transport occurred extracellularly, along the trigeminal nerve [278]. Similar findings have been reported for other radiolabeled protein and peptides [279]. The direct trigeminal neuronal pathway has been ascribed as the responsible for the rapid cerebral distribution of drugs administered by IN route [230].

On the other hand, and despite its reduced dimension and difficult access, olfactory mucosa is the “window of the brain”. Therefore, if drug formulation attains the olfactory region of nasal cavity, direct nose-to-brain delivery may occur through the olfactory nerve or olfactory epithelium pathways, attaining the cerebrospinal fluid (CSF) and cerebral parenchyma [280]. Thus, upon reaching the olfactory epithelium, drugs interact with the olfactory nerve endings and move along the axons to the olfactory bulb and CSF, and later to the other parts of the brain [281–283]. The olfactory nerve pathway hypothesis suggests an axonal intracellular transport of substances. IN administration of radioactive rubidium and thallium clearly showed their direct transport via the olfactory nerve attaining firstly the olfactory bulb and then other brain regions [284]. This transport, although direct, is slow and it can take hours or days to be complete [275]. Therefore, this is not the transport mechanism responsible for reaching peak concentrations almost immediately or in a few minutes, as desired for AEDs. In opposition, olfactory epithelium pathway allows drugs transfer along the olfactory axon to the CSF, which is covered by the subarachnoid space, in less than 30 minutes [242]. This hypothesis involves the paracellular transport across epithelium and *lamina propria*, followed by diffusion through subarachnoid extensions that involve the olfactory nerves from the epithelial base to the brain. In spite of fast, olfactory epithelium transport has the drawback of delivering the drug into CSF, which is completely renewed every 5 hours, contributing to a quick elimination of the drug [285].

Due to the wide variety of mechanisms that contribute for brain delivery after IN administration, it becomes difficult to distinguish which one(s) is(are) responsible for the direct transport to the brain [237, 286]. Nonetheless, pharmacokinetic and biodistribution *in vivo* studies can accurately distinguish both indirect and direct transports.

I.5. RELEVANCE OF BREAST CANCER RESISTANCE PROTEIN TO BRAIN DISTRIBUTION AND CENTRAL-ACTING DRUGS

The BCRP (gene symbol *ABCG2*) was discovered in 1998 in a human breast carcinoma cell line, when it triggered multidrug resistance or reduced the intracellular accumulation of anticancer drugs like mitoxantrone, daunorubicin and doxorubicin. BCRP is a 72-kDa half-transporter, composed by 655 amino acids and six transmembrane segments, four potential glycosylation sites and one nucleotide-binding domain (NBD) [287]. It actively extrudes substrates against the concentration gradient using ATP hydrolysis as a source of energy. Hence, BCRP belongs to the ABC superfamily of efflux transporters [287], which is one of the best characterized and most ubiquitously expressed families of efflux transporters. For this superfamily 49 genes are known to encode different proteins, classified into 7 subclasses (ABCA to ABCG) according to their functionalities and characteristics [288]. For these reasons, the Human Gene Nomenclature Committee renamed the protein *ABCG2* because it was the second protein discovered in the ABC superfamily subgroup G [289].

This section reviews the structure and localization of BCRP transporter, its highly specialized functions in specific types of physiological cells as well as the wide spectrum of drugs that interact with it. In this regard, it is important to remember that the overexpression of BCRP confers a multidrug-resistant phenotype, by transporting a diverse range of compounds out of the cell against the concentration gradient. This has been demonstrated for drugs that act at the CNS, as it will be herein focused on.

Information regarding single nucleotide polymorphisms (SNPs) of *ABCG2*, and the cooperation between BCRP and other ABC transporters, will also be herein highlighted as well as the subsequent changes in drugs pharmacokinetics, biodistribution and brain access.

I.5.1. BCRP: STRUCTURE AND LOCALIZATION

In opposition to the majority of ABC transporters, those from ABCG subfamily are ascribed as “half ABC transporters” or “incomplete transporters” since they comprise only one Transmembrane Domain (TMD) and one NBD, requiring homo or heterodimerization to attain adequate functionality [290]. As represented in **Figure I.8**, BCRP shows a distinct domain organization from that of P-gp (gene symbol *ABCB1*), as the NBD precedes the TMD (NBD-TMD arrangement) instead of the TMD-NBD arrangement characteristic of P-gp [291, 292]. Homology models suggest a large internal cavity formed by two bundles of six TMDs that is spacious enough to accommodate multiple drugs. Similarly to P-gp, BCRP has a high number of substances for which it has affinity, corroborating the possibility of having several binding sites [293]. Although the exact binding site in BCRP is still not completely known, several lines of biochemical evidence support the existence of multiple binding sites. Direct binding kinetic studies showed that there are possibly at least two distinct binding sites in BCRP, one for mitoxantrone and Hoechst 33342, and the other for prazosin [294, 295].

Thus, the feature of BCRP is its ability to interact with a broad range of structurally unrelated hydrophobic or partially hydrophobic compounds as it will be focused in-depth in **Section I.5.4**. That property has led BCRP to be described as a “multidrug transporter” and evidenced the BCRP importance on therapeutic responses regarding, at first, cancer chemotherapy. Indeed, BCRP was originally identified as a determinant of multidrug resistance in breast cancer cell lines, reducing cytoplasmic chemotherapeutic drug concentrations to levels below those required for cytotoxicity. Consequently, BCRP expression in tumors is correlated with poor prognosis, reduced remission rates and low cytostatic drug efficacy.

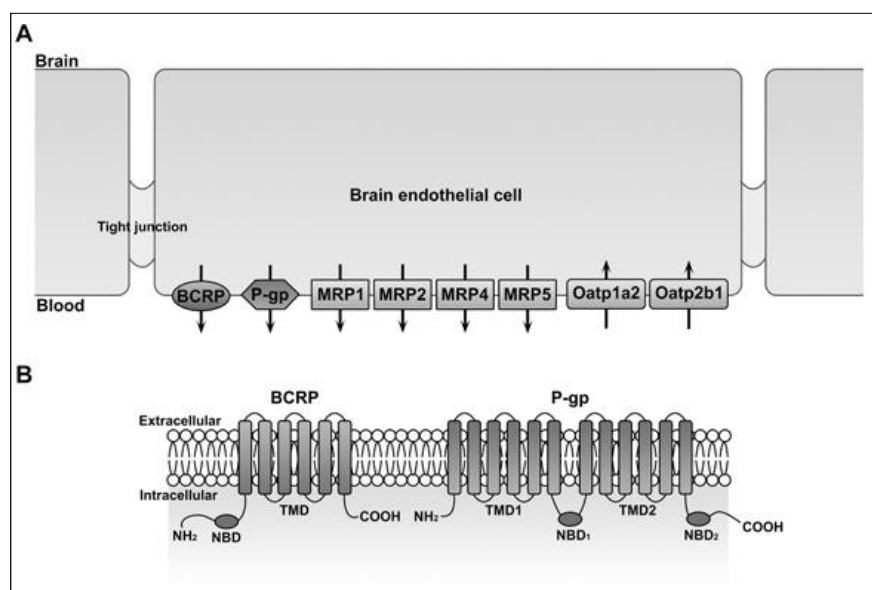


Figure 1.8 (A) Simplified distribution of efflux transporters across cerebral endothelial cells and **(B)** two-dimensional structural and topological models of P-glycoprotein (P-gp) and breast cancer resistance protein (BCRP). P-gp has six transmembrane domains (TMD) in two halves and two nucleotide binding domains (NBD), while Breast Cancer Resistant Protein (BCRP) has six transmembrane segments and only one efflux transporter nucleotide binding domain.

Among normal human tissues, the highest BCRP expression was observed on the apical membrane of the placental syncytiotrophoblasts in order to protect the fetus, avoiding the spread of possible toxins [296]. Jonker *et al.* demonstrated that the co-administration of topotecan and elacridar to pregnant female mice increased topotecan plasma levels twice in the fetus when compared to the levels observed after treatment with vehicle instead of elacridar [297]. Complementarily, BCRP is also expressed on the apical side of alveolar epithelial cells of mammary glands [298]. This is the main site of milk production during gestation and lactation periods, during which BCRP expression is exponentially increased. Evidence has showed that the main function of BCRP is to pump nutrients from the mother's diet to the milk as for example riboflavin [299]. In fact, the World Health Organization included it in the list of essential medicines that interact with BCRP [300]. As milk is a primary dietary source of riboflavin and BCRP is expressed in the lactating mammary gland, where it actively secretes its substrates into milk, the possible role of murine *Bcrp1* in riboflavin transport into milk was evaluated [299]. Accordingly, mice not expressing BCRP protein

presented a riboflavin secretion into milk at least 60 times lower than those animals expressing BCRP [299].

In addition, BCRP is prominently expressed on the apical membrane of the epithelium in the small intestine and colon and on the hepatic canalicular membrane [296]. This is extremely representative when regarding the oral administration of pharmacologically active substances. BCRP is also expressed on the apical membrane of human kidney proximal tubular cells [301, 302]; however, its level of expression in human kidney is relatively low compared to that in the liver and small intestine. The activity of BCRP as urate transporter is known and recognized as of great relevance in gout, the pathology related to the excessive levels of systemic uric acid due to its limited renal elimination.

Importantly, BCRP continues to gain force in research spotlight because it is a defense mechanism expressed at the BBB, where some drugs have demonstrated to inhibit or induce its expression in BBB [303]. Moreover, BCRP is not only expressed in the luminal side of endothelial cells of the BBB but also in the luminal face of the blood-spinal cord barrier, which separates the spinal cord tissue from peripheral blood circulation [304]. Changes in the expression levels of this transporter at both barriers altered drug concentrations in brain and spinal cord tissue. Therefore, a greater understanding of transporter activities at the BBB and blood-spinal cord barrier is essential to predict more accurately drug pharmacokinetics and pharmacodynamics in the CNS. Furthermore, this knowledge will allow new drug designs to avoid DDIs with these transporters and enhance CNS drug delivery or neuroprotection. At this point and in an attempt to facilitate the interpretation of *in vitro* and *in vivo* results, the diversified range of models and techniques that can be used to investigate BCRP interaction with drugs will be briefly explained in the following section.

I.5.2. HOW TO INVESTIGATE BCRP RELEVANCE AND DRUG-BCRP INTERACTIONS?

Distinct *in vitro* systems can be employed in the assessment of interactions with BCRP, each with its own advantages and limitations, as extensively reviewed in literature [305–307]. The most frequently used are accumulation and bidirectional transport assays, which are represented in **Figure I.9**. Taking into account Tables I.6 and I.7, it is undeniable that bidirectional transport assays using polarized cell monolayers are a classical approach to study the function of substrates and inhibitors of BCRP. The Transwell™ setup for these assays was recently reviewed [308]. Accordingly, these *in vitro* permeability assays are carried out in multi-well plates, where two compartments simulating the apical and basolateral sides are separated by a microporous filter on which the cells are seeded to form a cell monolayer. Monolayer integrity may be determined by measuring the transepithelial electrical resistance (TEER) or the paracellular transport of fluorescent markers such as lucifer yellow. The test compounds are added to apical or basolateral compartments and quantified in the opposite side, in order to estimate their apparent permeability (P_{app}). Differences in P_{app} from apical-to-basolateral (AP-BL) and basolateral-to-apical (BL-AP) compartments make it possible to identify the directional transport of the efflux pump and determine kinetic constants such as the affinity constant (K_m), that is in the μM range.

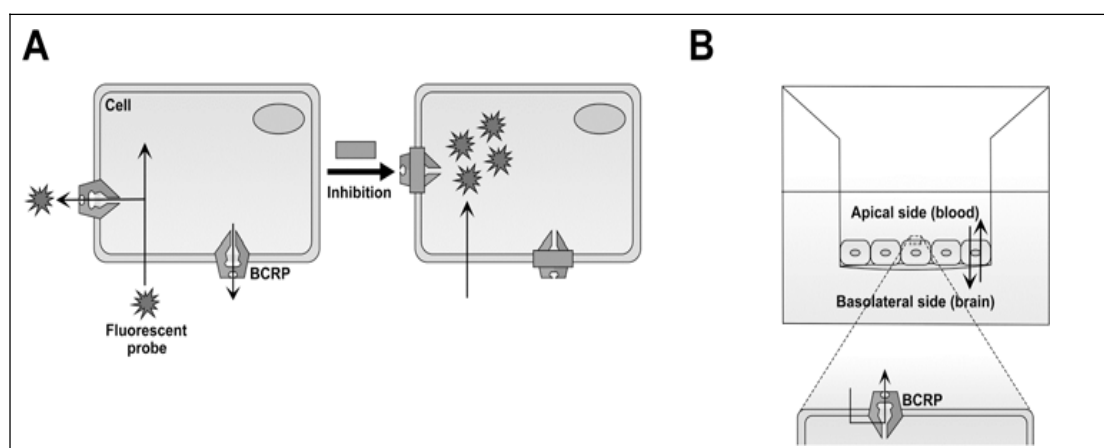


Figure I.9 Schematic representation of (A) intracellular accumulation (B) and bidirectional transport assays.

According to international guidelines, the efflux ratio [P_{app} (BL-AP)/ P_{app} (AP-BL)] or the net flux ratio [Efflux ratio (over-expressing cells)/Efflux Ratio (corresponding naïve

cells)] should be higher than 2.0 and decrease at least 50 % in the presence of a BCRP inhibitor. Although the preservation of the intact cell is advantageous for providing more information on compound permeability and interactions between compounds and transporters, this method also has some limitations, such as, being more laborious than membrane-based assays and requiring bioanalytical techniques for compound quantification. Furthermore, highly permeable compounds can give false-negative results in this model, as there is a risk of saturation of the efflux transporters and underestimation of the extrusion of compounds with rate-limited diffusion. These limitations result from the fact that highly permeable compounds easily get into the cells and may saturate the efflux transporters, particularly if the assay is carried out at high concentrations. Once efflux transporters are saturated, efflux will be lower and compounds will reach the acceptor chamber at higher concentrations than those that would be observed if no saturation occurred. In addition, the expression of multiple transporters by a cell line, including endogenous transporters, may complicate the interpretation of results, requiring the incubation with specific inhibitors of other transporters rather than BCRP. For instance, Madin-Darby canine kidney (MDCK) cells transfected with the human ABCG2 or murine Abcg2 genes can be incubated with zosuquidar to inhibit P-gp endogenously expressed by canine renal epithelial cells [309]. At this point, the selection of substrates and inhibitors is critical for designing definitive studies, and may circumvent the current issues with very high experimental inter-laboratory variability in in vitro assays [310].

Table I.6 Examples of BCRP substrates: evidence from *in vitro* and *in vivo* non-clinical studies.

BCRP Substrate	IN VITRO EVALUATION				IN VIVO NON-CLINICAL STUDIES			Refs.
	In vitro Assay	Cell line Type	Experimental Conditions	Main Results	Animal Model/ Administration Route and Dose	Study Design	Main Results	
Apixaban [Anticoagulant (Factor Xa inhibitor)]	Bidirectional Transport	Caco-2	Cells were cultured (density of 1×10^4 – 1.5×10^4 cells/well, 24-well plates), for 21 days until confluence (TEER > $150 \Omega \cdot \text{cm}^2$). Papp quantified at 2, 5, 10, 50 and 100 μM .	From 2-100 μM , ER ranged 36 - 22. Km: 8.5 μM	<i>Abcg2</i> (-/-), <i>Abcb1a/b</i> (-/-) and WT rats. IV (2 mg/Kg) PO (4 mg/Kg)	Plasma concentrations were determined up to 24 h post apixaban administration; Elacridar was administered orally (10 mg/kg) 1 h before apixaban administration.	<p><u>IV administration</u></p> <p>AUC_{0–∞} ↑ 66 % in <i>Abcg2</i> (-/-) rats AUC_{0–∞} ↑ 45 in <i>Abcb1a/b</i> (-/-) (compared with WT rats)</p> <p>Intestinal excretion: ↑ 21 to 42 % in <i>Abcg2</i>(-/-) rats ↑ 21 to 25 % in <i>Abcb1a/b</i>(-/-)</p> <p>Urinary excretion: ↓ 50 to 35 % in <i>Abcg2</i>(-/-) rats ↓ 50 to 44 % in <i>Abcb1a/b</i> (-/-)</p> <p><u>After PO administration</u></p> <p>AUC ↑ 300 % in <i>Abcg2</i> (-/-) rats AUC ↑ 100 % in <i>Abcb1a/b</i> (-/-) (vs. WT rats). GF-120918 ↑ AUC by 400 %.</p>	[311, 312]
BIA 9-1059 [Treatment of Parkinson’s disease (COMT inhibitor)]	Bidirectional Transport	MDCK-II WT BCRP	Cells seeded in 12-well Transwell [®] plates (6.0×10^5 cells/well), 7 days. Monolayer integrity assessed by TEER and sodium fluorescein flux. [BIA9-1059]: 60 μM Ko143 0.5 μM , 1h, both sides.	ER (MDCK-II): 1.14 ER (MDCK-BCRP): 7.04 Net flux ratio: 6.18 Net flux ratio (+Ko143): 0.64	NF			[313]

Ciprofloxacin (Antibacterial drug)	Bidirectional Transport	Caco-2	Caco-2 cells were sown for 14 days until confluence (TEER > 200 $\Omega \cdot \text{cm}^2$)	ER: 3.6	<i>Abcg2</i> (-/-) mice ♀ and WT mice	Plasma concentrations were determined up to 30 min post-oral administration; Plasm milk concentrations were determined 10 min after IV administration.	<u>PO administration:</u> Plasma concentration \neq more than 2-fold in <i>Abcg2</i> (-/-) than WT mice. <u>IV administration:</u> Plasma AUC \neq 1.5-fold in <i>Abcg2</i> (-/-) compared with that in WT mice. Milk-to-plasma ratio for WT mice \uparrow 2-fold in relation to <i>Abcg2</i> (-/-) lactating females.	[314, 315]
		MDCK-II-WT	MDCK monolayers considered confluent for differential ranging 60-80 mV	ER: 0.8	IV (10 mg/kg)			
		BCRP Bcrp1		ER: 7.6 Km: 94.7 μM		PO (10 mg/kg)		
Dabrafenib Anticancer drug (inhibitor of enzyme B-Raf)	Bidirectional Transport	MDCK-II-WT BCRP	Cells were cultured in 12-well Transwell® plates (density: 2×10^5 cells/well). Monolayer integrity assessed by TEER and [^{14}C] inulin. [Dabrafenib]: 5.0 μM Inhibition assays with Ko143.	ER (WT-MDCK): 1.2 ER (MDCK-BCRP): Alone: 21.0 + Ko143: 0.7	FVB-WT FVB-TKO ♀ ♂ mice IV (2.5 mg/kg) PO (25 mg/kg)	Blood and brain samples were collected: 5, 15, 30, 60 and 120 min after IV dosing; - 15, 30, 60, 120 and 240 min after PO dosing.	<u>IV administration:</u> Kp (FBV-WT) = 0.023 Kp (TKO) = 0.4 (18-fold greater than FBV-WT mice) <u>PO administration:</u> Plasma AUC (TKO) is 2-fold > than FBV-WT mice.	[316]
Dabigtran etexilate Anticoagulant drug (Factor Xa inhibitor)	Bidirectional Transport	Caco-2	Cells seeded in 24-well plates (1×10^4 – 1.5×10^4 cells/well), for 21 days until confluence (TEER > 150 $\Omega \cdot \text{cm}^2$). Papp was quantified at 2, 5, 10.5 and 100 μM .	From 2-100 μM , ER ranged from 8.5 to 1.4. Km: 39 μM	NF			[311]

Dasatinib Anticancer drug (Tyrosine kinase inhibitor)	Intracellular Accumulation Assay	MDCK-II-WT Bcrp1	Cells seeded (2×10^5 cells/well) in 12-well plates and pretreated or not with Ko143 (0.2 μ M, 30 min). Incubated for 3h with 1μ g/mL of [14 C] dasatinib. Ko143 in inhibition assays (0.2 μ M).	Dasatinib accumulation in the <i>Bcrp1</i> -MDCK cells was 25-fold $\$$ than WT cells. Ko143 abolished this difference.	σ WT mice, <i>Abcb1a/b(-/-)</i> <i>Abcg2(-/-)</i> TKO mice	All strains received dasatinib by IV or PO route with a pretreatment (or not) with Ko143 (IV, 10 mg/kg) 30 min before drug administration. Blood and brain were sampled at IV: 5, 20, 60, 120, and 180 min. PO: 120min.	<u>IV administration:</u> Brain concentrations: \uparrow <i>Abcb1a/b(-/-)</i> mice \leftrightarrow in <i>Abcg2(-/-)</i> mice \uparrow 10-fold in TKO mice (in relation to WT animals) Brain concentrations in WT animals remained — after elacridar administration.	[317]
	Bidirectional Transport	MDCK-II- WT MDCK-BCRP	Cells seeded in 6-well Transwell [®] plates (2×10^5 cells/well), 3-4days. Monolayer integrity assessed by TEER and mannitol flux. [Dasatinib]: 1.5 or 2.6 μ g/mL	ER (WT MDCK-II): 4.1 ER (MDCK-BCRP): 51.5 ER (MDCK-BCRP +Ko143): 9.0	IV (5 mg/kg) PO (10 mg/kg)		<u>PO administration</u> B/P concentration ratio \uparrow 4-fold in the <i>Abcb1a/b(-/-)</i> \uparrow more than 9-fold in TKO. \leftrightarrow after Ko143 administration.	
Donepezil Palliative treatment of Alzheimer's disease	Bidirectional Transport	MDCK-BCRP	MDCK cells seeded for 5 days on Transwell [®] filter membrane inserts (surface area 0.9 cm^2 , pore size 3 μ m, density 2.0×10^5 cells/ cm^2).	In MDCK- BCRP: Papp (BL-AP) significantly > than Papp (AP-BL). Km: 4.03 μ M	Wistar Rats ♀ IV (1 mg/Kg)	Animals were pretreated or not with 1 mg/kg of IV elacridar and then treated with donepezil.	After elacridar administration: - donepezil concentration in plasma, volume of distribution and clearance remained \leftrightarrow to those without elacridar.	[318]
	Accumulation Studies	Heart Tissue Slices from Wistar rats ♀	After preincubation or not with Ko143, heart slices were incubated with donepezil at 37 $^\circ$ C, 30 min with bubbling O_2 99.5 %.	Accumulation was evaluated as slice-to-medium concentration ratio, obtaining 4.78 and		Donepezil was determined in plasma, brain and heart tissues at 3 h post-administration.	- Kp \uparrow 44 % in the heart and 52 % in the brain.	

				5.78 in Ko143 absence or presence, respectively.			
Edoxaban Anticoagulant drug (Factor Xa inhibitor)	Bidirectional Transport	Caco-2	Cells seeded (1×10^4 – 1.5×10^4 cells/well) in 24- well plates, for 21 days until confluence (TEER > $150 \Omega \cdot \text{cm}^2$). Papp determined at 2, 5, 10, 50 and 100 μM .	From 2-100 μM , ER ranged from 21 to 11. Km: 40 μM	NF		[311]
Encorafenib Anticancer drug (Tyrosine kinase inhibitor)	Bidirectional Transport	MDCK- II-WT BCRP Bcrp	Cells seeded in 12- well Transwell [®] plates (5×10^5 cells/well). Mono- layer integrity assessed by TEER and ^[14C] inulin Papp. [Encorafenib]: 5.0 μM . Ko143 at 5.0 μM . Experiments with zosuquidar.	Transport ratio ^b WT MDCK-II: 10.3 MDCK-II BCRP: 13.4 Bcrp: 23.0 With Ko143: MDCK-II BCRP: 1.4 Bcrp: 1.0	FVB WT, <i>Abcb1a/b</i> (-/-) <i>Abcg2</i> (-/-) TKO mice PO and IV (10 mg/kg)	Plasma brain, liver, kidney and spleen concentrations of encorafenib up to 8 h after oral dosing were determined and up to 2 h after IV administration.	<u>PO administration:</u> No statistical differences <u>IV administration</u> Plasma AUC \uparrow 1.5-fold in TKO <i>versus</i> WT; TKO mice exhibited: 6.6-fold \uparrow in brain levels 3.7-fold \uparrow in B/P ratio 4-fold \uparrow in brain accumulation
Entacapone Treatment of Parkinson's	Bidirectional Transport	MDCK-II MDCK- BCRP	Cells seeded in 12- well plates Tran- swell [®] (6.0×10^5 cells per well), for 7 days. Monolayer integrity assessed by TEER and	ER (MDCK-II): 0.95 ER (MDCK- BCRP): 11.3 Net flux ratio: 11.9	NF		[313]

disease (COMT inhibitor)			fluorescein flux. [Entacapone]: 30 μM. Preincubation with Ko143 (1h, 0.5 μM, both sides.		Net flux ratio (+Ko143): 1.06			
Gefitinib Anticancer drug (EGFR inhibitor)	Intracellular Accumulation Assay	MDCK-II-WT BCRP Bcrp	[14C]-PhIP (1 μM) was used as a control substrate of the transport mediated by ABCG2/Abcg2. Papp determined at 0.1, 1 and 10 μM of [¹⁴ C]-gefitinib with or without elacridar (10 μM) or Ko143.	In MDCK-II-Abcg2 cells, [14C]-gefitinib levels ‡to levels close to those found in MDCK-II cell line, but restoration was not complete. In MDCK-ABCG2, elacridar completely offsetted ¹⁴ C gefitinib accumulation	♂ mice WT, <i>Abcb1a/b(-/-)</i> <i>Abcg2(-/-)</i> TKO mice IV (1 mg/Kg)	Elacridar (10 mg/kg) or vehicle was IV injected and, 15 min after, the [¹⁸ F] gefitinib was IV injected as a single bolus. PET scan was done, followed of CT imaging.	[18F]-gefitinib brain concentration in TKO mice was 2.3- fold ‡than WT mice. In the remaining animals: ↔ Brain/heart ratio ↑ 2.1-fold in TKO than WT mice. In the remaining animals: ↔ After elacridar treatment: Brain concentrations in WT, <i>Abcb1a/b(-/-)</i> and <i>Abcg2(-/-)</i> mice ↑ vs. vehicle-treated mice ↔ in TKO mice.	[319]
Imatinib Anticancer drug (Tyrosine kinase inhibitor)	Bidirectional Transport	MDCK-II-WT BCRP Bcrp	Imatinib was tested at 1, 10, 30 and 50 μM. Elacridar included at 5 μM. Samples collected up to 4 h.	Asymmetric transport in MDCK-Abcg2 and MDCK-ABCG2 but not in MDCK-II. Asymmetric transport ↓ as the imatinib concentration ↑.	FBV WT mice, <i>Abcb1a/b(-/-)</i> <i>Abcg2(-/-)</i> IV (12.5 mg/kg)	Plasma and brain were collected up to 2 h.	<u>After IV administration (versus WT mice)</u> Brain concentrations: ↑ 2.5-fold in <i>Abcg2(-/-)</i> mice ↑ 3.6-fold in <i>Abcb1a/b(-/-)</i> mice Clearance of imatinib: ↓ 1.6-fold in <i>Abcg2(-/-)</i> mice ↓ 1.3 fold in <i>Abcb1a/b(-/-)</i>	[320, 321]

Nebicapone Opicapone Treatment of Parkinson's disease (COMT inhibitor)	Bidirectional Transport	MDCK-II-WT BCRP	Cells seeded in 12-well Transwell [®] plates (6.0×10^5 cells per well) for 7 days. Monolayer integrity assessed by TEER and sodium fluorescein. [Nebicapone]: 10 μ M [Opicapone]: 30 μ M. Preincubation with Ko143 (1 h, 0.5 μ M, both sides.	ER (MDCK-II): 0.72 In MDCK-BCRP ER: 2.15 Net flux ratio: 2.99 With Ko143, net flux ratio \downarrow 1.07	NF	[313]		
Pilocarpine Cholinergic parasympatho mimetic agent	CETA	MDCK-II Bcrp	Cells were seeded in 6-Transwell [®] plates (density 0.4×10^6 cells/cm ²) for 5-7 days). Membrane integrity assessed by TEER and [¹⁴ C] mannitol.	MDCK-BCRP: pilocarpine moved into BL, contrarily to WT. Ko143 ablated, pilocarpine BL-AP transport.	WT mice <i>Abcb1a/b</i> (-/-) <i>Abcg2</i> (-/-) TKO mice IP (200 mg/Kg)	BCRP inhibitor Ko143 After 5, 10, 15, 20, 30, 60, and 120 minutes, mice were sacrificed	B/P ratio \uparrow in <i>Abcb1a/b</i> (-/-) and TKO mice in relation to WT. B/P ratio \downarrow in <i>Bcrp2</i> (-/-) in relation to WT.	[322]
Prazosin Sympatholytic drug (α/β -adrenergic antagonist)	Bidirectional Transport	Caco-2 MDCK-II WT BCRP	Cells seeded in 12-well Transwell [®] plates (6×10^4 cells/cm ²) for 21-28 days (Caco-2) or 7-11 days (both MDCK-II). Monolayer integrity assessed by TEER (>	ER: 10.5 ER (WT): 3.1 ER (MDCK-BCRP): 34.5	NF	[323]		

			450 Ω .cm ² for Caco-2 and > 1200 fi.cm ² for MDCK).					
Regorafenib Anticancer drug (Tyrosine kinase inhibitor)	Bidirectional Transport	MDCK-II-BCRP/PDZ K1	Cells were seeded in 12-well. Transwell® plates (3x10 ⁵ cells/well) and grown for 3 days. Regorafenib was tested at 0.1, 1 and 10 μ M.	ER (alone) = 4.31 ER (+ Ko143) = 1.69	FVB WT mice TKO mice ♂ IV (1 mg/kg)	30 min before drug administration, mice were treated with vehicle or elacridar (10mg/kg) by IV route.	Plasma concentrations in WT mice exhibited a peak at 4h post-dosing, in opposition to TKO mice. Skin, brain and lung concentrations \uparrow in TKO mice than in WT mice. Elacridar \nrightarrow drug skin and brain concentrations than in WT.	[324]
Riluzole Treatment of amyotrophic lateral sclerosis	Intracellular Accumulation Assay	BeWo	Cells seeded (10 ⁵ cells/well) in 24-well plates. 1 st treated (60 min) with FTC (10 μ M) or elacridar (10 μ M). 2 nd cells were treated (90 min) with riluzole (100 μ M).	Riluzole uptake: Vehicle: 4.00 \pm 0.43. + FTC: 4.90 \pm 0.63	CF1 <i>Abcb1a/b</i> (-/-) mice ♀ IP (10 mg/kg)	Mice were pre-treated (or not) with 100 mg/kg of elacridar and then treated with riluzole. Blood and brain were collected 15 min after injection.	Riluzole concentration remained whether pretreated or not with elacridar. $K_{p,brain}^a$ 1.34-fold in the elacridar-pretreated group compared with control group (5.90 \pm 0.57 vs 4.40 \pm 0.59, respectively).	[325]
Rivaroxaban Anticoagulant drug (Factor Xa inhibitor)	Bidirectional Transport	Caco-2	Incubation period of 12 days. Assays performed in the absence and presence of FTC (1 μ M) or LY335979 (1 μ M).	ER (alone): 2.82 ER (+ FTC): 1.88 ER (+LY335979): 1.61 ER (+ FTC + LY335979): 1.29	WT FVB mice <i>Abcb1a/b</i> (-/-) <i>Abcg2</i> (-/-) TKO mice PO (2 mg/kg)	Plasma samples were collected up to 4h post-dosing. Brain, liver and kidney were collected at 4h.	Plasma concentrations: \leftrightarrow in WT, <i>Abcb1a/b</i> (-/-) and <i>Abcg2</i> (-/-) \uparrow 2-fold in <i>Abcb1a/b</i> (-/-)/ <i>Bcrp1</i> (-/-) in relation to WT Clearance \leftrightarrow in WT, <i>Abcb1a/b</i> (-/-) and <i>Abcg2</i> (-/-) \uparrow 2-fold in TKO mice in relation to WT mice. Liver/Plasma ratio	[311, 326]

								↔ in WT, <i>Abcg2</i> ^{-/-} and <i>Abcb1a/b</i> (^{-/-})/ <i>Bcrp1</i> (^{-/-}) mice Brain/Plasma ratio ↔ in WT, <i>Abcb1a/b</i> (^{-/-}) and <i>Abcg2</i> ^{-/-} ↑ 2-fold in <i>Abcb1a/b</i> (^{-/-})/ <i>Bcrp1</i> (^{-/-}) in relation to WT	
Rosuvastatin HMG-CoA reductase Inhibitor	Bidirectional Transport	Caco-2 MDCK-II WT BCRP	Cells seeded in 12-well Transwell [®] plates (6x10 ⁴ cells/cm ²) for 21-28 days (Caco-2) or 7-11 days (MDCK). Monolayer integrity assessed by TEER (> 450 Ω.cm ² for Caco-2 and > 1200 Ω.cm ² for MDCK). Rosuvastatin was used at 2 μM.	ER: 83.2 Km: 2.02 Addition of Ko143: ↑ accumulation of rosuvastatin in the apical side. ER (WT): 1.1 ER (MDCK-BCRP): 5.8	FVB <i>Abcg2</i> (^{-/-}) and WT mice IV (infusion of 0.1nmol/min/kg after a bolus administration of 3 nmol/kg).	Blood samples collected from contralateral jugular vein; bile collected at 30-min intervals; 120 min post-dosing mice sacrificed and the entire liver was excised immediately.	% unchanged rosuvastatin in plasma, bile, and liver were, respectively: ↔ in WT and <i>Abcg2</i> (^{-/-}) 6.3-fold ↑ in WT mice 2.7-fold ↑ in WT mice Total clearance was 2-fold ↓ in <i>Abcg2</i> (^{-/-}) than WT mice.	[323, 327]	
Rucaparib Anticancer drug (PARP-1 inhibitor)	Bidirectional Transport	MDCK-II BCRP MDCK-II Bcrp	Cells seeded in 12-Transwell [®] plates (density 2.5x10 ⁵ cells/well) for 3 days. [Rucaparib]: 5.0 μM. Inhibition assays included Ko143 (5.0 μM) in both sides.	Transport ratio ^b WT MDCK-II: 1.0 MDCK-II BCRP: 3.0 MDCK-II Bcrp: 14.8 Ko143 completely inhibited the transport in overexpressing cells.	FBV mice ♀: WT, <i>Abcb1a/b</i> (^{-/-}) <i>Abcg2</i> (^{-/-}) TKO mice PO (10 mg/kg)	Blood samples were collected at 0.5, 1, 2, 4 and 8 h post-administration. Blood and brain were collected at 7.5, 15 and 30 min.	Relatively to WT mice, the oral plasma AUC ↑: 1.7-fold in <i>Abcg2</i> (^{-/-}), 2.5-fold in <i>Abcb1a/b</i> (^{-/-}) 4.0-fold in TKO mice Brain concentrations were: ↔ in <i>Abcg2</i> (^{-/-}) mice 4.1-fold ↑ in <i>Abcb1a/b</i> (^{-/-}) 7.9-fold in TKO animals	[328]	

						B/P ratio ↑2.9-fold in TKO animals, while brain accumulation ↑ 3.7 times.
Sildenafil Vasodilator	NF				FBV-WT FBV-TKO IV (50 mg/kg)	Brain penetration of sildenafil was more than 20-fold ↑ in TKO mice vs. WT. [329]
Silybin (A and B) Hepato-protective agent	Bidirectional Transport	MDCK-II WT BCRP	Cells seeded in Transwell® plates (2.0×10 ⁵ cells/cm ²) and grown for 4-5 days. Monolayer integrity was assessed by TEER and Papp of lucifer yellow. Silybin was tested at 10 μM. Ko143 (0.5 μM) or CsA (10 μM) were incorporated in AP and BL sides.	ER (Silybin A): 2.96 ER (Silybin A + Ko143): 1.31 ER (Silybin B): 3.04 ER (Silybin B + Ko143): 1.04	NF	[330]
Sorafenib Anticancer drug (Tyrosine kinase inhibitor)	Intracellular Accumulation Assay	MDCK-II WT BCRP	Cells seeded (2x10 ⁵ cells/well) in 24-well plates for 3 days. [^{3H}] sorafenib tested at 2 ng/mL	ER: 5.0	FVB <i>Bcrp1</i> ^{-/-} and WT mice	One cohort was pretreated with elacridar (10 mg/kg, IV), other with vehicle and the 3 rd cohort was not pre-treated; Blood and brain were collected 60 min after sorafenib administration.
	Bidirectional Transport	MDCK-II WT BCRP	Cells seeded (2x10 ⁵ cells/well) in 6-well Transwell® plates.	Papp (BL-AP) was 15-fold ↑ than Papp (AP-BL). Ko143 abolished this difference.	IV (10 mg/kg)	B/P ratio was 0.083 in WT mice and 0.37 in <i>Bcrp1</i> ^{-/-} . Elacridar ↑ brain concentrations by 5-fold in WT group and 3-fold in <i>Bcrp1</i> ^{-/-} mice, compared to 3 rd cohort group. Elacridar ↑ the B/P ratio to 0.76 in WT and 1.03 in the <i>Bcrp1</i> ^{-/-} mice. [331]

			^[3H] sorafenib tested at 2 ng/mL	Km: 5.5 nM				
Sulfasalazine Intestinal anti-inflammatory drug	Bidirectional Transport	Caco-2	Cells seeded for 21 days until confluence (TEER: 450-650 Ω .cm ²). Assays performed in the absence and presence of CsA (10 μ M) or FTC (10 μ M) or MK571 (30 μ M).	ER (alone): 87 ER (+ CsA): 87 ER (+ FTC): 2.6 ER (+ MK571): 2.4	FVB <i>Abcg2</i> (-/-) and WT mice. PO (20 mg/kg) IV (5 mg/kg)	Gefitinib was orally administered (50 mg/kg) 2 h before drug administration.	$AUC_{Abcg2(-/-)}/AUC_{WT} = 111$ After IV administration: $AUC_{Abcg2(-/-)}/AUC_{WT} = 13$ In WT animals, AUC \uparrow 13-fold times after Gefitinib administration.	[332, 333]
Topotecan Anticancer drug (Topoisomerase inhibitor)	Bidirectional Transport	Caco-2 MDCK-II WT BCRP	Caco-2 cells were incubated for 21 days when TEER values ranged 300-500 fi.cm^2 . Monolayers of 130-160 Ω .cm ² were feasible. FTC was used as inhibitor of BCRP.	Papp (BL-AP) depends on concentration and is saturable. Papp (BL-AP) significantly inhibited in FTC presence. Km: 213.28 μ M	<i>Abcb1a/b</i> (-/-) mice IV and PO administration	GF120918 or vehicle were orally administered 15 min before drug administration. Plasma levels were determined up to 4 h.	<u>PO administration:</u> AUC (GF120918) = 596 mg.h/L AUC (Vehicle) = 96 mg.h/L <u>IV administration:</u> AUC (GF120918) = 406 mg.h/L AUC (Vehicle) = 200 mg.h/L	[297, 334]
Vandetanib Anticancer drug	Bidirectional Transport	MDCK-II WT BCRP	Monolayers are confluent in 3-4 days. Samples (150 μ L) were withdrawn from the acceptor at 60, 120, 180 and 240 min of incubation.	ER: 7.5 In the presence of Ko143 (200 nM): ER \downarrow to 1.0	FVB WT mice σ 5 mg/kg IV route	LY335979 (25 mg/kg), Ko143 (10 mg/kg) or elacridar IV route 30 min before vandetanib. Brain and plasma concentration-time profiles determined up to 2 h.	LY335979 and Ko143 \uparrow brain concentrations only at 120 min post dose. Elacridar \uparrow the ratio $AUC_{\text{brain}}/AUC_{\text{plasma}}$ of vandetanib from 0.206 to 0.642.	[335]

↑ increase, ↓ decrease, ↔ unchanged; ^a $K_{p,brain} = C_{brain}/C_p$ where C_{brain} and C_p represent brain and plasma riluzole concentration. ^b Calculated by the ration between Papp (BL-AP) and Papp (AP-BL). AP-BL, *apical-to-basolateral*; AUC, *area under the curve*; BL-AP, *basolateral-to-apical*; B/P, *brain-to-plasma ratio given by the ratio between AUC in plasma and in brain*; CETA, *concentration equilibrium transport assay*; COMT, *catechol-o-methyl transferase*; CT, *computed tomography*; EGFR, *epidermal growth factor receptor*; ER, *efflux ratio calculated as Papp(BL-AP)/Papp(AP-BL)*; FTC, *fumitremorgin C*; FVB, *Friend leukemia virus strain B*; Km, *affinity constant*; Kp, *tissue-to-plasma concentration ratio*; IP, *intraperitoneal*; IV, *intravenous*; L/P, *liver-to-plasma ratio given by the ratio between AUC in plasma and in liver tissue*; MDCK, *Madin–Darby canine kidney*; NF, *not found*; Papp, *apparent permeability*; PET, *Positron emission tomography*; PhIP, *2-amino-1-methyl-6-phenylimidazo[4,5-b]pyridine*; PO, *per os*; TKO, *triple knockout animals which corresponds herein to Abcb1a/b(-/-)Abcg2(-/-)*; WT, *wild type*.

Table I.7 Examples of BCRP inhibitors and their influence on the disposition of drugs: evidence from *in vitro* and *in vivo* non-clinical studies.

IN VITRO EVALUATION						IN VIVO NON-CLINICAL STUDIES			
BCRP Inhibitors	<i>In vitro</i> Assay	Cell line type	Substrate	Experimental Conditions	Main Results	Animal Model Administration route and Dose	Substrate	Main Results	Refs.
Cyclosporin A Immuno-suppressant drug	Bidirectional Transport	MDCK-II-WT MDCK-BCRP MDCK-Bcrp	E3S (35 μ M) MTX (60 μ M) (60 min)	Cells seeded in 24- well Transwell [®] plates (1x10 ⁵ cells/well), for 3 days. CsA was added in donor side; Papp of E3S estimated from AP-BL and BL-AP.	In transfected MDCK-II cells, Papp of E3S was AP-BL 4.5-fold < BL-AP After incubation CsA (50 μ M): Papp (AP-BL) \leftrightarrow BL-AP Ki: 6.7 μ M Against MTX, Ki of CsA was 7.8 μ M	NF			[337]
Curcumin Food products	<i>Ex vivo</i> tissue permeability assay	Insolated and functionally active rat brain capillaries	Prazosin (2 μ M, 60 min)	Measurement of prazosin in the capillary lumen. FTC used as reference BCRP inhibitor.	IC50: 19.4 μ M IC50 (FTC): 5 μ M	WT mice <i>Abcg2</i> (-/-) mice TKO mice PO (40 mg/kg)	Sulfasalazine PO (20 mg/kg)	In WT mice, curcumin: \uparrow [sulfasalazine] in plasma \uparrow $t_{1/2}$ from 1.02 to 5.02 h \uparrow 5-fold AUC _{0-4 h} \uparrow 13-fold AUC _{0-24h} [sulfasalazine] in plasma remain \leftrightarrow in <i>Abcg2</i> (-/-) after curcumin dosing.	[338; 339]
						WT mice <i>Abcg2</i> (-/-) mice		[curcumin] of 150 mg/kg \leftrightarrow C _{max} of sulfasalazine,	

	Vesicular transport	hBCRP expressing membranes	Sulfasalazine (0.9 μ M)		IC ₅₀ : 1.6 μ M	PO (150, 300 and 400 mg/kg)	Sulfasalazine PO (10 mg/kg)	↑the systemic exposure of sulfasalazine [curcumin] of 300 mg/kg ↑ 8.5-fold AUC _{0-8h} [curcumin] of 400 mg/kg ↑ 8.0-fold AUC _{0-8h}
Delavirdine NNRTI	Intracellular accumulation	MDCK-BCRP	PhA (1 μ M, 30 min)	Cells seeded in 24- well Transwell [®] plates 1x10 ⁶ cells/mL	[Inhibitor]: 1 - 100 μ M IC ₅₀ : 18.7 μ M	NF		[340]
Efavirenz NNRTI					[Inhibitor]: 5 - 100 μ M. IC ₅₀ : 20.6 μ M			
Elacridar	Intracellular accumulation	MCF-7/Topo ^b	MXR (20 μ M, 60 min)	1x10 ⁶ cells/mL [Inhibitor]: 0.001 - 10 μ M	IC ₅₀ : 0.25 μ M		Several investigations as mentioned in text and Table 1.6	[340]
	Intracellular accumulation	K562 WT K562/BCRP		Cells seeded (5x10 ⁵ cells/mL). MXR (300 μ M) incubated 40 min. FTC added at 1 and 10 μ M.	Ki: 0.55 μ M IC ₅₀ : 0.25 μ M			[341]
FTC			MXR (300 μ M, 40 min/10 μ M 60 min)			MXR accumulation significantly ↓ in Bcrp1/BCRP1 cells.	ND	
	Intracellular accumulation	MDCK-II-WT MDCK-BCRP MDCK-Bcrp		Cells seeded in 24- well plate for 36 h. FTC added at 1-10 μ M.	IC ₅₀ (MDCK-BCRP): 1.04 μ M			[342]

				IC ₅₀ (MDCK-Bcrp): 8.29 μM				
Ko143	Intracellular accumulation	MEF3.8 parent cell line and T6400 cell line ^a	MXR	-	EC ₅₀ : 25 nM (2-fold more potent than elacridar).	<i>Mdr1a/b</i> (-/-) mice PO(10 mg/kg)	Topotecan PO (1 mg/kg)	Ko143 ↑ 4-6-fold in plasma topotecan concentrations in the <i>Mdr1a/b</i> (-/-) mice. [343]
Lansoprazole Proton pump inhibitor	Vesicular transport	BCRP-expressing membrane vesicles, in an 'inside-out' direction	MXR (100 μm)	[Lansoprazole]: 5, 20, 100 μM	IC ₅₀ : 14.4 μM	NF		[344]
Lopinavir HIV-protease inhibitor	Intracellular accumulation	MDCK-BCRP	PhA (1 μM, 30 min)	Cells seeded at 1x10 ⁶ cells/mL [Inhibitor]: 0.2 - 20 μM.	IC ₅₀ : 7.66 μM	NF		[340]
Nelfinavir HIV-protease inhibitor					IC ₅₀ : 13.5 μM			
Nebicapone COMT inhibitor	Intracellular accumulation	MDCK-BCRP	Hoechst 33342 (10 μM)	Cells seeded in 12- well plates (3.0 x 10 ⁵ cells per well) for 48 h [Ko143]: 0.5 μM	IC ₅₀ : 18.4 μM	NF		[314]
Novobiocin Antibacterial drug	Intracellular accumulation	HEK293-BCRP	Topotecan (10 μM)	Cells seeded in 24-well plates (2x10 ⁵ cells/well) until confluence. Topotecan uptake studied 1 day after confluence.	Novobiocin significantly ↑ the cellular uptake of topotecan.	Sprague Dawley rats ♂ PO (50 mg/kg)	Topotecan: PO (2 mg/kg) IV (1 mg/kg)	After novobiocin administration: PO administration AUC _{0-inf} ↑ 3-fold Cmax ↑ 4.7-fold MRT ↑ 1.3-fold IV administration AUC _{0-inf} ↑ 1.5-fold MRT ↑ 5.5-fold [345]

Omeprazole Proton pump inhibitor					IC ₅₀ : 17.6 μM		
Pantoprazole Proton pump inhibitor	Vesicular transport assay	BCRP-expressing inside-out mem- brane vesicles	MXR (100 μm)	[PPI]: 5, 20, 100 μM	IC ₅₀ : 5.5 μM	NF	[344]
Rabeprazole Proton pump inhibitor					IC ₅₀ : 8.5 μM		
Risperidone Antipsychotic drug	Intracellular accumulation	MCF7/MX100 ^b	MXR (5 μM)	1x10 ⁶ cells/mL [Sirolimus]: 0 - 100 μM Ko143 used as positive control	IC ₅₀ (Ko143): 0.1 μM IC ₅₀ : 38.1 μM	NF	[346]
Saquinavir HIV-protease inhibitor	Intracellular accumulation	MDCK-BCRP	PhA (1 μM, 30 min)	Cells seeded at 1x10 ⁶ cells/mL [Saquinavir]: 1.0 - 50 μM	IC ₅₀ : 27.4 μM	NF	[340]
Sirolimus Immuno-suppressant drug	Intracellular accumulation	HEK293- BCRP	PhA (1 μM) MXR (10 μM) 30 min	Cells seeded at 1x10 ⁶ cells/mL [Sirolimus]: 0 - 25 μM	IC ₅₀ : 1.9 μM ↓ the resistance induced by topotecan.	NF	[347]
Sorafenib Anticancer drug (Tyrosine kinase inhibitor)	Intracellular accumulation	HEK293-BCRP	MXR (2.5-20 μM, 30 min)	Cells seeded at 1x10 ⁶ cells/mL [Inhibitor]: 2.5 μM	IC ₅₀ : 1.31 μM < potency than Ko143. No effect on P-gp.	NF	[348]
Tacrolimus Immuno-suppressant drug	Intracellular accumulation	HEK293/BCRP	PhA (1 μM) MXR (10 μM) 30 min	Cells seeded at 1x10 ⁶ cells/mL [Inhibitor]: 0 - 25 μM	IC ₅₀ : 3.6 μM ↓ the resistance induced by topotecan.	NF	[347]

Tariquidar	Intracellular accumulation	MCF-7/Topo ^b	MXR (20 μ M, 60 min)	Cells seeded at 1×10^6 cells/mL [Inhibitor]: 0.001 - 10 μ M	IC ₅₀ : 0.92 μ M	NF		[348]	
Telatinib VEGFR inhibitor	Intracellular accumulation	HEK293-BCRP	MXR (0.1 μ M, 2 h)	Cells seeded at 12×10^6 cells/mL [Inhibitor]: 0.25 - 1.0 μ M	IC ₅₀ : 66.5 nM (vs 64.1 nm for FTC)	Athymic nude σ mice ABCG2-overexpressing. PO (15 mg/kg)	Doxorubicin (1.8 mg/kg)	Growth rate and tumor size \downarrow after administration of Telatinib + Doxorubicin vs Doxorubicin group.	[348]
Tolcapone COMT inhibitor	Intracellular accumulation	MDCK-BCRP	Hoechst 33342 (10 μ M)	Cells seeded in 12- well plates (3.0×10^5 cells/well), 48 h. [Ko143]: 0.5 μ M.	IC ₅₀ : 32.5 μ M	NF		[314]	
Zidovuvir NRTI	Intracellular accumulation	MDCK-BCRP	PhA (1 μ M, 30 min)	Cells seeded at 1×10^6 cells/mL. [Inhibitor]: 10 - 1000 μ M	Inhibition observed only at concentrations \leq 500 μ M.	NF		[340]	

\uparrow increase, \downarrow decrease, \leftrightarrow unchanged; ^a MEF3.8 parent cell line express low Bcrp while T6400 cell line lacks P-gp and MDR1 and overexpress *Bcrp1*. ^b ABCG2 overexpressing subclone of MCF-7 breast cancer adenocarcinoma cells. AP-BL, *apical-to-basolateral*; AUC, *area under the curve*; BL-AP, *basolateral-to-apical*; B/P, *brain-to-plasma ratio given by the ratio between AUC in plasma and in brain*; COMT, *catechol-o-methyl transferase*; ER, *efflux ratio*; E3S, *estrone-3-sulfate*; FVB, *Friend leukemia virus strain B*; HEK, *human embryonic kidney*; IC₅₀, *inhibitor concentration causing 50 % inhibition*; Ki, *inhibitory constant*; Kp, *tissue-to-plasma concentration ratio*; IP, *intraperitoneal*; IV, *intravenous*; MTX, *methotrexate*; MXR, *mitoxantrone*; NNRTI, *Non- nucleoside reverse transcriptase inhibitor*; NRTI, *nucleoside reverse transcriptase inhibitor*; NF, *not found*; Papp, *apparent permeability*; P-gp, *P-glycoprotein*; PO, *per os*; TKO, *triple knockout animals which corresponds herein to Mdr1a/b(-/-)Bcrp1(-/-)*; t_{1/2}, *half-life time*; VEGFR, *vascular endothelial growth factor receptors*; WT, *wild type*.

Specifically regarding BCRP, the MDCK cell line and the human epithelial colorectal adenocarcinoma (Caco-2) cell line are the most widely used (**Tables I.6** and **I.7**). One of the greatest advantages of the former is that they are easy to grow, requiring few days of culture to be ready for assays (**Table I.6**). Importantly they can be transfected with the *ABCG2* or *abcg2* genes in order to polarize the expression of BCRP and subsequently study its interaction with xenobiotics. On the other hand, results achieved in MDCK cells over-expressing BCRP can be normalized through the results observed in the wild type (WT) cell line that only considers the endogenously expressed transporters. In opposition, the Caco-2 cell line takes almost 21 days to develop a mature cellular monolayer. Furthermore, they are tumoral and consequently, P-gp expression seems to be increased in relation to other efflux transporters. Nevertheless, when the objective regards intestinal permeability and the influence of intestinal BCRP, the Caco-2 line is preferable to be used [308].

Vesicular transport assays are also used to distinguish efflux substrates from inhibitors, but not inducers. In brief, plasma membranes are obtained from transporter-expressing cells and utilized to form inside-out vesicles where substrates are effluxed into the vesicle, in the presence of ATP. While efflux substrates demonstrate concentration and ATP-dependent accumulation into the vesicles, inhibitors are detected by the reduction of the concentration of probe substrate in the vesicles. However, preparation and purification protocols are complex and the assay is suitable for compounds with low passive permeability and low non-specific binding drugs [305].

At this point, it is important to emphasize that a drug that reveals to be a substrate of *ABCG2/Abcg2* *in vitro* may not have impact in *in vivo* disposition. Indeed, *in vivo* methods have been crucial in understanding the relevance of the BCRP transporter in absorption, distribution, metabolism, and excretion (ADME) of drugs as well as in physiology (**Table I.6**). Judging by early tissue distribution and *in vitro* functionality data, the most prominent *in vivo* models are based on Bcrp null mice that do not express BCRP [the *Bcrp(-/-)*]; they have been applied and the pharmacokinetic results compared with those attained in WT animals to determine the effect of BCRP on absorption, extent of elimination and brain penetration. In addition to Bcrp1 knockout

(KO) animals, triple knockout (TKO) mice, in combination with *Abcb1a/b*, have also been generated and have been essential in clarifying the relationship between *Bcrp* and P-gp at the BBB on compounds that are shared substrates.

I.5.3. BCRP IN DRUGS PHARMACOKINETICS AND BRAIN DISTRIBUTION

From a pharmacokinetic perspective, BCRP functions primarily as an apical efflux pump in enterocytes and hepatocytes, attenuating drug uptake from intestinal lumen and enhancing hepatobiliary excretion after oral drug administration. In opposition to intestinal BCRP, which is rate-determining of the absorption of low-permeability drugs, hepatic canalicular BCRP transports the drug from the hepatocytes into the bile and its function is rate-limited by the hepatic clearance of drugs that are predominantly transported to the liver by carrier-facilitated proteins before being excreted into the bile. In fact, one of the first investigations that directly evaluated the role of hepatic *Abcg2* was performed by van Herwaarden and colleagues, who cannulated the gall bladder of *Abcg2*(-/-) and WT animals [348]. The kinetics of the dietary carcinogen, 2-amino-1-methyl-6-phenylimidazo(4,5-b)pyridine, was assessed and the area under the curve (AUC) plasma concentration vs. time was nearly 3-fold higher in *Abcg2*(-/-) mice. They revealed that approximately 75 % of the biliary excretion of 2-amino-1-methyl-6-phenylimidazo(4,5-b)pyridine could be attributed to hepatic *Abcg2* function. Moreover, it was demonstrated that murine BCRP is a major factor in the hepatobiliary and intestinal excretion of 2-amino-1-methyl-6-phenylimidazo(4,5-b)pyridine, which was shifted predominantly toward urinary elimination in mice lacking *Abcg2*. In humans, BCRP has also already demonstrated an important role in combination with P-gp. Eight patients who received an oral administration of topotecan (1 mg/m²) and elacridar (1000 mg) exhibited a 2.4-fold higher oral bioavailability of topotecan as elacridar decreased its biliary and renal excretion, in addition to its increased intestinal absorption [349].

Based on **Table I.6**, BCRP undoubtedly demonstrated to determine the bioavailability of the novel anticoagulant drugs Factor Xa inhibitors, including apixaban

and rivaroxaban. Regarding apixaban, the total AUC increment in *Abcg2(-/-)* rats in relation to that of WT animals was higher after oral administration than IV administration (300 % vs 66 %), suggesting that intestinal uptake is determined by BCRP. The primary mechanism by which BCRP reduced oral bioavailability was by decreasing intestinal absorption (evidenced by the increment of intestinal excretion depicted in **Table I.6**) and urinary excretion. Interestingly, WT and *Abcg2(-/-)* mice presented similar plasma concentrations of rivaroxaban after its oral administration, suggesting that BCRP may have a limited effect on the intestinal rivaroxaban absorption; however, the TKO (lacking *Abcb1a/b* and *Abcg2* genes) exhibited 2-fold higher plasma concentrations than those observed in WT mice. The lack of differences on rivaroxaban clearance between the individual transporter KO mice and its significant reduction in the *Abcb1a/b(-/-)/Abcg2(-/-)* mice, clearly support that rivaroxaban is a shared substrate of both P-gp and BCRP. Extremely important is also the fact that rivaroxaban brain-to-plasma ratio was significantly elevated in TKO mice by over 2 times [326]. This finding brings important mechanistic reasons that can underlie the elevated risk of rivaroxaban to trigger hemorrhages such as intracranial bleeding including the life-threatening hemorrhagic stroke in some patients [350]. In fact, the risk of rivaroxaban associated adverse events has been confounded by poor renal function, driven by increased systemic levels of the drug [351], suggesting that rivaroxaban is expected to modulate the extent of bleeding risk in patients. However, the higher brain concentrations of rivaroxaban observed in TKO mice relatively to WT animals hint that patients at the highest bleeding risk may have not only poor renal function but also reduced P-gp and BCRP function. The net effect would include an increment of gastrointestinal rivaroxaban absorption, which would lead to an increased bioavailability, worsened by a reduced rivaroxaban renal secretion. At present, clinical studies should be performed regarding the new oral anticoagulant drugs to clarify the relevance of DDI and genotypes at BCRP levels.

Besides anticoagulant drugs, it is noticeable that BCRP also influences the oral bioavailability, excretion and BBB penetration of several anticancer agents (**Table I.6**). Among them, dabrafenib, dasatinib, encorafenib, rucaparib and topotecan were orally and intravenously administered to WT mice, as well as to *Abcg2* and/or *Abcb1a/b* KO

strains. With exception of encorafenib, all revealed plasma bioavailability values (given by plasma concentrations or AUC values) substantially higher in *Abcg2*(-/-) strains or TKO mice than in WT animals (**Table I.6**). In turn, the oral administration of encorafenib revealed a strong inter-individual variability which could minimize the differences between each group. To overcome this limitation, drugs are often administered by IV route. Although no information is provided regarding intestinal absorption, the influence of BCRP on BBB drug penetration and drug elimination is more accurately assessed. Thus, analyzing the results obtained after IV administration, it is noteworthy that all anticancer drugs demonstrated higher brain-to-plasma ratios when administered to TKO animals than those found after administration to WT animals, suggesting that both P-gp and BCRP contribute similarly to their efflux at the BBB. Nonetheless, the brain accumulation of sorafenib was mainly restricted by BCRP [352]. Contrariwise, *in vivo* studies with dasatinib suggest that its access to CNS is mainly dependent of P-gp, as brain dasatinib concentrations significantly increased in *Mdr1a/b*(-/-) mice compared with those in WT mice, while brain concentrations in *Bcrp1*(-/-) mice remained unchanged in relation to WT animals. Although this finding could suggest that BCRP did not influence the BBB permeability of dasatinib, dasatinib brain concentrations increased by more than 10-fold in the *Mdr1a/b*(-/-)/*Bcrp1*(-/-) mice and the brain-to-plasma concentration ratio increased approximately 4-fold in the *Mdr1a/b*(-/-) mice and by more than 9-fold in the *Mdr1a/b*(-/-)/*Bcrp1*(-/-) mice in relation to WT animals. These findings suggest that both transporters limit brain distribution of this anticancer drug [317]. One possible reason could be that in single-KO mice, the remaining transporter can largely compensate for the loss of function of the deleted one while in *Abcb1a/b/Abcg2* TKO mice, the capacity to compensate appears to be exhausted with no additional transporter is able to fill the breach. Remarkably, similar results have been reported for imatinib, with the brain distribution increasing in the absence of both P-gp and BCRP [320, 353].

The finding of the synergistic effect that P-gp and BCRP have on anticancer drug delivery into the brain has important consequences for the treatment of CNS metastasis in chronic myeloid leukemia and other CNS tumors. Thus, we suggest that “pharmacological knockout” studies should be performed to identify the transporter(s)

that limit brain penetration, because *Abcg2* KO mice model often fails to affect the brain penetration and overall disposition of anticancer drugs. Accordingly, specific (or non-specific) BCRP inhibitors should be co-administered with the drugs to WT and TKO animals and brain exposure or brain-to-plasma ratios should be determined and compared. Elacridar is a BCRP and P-gp inhibitor while Ko143 specifically inhibits BCRP and zosuquidar specifically inhibits P-gp. If plasma and brain exposures are not altered by any of these inhibitors, it is probable that BCRP does not influence its access into the brain.

These findings strongly evidence the clear influence of BCRP in drugs pharmacokinetics and pharmacodynamics, making BCRP a drug transporter that both the FDA and European Medicines Agency (EMA) required to investigate those liabilities for NCEs. Drugs for which ADME, bioavailability and BBB permeation are influenced by BCRP may require further clinical investigations with clinical BCRP inhibitors to reveal a potential DDI. Nevertheless, it is important to bear in mind that the significance of transporters *in vivo* is related to drug permeability: the impact of efflux transport activity increases as the bioavailability and intrinsic permeability of the drug decrease along with a narrow therapeutic index [354–356]. In opposition, for highly permeable molecules, the transporter effect in humans will be minimal.

1.5.4. DRUGS-BCRP TRANSPORTER INTERACTION

Since its discovery in the last decade of the 20th century, much has been revealed about the broad range of BCRP substrates and inhibitors. In fact, given the relevance of BCRP in multidrug resistance and its impact in ADME, toxicity and DDIs, BCRP substrate or inhibitor screening methods are currently required by the FDA and EMA to be incorporated into drug discovery. The major driving forces behind the identification of substrates/inhibitors of BCRP are to explain the mechanisms behind the DDI found in humans and animals and anticipate potentially associated toxicities.

I.5.4.1. BCRP Substrates

The list of BCRP substrates is large and diverse at least regarding non-clinical *in vitro* and *in vivo* investigations (**Table I.6**); nonetheless few are currently clinical BCRP probe substrates. In fact, observed interspecies differences demand that the pharmacokinetics of candidate drugs must be demonstrated in human studies and not only in animals. For instance, observing **Table I.6**, it is evident that gefitinib is transported *in vitro* by human and murine *ABCG2/Abcg2*. However, it appears that the overexpression of murine *Abcg2* has a more pronounced effect than that of human BCRP, because the accumulation of gefitinib in human ABCG2 over-expressing cells was completely offset by elacridar while it was not complete in murine *Abcg2* over-expressing cells [319]. Two reasons were suggested to underlie the inter-species differences observed on gefitinib pharmacokinetics: species-specific difference in transport affinity or capacity of ABCG2 for gefitinib; and the lower expression of ABCG2 protein in the human ABCG2-overexpressing cells compared to murine *Abcg2*-overexpressing cells [319]. In this context, probe BCRP substrates supported by clinical evidence will be herein focused.

Statins revealed early differences among their exposure and severity of adverse effects as well as significant inter-individual variability, particularly between Caucasian and Asian subjects [357]. Although statins share similar molecular weight, pKa and anionic charge, their lipophilicity considerably differs and, consequently, their passive permeability and enzymatic metabolism. For instance, pitavastatin, pravastatin and rosuvastatin undergo minimal metabolism and are mainly cleared through biliary and urinary excretion [358, 359]. Almost all statins are substrates of hepatic uptake transporters while only rosuvastatin is undeniably a BCRP substrate (**Table I.6**). Particularly, rosuvastatin is recognized by the FDA and EMA as a BCRP clinical substrate probe once it has already revealed clinically significant interactions with critical drugs [354]. Thus, besides the non-clinical *in vitro* and *in vivo* studies demonstrating its interaction with BCRP and pharmacokinetic consequences, particularly regarding its biliary and systemic clearance (**Table I.6**), several clinical studies, including reverse translational studies, showed the impact of BCRP polymorphisms in the

pharmacokinetics and pharmacodynamics of rosuvastatin [300]. Focusing on healthy Chinese male volunteers, when controlling for CYP2C9 and SLCO1B1 variations, the BCRP c.421C.A variant significantly increased the AUC and decreased the apparent clearance of rosuvastatin [360]. Similarly a clinical study enrolling healthy Finnish volunteers showed that even in European subjects, the BCRP c.421C.A variant markedly affected rosuvastatin exposure [361]. More recent studies also corroborated these results, emphasizing the importance of BCRP in statins disposition, particularly due to their potential for rare, but life-threatening, adverse effects [362]. Because the BCRP c.421C.A variant does not represent a complete knockout of BCRP activity, it is likely that more profound changes may be observed if rosuvastatin is administered with a potent BCRP inhibitor/inducer or in the Jr(-a) population, which lacks BCRP altogether [363]. In fact, in clinical DDI studies, eltrombopag, ritonavir, and cyclosporine A, which are BCRP inhibitors, increased rosuvastatin plasma exposure up to 7-fold [310, 364]. However, it is important to remember that these perpetrators are also strong organic anion transporting polypeptide (OATP) inhibitors, a significant distribution and elimination pathway of rosuvastatin. These findings were a turnaround point to international guidelines which currently recommend screening new molecular entities for their inhibition or transport by BCRP to avoid DDIs [354, 365]. Nonetheless, both agencies recognize that drugs with high permeability and high solubility can be exempt from *in vivo* evaluation of BCRP interactions (as victim) because they tend to be well absorbed even if substrates of active transport.

In opposition to rosuvastatin that is ascribed as a systemic probe substrate of BCRP, sulfasalazine is an intestinal probe substrate [366]. After oral administration of sulfasalazine (20 mg) to *Bcrp(-/-)* mice, the plasma $AUC_{(0-\infty)}$ of the drug was 111-fold higher than that in WT mice (**Table I.6**), suggesting that BCRP is a major contributor to the reduced oral bioavailability of sulfasalazine (only 10 % in humans) and one of the causes for the highly variable absorption observed in humans. However, in humans, inconsistent findings have demonstrated that the pharmacokinetics of sulfasalazine may not be as sensitive to BCRP as it would be desirable. Most important is the high variability observed in sulfasalazine exposure (that can be as high as 81-fold), demanding a crossover study when investigating DDIs that involve sulfasalazine. In

addition, on one hand, the inhibition of BCRP increased intestinal absorption of sulfasalazine and consequently reduced its metabolism mediated by the *N*-acetyltransferase 2 and the production of sulfapyridine. As such, the metabolite-to-parent AUC ratio was proposed to be a more sensitive indicator of intestinal BCRP modulation in humans than parent sulfasalazine AUC, but only in intermediate and rapid acetylator phenotypes [367]. Furthermore, some pharmacogenetic clinical studies demonstrated that the SNP on human BCRP c.421C.A influences the pharmacokinetics of sulfasalazine: subjects with the ABCG2 c.34GG/c.421CA genotype exhibited an $AUC_{(0-\infty)}$ value 2.5-fold higher than those subjects with the reference c.34GG/c.421CC genotype, with a ranking of AUC values of ABCG2 c.421AA > CA > CC [367, 368]. In opposition, the co-administration of pantoprazole (BCRP inhibitor) with sulfasalazine did not significantly affect the pharmacokinetics of sulfasalazine or its metabolite. These findings suggest that other transporters may compensate the absorption of sulfasalazine (*e.g.* P-gp and MRP2) or its uptake from enterocytes (OATP2B1) and therefore the metabolite-to-parent AUC ratio should be used when performing DDI studies with sulfasalazine [369].

At this point it is important to highlight that FDA recently updated the guideline on DDIs, suggesting that only rosuvastatin and sulfasalazine should be seen as clinical BCRP substrate probes as their AUC increased more than 2-fold in ABCG c.421C.A genotype and they demonstrated to be transported by BCRP *in vitro* expression systems [366].

Nevertheless, multiple anticancer agents demonstrated to be BCRP substrates in *in vitro* and in *in vivo* assays performed with WT and KO animals (**Table I.6**). Among them, topotecan is the one with the most attractive clinical evidence to be used as a BCRP probe substrate particularly due to the influence of the BCRP c.421C.A SNP in its pharmacokinetics (1.3-fold increment of oral bioavailability in c.421C.A genotype vs. c.421C.C) [370, 371]. Important DDI clinical studies demonstrated that the co-administration of elacridar with topotecan to cancer patients increased its plasma exposure 3-fold, which is the upper limit of the possible increase in humans, where baseline bioavailability is 40 % [349]. Accordingly, topotecan is obviously attractive as a BCRP clinical probe substrate in oncological patients, although it is impractical for

routine use in healthy volunteers DDI studies due to its safety profile as a cytotoxic agent.

I.5.4.2. BCRP Inhibitors

BCRP inhibitors have been investigated in an attempt to reverse BCRP multidrug resistance in chemotherapy and improve the pharmacokinetic profiles of drugs that are its substrates. However, in contrast to P-gp, for which several compounds have been identified as inhibitors in clinical studies, only few suitable BCRP inhibitors have been reported *in vitro* and/or *in vivo* non-clinical studies (**Table 1.7**) currently presenting a questionable clinical relevance. For example, sulfasalazine did not exhibit pharmacokinetic alterations when co-administered with pantoprazole, a well-known inhibitor of BCRP in *in vitro* conditions; moreover, its plasma AUC increased 3.2-fold after sulfasalazine had been administered with high doses of curcumin to humans [338]. These are particularly unexpected findings, given the pre-clinical observations (111-fold change in AUC) and BCRP effect polymorphism effect (up to 4-fold change in AUC) regarding sulfasalazine and curcumin [337, 338]. On the other hand, when rosuvastatin and topotecan were co-administered with marketed drugs identified as BCRP inhibitors *in vitro* (omeprazole, pantoprazole, ritonavir and cyclosporine A), their pharmacokinetic/toxicological profiles were affected. However, these inhibitors are not specific for BCRP, and they also inhibit other transporters and enzymes [310].

In fact, identifying compounds that can be used as selective BCRP inhibitors in a clinical DDI study is challenging, as currently available compounds are not selective for BCRP and inhibit other transporters and drug-metabolizing enzymes [305, 310]. In this context, to identify potential clinical BCRP inhibitors based on non-clinical studies, it is suggested that the inhibitor concentration causing 50 % inhibition (IC_{50}) or inhibitory concentration (K_i , given as $IC_{50}/2$) must be lower than 10 μ M. For IC_{50} determination, a unidirectional assay (*e.g.* BL-AP) based on BCRP over-expressing cells and the probe substrate must be performed using different concentrations of inhibitor [354]. Furthermore $[I]_1/IC_{50}$ (where $[I]_1$ represents the mean steady-state maximum

concentration (C_{\max}) of total drug following administration of the highest proposed clinical dose) must be inferior to 1.0 [372].

The first reported BCRP inhibitor was fumitremorgin C, which, despite its high potency (**Table I.7**), cannot be used in clinical practice due to neurotoxicity. The most remarkable and selective BCRP inhibitor with no toxic effects in mice is a fumitremorgin C derivative, Ko143. However, it was recently published that its use in *in vivo* non-clinical studies should be precluded because it is unstable in rat plasma [373]. Similarly to fumitremorgin C, elacridar is a potent BCRP inhibitor but not chronically tolerated at the doses required to inhibit BCRP [374]. Particularly regarding elacridar, it was originally designed and developed as a reversal agent of P-gp and BCRP to overcome multidrug resistance. It is a 3rd generation P-gp inhibitor and a more potent inhibitor of P-gp than BCRP, requiring caution when analyzing the results. Furthermore, elacridar increases the oral bioavailability of topotecan by inhibiting BCRP, emerging as an intestinal inhibitor [375]. Although its use is not currently authorized in humans, elacridar is widely employed in *in vitro* and non-clinical *in vivo* studies (**Tables I.6** and **I.7**). Amongst other potent dual inhibitors of P-gp and BCRP is tariquidar, which acts, at low concentrations, as a selective inhibitor of P-gp, but, at higher concentrations (≤ 100 nM), as a dual P-gp/BCRP inhibitor. Thus, the *in vivo* specificity of tariquidar is dependent on both the concentration and the relative density and capacity of ABCB1 and ABCG2 [376].

Tyrosine kinase inhibitors stand out as potent BCRP inhibitors (**Table I.7**), with acceptable safety margins that can be used in healthy volunteers [372]. Moreover, they demonstrated usefulness as intestinal and systemic BCRP inhibitors with high BCRP selectivity. Indeed, the finding that several of these drugs efficiently block BCRP function has prompted the design of novel therapeutic drug-combination strategies [377]. Tyrosine kinase inhibitor-based compounds and their function as selective BCRP modulators were recently reviewed [378].

Table I.7 shows other two major pharmacological groups as *in vitro* BCRP inhibitors: proton pump inhibitors (PPI) and protease inhibitors of the human immunodeficiency virus (HIV) [336, 339, 379, 380, 340–347]. Two PPIs, pantoprazole and rabeprazole, fulfil the aforementioned criteria defined by international guidelines

to identify clinical BCRP inhibitors. Nevertheless, pre-clinical and clinical proof-of-concept studies have not yet been published. For instance, a retrospective study on plasma methotrexate concentrations of 171 cycles of high-dose methotrexate therapy in 74 patients supported the co-administration of PPIs (*i.e.*, omeprazole, lansoprazole, rabeprazole, pantoprazole) as a risk factor for delayed elimination, as well as, renal and liver dysfunction [343]. Although all four PPIs inhibited BCRP-mediated transport of methotrexate *in vitro* (**Table I.7**), IC_{50} values were higher than the plasma concentrations of PPIs and, therefore, the DDI is likely not solely a result of the PPI effects on BCRP-mediated methotrexate transport. In fact, PPIs are not as potent BCRP inhibitors as tyrosine kinase inhibitors, for which pre-clinical proof-of-concept has been demonstrated [333]. Indeed, pantoprazole marginally met the predefined criterion for systemic BCRP inhibition (it has an $[I_1]/IC_{50}$ of only 1.2). Regarding protease inhibitors of HIV, clinical studies supporting that anti-HIV drugs are BCRP inhibitors do not exist [378]. However, it is interesting to highlight that the protein expression of BCRP seems to be significantly lower in HIV⁺ naïve group compared to HIV⁻ naïve control group and it was partially restored to baseline levels in HIV⁺ subjects receiving antiretroviral therapy [381]. In addition, the influence of several anti-HIV drugs on BCRP activity was assessed *in vitro* by measuring the increase of the ABCG2 substrate pheophorbide A (PhA) accumulation in MDCK-BCRP cells using fumitremorgin C and Ko143 as reference compounds (IC_{50} of 0.47 and 0.01 μ M). The protease inhibitors lopinavir, nelfinavir, delavirdine, efavirenz, and saquinavir showed to be potent BCRP inhibitors with IC_{50} values of 7.66, 13.5, 18.7, 20.6, and 27.4 μ M, respectively [339]. Nevirapine and zidovudine showed low inhibition, whereas indinavir, didanosine, emtricitabine, lamivudine, stavudine, tenofovir, and zalcitabine had no inhibitory effect [339, 382, 383]. Importantly, HIV-protease inhibitors that inhibit BCRP are not substrates of this transporter [382].

In addition, it is important to highlight that several commonly used antipsychotic drugs have exhibited various degrees of inhibitory effects on BCRP activity. Among them, risperidone (IC_{50} = 38.1 μ M), clozapine (IC_{50} = 42.0 μ M), paliperidone (IC_{50} = 51.0 μ M), chlorpromazine (IC_{50} = 52.2 μ M) and quetiapine (IC_{50} = 66.1 μ M) clearly exhibited moderate to mild inhibitory effects on BCRP activity and its transport

efficiency (**Table I.7**), while olanzapine ($IC_{50} > 100 \mu M$) and haloperidol ($IC_{50} > 100 \mu M$) exhibited no apparent inhibitory effect on BCRP activity. Taking these data into account, risperidone was the most potent antipsychotic drug inhibitor of BCRP [345]. These results were, up to this day, demonstrated in cell lines over-expressing BCRP (**Table I.7**), but it is expected that several antipsychotics at clinical circumstances may inhibit BCRP activity and cause DDIs with BCRP substrates [384]. Aripiprazole also demonstrated to inhibit BCRP [385].

Despite the aforementioned pre-clinical and clinical evidence, it is interesting to note that FDA suggests the immunosuppressant cyclosporine A and the platelet-increasing agent eltrombopag as clinical BCRP inhibitors. Cyclosporine A has been recognized as a potent inhibitor of BCRP for a long time, with an IC_{50} value for BCRP inhibition of $4.3 \mu M$ [346]. Nevertheless, it also inhibits CYP3A4 and compromises the immunological system if chronically used, becoming, hence, impractical [372]. Regarding eltrombopag, pre-clinical and clinical studies clearly support that it inhibits BCRP, triggering DDIs with pharmacokinetic and pharmacodynamic consequences that compromise the safety and efficacy of rosuvastatin [364, 386]. Curcumin has been also suggested as a clinical BCRP inhibitor, probably due to its relevant effect on pharmacokinetics of sulfasalazine in rodents (**Table I.7**), and clinical investigations [338, 387, 388].

Direct clinical evidence of the contribution of BCRP inhibition to DDIs is limited by cross-specificity with P-gp and CYP3A substrates and inhibitors, and by the activity of other transporters such as OATPs. In fact, hepatic BCRP inhibition may decrease biliary excretion and increase liver/plasma concentrations ratio, enhancing drug availability in hepatocytes and, consequently, its metabolism. In cases where metabolites are active and toxic, this may not only compromise the therapeutic effect but also increase drug toxicity. Although BCRP is involved in a number of clinically relevant DDIs, none of the cited clinical probe substrates or inhibitors is truly specific for this transporter. The current recommendation for investigating BCRP-related DDIs involves oral sulfasalazine for intestinal BCRP, oral rosuvastatin for both intestinal and hepatic BCRP, and intravenous rosuvastatin for hepatic BCRP only, with curcumin or eltrombopag or cyclosporine A as reference inhibitors [366].

I.5.4.3. BCRP Inducers

Regarding BCRP inducers, few have been reported in literature until today (**Table I.8**). In fact, due to its physiological and pathophysiological functions, BCRP is a good therapeutic target to be inhibited instead of being induced. Inducing the gene expression of *ABCG2* and the biosynthesis of functional BCRP seem to be therapeutically useful only for the possible treatment of gout [389]; probably, for this reason, research of BCRP inducers is not as explored as inhibitors. Gout is a consequence of elevated serum levels of urate, whose elimination is dependent of the BCRP transporter and has a strong genetic influence. The common BCRP c.421C.A variant has been shown to be significantly associated with elevated serum uric acid levels and the subjects carrying that SNP are likely at an increased risk for developing gout [390–393].

However, it is noteworthy that imatinib is a substrate of BCRP (**Table I.8**), but it also induces the same transporter. The continuous exposure of imatinib in Caco-2 cells upregulated the expression of BCRP (approximately 17-fold) and P-gp (approximately 5-fold), and decreased 50 % of the accumulation of imatinib into the cells [394]. Since both BCRP and P-gp are expressed in the gastrointestinal tract, it might be anticipated that drug-induced upregulation of these intestinal pumps can reduce the oral bioavailability of imatinib or other BCRP substrates after chronic treatment of imatinib [395]. In fact, this observation enlarges many other drugs currently used in clinical practice as summarized in **Table I.8** [396–401]. As it will be focused in the following section, this inducing effect on BCRP expression has been associated with the development of mechanisms of resistance against CNS-acting drugs, whose access into the brain becomes compromised due to BCRP expression at the BBB.

Table I.8 Example of drugs that demonstrated to be BCRP inducers. The principal experimental conditions and results are presented.

BCRP Inducer	Experimental Conditions and Main Results	Ref.
5-Fluorouracil	For 5 consecutive days, rats were orally administered with 5-fluorouracil (30 mg/kg/day). The mRNA and protein expression levels of P-gp and BCRP transporters in each intestinal segment were determined using quantitative real-time PCR and Western blotting, respectively. Bcrp protein levels of were 2.6-fold higher in the upper intestinal segment in relation to those found in the same region of the non-treated group. In the remaining intestinal segments, the levels of Bcrp remained unaffected by 5-fluorouracil.	[396]
Elvitegravir Maraviroc	LS180 human adenocarcinoma cells were treated with different antiretroviral drugs for three days in order to evaluate their effect on BCRP mRNA expression. These levels were quantified by real-time RT-PCR. BCRP mRNA was weakly induced by elvitegravir (1.6+0.4 at 10 mM,) and maraviroc (1.7+0.4 at 1 mM).	[397]
Etravirine	The <i>in vitro</i> induction assay was performed on LS180 human adenocarcinoma cells treated with etravirine at 0.1 and 1.0 μ M. At the end, the expression of mRNA BCRP was quantified by real-time RT-PCR. At 1.0 μ M, etravirine increased the expression of BCRP mRNA 3.5 times in relation to untreated cells.	[398]
Imatinib	Caco-2 cells were treated every day with imatinib (10 μ M) up to 100 days. Gene expression increased significantly after 3 days of exposure to imatinib, with an induction of approximately 17 times	[394]
Oltipraz Phenobarbital Rifampicin	Human hepatocytes were treated with several xenobiotics for 72 h. mRNA levels were determined by real-time RT-PCR. Oltipraz, phenobarbital and rifampicin increased, the BCRP gene expression 2.6, 3.7 and 2.7 times respectively.	[399]
Phenobarbital Venlafaxine Promazine	Several compounds were tested on human hepatocytes for 48 h, at the concentration of 5 μ M; quantitative analysis of BCRP mRNA expression was performed by real-time RT-PCR. Increases in BCRP mRNA expression of 3.4, 1.8 and 1.5 were obtained after incubation with phenobarbital, venlafaxine and promazine, respectively, in comparison with DMSO-treated cells.	[400]
Telaprevir	The inducing capacity of telaprevir on BCRP was evaluated on LS180 human adenocarcinoma cells. After seeding and culturing for 3 days, the cells were treated with telaprevir (1, 3, 10 and 30 μ M) for 4 consecutive days. Rifampicin (20 μ M) was used as a positive control. A quantitative analysis of mRNA expression was performed by real-time RT-PCR. Telaprevir induced BCRP mRNA levels at 10 and 30 μ M.	[401]

BCRP, *breast cancer resistance protein*; DMSO, *dimethyl sulfoxide*; HT-29DxR, *HT-29 doxorubicin-resistant colon cancer cells*; P-gp, *P-glycoprotein*; RT-PCR, *reverse transcription polymerase chain reaction*; WT, *wild type*.

I.5.5. BCRP AND EPILEPSY

As explored in **Section I.2.4.**, the two key theories that have been advocated to explain medical refractoriness of epilepsy are based on the target hypothesis and the multidrug-transporter hypothesis [150]. While the target hypothesis postulates that acquired alterations in the structure and/or functionality of target ion channels and neurotransmitter receptors result in the loss of AED affinity and efficacy; the multidrug-transporter hypothesis suggests that an over-expression of efflux proteins at the BBB restricts drug uptake into the brain leading to insufficient AED levels at their target sites [77, 402, 403].

The first evidence of the role of ABC efflux transporters in AED pharmacoresistance was provided by Tishler and collaborators, who detected high expression of P-gp in capillary endothelial cells isolated from the brain tissue of refractory epileptic patients [156]. Since then, the over-expression of P-gp and other ABC efflux transporters such as BCRP and MRP have been confirmed by *in vitro*, *in vivo* and clinical studies [404, 405]. Importantly, although for P-gp this is already supported by clinical investigations, the clinical information regarding other transporters, namely BCRP, is scarce, controversial and frequently inconclusive mainly because the number of patients is small [406–409]. Only recently, it was demonstrated the significant up-regulation of BCRP in epileptic tissue from patients with mesial temporal lobe epilepsy as compared to non-epileptic controls in which tissues were dissected from tumor periphery and autopsy tissues [409]. This means that, during chronic/prolonged treatment, the induction effect of AEDs on the expression of efflux transporters and the morphological alterations triggered by successive seizures restrict the BBB and blood-spinal cord barrier even more, hampering the entry of AEDs into the biophase (*i.e.* epileptogenic focus). Consequently, patients can successfully respond to AEDs at the beginning of the treatment, but the probability of developing drug-resistant epilepsy enhances as the treatment is prolonged. Nevertheless, although the influence of BCRP on the brain disposition of AEDs is not as clear as that of P-gp, it must be kept in mind that BCRP expression in other organs, namely small intestine and liver, is highly probable to determine the pharmacokinetics and pharmacodynamics of AEDs. Consistent with

these findings are the unquestionable *in vitro* results reported supporting that some AEDs are BCRP substrates (*e.g.* lamotrigine). In this context, the co-administration of BCRP inhibitors is expected to enhance the brain penetration and efficacy of AEDs.

Until this day, only the AED lamotrigine demonstrated to be a BCRP substrate, applying MDCK-II cells transfected with murine and human efflux transporters. A marked Bcrp-mediated transport was observed in these cells (in the presence of tariquidar), which was completely inhibited by Ko143 [410]. This observation has important consequence for epilepsy treatment because in AED resistant patients the expression of both transporters is markedly increased. Since lamotrigine is a substrate of both human P-gp and BCRP, the over-expression of these transporters may synergistically decrease its brain concentrations, thus causing or contributing to pharmacoresistance [410]. More pre-clinical and clinical experiments should be performed, in order to understand the impact of this transporter in the pharmacokinetics and pharmacodynamics of other AEDs, namely those from 2nd and 3rd generations (*e.g.* lacosamide, levetiracetam, zonisamide) that will be investigated in the present thesis.

CHAPTER II

OBJECTIVES



II.1. GENERAL OBJECTIVES

In spite of all the efforts and advances regarding the scientific knowledge of physiopathology and drug discovery, pharmacoresistance continues to represent a challenge for effective treatments, since the organism has the capacity to develop physiological defense mechanisms that prevent the access of external agents, namely drugs, to the target organ. Poor tolerability and adverse effects are other concerns that can also lead to drug withdrawal and treatment changes.

Pharmacoresistance is observed in one-third of the epileptic patients, reinforcing that epilepsy treatment remains an unmet clinical need, despite the currently available AEDs. Consequently, it is important to investigate the mechanisms inherent to pharmacoresistant epilepsy and test new approaches to overcome the restrictiveness of the BBB. Even though the expression of the ABC efflux transporter BCRP in epilepsy is increased as the disease progresses, its interaction with AEDs remains unclear, namely for lacosamide, levetiracetam and zonisamide.

Therefore, the main objective of the present thesis was to develop an *in vitro/in vivo* combo-strategy to overcome the BBB making use of IN administration, and assess whether this route could circumvent the impact of BCRP in AEDs brain delivery. The olfactory epithelium is the unique part of our body that allows the direct contact of external environment with the brain and, hence, direct nose-to-brain delivery is expected to be a powerful strategy to circumvent the BBB and BCRP activity. This is expected to improve the delivery of lacosamide, levetiracetam and zonisamide into the brain, with probable avoidance of pharmacoresistant mechanisms, and decrease peripheral systemic exposure.

Lacosamide, levetiracetam and zonisamide were herein selected for investigation because they are new-generation AEDs widely used in clinical practice, as first-line and adjuvant treatments. In particular, levetiracetam is the most frequently administered AED nowadays, even though with inter- and intra-individual variability. In turn, besides their unclear interaction with BCRP, lacosamide and zonisamide are metabolized by polymorphic enzymes and highly susceptible to develop DDIs that may change AEDs

systemic and brain exposures. By avoiding an intestinal/hepatic first-pass effect, IN administration will decrease the potential of AEDs to interact with other drugs and reduce response variability. Complementarily, our choice resulted from the fact that lacosamide, levetiracetam and zonisamide are indicated not only for epilepsy but also in seizures inherent to other pathologies, requiring pharmacological treatments that quickly reach the CNS, such as *status epilepticus*. IV administration is the current option for this clinical situation, but it is invasive and unavailable for zonisamide. As a non-invasive route, IN administration gains momentum since it may attain effective brain concentrations in a few minutes with lower peripheral systemic exposure.

II.2. SPECIFIC OBJECTIVES

The following specific objectives were established:

- To develop and fully validate an analytical technique for the simultaneous quantification of lacosamide, levetiracetam and zonisamide in human plasma, using high performance liquid chromatography (HPLC) with diode array detection (DAD).
- To adopt, validate and implement an HPLC-DAD technique to quantify lacosamide, levetiracetam and zonisamide in plasma, brain, lung and kidney tissue homogenates of mice.
- To investigate whether the selected AEDs are BCRP substrates or inhibitors, resorting to *in vitro* bidirectional and accumulation studies, respectively. This was performed with MCDK-II and MDCK-BCRP cell lines.
- To determine the *in vitro* apparent permeability (P_{app}) of lacosamide, levetiracetam and zonisamide through human nasal septum (RPMI-2650) cell monolayers and establishment of a correlation with the results obtained from *in vivo* studies.

- To investigate the influence of lacosamide, levetiracetam and zonisamide and the thermoreversible gel to be used in the *in vivo* studies on the viability of RPMI-2650 and pulmonary adenocarcinoma (Calu-3) cells.

- To characterize the *in vivo* pharmacokinetics of lacosamide, levetiracetam and zonisamide following single IN and IV administration in mice to determine drug targeting efficiency (DTE) and direct transport percentage (DTP). Zonisamide was also orally administered, as this is the only clinically recommended administration route.

- To assess the impact of BCRP inhibition mediated by elacridar on brain drug distribution after IN and IV administration of the previously identified BCRP substrate(s).

CHAPTER III

ANALYTICAL DRUG QUANTIFICATION



III.1. INTRODUCTION

Affecting more than 50 million people worldwide, epilepsy is associated with high morbidity and mortality rates [411, 412]. Furthermore 20–40 % of the patients with idiopathic generalized epilepsy and up to 60 % of patients with focal epilepsies do not successfully respond to AEDs therapy [413]. Due to the high inter- and intra-individual variability observed, the dose of administered AEDs does not mandatorily correlate with drugs effects and, therefore, epileptic patients under therapy with AEDs should be monitored through video-electroencephalography and plasma drug concentrations. Even the new AEDs, characterized by wider therapeutic plasma ranges and less severe side effects than those from first generation, should be monitored due to their high inter-individual variability. At this point, has promoted the concept of "individual therapeutic concentrations" [74, 414], employing plasma drug concentrations in parallel with clinical observations and video-electroencephalography for a personalized treatment. Thus, regarding new AEDs, therapeutic drug monitoring based on plasma drug concentrations is extremely important to assess patient compliance and manage suspected toxicity. Moreover, pregnancy and puerperium are states where pharmacokinetic changes are more pronounced and faster than other life-period, requiring AED adjustments that guarantee seizures control in equilibrium with no toxic effects.

In this context, plasma drug concentrations monitoring is fully justified for new-generation AEDs, namely, levetiracetam, lacosamide and zonisamide, in order to personalize the pharmacotherapy. Moreover, the high inter-individual variability resulting from the metabolism of lacosamide and zonisamide, mainly mediated by hepatic CYP 450, is the major reason to perform an individualized monitoring of plasma drug concentrations. Variability in metabolism has been ascribed to impaired organ function, genetic factors (polymorphic enzymes, e.g., CYP2C9 and CYP2C19), or DDIs particularly with zonisamide, which plasma levels seem to be reduced by co-medication with enzyme-inducing AEDs and enhanced by lamotrigine [415]. Therefore, it may be necessary to modify zonisamide doses based on concomitant AEDs. On the other hand, levetiracetam, a third-generation AED mainly eliminated by renal route

shows significant variations and 'on-need' monitoring has recently been demonstrated to be useful, including during pregnancy [416–418] and renal failure [415].

The aforementioned new AEDs may be administered in mono or polytherapy to epileptic patients, including the pediatric ones [419–421]. In particular, it was recently stated that the administration of levetiracetam and lacosamide to pediatric patients in *status epilepticus* seems to be efficacious [225]. Therefore, monitoring AEDs plasma concentrations simultaneously within one sample is of utmost relevance, but requires HPLC techniques. To the best of our knowledge, to this day, there are only two developed and fully validated analytical methods that simultaneously quantify levetiracetam, lacosamide and zonisamide in a single chromatographic run [422, 423]; however, one of them involves postmortem plasma samples [423] and both of them require liquid chromatography–mass spectrometry (LC–MS/MS) methods. Although their high sensitivity and selectivity are undeniable, they may also conduct to some pitfalls [424].

Thus, we herein propose the first HPLC method with diode array detection (DAD) to simultaneously, accurately and precisely quantify levetiracetam, lacosamide and zonisamide in human plasma.

III.2. MATERIAL & METHODS

III.2.1. CHEMICALS & REAGENTS

Lacosamide solution, levetiracetam, zonisamide and antipyrine (ref. A5882), used as internal standard (IS), were purchased from Sigma-Aldrich (MO, USA). Methanol, acetonitrile (both HPLC gradient grade) and ethyl acetate were purchased from Thermo Fisher Scientific (Loughborough, UK). Ultra-pure water (HPLC, 18.2 MΩ.cm) was obtained by means of a Milli-Q water apparatus from Millipore (MA, USA). Reagents used during method optimization, such as sodium dihydrogen phosphate dehydrate, 37 % fuming hydrochloric acid and triethylamine, were acquired from Merck KGaA (Darmstadt, Germany).

Blank human plasma samples from healthy donors were kindly provided by the Portuguese Blood Institute after written consent of each subject.

III.2.2. PREPARATION OF SOLUTIONS

III.2.2.1. Stock & Working Sample Solutions

Stock solutions of levetiracetam and zonisamide (4 mg/mL) were individually prepared by dissolving each compound in pure acetonitrile and then appropriately diluted with acetonitrile in order to achieve intermediate solutions of 2 mg/mL and 100 µg/mL. Stock and intermediate solutions of each AED were combined and diluted with acetonitrile to obtain two sets of combined working solutions that were used to spike human plasma samples. One set, used to achieve the calibration standard samples, was prepared at final concentrations of 25, 50, 75, 100, 200, 300 and 400 µg/mL for levetiracetam, 5, 10, 25, 50, 150, 250 and 300 µg/mL for lacosamide and 5, 10, 50, 100, 250, 400 and 500 µg/mL for zonisamide. The second set, used to prepare the quality control (QC) samples, included four spiking solutions with the final concentrations of 5, 20, 100 and 270 µg/mL for lacosamide, 25, 60, 150 and 360 µg/mL for levetiracetam and 5, 20, 200 and 450 µg/mL for zonisamide. Another spiking working sample composed of 1.5, 2.0 and 2.5 mg/mL of lacosamide, levetiracetam and zonisamide, respectively, was used to evaluate the dilution effect.

The stock solution of IS (antipyrine) was prepared at 1 mg/mL in acetonitrile and daily diluted to prepare a working standard solution at 50 µg/mL.

All stock and intermediate standard solutions were stored in amber vials at 4 °C and were found to be stable for up to 30 days. The working standard solutions were stored at 4 °C in Eppendorf® Tubes.

III.2.2.2. Calibration Standards & QC Samples

Aliquots (10 μ L) of the appropriate mixed working standard solutions were further added to blank human plasma (100 μ L) to obtain calibration standards and QC samples. Calibration standards spiked plasma were prepared by spiking blank plasma at seven different concentration levels: 2.5, 5.0, 7.5, 10.0, 20.0, 30.0 and 40.0 μ g/mL for levetiracetam; 0.5, 1.0, 2.5, 5.0, 15.0, 25.0 and 30.0 μ g/mL for lacosamide and 0.5, 1.0, 5.0, 10.0, 25.0, 40.0 and 50.0 μ g/mL for zonisamide.

The QC samples were prepared independently, in an analogous manner as the calibration standards, using the second set of aforementioned working solutions. Thus, QC samples were prepared at the lower limit of quantification (LLOQ) and three concentration levels – low (QC₁), medium (QC₂) and high (QC₃) – representative of the entire calibration ranges. The nominal concentrations were, for levetiracetam, lacosamide and zonisamide as follow: 2.5, 0.5 and 0.5 μ g/mL in LLOQ; 6.0, 2.0 and 2.0 μ g/mL in QC₁; 15.0, 10.0 and 20.0 μ g/mL in QC₂; and 36.0, 27.0 and 45.0 μ g/mL in QC₃. Finally, a QC sample was prepared (QC_{Dil}) at a concentration five-times higher than the upper limit of calibration curve in order to evaluate the sample dilution effect (1:5).

III.2.3. SAMPLE PREPARATION

Cleanup of human plasma samples was herein developed and optimized in order to achieve the best recovery yields for all the three AEDs. Briefly, the final sample preparation protocol combined a liquid–liquid extraction (LLE) procedure followed by organic solvent evaporation and solid residue reconstitution. Plasma samples (standard calibration samples and QC samples), when stored at -30 °C, were thawed on the extraction day at room temperature, followed by a fast centrifugation of 15 seconds at 12,045 *g* to ensure precipitation of any solid particle. To each spiked plasma aliquot (100 μ L), 40 μ L of methanol, 10 μ L of IS working solution and 1 mL of ethyl acetate were added. Then the mixture was vortex-mixed for 30 s and centrifuged at 12,045 *g* for 3 min in order to extract the drugs and the IS. The resulting upper organic

layer was transferred to a clean glass tube and the aqueous layer was re-extracted using the aforementioned LLE procedure. To concentrate the analytes, both organic phases were combined and evaporated to dryness under a gentle nitrogen stream at 45 °C, and the resulting solid residue was reconstituted with 100 µL of a mixture of water and acetonitrile (90:10, v/v) by vortex-mixing for approximately 1 min and placing in an ultrasonic bath at room temperature for approximately 1 min. Afterward, the extracts were transferred to a 0.22 µm Costar® Spin-X®R centrifugal filter (Corning, Inc., NY, USA), centrifuged at 12,045 *g* for 2 min and 20 µL of the final filtered samples were injected into the HPLC system.

III.2.4. CHROMATOGRAPHIC SYSTEM & CONDITIONS

A Shimadzu HPLC system (Shimadzu Corporation, Kyoto, Japan) equipped with a solvent delivery model (LC-20A), a degasser (DGU-20A5), an autosampler (SIL-20AHT), a column oven (CTO-10ASVP) and DAD (SPD-M20A) was used to perform the chromatographic analysis herein proposed. The HPLC apparatus and data acquisition were controlled by LCsolution software (Shimadzu Corporation).

The chromatographic separation of levetiracetam, lacosamide, zonisamide and IS was accomplished in 14 min, using a reversed-phase LiChroCART® Purospher® Star C₁₈ column (55x4 mm, 3 µm particle size; Merck KGaA, Darmstadt, Germany) thermostated at 40 °C. The mobile phase was composed of water and acetonitrile pumped at a flow rate of 1.0 mL/min under the following time gradient elution program: during the first 10 min of the run, a linear gradient was applied by varying the proportion of acetonitrile from 3 to 10 % and, subsequently, restoring it to 3 % within 2 min. This was maintained until the end of the run, leading to a total run time analysis of 14 min. The detection wavelengths of the AEDs and the IS were set after optimization at 239 nm for zonisamide and 220 nm for the remaining compounds.

III.2.5. METHOD VALIDATION

Method validation is a crucial step in bioanalysis as it demonstrates the ability of developed methods to provide reliable and reproducible data and thus their suitability for the intended use [425, 426].

Therefore, once developed, the method was fully validated considering the acceptance criteria defined by the international guidelines for bioanalytical methods validation published in 2013 and 2011 by FDA and EMA as well as other international recommendations for bioanalytical method validation [427, 428] according to the following validation parameters.

III.2.5.1. Selectivity

Selectivity is defined as the ability of an analytical method to unambiguously quantify and differentiate the analyte(s) of interest from other interfering components that may be expected to be present in the sample, typically, endogenous biological matrix substances, metabolites, degradation products or co-administered drugs [425, 429]. Even though the FDA guidance does not provide specific recommendations for selectivity, EMA guideline states that the absence of interfering components is accepted when the peak response in blank matrices at the retention time of the analyte(s) is less than 20 % of the response for the LLOQ samples, and lower than 5 % for the IS [427, 428].

To assess the selectivity of the method, blank samples from six different subjects were processed using the proposed preparation method and analyzed to evaluate the potential chromatographic interference from endogenous compounds at the retention time windows of lacosamide, levetiracetam, zonisamide and IS. Furthermore, interference from other commonly prescribed drugs was also tested and included acetylsalicylic acid, amitriptyline, atenolol, carbamazepine, carbamazepine-10,11-epoxide, chloramphenicol, chlorpromazine, diazepam, eslicarbazepine, fluoxetine, furosemide, hydrochlorothiazide, ibuprofen, imipramine, ketoprofen, lamotrigine,

lorazepam, meloxicam, metoprolol, mirtazapine, naproxen, oxcarbazepine, paracetamol, paroxetine, phenytoin, piroxicam, ranitidine, retigabine, risperidone, sertraline, theophylline, tamoxifen, topiramate, trazodone, venlafaxine and verapamil.

III.2.5.2. Linearity of the Calibration Curve

The calibration curve was prepared in the human plasma matrix using seven standards, and defined for each AED in order to cover the expected therapeutic range concentrations [430–432]. Five calibration curves were prepared and analyzed on five consecutive days by plotting the peak area ratios against the corresponding nominal plasma concentrations. The peak area ratios were calculated as the ratio between the peak area from the analyte and that of the IS.

The homoscedasticity of the data obtained for standard calibration samples was assessed in unweighted linear regression by plotting residuals *versus* concentration and by applying an F-test in accordance to [433]. The weighting factor was chosen according to the percentage of relative error (RE), which compares the experimental concentration estimated by the equation constructed with each weighted factor with the nominal concentration. Herein, the sum of absolute % RE values was used as indicator of goodness of fit in the evaluation of the effectiveness of a weighting factor; the best factor was the one with lowest value of % RE sum.

Thus, after evaluating the best fit of peak area ratios *versus* concentration for all AEDs under investigation, the weighted linear regression was performed on calibration data using $1/x^2$ as weighting factor as it was the one with the best fit.

III.2.5.3. Precision & Accuracy

Intraday and interday precision and accuracy were assessed by analyzing the three QC samples (QC₁, QC₂ and QC₃). The intraday precision and accuracy were determined by analyzing each QC sample five-times on the same day while the interday data were

obtained by analyzing each QC sample on five different days. The acceptance criterion for precision was a coefficient of variation (CV, 100 % standard deviation/mean) equal to or lower than 15 %. Accuracy was determined by comparing the estimated concentrations of the three QC samples with their nominal concentrations. The acceptance criterion for accuracy was a % RE value within ± 15 %. Again, RE corresponds to the percentage of the deviation from nominal value in relation to the nominal concentration.

III.2.5.4. LLOQ & Limit of Detection

The LLOQ was defined as the lowest concentration on the calibration curve that can be measured with precision (expressed as % CV) not exceeding 20 % and accuracy (expressed as % RE) within ± 20 %. The LLOQ was evaluated by analyzing plasma samples independently prepared in five replicates ($n = 5$).

Limit of detection (LOD) corresponds to the lowest concentration which signal can be distinguished from the noise level. Through the analysis of plasma samples fortified with the three AEDs at known concentrations successively diluted, the minimum level at which the analytes were reliably detected was defined as the LOD.

III.2.5.5. Sample Dilution

In order to ensure that human plasma samples with concentrations higher than the upper limit of calibration curve of the calibration range could be accurately quantified after dilution with human blank plasma, an appropriate plasma diluted QC sample was used and the dilution effect of 1:5 was investigated.

For this purpose, the spiked samples were diluted with blank drug-free plasma five-times and 100 μ L aliquots were subsequently processed according to the sample preparation procedure and analyzed by the proposed HPLC-DAD method. The intra- and interday accuracy and precision of a five-fold dilution were investigated in human

plasma using diluted QC samples ($n = 5$). The acceptance criteria for accuracy and precision were an RE value within $\pm 15\%$ and a $CV \leq 15\%$, respectively.

III.2.5.6. Recovery

Drugs absolute recovery from human plasma samples was determined comparing the analyte peak area from QC samples submitted to the pretreatment process herein proposed with the areas obtained from non-extracted solutions at the same nominal concentrations. This procedure was performed with QC₁, QC₂ and QC₃ samples and repeated five-times ($n = 5$); in addition, the same protocol was employed for IS.

III.2.5.7. Carry-over Effect

During validation, carry-over was assessed by injecting blank samples after the upper limit of the calibration curve. Acceptability criteria were established in accordance to EMA guideline [427], which defines that the carry-over in the blank sample following the high concentration standard should not be greater than 20 % of LLOQ and 5 % of the IS.

III.2.5.8. Stability

Stability was assessed by comparing the data of QC₁ and QC₃ samples ($n = 5$) analyzed before (reference samples) and after being exposed to the conditions for stability assessment (stability samples). Stability conditions reflected the conditions of sample storage, handling and analysis. The stability of lacosamide, levetiracetam and zonisamide in human plasma was assessed at room temperature for 3 h, at 4 °C for 24 h and at -30 °C for 30 days to simulate sample handling and storage time in the freezer before sample analysis. Freeze-thaw stability was also evaluated by successive cycles

of freezing and thawing. Three complete freeze-thaw cycles were performed with QC₁ and QC₃ samples frozen at -30 °C for 24 h per cycle and thawed unassisted at room temperature. To resemble the residence time in the autosampler before analysis, the stability of the three AEDs was also studied at room temperature for 2 h and at 4 °C during 24 h in the reconstitution solvent.

Results obtained from the analysis of the stored samples were compared with those that were obtained from the analysis of freshly prepared samples spiked with the analytes in human plasma. Stability acceptance criteria included a stability/reference samples ratio between 85 and 115 % and a RE within ± 15 %.

III.2.6. METHOD APPLICATION TO REAL SAMPLES FROM EPILEPTIC PATIENTS

The method herein optimized and validated was then used to identify and quantify levetiracetam, lacosamide and zonisamide in plasma samples of epileptic patients treated with each AED. Blood samples were collected to heparin–lithium tubes and centrifuged, for 10 min at 2088 *g* (4 °C) to obtain plasma, which was immediately separated and frozen at -30 °C prior to the analysis. Incurred sample reanalysis was conducted by reanalyzing 75 % of study samples in separate runs at different days. According to EMA guideline, the percent difference between the initial concentration and the concentration measured during the repeat analysis should not be greater than 20 % of their mean for at least 67 % of the samples [427].

III.3. RESULTS & DISCUSSION

III.3.1. METHOD DEVELOPMENT

III. 3.1.1. Chromatographic Separation of the Analytes

In order to achieve the best chromatographic conditions to separate all the analytes in the reversed-phase LiChroCART® Purospher® Star C₁₈ column, individual and combined drug solutions were directly injected in the HPLC-DAD system. A 20 min constant gradient (1 mL/min) was first established, initiating with 100 % water and finalizing at 100 % of methanol. Levetiracetam was detected with a retention time of approximately 6.42 min, followed by zonisamide and lacosamide (retention times of 7.87 and 9.30 min, respectively). In theory, this means that the first AED would require at least 30 % of methanol to be eluted. Therefore, the first investigated mobile phase was composed of a water–methanol–acetonitrile (64:30:6, v/v/v) solution, pumped at 1 mL/min at 40 °C. Under these conditions, the retention times of levetiracetam, zonisamide and lacosamide were 0.70 min, 1.09 min and 1.38 min, respectively. These findings suggest that particularly levetiracetam and zonisamide weakly interact with the C₁₈ stationary phase probably due to their considerable hydrophilicity. As aqueous endogenous human plasma interferences are expected to elute at initial times, the percentage of the organic methanol incorporated in the mobile phase was reduced to 20 and 10 %, while acetonitrile remained unchanged. The retention times of the analytes increased, but the peak shape, particularly those of levetiracetam and lacosamide, revealed an increased bandwidth, compromising their symmetry and resolution (**Table III.1**).

As several articles used phosphate buffer [434–439] or ammonium acetate buffer in mobile phase [440] to quantify lacosamide, levetiracetam or zonisamide, the influence of mobile phase pH on peak shape, resolution and retention times was evaluated. Even though a pH range between 3.5 and 9.0 was tested, no differences were observed in those chromatographic parameters. Furthermore, as the AEDs

include amine basic groups that may interact with the free silanol groups of silica-based column, thereby compromising their fast elution from the stationary phase, triethylamine was integrated in the mobile phase as an amine additive to compete with the drugs in an attempt to reduce the peak tailing effect [441]. However, no differences were found, and therefore the authors tested a mobile phase composed of acetonitrile and water at the proportion of 1:9 (v/v), which yielded symmetric and sharp peaks for zonisamide and lacosamide (**Table III.1**). Under these conditions, the asymmetry factor of levetiracetam is 1.329, which, together with its poor resolution (0.492), may compromise its accurate quantification. Thus, in order to enhance the symmetry and resolution of the levetiracetam peak, the composition of the mobile phase was slightly modified to the gradient mode described in the **Section III.2.4**, revealing an optimal symmetry and resolution among all three AEDs and the IS (**Table III.1**).

Table III.1 Chromatographic characteristics of the peaks corresponding to levetiracetam (LEV), zonisamide (ZNS) and lacosamide (LAC) under the chromatographic conditions tested during method development.

Mobile Phase Composition	AED	Rt (min)	Peak Area	As ^a	Rs ^b	W
H ₂ O/MeOH/ACN (64:30:6, v/v/v)	LEV	0.728	343437	1.532	1.336	0.121
	ZNS	1.096	768246	1.231	2.937	0.130
	LAC	1.381	256286	1.320	1.149	0.150
H ₂ O/MeOH/ACN (74:20:6, v/v/v)	LEV	0.883	343285	1.414	0.645	0.133
	ZNS	1.727	831511	1.163	5.474	0.176
	LAC	2.304	403325	0.895	2.647	0.260
H ₂ O/MeOH/ACN (84:10:6, v/v/v)	LEV	1.209	337651	1.308	4.066	0.154
	ZNS	3.200	835830	1.050	2.470	0.271
	LAC	4.480	391004	1.321	3.585	0.443
H ₂ O/ACN (90:10, v/v)	LEV	1.195	337894	1.329	0.492	0.147
	ZNS	4.273	836008	1.012	12.657	0.339
	LAC	5.031	309588	1.078	2.031	0.407
0 min: 3 % ACN	LEV	3.716	332385	1.132	3.7075	0.366
10 min: 10 % ACN	ZNS	9.336	830014	0.960	12.735	0.516
12 min: 3 % ACN	LAC	12.126	307493	1.017	5.378	0.521
14 min: 3 % ACN						

^aCalculated in accordance with the equation: $W_{0.05}/2f$, where $W_{0.05}$ is the width of the peak at 5 % height and f is the distance from the peak maximum to the leading edge of the peak, the distance being measured at a point 5 % of the peak height from the baseline.

^bCalculated in accordance with the equation: $[(Rt_2 - Rt_1)/0.5(W_1 + W_2)]$, where Rt_2 and Rt_1 correspond to the retention times of two adjacent peaks ($Rt_2 > Rt_1$) while W_1 and W_2 correspond to their width.

ACN: Acetonitrile; As: Symmetry factor; H₂O: Water; MeOH: Methanol; Rs: Resolution; Rt: Retention time; W: Peak width defined by United States Pharmacopeia.

At this point, several structurally related compounds were tested for potential use as IS, among which antipyrine was selected as it presented a retention time between zonisamide and lacosamide as well as similar recovery values from those of the AEDs, corroborating that antipyrine has a similar behavior to the analytes throughout sample pretreatment and chromatographic procedures. Moreover, it is commercially available, allowing the method to be easily applied by other research groups or clinical departments. It is worthy to note that several chromatographic techniques use other

AEDs as IS, a fact that will hamper the application of the method if the patient is co-administered with the IS. In the method herein proposed, antipyrine is advantageous as it is uncommonly co-administered with AEDs.

III.3.1.2. Optimization of Sample Preparation

Before using the LLE procedure to extract the analytes, protein precipitation was tested with methanol, acetonitrile and trichloroacetic acid 20 %. No successful results were achieved with methanol or acetonitrile because the resulting processed samples were relatively unclean. On the other hand, the use of trichloroacetic acid 20 % was also not possible because the acidic environment partially degraded the AEDs.

As solid phase extraction and microextraction by packed sorbent have been associated to high and reliable extraction of AEDs from plasma matrices [442–445], they were herein tested. Solid phase extraction was performed with Oasis® HLB (30 mg, 1 mL) cartridges (Waters, MA, USA); whereas microextraction by packed sorbent 250 µL syringe and microextraction by packed sorbent BIN (barrel insert and needle) containing 4 mg of solid phase silica–C18 sorbent activated with methanol and water were used for microextraction by packed sorbent extraction. Several types and volumes of washing solvents as well as several elution solvents were investigated, but none reached a good relationship between analytes recovery and selectivity. Indeed, after employing solid phase extraction procedures, the AEDs were not detected at therapeutic concentrations; on the other hand, similar results were found for levetiracetam after its extraction through microextraction by packed sorbent procedure. In this way, LLE emerged as a new hypothesis and hexane, ethyl acetate, dichloromethane and tetrahydrofuran were tested. A double extraction with ethyl acetate of the aqueous phase was chosen because it enhanced the quantity of detected AED and decreased the influence of the impurities in relation to remaining options.

III.3.1.3. Optimization of Diode-Array Detection

In an attempt to ameliorate the recovery/selectivity ratio and lower the LLOQ of the analytical technique, a potential of the DAD instrument was explored. To decrease the LLOQ of AEDs without compromising selectivity, the absorption peak on the ultraviolet (UV) and visible spectrum defined by the DAD detector was selected for each analyte (**Figure III.1**). Accordingly, the highest signal intensity for levetiracetam, lacosamide and IS, with minimal interference of endogenous substances, was achieved at the wavelength of 220 nm while 239 nm seemed to be the best wavelength for zonisamide. Representative chromatograms of the extracts of blank and spiked plasma samples are shown in (**Figure III.2**).

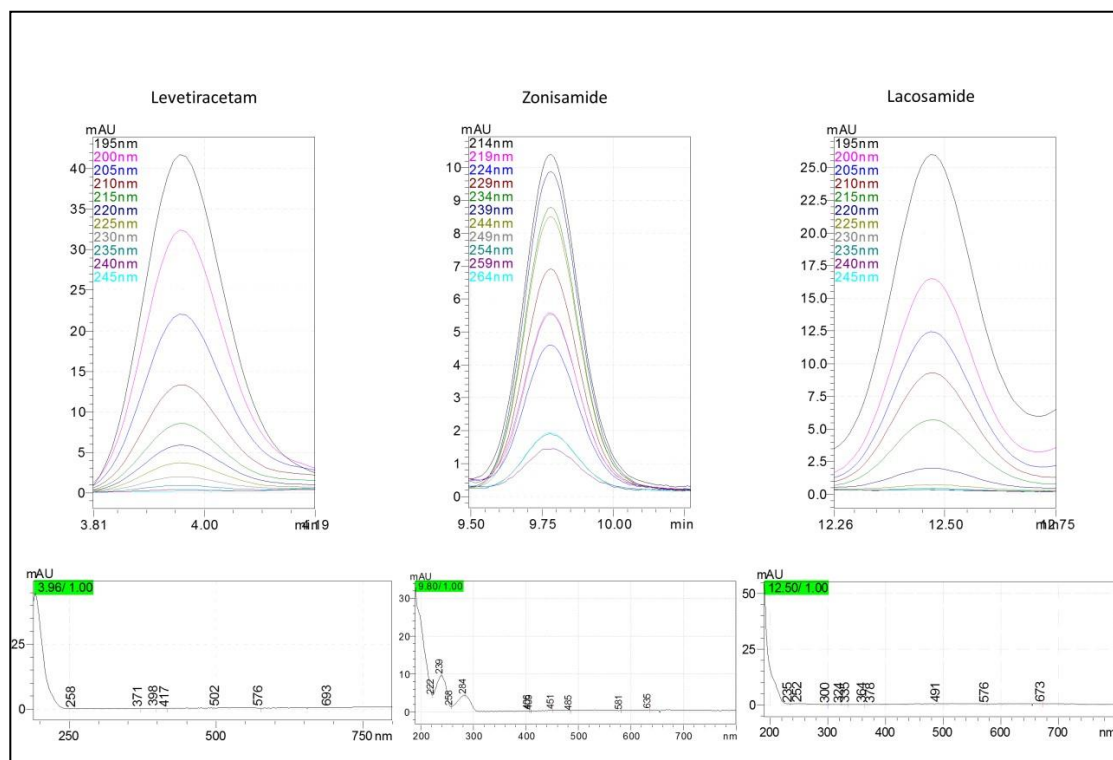


Figure III.1 UV and visible absorption spectrum of levetiracetam, zonisamide and lacosamide. Upper line: absorbance intensity of each AED in function of specific wavelengths; Lower line: complete UV-Vis absorption spectrum of each AED.

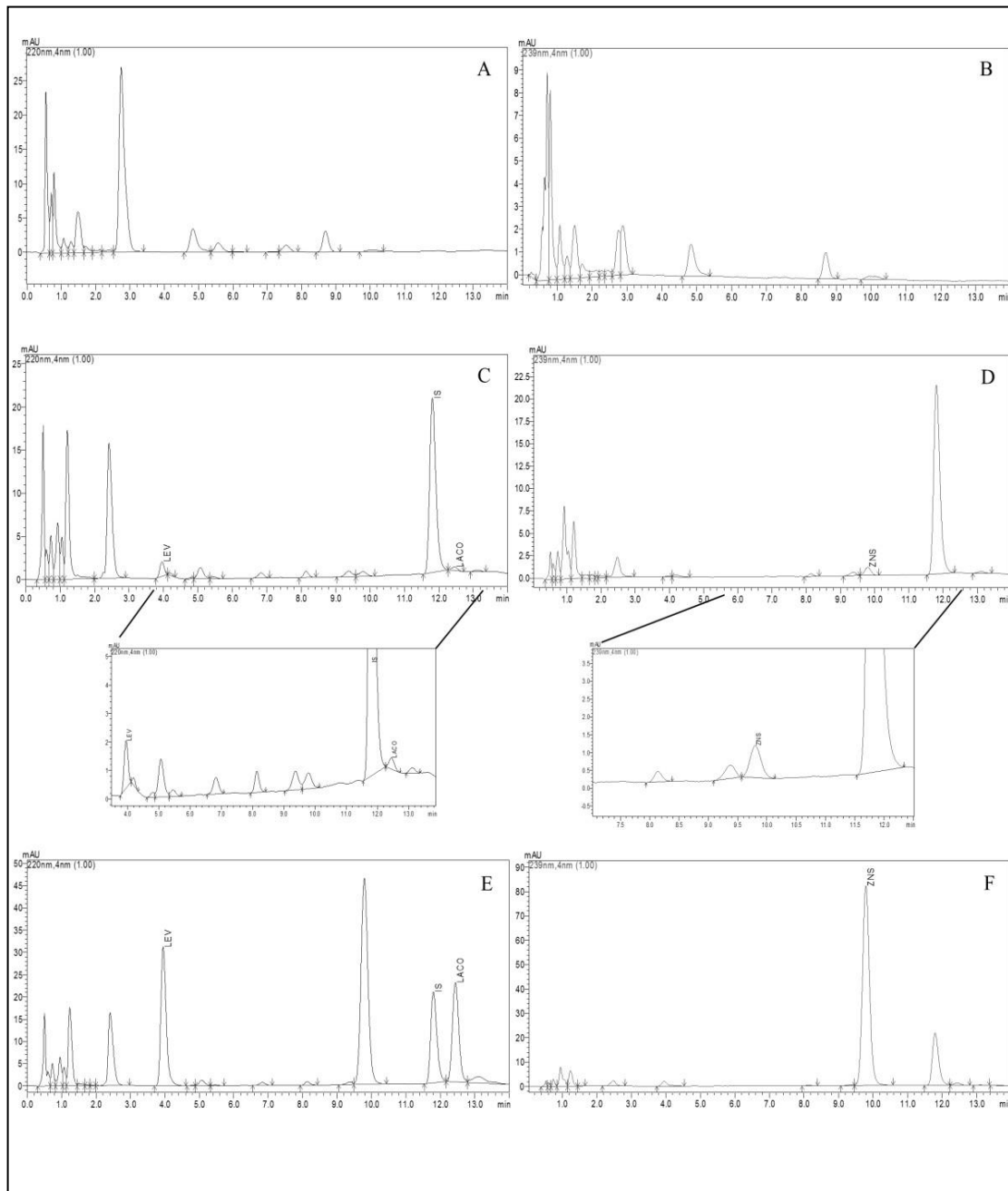


Figure III.2 Typical HPLC-DAD chromatograms of extracted human plasma samples. Blank sample at 220 nm **(A)** and at 239 nm **(B)**, sample spiked at level of the lower limit of quantification at 220 nm **(C)** and at 239 nm **(D)**, and sample spiked at level of the upper limit of the calibration range at 220 nm **(E)** and at 239 nm **(F)**. DAD, diode array detection; IS, internal standard; LACO, lacosamide; LEV, levetiracetam; ZNS, zonisamide.

III.3.2. METHOD VALIDATION

III.3.2.1. Selectivity & Sensitivity

The chromatographic separation of levetiracetam, lacosamide, zonisamide and antipyrine (IS) in spiked human plasma samples was successfully achieved using the previously described chromatographic conditions since the analysis of the six blank human plasma samples showed no interfering peaks in the retention times of the AEDs and IS (**Figure III.1**).

Table III.2 Retention time (initial-final) presented by some drugs potentially co-administered with levetiracetam, lacosamide and zonisamide, after submitted to plasma sample preparation and HPLC-DAD methodology herein developed.

Drug	Retention Time (min)
Acetylsalicylic acid	1.264 (1.114-1.965)
Amitriptyline	ND
Atenolol	8.714 (7.648-12.960)
Carbamazepine	ND
CBZ-10,11-epoxide	ND
Chloramphenicol	2.765 (2.464-3.584)
Chlorpromazine	8.162 (7.691-9.515)
Diazepam	ND
Eslicarbazepine	ND
Fluoxetine	ND
Furosemide	1.084 (0.984-1.111)
Hydrochlorothiazide	< 1.0
Ibuprofen	ND
Imipramine	ND
Ketoprofen	ND
Lamotrigine	ND
Lorazepam	ND
Meloxicam	ND
Metoprolol	ND
Mirtazapine	ND
Naproxen	ND
Oxcarbazepine	ND
Opicapone	ND
Paracetamol	< 1.0
Paroxetine	ND
Phenytoin	ND
Piroxicam	ND
Ranitidine	ND
Retigabine	1.466 (1.291-1.899)

CBZ-10,11-epoxide – *Carbamazepine-10,11-epoxide*; ND – *Not detected* within 14 min after the injection

Under these analytical conditions, the last-eluting analyte was lacosamide, with a retention time of approximately 12.45 min, and the order of elution of the compounds was as follow: levetiracetam (3.95 min), zonisamide (9.79 min), IS (11.80 min) and lacosamide.

On the other hand, none of the tested drugs potentially co-prescribed with the three new-generation AEDs were found to interfere with their peaks (**Table III.2**).

III.3.2.2. Linearity, LLOQ & LOD

Analyte concentrations in biological samples are typically interpolated using the regression results obtained from calibration curves, the linear regression being the most commonly adopted model [433]. The ordinary least square model is one of the simplest and most commonly used linear regression models; however, it only can be applied when the condition of homoscedasticity, i.e., constant variance over the whole calibration range (assessed by plotting the residuals versus concentration values), is confirmed for the analytical data [429].

Employing the least square model, linearity was observed ($r^2 \geq 0.999$) but accuracy of LLOQ revealed to be higher than 20 % as well as the accuracy of the smallest standards. As heteroscedasticity was demonstrated for lacosamide, levetiracetam and zonisamide, several weighting factors were tested and the results are summarized in **Table III.3**. Accordingly, the weighting factor of $1/x^2$ was chosen for all AEDs as it originated the least sum for this dataset, providing the most adequate approximation of variance. The correspondent calibration curves prepared in human plasma showed a consistent linear relationship between the ratios of the peak area signals of the AEDs to that of the IS and the corresponding concentration ranges defined in **Section III.2.2.2** ($r^2 \geq 0.998$; **Table III.4**).

Table III.3 Regression parameters of the calibration curve generated for each weighting factor (w_i) and the respective sum of the relative errors (Σ % RE) for the calibration standard data; $n = 35$.

Drug	w_i	Slope	Interception	r	% RE
Levetiracetam	1	0.02530	-0.00430	0.9949	158.7028
	$1/x$	0.02541	-0.00659	0.9969	155.9489
	$1/x^2$	0.02554	-0.00744	0.9982	154.9099
	$1/\sqrt{x}$	0.02533	-0.00563	0.9964	156.8933
	$1/y$	0.02536	-0.00701	0.9968	155.0918
	$1/y^2$	0.02537	-0.00779	0.9946	165.0316
	$1/\sqrt{y}$	0.02531	-0.00596	0.9964	156.9943
Zonisamide	1	0.07410	-0.00540	0.9974	154.0891
	$1/x$	0.07404	-0.00470	0.9989	148.6667
	$1/x^2$	0.07393	-0.00450	0.9981	147.5168
	$1/\sqrt{x}$	0.07403	-0.00451	0.9988	147.5203
	$1/y$	0.07387	-0.00491	0.9986	150.6094
	$1/y^2$	0.07325	-0.00435	0.9968	148.6231
	$1/\sqrt{y}$	0.07398	-0.00489	0.9988	149.9129
Lacosamide	1	0.03740	-0.00400	0.9954	186.2047
	$1/x$	0.03740	-0.00422	0.9979	187.4400
	$1/x^2$	0.03686	-0.00334	0.9980	184.5687
	$1/\sqrt{x}$	0.03741	-0.00439	0.9981	188.3976
	$1/y$	0.03727	-0.00428	0.9979	187.7342
	$1/y^2$	0.03641	-0.00329	0.9949	185.9483
	$1/\sqrt{y}$	0.03736	-0.00448	0.9981	188.8880

Calibration curve is given by the general equation of $y = mx+b$, with m corresponding to the slope and b to the intercept. r , correlation coefficient.

Table III.4 Calibration curve parameters of levetiracetam, zonisamide and lacosamide, in human plasma. Regression equation and correlation coefficient (r) are expressed as the mean of five calibration curves ($n = 5$).

Drug	Concentration Range ($\mu\text{g/mL}$)	Regression Equation ^a	r^2	Standard Deviation	Slope Intercept
Levetiracetam	2.5 – 40	$y = 0.02554C_{Lev} - 0.00744$	0.9982	0.0013	0.0034
Zonisamide	0.5 – 50	$y = 0.07393C_{ZNS} - 0.00453$	0.9981	0.0032	0.0023
Lacosamide	0.5 – 30	$y = 0.03686C_{LAC} - 0.00334$	0.9980	0.0025	0.0013

^aEquation of the calibration curve is given by the general equation of $y = mx+b$, with m corresponding to the slope and b to the intercept. The equation represents the peak areas signals of each drug to that of the internal standard (y), versus the corresponding plasma concentration of levetiracetam (C_{Lev}), zonisamide (C_{ZNS}) and lacosamide (C_{LAC}).

The LLOQ was experimentally defined as 2.5 $\mu\text{g/mL}$ for levetiracetam, 0.50 $\mu\text{g/mL}$ for lacosamide and zonisamide with acceptable precision ($CV \leq 8.11\%$) and accuracy (RE varied from 0.68 to 3.87%) as depicted in **Table III.5**. Interestingly, the LLOQ values obtained with the proposed method are often lower than those achieved with other HPLC–UV techniques reported in literature [436, 437, 446–448] and similar those achieved with MS/MS detection [423, 435].

After successive dilutions of the lowest calibration standard, the LOD was reliably established at 0.625 $\mu\text{g/mL}$ for levetiracetam, 0.20 $\mu\text{g/mL}$ for zonisamide and 0.25 $\mu\text{g/mL}$ for lacosamide.

Table III.5 Intra-day and interday accuracy and precision data of levetiracetam, zonisamide and lacosamide employing the novel HPLC-diode array detection technique herein developed.

	Levetiracetam	Nominal concentrations of quality control sample ($\mu\text{g/mL}$)				
		2.5	6.0	15.0	36.0	200.0 (QC _{Dil})
Overall C _{exp} (Mean \pm SD, n = 12)		2.570 \pm 0.204	5.832 \pm 0.437	14.484 \pm 1.195	37.804 \pm 1.142	198.033 \pm 2.001
Accuracy (% RE)						
	Intraday	0.832	-4.354	-8.536	4.195	-0.974
	Interday	0.684	-1.253	0.640	5.827	-1.328
Precision (CV %)						
	Intraday	3.948	8.875	3.944	1.185	1.014
	Interday	8.114	8.423	8.525	4.023	1.008
	Zonisamide	0.5	2.0	20.0	45.0	250.0 (QC_{Dil})
Overall C _{exp} (Mean \pm SD, n = 12)		0.507 \pm 0.029	2.063 \pm 0.118	20.144 \pm 1.133	45.567 \pm 2.583	250.964 \pm 2.418
Accuracy (% RE)						
	Intraday	1.335	1.431	-3.307	0.378	0.790
	Interday	1.395	4.853	4.742	2.139	0.265
Precision (% RE)						
	Intraday	2.480	4.902	2.420	5.558	0.901
	Interday	5.642	5.125	4.905	6.288	1.000
	Lacosamide	0.5	2.0	10.0	27.0	150.0 (QC_{Dil})
Overall C _{exp} (mean \pm SD, n = 12)		0.515 \pm 0.040	1.779 \pm 0.140	9.348 \pm 0.480	28.462 \pm 1.651	152.366 \pm 4.005
Accuracy (% RE)						
	Intraday	0.995	-12.410	-9.770	8.303	1.441
	Interday	3.871	-9.717	-3.274	2.525	2.004
Precision (CV %)						
	Intraday	4.560	8.434	2.249	4.233	1.734
	Interday	7.689	8.759	4.843	6.373	3.629

The data corresponds to the LLOQ, QC1, QC2, QC3 and QC_{Dil} and were obtained with five replicates in the same day or in consecutive days, respectively (n = 5).

% RE: *percentage relative error*; CV: *coefficient of variation*; QC: *quality control*; QC_{Dil}, *quality control with 1:5 diluted*

III.3.2.3. Precision & Accuracy

The quality of a calibration curve is guaranteed not only by its linearity but also if the back calculated concentrations of all the calibration standards do not deviate more than $\pm 15\%$ of the nominal value with the exception of the LLOQ as discussed in the previous section.

Results presented in **Table III.5** indicate that intra and interday precision given by CV values was between 1.19 and 8.88 % for levetiracetam, between 2.42 and 6.29 % for zonisamide and between 2.25 and 8.76 % for lacosamide in human plasma; whereas the overall accuracy, which was assessed by the RE %, ranged from -8.54 to 5.83 % for levetiracetam, from -3.31 to 4.85 % for zonisamide and from -12.41 to 8.30 % for lacosamide. Accordingly, it is undeniable that the acceptance criteria defined by EMA and FDA were fulfilled for all the compounds at the three assessed concentration levels.

In addition, the overall experimental concentrations of levetiracetam, zonisamide and lacosamide estimated in plasma samples above the high concentration sample diluted quality control were found to be 198.03 ± 2.00 , 250.96 ± 2.42 and 152.37 ± 4.01 $\mu\text{g/mL}$, respectively (**Table III. 5**). Furthermore, while the accuracy varied from -1.33 to 2.00 %, the precision was inferior to 3.63 %. These results suggest that the method can be successfully applied to the analysis of human plasma samples that exceed the upper limit of calibration curve after a five-fold dilution with blank human plasma.

III.3.2.4. Recovery & Carry-Over Effect

The overall recovery values obtained using the sample preparation methodology herein developed are presented in **Table III.6**. Although protein precipitation is particularly use when samples are analyzed by LC-MS/MS methods, LLE is preferable for DAD methods. It is worthy to mention that several methods reported in literature that can individually quantify lacosamide, levetiracetam and zonisamide required a protein precipitation procedure before LLE or solid phase extraction [449–451]. At this

point, strength of the methodology herein proposed is that it only requires a LLE procedure. Furthermore, the absolute recovery found for the three AEDs with the present procedure varied from 72.87 to 99.28 %, and showed CV values lower than 9.99 %, suggesting a consistent average recovery over the evaluated concentration ranges. Importantly, the recovery of the IS was also consistent, precise and reproducible, with a mean value of 94.7 %.

No interfering peaks with areas greater than 5 % of the peak areas at the LLOQ level of each AED were detected in blank human plasma samples injected after the upper limit of calibration curve standard.

Table III.6 Absolute recovery from human plasma (%) of Levetiracetam, zonisamide and lacosamide employing the sample treatment and extraction procedures herein optimized. Low, medium and high-quality control samples were used (n = 5). The absolute recovery is also presented for the internal standard (n = 5).

Analyte	Nominal Concentration ($\mu\text{g}/\text{mL}$)	Recovery	
		Mean \pm SD	CV (%)
Levetiracetam	6.0	81.306 \pm 7.554	9.291
	15.0	82.476 \pm 7.075	8.578
	36.0	99.276 \pm 6.976	7.027
Zonisamide	2.0	72.866 \pm 5.362	7.359
	20.0	74.178 \pm 6.173	8.322
	45.0	77.048 \pm 5.551	7.205
Lacosamide	2.0	90.493 \pm 9.043	9.993
	10.0	91.038 \pm 2.192	2.406
	27.0	97.771 \pm 3.261	3.336
Internal Standard	5.0	82.021 \pm 7.394	9.014

CV, coefficient of variation; SD, standard deviation.

III.3.2.5. Stability

The stability results presented in **Table III.7** indicate that the AEDs can be considered stable under the various investigated conditions, since their concentrations deviated by no more than 11.76 % in relation to the reference for any of the analytes and the stability varied within 86.05 and 112.47 %. Human plasma samples containing the analytes may therefore be kept for up to 3 h, at ambient temperature, 24 h at 4 °C,

30 days at -30 °C and after three freeze–thaw cycles (24 h per cycle) at -30 °C, without any significant degradation. In addition, for all the compounds, stability of processed plasma samples was also ensured for at least 24 h at 4 °C and 3 h at room temperature.

Table III.7 Stability data for levetiracetam, zonisamide and lacosamide under several conditions of sample handling and storage (n = 5).

Drug	RT, 3 h	Unprocessed plasma samples			Processed plasma samples		
		4 °C, 24 h	-30 °C, 30 days	3 freeze/thaw cycles	RT, 3 h	4 °C, 24 h	
Levetiracetam	6.9 µg/mL						
	C _{exp} (Mean ± SD)	5.853 ± 0.24	6.70 ± 0.39	6.57 ± 0.37	5.81 ± 1.25	6.05 ± 0.14	6.63 ± 0.21
	% RE	-2.45	11.76	9.550	-3.15	0.77	10.50
	Stability (%) ^a	98.73	112.47	110.58	97.80	101.441	111.767
	36.0 µg/mL						
	C _{exp} (Mean ± SD)	35.594 ± 2.42	34.38 ± 0.99	33.179 ± 1.401	32.35 ± 1.34	38.64 ± 1.183	38.49 ± 1.57
% RE	-6.767	-4.495	-7.84	-10.15	7.33	6.92	
Stability (%) ^a	93.46	97.06	90.887	96.774	102.718	101.423	
Zonisamide	2.0 µg/mL						
	C _{exp} (Mean ± SD)	2.187 ± 0.16	2.09 ± 0.05	1.96 ± 0.03	1.95 ± 0.07	2.22 ± 0.08	2.11 ± 0.09
	% RE	9.350	4.25	-2.150	-2.60	11.20	5.70
	Stability (%) ^a	104.43	100.41	98.48	97.68	105.15	109.76
	45.0 µg/mL						
	C _{exp} (Mean ± SD)	45.72 ± 4.13	47.49 ± 4.60	44.36 ± 5.16	44.03 ± 2.12	46.21 ± 1.74	47.51 ± 1.61
% RE	1.61	5.55	-1.43	-2.14	2.69	5.57	
Stability (%) ^a	100.09	103.84	99.41	97.98	100.54	104.29	
Lacosamide	2.0 µg/mL						
	C _{exp} (Mean ± SD)	2.051 ± 0.26	1.80 ± 0.12	1.77 ± 0.05	1.71 ± 0.01	1.83 ± 0.09	1.99 ± 0.07
	% RE	2.55	-10.25	-11.3	-14.4	-8.75	-0.35
	Stability (%) ^a	101.48	89.851	88.701	86.050	91.530	99.667
	27.0 µg/mL						
	C _{exp} (Mean ± SD)	29.311 ± 1.16	27.98 ± 1.022	24.21 ± 2.624	26.50 ± 2.01	25.70 ± 1.48	28.77 ± 1.21
% RE	8.559	2.96	-10.32	-1.48	-4.81	6.57	
Stability (%) ^a	107.64	102.87	89.99	98.57	95.19	105.41	

^aGiven as the percentage of overall experimental concentration of the drug in sample after and before being exposed to stability assessment.

C_{exp}, Experimental concentration estimated employing the correspondent mean calibration equation; CV: Coefficient of Variation; RE: Relative percentage error given by [(overall mean experimental concentration: nominal concentration)/(nominal concentration) x 100]; RT: Room temperature; SD: Standard deviation.

III.3.3 METHOD APPLICATION TO CLINICAL SAMPLE ANALYSIS & INCURRED SAMPLE REANALYSIS

By employing the bioanalytical method herein presented, plasma concentrations of levetiracetam, lacosamide and zonisamide were determined on 12 plasma samples collected from 11 distinct epileptic patients. The drug, administration route, dose, blood collection time and the co-administered AEDs as well as the determined respective drug concentrations are summarized in **Table III.8**. Representative chromatograms are depicted in **Figure III.3**, and it is clearly seen that peak shape and resolution are very similar to those obtained using spiked blank plasma with no interferences. All estimated concentrations depicted in **Table III.8** are within the calibration ranges herein defined, with exception of levetiracetam in plasma samples from patients 8, 9 and 11. However, these results were expected taking into account the postdosing time of samples collection (>15 h postdosing). Furthermore, the co-administered drugs (**Table III.8**) were not detected during the chromatographic analysis or, when detected, they did not interfere with the retention time of the AEDs or IS.

From patient 1 administered with levetiracetam, two samples were collected: one at 3 h postdosing (suggesting the peak concentration) and the other immediately before the subsequent administration (corresponding to the trough concentration). According to **Table III.8**, it is worthy to note that although the first concentration is within the therapeutic range, the last is not. This suggests that the interval of administration can be decreased if uncontrolled seizures occur. An increase of the administered dose to 1500 mg could also be hypothesized; however, there would be the risk of toxicity and drug monitoring must be performed. It is interesting to highlight that zonisamide concentration estimated in plasma from the orally treated patient 3 was below the plasma therapeutic range defined in literature [432]. As the sample was collected in ambulatory, immediately before oral drug administration, the result suggests that the patient is probably not correctly adhering to the therapy.

To demonstrate reproducibility of the validated method, incurred sample reanalysis was assessed for 75 % of the epileptic patient samples herein enrolled. As

depicted in the **Table III.9**, the percent difference between the initial concentration and the concentration measured during the repeat analysis was lower than 20 % as it is required by international guidelines. The incurred sample reanalysis was herein assessed according to EMA guidelines. The percentage of difference estimated according to the equation defined by EMA [(original value - incurred sample reanalysis value)/mean value × 100], and the results are within the ranges internationally defined.

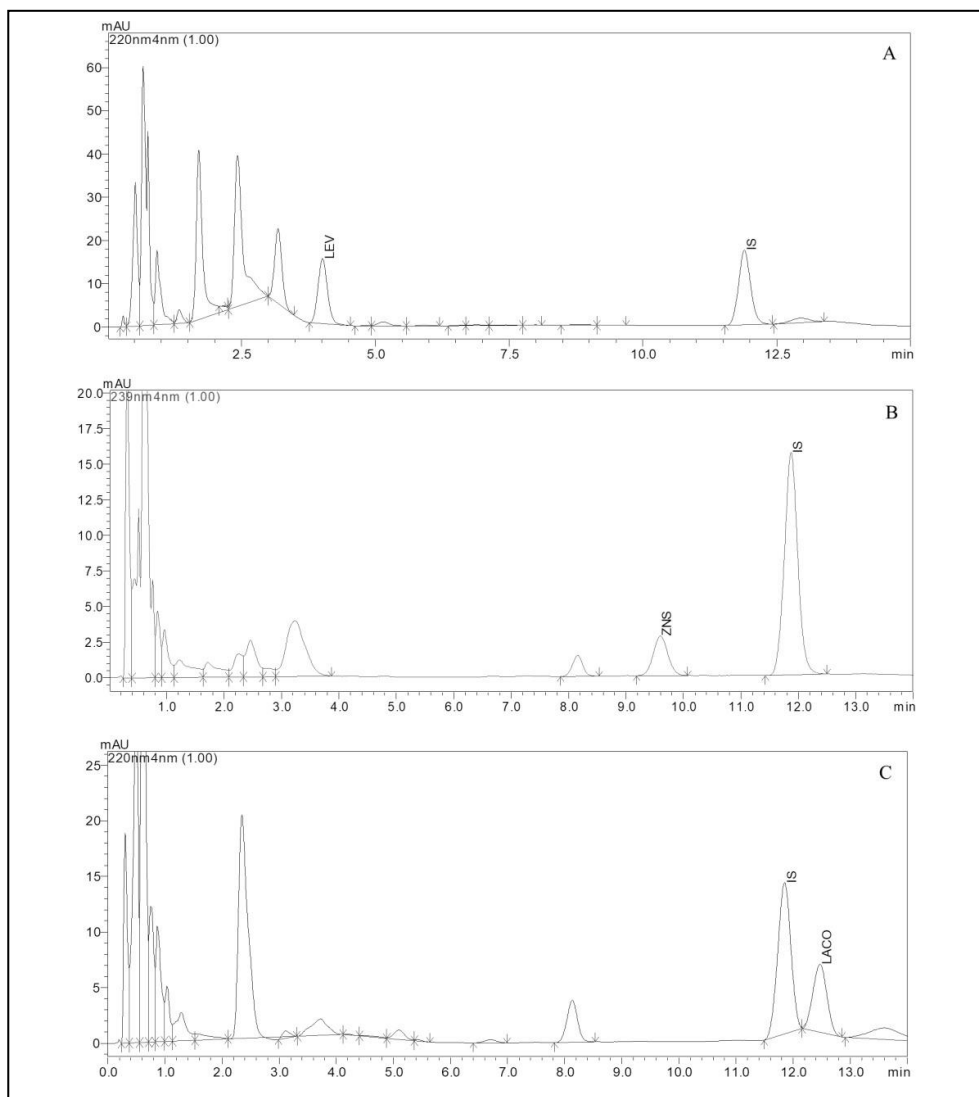


Figure III.3 Representative chromatograms of plasma samples obtained from epileptic patients treated with different AEDs. **(A)** Levetiracetam (LEV) administered by intravenous route (dose of 1000 mg each 24 h); **(B)** orally administered zonisamide (ZNS) at the dose of 300 mg each 24 h; and **(C)** intravenous administration of lacosamide (LAC) at 600 mg each 24 h. The determined plasma concentrations correspond to those exposed in **Table III.8**. IS, *Internal standard*.

Table III.8 Characteristics regarding drug posology and co-administered antiepileptic drugs instituted to the epileptic patients and the corresponding plasma concentration of levetiracetam, zonisamide and lacosamide assessed after employing the method herein developed.

Patient number ^a	Monitored AED	Route (dose) and frequency	Time sample collection	Plasma concentration (µg/mL)	Co-administered AEDs
1	Levetiracetam	IV (1000 mg) 24/24 h	3 h postdosing	26.602	Valproic acid
			Pre dosing ^b	8.408	Valproic acid
2	Lacosamide	IV (600 mg) 24/24 h	1 h postdosing	9.738	NR
3	Zonisamide	Oral (300 mg) 24/24 h	Pre dosing ^b	2.816	NR
4	Levetiracetam	IV (1000 mg) 8/8 h	Pre dosing ^b	19.407	CLN, ESL, LTG
5	Levetiracetam	IV (1500 mg) 12/12 h	24 h postdosing	3.116	CBZ, CLB, PER
			Oral (200 mg) 12/12 h	Pre dosing ^b	39.815
6	Lacosamide	IV (200 mg) 12/12 h	Pre dosing ^b	6.241	CLB, valproic acid
			Levetiracetam	IV (1500 mg) 12/12 h	Pre dosing ^b
7	Levetiracetam	IV (1000 mg) 8/8 h	24 h postdosing	8.226	CBZ
			Zonisamide	Oral (100 mg) 8/8 h	12 h postdosing
8	Levetiracetam	IV (800 mg) 12/12 h	15 h postdosing	ND	ESL, midazolam, diazepam
9	Levetiracetam	IV (500 mg) 12/12 h	24 h postdosing	BLLOQ	–
10	Lacosamide	IV (200 mg) 12/12 h	Pre dosing ^b	4.712	LTG, alprazolam
			Levetiracetam	IV (500 mg) 12/12 h	24 h postdosing
11	Levetiracetam	IV (1000 mg) 12/12 h	24 h postdosing	3.962	CBZ, LTG

Plasma concentration of AED corresponds to the original sample analysis.

^aThe patient number herein inserted was randomly selected.

^bBlood was collected immediately before drug administration.

AED, Antiepileptic drug; BLLOQ, Below the LLOQ; CLB, Clobazam; CLN: Clonazepam; ESL, Eslicarbazepine acetate; IV, Intravenous; LTG, Lamotrigine; ND, Not detected; N, Not reported; PE, Perampanel

Table III.9 Incurred samples reanalysis (ISR) of plasma samples obtained from epileptic patients.

Patient Number ^a	Monitored AED	Original Plasma Concentration (µg/mL)	ISR Plasma Concentration (µg/mL)	% Difference ^b
1	Levetiracetam	27.0261	26.6026	- 1.58 %
		8.6251	8.4081	- 2.55 %
4	Levetiracetam	19.4073	16.2744	-17.56 %
5	Levetiracetam	2.9172	3.1156	6.58 %
		Zonisamide	39.8150	33.7768
6	Lacosamide	6.2407	6.1580	-1.33 %
		Levetiracetam	21.9980	21.3063
7	Levetiracetam	8.2261	7.8246	-5.00 %
		Zonisamide	7.5473	7.0404

^aThe patient number herein inserted was randomly selected and correspond to those from **Table III.8**; ^bPercent of difference was estimated according to the equation: [(original value – ISR value)/mean value x 100].

III.4 CONCLUSION & FUTURE PERSPECTIVE

A reliable, accurate and precise HPLC-DAD method was developed and fully validated for the quantification of new-generation AEDs in human plasma. It is the first HPLC-DAD method that allows the simultaneous quantification of levetiracetam, lacosamide and zonisamide in human plasma. Indeed, there are only two chromatographic methods that simultaneously quantify levetiracetam, zonisamide and lacosamide but LC-MS/MS techniques as well as deuterated IS are required. The main strength of the proposing work is the HPLC-DAD technique, which can be more widely used than LC-MS/MS in clinical laboratories. Validation results as well as the method application to real plasma samples from epileptic patients demonstrated that the analytes can be accurately and precisely quantified. The present method is therefore expected to be employed in the near future in routine pharmacokinetic drug monitoring of patients treated with such AEDs either in monotherapy, transitional or chronic polytherapy regimens as well as in other pharmacokinetic-based studies involving those drugs. The wide calibration range and the evaluation of the fivefold

dilution effect support the application of the present technique when suspecting of toxicity.

It is worthy to note that the HPLC-DAD procedure was coupled to a sample preparation procedure based on LLE with ethyl acetate, only required 100 μL of plasma, which allow the method application to pediatric epileptic patients. The LLOQs achieved for lacosamide, levetiracetam and zonisamide were considerably low, reaching the values reported with LC-MS or LC-MS/MS. Moreover, the mobile phase with more than 90 % of water, the simplicity of sample preparation and a chromatographic retention time of less than 14 min give the method the capability of being used in high sample throughput analysis in the future.

CHAPTER IV

NOSE-TO-BRAIN DELIVERY OF LEVETIRACETAM AFTER INTRANASAL ADMINISTRATION TO MICE



IV.1. INTRODUCTION

With an estimated burden of disease between 1–2 %, epilepsy is the fourth most common neurological condition that currently affects more than 50 million people worldwide [452, 453]. It affects patient quality of life, independently of age or social status. For this reason, epilepsy is one of the most impairing brain diseases and requires daily pharmacological treatment with antiepileptic drugs (AEDs).

In the last decade, levetiracetam, (S)-2-(2-oxopyrrolidin-1-yl)butanamide (Keppra®), has been the most frequently prescribed AED to treat partial and generalized seizures in both adults and children more than one month old [454]. Aside from its few neurological adverse effects, levetiracetam is authorized in Europe as monotherapy in adults and adolescents older than 16 years of age, with newly diagnosed epilepsy with partial-onset seizures, and, as adjunctive, in patients aged with at least one month old [454]. Interestingly, the nearly perfect efficacy and tolerability profiles observed in children are promoting the off-label use of levetiracetam in neonate seizures, which are the most frequent clinical manifestation of CNS dysfunctions of newborns [150, 455].

As a member of the “racetam” family, levetiracetam exhibits an innovative mechanism of action, primarily characterized by its interaction with the SV2A and consequent reduction of neuronal hyper-synchronization. This contributes to its anticonvulsant activity, together with the potentiation of GABA and glycine inhibitory systems, and partial depression of N-calcium current of AMPA glutamatergic receptors. Its unique multiple pharmacodynamic activity reduces the need of its co-administration with other AEDs with distinct therapeutic targets [456–458]. Moreover, in contrast to classic AEDs, levetiracetam has a wider therapeutic index and excellent safety. Its pharmacokinetic profile is linear and clean, characterized by an almost complete intestinal absorption, non-significant plasma protein binding and no hepatic metabolism mediated by CYP450 enzymes [458, 459]. Levetiracetam is mainly excreted by renal route, 60 % as unchanged form and 40 % as UCB L057, an inactive metabolite formed by plasmatic hydrolysis of the parent drug [226]. All the aforementioned advantages, together with being available in oral and IV formulations, are prompting

the use of levetiracetam in status *epilepticus*, one of the most frequent neurological emergencies. In addition to its dramatic and shocking nature, status epilepticus is coupled to significant morbidity and mortality and requires prompt treatment, in order to avoid cerebral damage and systemic complications [460, 461]. From 2007 to 2010, the utilization of levetiracetam by IV route in status *epilepticus* episodes increased from 30 to more than 50 %. It is currently the second-line treatment, only preceded by benzodiazepines [460].

Nevertheless, real-life studies regarding the efficacy and tolerability of levetiracetam are evidencing pitfalls that highly compromise its therapeutic efficacy, particularly in poly-medicated and critically ill epileptic patients [462]. Indeed, DDIs with levetiracetam were unexpected, since it is not metabolized by CYP enzymes [459, 463]. However, pediatric and adult studies undoubtedly demonstrate a significant increase of levetiracetam clearance and a reduction of its systemic bioavailability when patients are co-medicated with enzyme inducing AEDs, including carbamazepine, phenytoin and phenobarbital [226, 431, 452, 463, 464] and drugs from other pharmacotherapeutic groups [431, 452, 465]. It has been suggested that these findings probably result from the induction of the enzymatic hydrolysis of levetiracetam, as well as from efflux transporters from the ABC superfamily including P-gp [226], which has been identified as one of the responsible transporters for the development of pharmacoresistance against AEDs. At this point, it is noteworthy that 30-40 % of medicated epileptic patients are refractory to treatment and develop drug-resistant epilepsy [149]. Also known as refractory epilepsy, drug-resistant epilepsy is defined as the failure of two rationally chosen AED dosage schedules, in monotherapy or in combination with other AEDs, to achieve seizure control or freedom [144, 466]. Among several theories attempting to explain drug-resistant epilepsy, emerges the pharmacokinetics hypothesis, which postulates that efflux transporters located in peripheral organs reduce the systemic bioavailability of AEDs and consequently, the concentration available to cross the BBB and reach the biophase [144, 467]. Complementarily, the transporter hypothesis emphasises that consecutive seizures and/or chronic treatment with AEDs induce the expression of ABC transporters in

endothelial cells of the BBB and in other cells of epileptic brain, hampering access of AEDs into the epileptogenic focus [468].

Despite being ascribed as an “almost perfect” drug, the truth is that epileptic patients medicated with levetiracetam also develop drug resistance, in part, because systemic treatments available in clinical practice are a daunting challenge due to the unique protective barriers of the CNS. Such innate barriers, mainly the BBB and the blood–cerebrospinal fluid barrier, play a critical role in protecting the CNS against toxic agents. However, they become an obstacle for effective systemic drug delivery to the CNS, particularly when ABC transporters are overexpressed, as in drug-resistant epilepsy, hampering the passage of levetiracetam to the biophase (the brain) and reducing drug efficacy.

Thus, in the present work, a novel alternative route to administer levetiracetam is described, which enables a partial circumvention of the BBB and the cardiovascular system. Through a noninvasive nose-to-brain delivery, levetiracetam is expected to be, in part, quickly delivered into the CNS by resorting to neural pathways that connect the nasal mucosa and the brain, avoiding the passage across the BBB. Several studies and marketed nasal drugs offer concrete evidence showing the potential advantage of IN delivery over systemic routes of administration [234, 469, 470]. The herein proposed nose-to-brain delivery of levetiracetam is also expected to become a comfortable and convenient approach that overcomes drug resistance mechanisms at the BBB. Furthermore, it may be applied in emergency situations and reduce potential DDI.

IV.2. MATERIAL & METHODS

IV.2.1. DRUGS & REAGENTS

Levetiracetam was purchased from Molekula SRL (Rimini, Italy). Antipyrine, used as IS, was obtained from Sigma-Aldrich (St. Louis, MO, USA).

For the quantification of levetiracetam in biological samples, acetonitrile of HPLC gradient grade was used and acquired from Fisher Scientific (Leicestershire, UK). Ultrapure water (HPLC grade, 18.2 MΩ.cm) was obtained from a Milli-Q water apparatus from Millipore (Milford, MA, USA). For the preparation and optimization of the IN gel, pluronic F-127 was purchased from Sigma–Aldrich (St. Louis, MO, USA) while Carbopol® 974P and Noveon® Polycarbophil were kindly supplied by Lubrizol (Wickliffe, OH, USA). Reagents such as methanol, ethyl acetate and dimethyl sulfoxide (DMSO) were obtained from Fisher Scientific (Leicestershire, UK) while sodium dihydrogen phosphate dihydrate, disodium hydrogen phosphate dihydrate and hydrochloric acid fuming 37 %, used to prepare 0.1 M sodium phosphate buffer pH = 5.0, were purchased from Merck KGaA (Darmstadt, Germany). Anesthesia was performed with ketamine (Imalgene 1000®, 100 mg/mL) and xylazine (Vetaxilaze 20®, 20 mg/mL), both commercially acquired. Sodium chloride 0.9 % solution was purchased from B. Braun Medical (Queluz de Baixo, Portugal). All remaining chemicals were obtained from Sigma-Aldrich (St. Louis, MO, USA) unless otherwise stated.

IV.2.2. DEVELOPMENT AND CHARACTERIZATION OF THERMOREVERSIBLE GEL

For IN administration, a thermoreversible gel loaded with levetiracetam was optimized in order to exhibit a thermosensitive profile. Below room temperature, it is a user-friendly and easily measurable liquid solution, which becomes a semisolid gel at the physiological temperature of the nasal mucosa (approximately 35 °C). Thus, the thermoreversible gel was initially prepared based on the cold method described by

[471]. Accordingly, 1.8 g of Pluronic F-127 (final concentration 18 %, w/v) were slowly added to 10 mL of cold Milli-Q water (5-10 °C) under magnetic stirring and kept overnight at 4 °C, in order to attain an efficient flocculation. Pluronic F-127 was chosen because it is a triblock copolymer composed of poly(ethylene oxide) and poly(propylene oxide) units that are fluid at or below room temperature, turning to a semisolid gel as the temperature increases, as a result of the micelle packing disorder-order transition phenomenon [472]. In an attempt to increase the bioadhesive properties of the gel, enhance its residence time and improve the central delivery of levetiracetam, two distinct polymers were tested at 0.2 % (w/v), Carbopol® 974P and Noveon® Polycarbophil. The textural characteristics (hardness, compressibility, adhesiveness, cohesiveness and elasticity) of both formulations were assessed resorting to the texture analyzer TA.XT Plus (Stable Micro System Ltd., Surrey, UK) as previously described [473]. The best formulation was loaded with levetiracetam in two concentrations (15 and 25 mg/mL) in order to evaluate the influence of drug incorporation in the characteristics of the thermogel.

IV.2.3. IN VITRO STUDIES

Two human cell lines were used for viability studies: the human lung adenocarcinoma cell line (Calu-3, ATCC® HTB-55TM) and the Human nasal septum cell line (RPMI-2650, ECACC 88031602). The Calu-3 cell line was cultured in Dulbecco's modified Eagle's medium (Sigma-Aldrich) containing 0.04 M sodium bicarbonate. The RPMI-2650 cell line was cultured in sterile Minimum Essential Medium Eagle with Earle's salts and sodium bicarbonate, supplemented with 2 mM glutamine and 1 % non-essential amino acids. For both cell types, media were supplemented with 10 % of heat-inactivated fetal bovine serum (FBS) and 1 % penicillin-streptomycin mixture. The cells were grown in T-75 flasks (Orange-Scientific, Braine-l'Alleud, Belgium), passaged 2-3 times a week using a 0.25 % Trypsin-EDTA solution and cultured at 37 °C in 5 % CO₂ and 95 % relative humidity.

The viability of Calu-3 and RPMI-2650 cells was assessed in 96-well plates (3.5×10^4 cells per well and 3×10^5 cells per well, respectively) by the Alamar Blue assay in accordance to [474]. Viable cells reduce the non-fluorescent compound, resazurin, into the fluorescent compound, resorufin, which accumulates inside viable cells and is then quantified. Hence, after 24 h of seeding, the culture medium was removed and 200 μ L of medium (control cells) or levetiracetam at different concentrations (1, 5, 10, 25, 50, 100 μ M) were added to the wells and incubated for 24 h. Then, treatment solutions were removed and the Alamar Blue solution (10 %) was added to each well and incubated for 3 h at 37 °C in 5 % CO₂. Lastly, fluorescence was measured (excitation and emission wavelengths of 530/590 nm) in a Biotek Synergy HT microplate reader (Biotek® Instruments, Winooski, VT, USA). Cell viability (%) was calculated according to **Equation IV.1**.

$$\text{Cell viability (\%)} = \frac{FL_{\text{Lev}} - FL_{\text{W}}}{FL_{\text{Control}} - FL_{\text{W}}} \times 100 \quad \text{Equation IV. 1}$$

FL_{lev} is the mean fluorescence observed after incubation with levetiracetam, FL_{control} is the mean fluorescence observed in controls and FL_{W} is the mean fluorescence observed in wells with no cells. For each condition, 9 replicates were performed in three independent assays.

IV.2.4. IN VIVO STUDIES

IV.2.4.1. Animals and Ethics

Healthy adult male CD-1 mice, weighing between 25-30 g, were supplied by Charles River Laboratories (France) and allowed to acclimate to the local animal facilities for at least 1 week before experiments. Animals were housed under controlled environmental conditions (temperature 20 ± 2 °C; relative humidity 55 ± 5 %; 12 h light/dark cycle), with *ad libitum* access to tap water and standard rodent diet (4RF21, Mucedola®, Italy) during all experimental procedures.

All experiments involving animals and their care were conducted in conformity with the international regulations of the European Directive (2010) regarding the protection of laboratory animals used for scientific purposes (2010/63/EU) [475] and the Portuguese law on animal welfare [475]. The applied experimental procedures were reviewed by the Portuguese National Authority for Animal Health, Phytosanitation and Food Safety (DGAV – *Direção-Geral de Alimentação e Veterinária*). All efforts were made to minimize the number of animals used and their suffering.

IV.2.4.2. *In Vivo* Pharmacokinetic Single-Dose Study

The aim of pharmacokinetic *in vivo* studies was to compare the pharmacokinetic profiles of levetiracetam in plasma, brain, lungs and kidneys after a single dose administration by IN and IV routes to mice.

The animals were divided into two groups; one group received 25 μ L of the thermoreversible gel loaded with levetiracetam (25 mg/mL) while the other received the same dose of levetiracetam by IV route. The IV solution was an injectable levetiracetam solution (Keppra[®], 100 mg/mL) previously diluted with physiological saline solution (0.9 % NaCl) to attain the final concentration of 5.2 mg/mL.

Before treatment, both groups were anaesthetized by an intraperitoneal injection of a mixture of ketamine (100 mg/kg) and xylazine (10 mg/kg), and kept in a heated environment to maintain the body temperature. In each set of experiments, animals were randomly divided into 7 subgroups ($n = 5$) and each was sacrificed at predefined time points post-administration (5, 15, 30, 60, 90, 120 and 240 min).

The anesthetized animals from IN group were placed in right lateral recumbency and the instillation took place unilaterally into the left nostril using a MicroSprayer[®] Aerosolizer (Model IA-1B from Penn-Century, Inc., Wyndmoor, PA) coupled to a high-pressure syringe (Model FMJ-250 from Penn-Century, Inc., Wyndmoor, PA). The tip of the delivery tube was inserted for approximately 1 mm into the nostril. Together, both devices produce a highly concentrated, air-free aerosol from the end of the small diameter delivery tube to aerosolize the thermoreversible gel. This system only allows

the administration of a fixed-volume of 25 μL or multiple. Therefore, each animal received 625 μg of levetiracetam by administering 25 μL of the optimized thermoreversible gel with the concentration of 25 mg/mL.

In the IV group, the administration of levetiracetam was performed by means of a single injection (120 μL) of the formulation into the preheated lateral tail vein using an insulin syringe (27 G x 1/2 in., 1.0 mL).

At the aforementioned time points after drug administration, both animal groups were sacrificed by cervical dislocation followed by decapitation and the blood was immediately collected into heparinized tubes. The brain, lungs and kidneys were quickly removed, carefully washed with physiological saline and weighed. Blood samples were centrifuged at 4 $^{\circ}\text{C}$ and 2880 g for 10 min to obtain plasma supernatants which were stored at -80 $^{\circ}\text{C}$ until preparation and analysis by HPLC, as described in **Section IV.2.4.2.1**. Mice brain, lungs and kidneys were homogenized in 0.1 M sodium phosphate buffer pH 5.0 (4 mL per gram of tissue) using a THOMAS[®] Teflon pestle tissue homogenizer. Tissue homogenates were centrifuged at 4147 g for 15 min at 4 $^{\circ}\text{C}$ and the resultant supernatants were also frozen at -80 $^{\circ}\text{C}$ until analysis.

IV.2.4.2.1. Quantification of Levetiracetam in Biological Samples

Levetiracetam concentrations were determined in plasma and tissue samples obtained during *in vivo* pharmacokinetic single-dose studies using a liquid-liquid extraction procedure. This was followed by HPLC analysis, based on the previously developed and validated method by [476] with slight alterations.

Briefly, 40 μL of methanol were added to plasma aliquots (100 μL) or tissue homogenate supernatant (150 μL) for protein precipitation. Then, 10 μL of IS working solution (50 $\mu\text{g}/\text{mL}$) in acetonitrile and 1 mL of ethyl acetate were also added, vortex-mixed for 30 seconds, and centrifuged at 12,045 g (3 min for plasma and 5 min for tissues samples) in order to extract the drug and the IS. The resulting upper organic layer was transferred to a clean glass tube and the aqueous layer was re-extracted using the aforementioned LLE procedure. To concentrate the analytes, both organic

phases were combined and evaporated under a gentle nitrogen stream at 45 °C. The resulting solid residue was reconstituted in 100 µL of water and acetonitrile mixture (90:10, v/v) by vortex-mixing for approximately 1 min and sonication in an ultrasonic bath at room temperature for approximately 1 min. Afterwards, the extracts were transferred to a 0.22 µm Costar® Spin-X® centrifugal filter (Corning, Inc., NY, USA), centrifuged at 12,045 g for 3 min or 5 min (plasma and tissues respectively). Lastly, 20 µL of the final filtered samples were injected into the HPLC system.

HPLC analysis was carried out in a Shimadzu HPLC system (Shimadzu Corporation, Kyoto, Japan) equipped with a solvent delivery model (LC-20A), a degasser (DGU-20A5), an autosampler (SIL-20AHT), a column oven (CTO-10ASVP) and a DAD (SPD-M20A). The HPLC apparatus and data acquisition were controlled by LCsolution software (Shimadzu Corporation, Kyoto, Japan). Levetiracetam and IS, present in the pre-treated samples, were separated in a reverse-phase LiChroCART® Purospher® Star C₁₈ column (55 × 4 mm, 3 µm particle size; Merck KGaA, Darmstadt, Germany) at 40 °C with the wavelength set at 220 nm. The mobile phase was composed of water and acetonitrile, and pumped at a flow rate of 1.0 mL/min according to the following time gradient elution program: a linear gradient was applied by varying the proportion of acetonitrile from 3 to 10 % in the first 10 min; subsequently, within 2 min, the percentage of acetonitrile was restored to 3 %, and maintained until the end of the run (14 min).

The main validation parameters of the analytical method are summarized in **Table IV.1** and in agreement with the international bioanalytical guidelines issued by the EMA [427] and FDA [418].

Table IV.1 Main parameters of the HPLC-DAD method validation employed to quantify levetiracetam in plasma, brain, lung and kidney matrices (n = 5).

Validation Parameter	Plasma	Brain	Lungs	Kidneys
Calibration range^a ($\mu\text{g/mL}$)	2.5 - 40	2.5 - 160 ^b	10 - 160 ^b	10 - 160 ^b
Regression Equation^a	$Y = 0.022641x - 0.013985$	$Y = 0.037154x - 0.013824$	$Y = 0.034421x - 0.018505$	$Y = 0.035198x - 0.025702$
Coefficient of determination (r^2)	0.9948	0.9920	0.9965	0.9970
LLOQ ($\mu\text{g/mL}$)	2.5	0.625	2.5	2.5
Interday				
Precision (% CV)	2.88 - 9.48	5.79 - 9.42	3.65 - 5.23	4.92 - 14.30
Accuracy (% RE)	-1.52 - 13.42	-4.70 - 2.07	-6.44 - 3.55	-10.16 - 9.63
Intraday				
Precision (% CV)	2.81 - 9.91	2.17 - 6.33	1.12 - 3.59	3.08 - 13.79
Accuracy (% RE)	0.60 - 8.88	-7.61 - 4.45	-6.50 - 2.39	-12.89 - 9.04
Recovery (%)	58.86 - 79.18	69.10 - 87.07	63.26 - 86.06	77.55 - 81.74

^a Interday values, n = 5; ^b values expressed in $\mu\text{g/g}$

LLOQ, lower limit of quantification; CV, coefficient of variation; RE, relative error

IV.2.4.2.2. Pharmacokinetic Analysis and Calculations

The pharmacokinetic parameters were estimated by a non-compartmental pharmacokinetic analysis employing the WinNonlin version 5.2 (Pharsight Co, Mountain View, CA, USA), based on mean concentration values (n = 5) determined for each time point.

The maximum peak concentration (C_{max}) of levetiracetam in plasma and tissues and the corresponding time to reach C_{max} (t_{max}) were determined. Other estimated pharmacokinetic parameters included the area under the drug concentration time-curve (AUC) from time zero to the time of the last quantifiable drug concentration (AUC_t), calculated by the linear trapezoidal rule; the AUC from time zero to infinity (AUC_{inf}), calculated by $\text{AUC}_t + (C_{\text{last}}/k_{\text{el}})$, where C_{last} is the last quantifiable concentration and k_{el} is the apparent elimination rate constant, estimated by log-linear regression of the terminal segment of the concentration–time profile; and the percentage of AUC

extrapolated from t_{last} to infinity [$AUC_{extrap}(\%)$], where t_{last} is the time of the C_{last} . The apparent terminal elimination half-life ($t_{1/2el}$) and the mean residence time (MRT) were additionally determined.

The absolute bioavailability (F) of levetiracetam after IN administration was calculated in accordance with **Equation IV.2**.

$$F = \frac{AUC_{tIN} \times Dose_{IN}}{AUC_{tIV} \times Dose_{IV}} \times 100 \quad \text{Equation IV. 2}$$

AUC_{infIN} and AUC_{infIV} are the AUC_{inf} values observed following IN and IV administration, respectively; $Dose_{IV}$ and $Dose_{IN}$ represent the drug dose (mg) administered by IV and IN routes to mice.

To evaluate drug distribution into the brain, lungs and kidneys after IN and IV administration, the ratios were determined based on the quotient $AUC_{tissue}/AUC_{plasma}$.

With the objective of determining the brain targeting efficiency of nasally delivered levetiracetam, the drug targeting efficiency (DTE) percentage was calculated following **Equation IV.3**. The DTE index represents the brain-to-plasma partitioning ratio of the drug administered by IN route compared to IV injection.

$$DTE (\%) = \frac{(AUC_{brain}/AUC_{plasma})_{IN}}{(AUC_{brain}/AUC_{plasma})_{IV}} \times 100 \quad \text{Equation IV. 3}$$

AUC_{brain} and AUC_{plasma} are, respectively, the AUC_t observed in brain and plasma after both administration routes to mice. It is ensured that a preferential drug transport to the brain following IN administration, compared to systemic administration, occurs when DTE (%) is greater than 100 % [477].

In order to estimate the drug fraction that is transported through the olfactory and trigeminal nerve pathways, the direct transport percentage (DTP) was calculated by

subtracting the contribution of the indirect pathway (via absorption into the systemic circulation) from the total IN brain AUC, in accordance with **Equation IV.4**.

$$\text{DTP (\%)} = \frac{\text{AUC}_{\text{brain IN}} - \left[\frac{\text{AUC}_{\text{brain IV}}}{\text{AUC}_{\text{plasma IV}}} \times \text{AUC}_{\text{plasma IN}} \right]}{\text{AUC}_{\text{brain IN}}} \times 100 \quad \text{Equation IV. 4}$$

Hence, the smaller the ratio of IV brain AUC to IV plasma AUC is, the larger DTP values are. Consequently, DTP values higher than 0 indicate the presence of brain targeting through direct pathways, in opposition to values from $-\infty$ to 0, which indicate a more efficient brain targeting by IV route [478].

The comparative brain bioavailability between IN and IV routes ($B_{\text{brain IN/IV}}$) was also measured as an indicator of brain drug accumulation through the IN route over the IV. It only considers brain AUC_t values, excluding those in plasma and it was estimated in accordance with **Equation IV.5** [479].

$$B_{\text{brain IN/IV}} = \frac{\text{AUC}_{\text{brain IN}}}{\text{AUC}_{\text{brain IV}}} \quad \text{Equation IV. 5}$$

IV.2.4.3. *In Vivo* Intranasal Repeated Dose Toxicity Study

During seven consecutive days, mice were administered levetiracetam thermoreversible gel (1250 µg daily, n = 5) or ultra-purified water (control group, n = 5) by IN route twice-daily. On the morning after the last dose of the 7th day, mice were anaesthetized with ketamine/xylazine (100/10 mg/kg, intraperitoneal), the trachea was exposed by snipping the covering tissue and the inferior vena cava and aorta were snipped near the kidneys, in order to exsanguinate the animal [480, 481]. Immediately afterwards, the animals were perfused by cardiac route with 10 mL of 0.9 % sodium chloride by inserting a syringe attached to a needle (25 G x 5/8 in) into the right heart ventricle. Exsanguination was performed by opening the abdominal cavity and severing the abdominal aorta with scissors. This aimed to prevent blood flow into the

base of the lungs. After cardiac perfusion, a small incision was made on the ventral surface of the trachea, where the sheath of a 20 G angiocatheter was slid to insufflate the lungs with 1 mL of phosphate buffered saline (pH 7.4) and 1 mL of the fixative (paraformaldehyde 4 %). The lungs were collected and stored in PAF at room temperature until histological analysis.

In order to detect if any significant histological changes occurred during the repeated-dose experiment, a histological study of excised lung tissues was conducted by comparing lung tissues from animals subjected to the repeated-dose IN study with those collected from non-treated CD-1 male mice. Thus, lung tissues from control and treated animals were fixed in 10 % formalin solution, embed in paraffin and sliced into 4- μ m thick sections using a rotary microtome (Leica Model DM 1000 LED).

Representative blocks were collected from both left and right lobes. The sectioned tissues were routinely stained with hematoxylin and eosin and examined under an optical microscope by a pathologist with no knowledge of the treatment. The photographs were taken using the software Leica Application Suite Version 4.13.0.

IV.2.5. STATISTICAL ANALYSIS

Data from the *in vivo* pharmacokinetic single-dose study were processed using Graphpad Prism® 5.03 (San Diego, CA, USA) and expressed as mean \pm standard error of the mean (SEM). At each time point, statistical comparisons were performed between IN and IV administration groups using the unpaired two-tailed Student's t-test.

Similarly, data from *in vitro* studies were processed using Graphpad Prism® 5.03 (San Diego, CA, USA) and expressed as mean \pm standard deviation (SD). An ANOVA test was used to determine differences of cell viability (%) after incubation with levetiracetam compared with untreated control cells (100 % cell viability).

Differences were considered statistically significant for *p*-values lower than 0.05.

IV.3. RESULTS

IV.3.1. OPTIMIZATION AND CHARACTERIZATION OF THE INTRANASAL THERMOREVERSIBLE GEL

In order to optimize the thermosensitive profile of the gel intended for IN administration to mice, the mechanical properties of the pharmaceutical products were investigated by texture profile analysis at three temperatures (5 °C, 25 °C and 35 °C). Moreover, the influence of two polymers, Carbopol® 974P and Noveon® Polycarbophil USP, and the loaded levetiracetam concentration on compressibility, hardness, adhesiveness, elasticity and cohesiveness of the formulation was also assessed. The overall results are presented in **Table IV.2**.

Regarding the hardness of the polycarbophil gel, which expresses the ease with which the gel is applicable on the nasal mucosa, a slight decrease was observed when temperature increased from 5 °C to 25 °C. Then, at 35 °C, it returned to values similar to those reported at 5 °C. In opposition, using Carbopol® 974P instead of Noveon® Polycarbophil, hardness remained practically constant from 5 to 25 °C (approximately 11 g), but increased significantly at 35 °C (mean value of 19.36 g). Similar trends were observed for compressibility, which is correlated to the spreadability of the gel.

Indeed, as shown in **Table IV.2**, the compressibility of polycarbophil gel was almost independent of the temperature (mean values of 14.13, 10.93 and 17.40 g.s) while the gel carrying Carbopol® 974P exhibited an increased compressibility, as temperature rose (mean values of 8.50, 10.78 and 17.78 g.s). Note that the compressibility value must be low to extract the prepared gel from the container more easily and accurately spread it on the nasal mucosa. This was achieved with the Carbopol® 974P gel by preparing it on ice (approximately 5 °C) and aspirating it into the cold high-pressure syringe coupled to the refrigerated MicroSprayer® Aerosolizer system. These advantages of the Carbopol® 974P gel in relation to the Noveon® polycarbophil gel did not seem to compromise its adhesiveness, which determines the bioadhesion of the gel onto the nasal surface and its retention time at the site of application. In fact, at 35

°C, both gels displayed similar values of adhesiveness (absolute values of 3.45 and 3.25 g.s, **Table IV.2**). This is consistent with the information provided by the manufacturer. A similar trend was observed for cohesiveness and elasticity parameters. Cohesiveness provides information on the structural reformation of the gel after its application, and higher values are ascribed to a full structural recovery. Regarding elasticity, defined as the rate at which the deformed sample returns to its original condition after the removal of the deforming force, a lower value was observed at 5 °C with Carbopol® 974P, which is, hence, associated to an increased hydrogel elasticity [473].

The influence of the inclusion of levetiracetam in the hydrogels was assessed at 15 and 25 mg/mL. In accordance to **Table IV.2**, it is evident that in the carbopol gel, the hardness and compressibility decreased slightly at 5 °C, as the drug quantity loaded in the gel increased. This suggests a more user-friendly and easier to handle final pharmaceutical product. Irrespectively of temperature, the hardness, compressibility and adhesiveness were higher for levetiracetam at a concentration of 25 mg/mL. Particularly, at the physiological temperature of nasal mucosa (35 °C), the adhesiveness of the formulation approximately doubled comparing the obtained values in the absence and presence of levetiracetam at 25 mg/mL (absolute value of 3.25 *versus* 6.43, respectively; **Table IV.2**). In opposition, inclusion of levetiracetam in the Noveon® polycarbophil gel generally decreased the hardness, compressibility and adhesiveness of the gel at all the temperatures, corroborating that it does not gellify in the nasal cavity.

Taking the aforementioned data into consideration, the carbopol gel revealed to be the preferable option in the present research work, given that in the presence of levetiracetam (25 mg/mL) it was syringeable at 5 °C, gelling at the physiological temperature of nasal cavity.

Table IV.2 Mechanical properties of the several nasal gel formulations prepared to incorporate levetiracetam. Results are indicated as a mean of six replicates \pm standard deviation ($n = 6$).

Gel Formulations	Hardness (g)	Compressibility (g.s)	Adhesiveness (g.s)	Cohesiveness	Elasticity
5 °C					
Polycarbophil Gel	13.62 \pm 2.13	14.13 \pm 6.56	-4.97 \pm 2.82	0.05 \pm 0.03	0.14 \pm 0.15
+ Levetiracetam (15 mg/mL)	3.72 \pm 0.82	4.99 \pm 0.33	-1.84 \pm 2.49	0.18 \pm 0.19	0.21 \pm 0.09
+ Levetiracetam (25 mg/mL)	4.33 \pm 0.45	2.02 \pm 0.53	NC	0.34 \pm 0.16	0.39 \pm 0.21
Carbopol® 974P Gel	11.41 \pm 3.00	8.50 \pm 5.94	-3.52 \pm 1.93	-0.04 \pm 0.48	0.06 \pm 0.40
+ Levetiracetam (15 mg/mL)	10.87 \pm 3.40	11.96 \pm 5.55	-1.98 \pm 2.02	0.38 \pm 0.49	0.03 \pm 0.04
+ Levetiracetam (25 mg/mL)	6.90 \pm 1.97	6.37 \pm 4.43	-4.85 \pm 1.91	0.16 \pm 0.28	0.06 \pm 0.64
25 °C					
Polycarbophil Gel	9.08 \pm 5.79	10.93 \pm 10.02	-3.08 \pm 1.19	-0.12 \pm 0.33	0.08 \pm 0.06
+ Levetiracetam (15 mg/mL)	3.98 \pm 0.90	1.27 \pm 0.10	-0.34 \pm 0.48	0.20 \pm 0.14	0.24 \pm 0.11
+ Levetiracetam (25 mg/mL)	2.47 \pm 2.98	1.12 \pm 0.11	-0.59 \pm 0.81	0.30 \pm 0.08	0.28 \pm 0.10
Carbopol® 974P Gel	11.27 \pm 4.19	10.78 \pm 9.67	-2.39 \pm 2.67	0.06 \pm 0.64	0.15 \pm 0.09
+ Levetiracetam (15 mg/mL)	16.38 \pm 3.84	19.03 \pm 9.59	-2.60 \pm 1.50	0.07 \pm 0.03	0.186 \pm 0.13
+ Levetiracetam (25 mg/mL)	17.22 \pm 3.79	25.30 \pm 9.53	-4.67 \pm 2.68	0.06 \pm 0.04	0.22 \pm 0.10
35 °C					
Polycarbophil Gel	14.75 \pm 4.31	17.40 \pm 8.98	-3.45 \pm 2.30	0.06 \pm 0.02	0.12 \pm 0.06
+ Levetiracetam (15 mg/mL)	3.81 \pm 0.94	0.90 \pm 0.52	-3.34 \pm 3.49	0.16 \pm 0.1	0.20 \pm 0.04
+ Levetiracetam (25 mg/mL)	3.72 \pm 1.02	0.98 \pm 0.35	-1.76 \pm 2.17	0.52 \pm 0.36	0.32 \pm 0.11
Carbopol® 974P Gel	19.36 \pm 5.85	17.73 \pm 9.10	-3.25 \pm 2.79	0.24 \pm 0.36	0.19 \pm 0.11
+ Levetiracetam (15 mg/mL)	12.58 \pm 3.65	11.38 \pm 5.02	-4.89 \pm 2.41	0.19 \pm 0.08	0.33 \pm 0.12
+ Levetiracetam (25 mg/mL)	16.82 \pm 3.82	24.24 \pm 7.15	-6.43 \pm 5.03	0.03 \pm 0.04	0.09 \pm 0.09

NC, not calculate

IV.3.2. *IN VITRO* CELLULAR VIABILITY OF RPMI-2650 AND CALU-3 CELLS

The Alamar Blue assay revealed that the viability of RPMI-2650 cells following 24 h of incubation with levetiracetam, empty gel vehicle and gel loaded with levetiracetam at 25 mg/mL were within $\pm 15\%$ in relation to the negative control, without significant statistical differences ($p = 0.785$; **Figure IV.1**). Similarly, there were no significant losses ($p = 0.0788$) of Calu-3 cell viability following 24 h of incubation with levetiracetam at the concentration range of 1–100 μM (**Figure IV.2**). Variations in relation to the negative control were also far from 15 %, as evidenced in **Figure IV.2**.

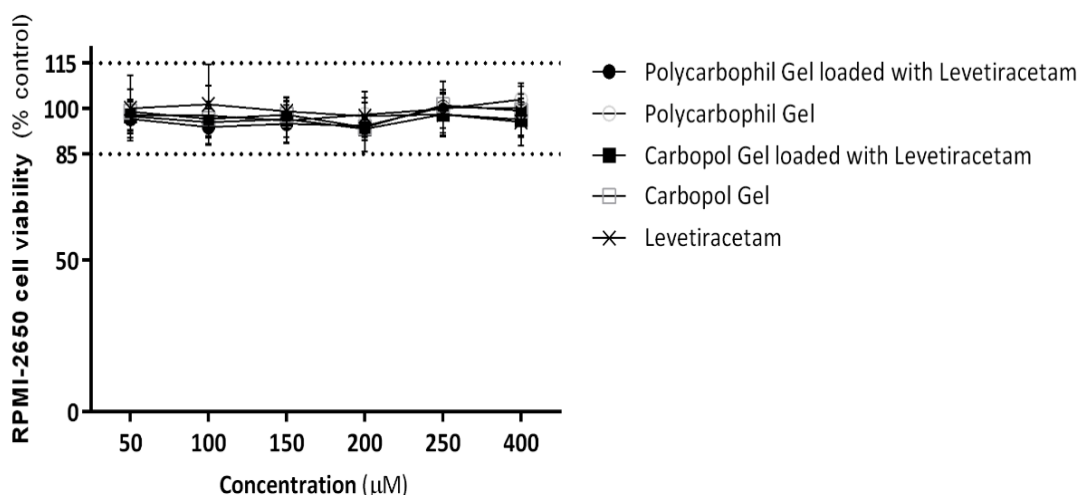


Figure IV. 1 Viability (%) of RPMI-2650 cells after incubation with levetiracetam for 24 h (50–400 μM); empty Polycarbophil and Carbopol® thermoreversible gels; and thermoreversible gels loaded with levetiracetam at the same concentrations. Data represented as mean \pm standard deviation (9 replicates in three independent replicates).

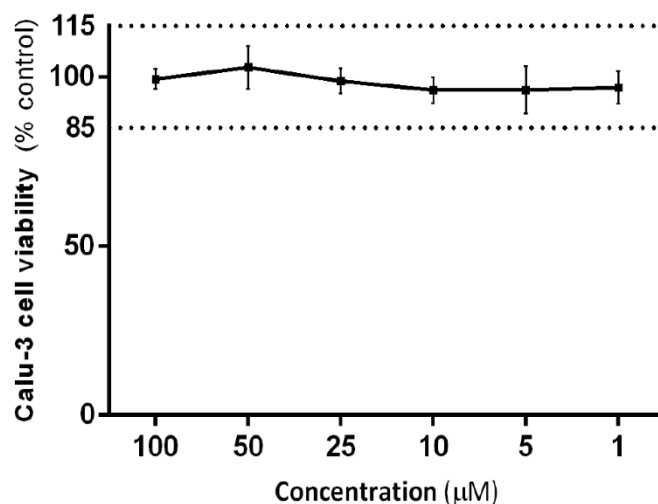


Figure IV. 2 Viability (%) of Calu-3 cells after incubation with levetiracetam for 24 h (1, 5, 10, 25, 50 and 100 µM). Data represented as mean ± standard deviation (9 replicates, three independent replicates).

IV.3.3. PHARMACOKINETICS OF LEVETIRACETAM AFTER SINGLE-DOSE ADMINISTRATIONS

The mean plasma, brain, lung and kidney concentration–time profiles of levetiracetam after administration of an IV solution and the nasal gel to mice are shown in **Figure IV.3**. The corresponding main pharmacokinetic parameters estimated by noncompartmental analysis are displayed in **Table IV.3**.

Accordingly, plasma pharmacokinetic profiles of levetiracetam are fairly comparable in both administration routes, with no statistically significant differences in any time points post-dosing (**Figure IV.3A**). Furthermore, C_{max} and t_{max} as well as the extent of systemic exposure (assessed by AUC_t and AUC_{inf}) are also similar after IN and IV administrations (**Table IV.3**). Indeed, the absolute bioavailability estimated for levetiracetam delivered by IN route was very high (107.44 %), suggesting that a similar drug amount is easily and rapidly accessible in the systemic circulation following the IN route and the classic IV injection. However, taking a closer look at **Figure IV.3**, it is noteworthy that, in spite of the parallel plasma profiles, levetiracetam concentrations in tissues depend on the administration route, particularly up to 30 min post-administration.

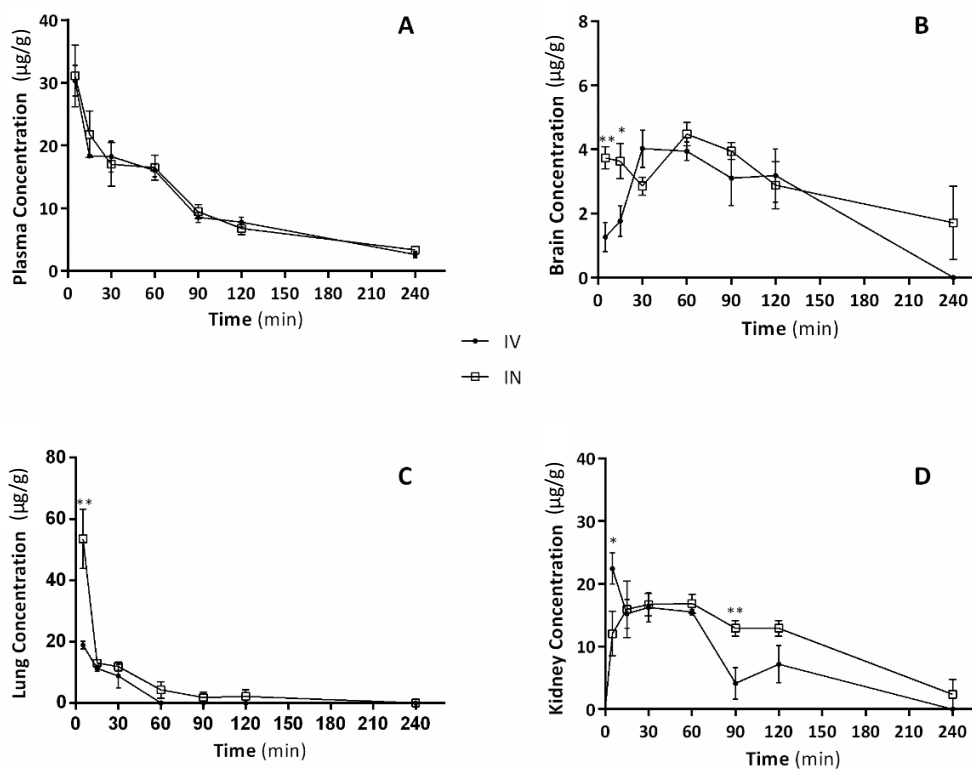


Figure IV. 3 Concentration-time profiles of levetiracetam up to 240 min post-dosing in plasma (A), brain (B), lung (C) and kidney (D) following intranasal (IN) and intravenous (IV) administration (625 µg/animal) to mice. Symbols represent the mean values \pm SEM of five determinations per time point ($n = 5$). * $t(8) = 0.729$, $p = 0.033$; ** $t(8) = 4.36$, $p = 0.0024$; # $t(8) = 3.56$, $p = 0.0074$; Y $t(8) = 2.41$, $p = 0.0424$; YY $t(8) = 3.11$, $p = 0.014$.

Concerning brain concentration–time profiles (**Figure IV.3B**), the concentrations observed at 5 and 15 min post-dosing are considerably higher after IN administration (3.73 ± 0.77 and 3.63 ± 1.23 µg/g, respectively) than those observed after IV injection (1.27 ± 1.00 and 1.76 ± 1.07 µg/g, respectively) even though no differences have been detected in plasma at those time points.

Table IV.3 Pharmacokinetic parameters of levetiracetam in plasma, brain, lung and kidney tissues following its intranasal (IN) and intravenous (IV) administration (20.8 mg/kg) to mice.

Pharmacokinetic Parameters ^a	Plasma		Brain		Lung		Kidney	
	IN	IV	IN	IV	IN	IV	IN	IV
t_{max} (min)	5.00	5.00	60.00	30.00	5.00	5.00	30.00	5.00
C_{max} ($\mu\text{g/mL}$) ^b	31.11	30.330	4.48 ^b	4.02 ^b	53.54 ^b	17.87 ^b	16.90	22.46
AUC_t ($\mu\text{g}\cdot\text{min/mL}$)	2407.07	2309.35	742.41 ^c	381.93 ^c	1163.08 ^c	444.15 ^c	2473.28	1445.45
AUC_{inf} ($\mu\text{g}\cdot\text{min/mL}$)	2685.90	2499.80	NC	NC	1329.59 ^c	505.05 ^c	2682.68	2105.23
AUC_{extrap} (%)	10.38	7.62	NC	NC	12.52	12.06	7.81	31.34
k_{el} (min^{-1})	0.0088	0.0107	NC	NC	0.0130	0.0342	0.0115	0.0109
$t_{1/2el}$ (min)	78.56	65.03	NC	NC	53.19	20.30	60.48	63.61
MRT (min)	99.21	92.66	NC	NC	40.79	28.98	102.5	98.72
F (%) ^d	107.44							
AUC_t Ratios	IN	IV	DTE (%)	DTP (%)				
AUC_{brain}/AUC_{plasma}	0.31	0.17	182.35	46.38				
AUC_{lung}/AUC_{plasma}	0.48	0.19	253.63					
$AUC_{kidney}/AUC_{plasma}$	1.02	0.63	162.90					

^a Parameters were estimated using the mean concentration-time profiles obtained from five different animals per time point (n = 5). ^b Values expressed in $\mu\text{g/g}$; ^c Values expressed in $\mu\text{g}\cdot\text{min/g}$; ^d Absolute intranasal bioavailability (F) was calculated based on AUC_{inf} values; AUC_{extrap} , Extrapolated area under the drug concentration time-curve; AUC_{inf} , Area under the concentration time-curve from time zero to infinite; AUC_t , Area under the concentration time-curve from time zero to the last quantifiable drug concentration; C_{max} , Maximum peak concentration; DTE, Drug targeting efficiency index; k_{el} , Apparent elimination rate constant; MRT, Mean residence time; NC, not calculated; $t_{1/2el}$, Apparent terminal elimination half-life; t_{max} , Time to achieve the maximum peak concentration

The brain-to-plasma concentration ratios (**Figure IV.4A**) are higher after IN instillation of the gel than IV injection at 5, 15 and 60 min, although statistically significant differences were only found at the first time-point. It is also evident that there is an increase of the brain-to-plasma ratio from 1 h to 2 h post-dosing after both delivery routes (**Figure IV.4A**), demonstrating that levetiracetam also reached the brain through systemic absorption followed by BBB crossing. Consistently, the value of DTE in the brain was 182.35 % and DTP was 46.38 %. Furthermore, in comparison to IV delivery, a slight delay in the time to reach C_{max} was observed for IN administration (30 and 60 min, respectively). It was particularly interesting that the magnitude of the peak concentration of levetiracetam achieved in IN delivery was higher than that observed in IV delivery, together with its exposure at the biophase, given by AUC_t (**Table IV.3**). It was not possible to calculate k_{el} in the brain, but t_{max} and AUC_t could be estimated, and $B_{brain\ IN/IV}$ was determined. The obtained value was 1.94,

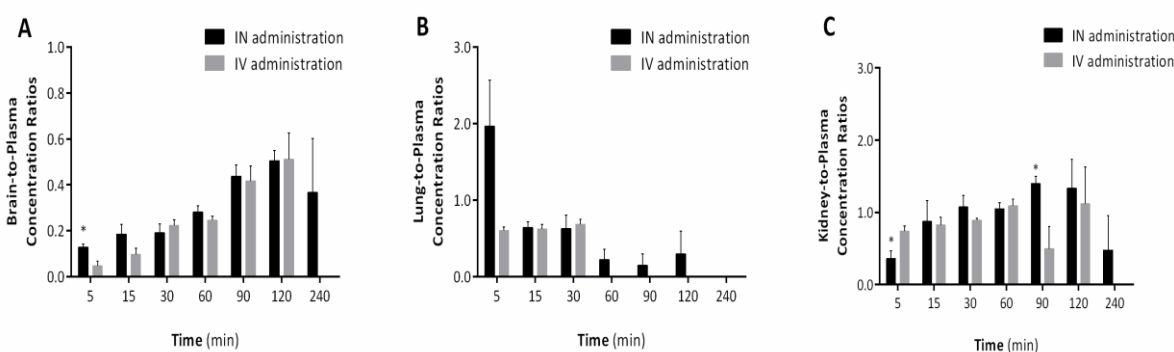


Figure IV. 4 Tissue-to-plasma concentration ratios of levetiracetam at 5, 15, 30, 60, 90, 120 and 240 min after administration of the drug by intranasal (IN) or intravenous (IV) route. **(A)** represents the brain-to-plasma concentration ratios variation *versus* time; **(B)** represents the lung-to-plasma concentration ratios variation *versus* time and **(C)** represents the kidney-to-plasma concentration ratios variation *versus* time. * $t(8) = 0.024$, $p = 0.011$.

Regarding lung concentrations, both administration routes revealed a t_{max} for levetiracetam of approximately 5.00 min (**Table IV.3**). However, unsurprisingly, the C_{max} was considerable higher after IN administration relatively to IV administration (53.54 ± 21.56 and 22.46 ± 5.46 $\mu\text{g/g}$; **Figure IV.3C**) and the lung-to-plasma concentration ratio was also higher in IN route, although no significant statistical differences were identified (**Figure IV.4B**). These findings, together with the DTE value of 253.63 %, evidence a certain potential of the IN route to deliver levetiracetam

directly into the lung. It is important to emphasize that, in intranasally administered mice, levetiracetam concentrations declined steeply to values similar to those observed after IV administration (**Figure IV.3C**). Nevertheless, the drug was more slowly cleared from the organ, as suggested by the lower value of k_{el} after IN administration (0.0130 *versus* 0.0342 min^{-1}). Consequently, levetiracetam remained in the lung for a longer period of time (MRT of 40.79 *versus* 28.98 min in comparison to IV injection, **Table IV.3C**). Therefore, the viability of Calu-3 cells was assessed after exposure to levetiracetam formulations and the histological lung toxicity was evaluated *in vivo* after repeated IN administrations. The results are presented in **Sections IV.3.2** and **IV.3.4**, respectively.

By analyzing the temporal evolution of levetiracetam concentrations in its major excretory organ, the kidney, it is possible to notice that, following IN delivery, there is an initial increase of drug concentrations, while after IV administration the trend is a decreasing throughout the 240 min of the study (**Figure IV.3D**). Thus, aside from C_{max} and the extent systemic exposure given by AUC_{inf} , which are diminished in IN route, the remaining pharmacokinetic parameters are very similar in both administration routes (**Table IV.3**). Moreover, the kidney-to-plasma ratios (assessed by AUC_t) were 1.02 and 0.63 after IN and IV deliveries, respectively, and the DTE value was the lowest (161.90 %, **Table IV.3**). At this point, it is important to mention that the percentage of AUC_{extrap} is higher than 20 % when considering the biodisposition of levetiracetam in kidney tissue after IV injection (**Table IV.3**). This was the only situation that may underestimate the kidney-to-plasma ratio and overestimate the value of DTE. Moreover, analyzing (**Figure IV.4C**), it is noticeable that kidney-to-plasma concentration ratios increase through most of the study, with the exception of the last time point (240 min).

IV.3.4. HISTOLOGICAL EVALUATION OF LUNG TISSUE FROM *IN VIVO* MULTIPLE-DOSE STUDY

All animals subjected to the repeated-dose IN study survived and revealed no significant weight variation (within $\pm 5\%$). No signals of anxiety or stress were observed throughout the 7 days of treatment.

In general, histological examination of IN treated mice at the 7th day showed no histopathological changes in the lung, compared to non-treated control animals (**Figure IV.5**). Staining with hematoxylin and eosin revealed maintenance of the pulmonary architecture, without widening of the inter-alveolar septa, as described in literature [482]. No edema, emphysema or fibrotic lesions were observed as well as any signs of inflammation in the interstitial tissues of bronchioles.

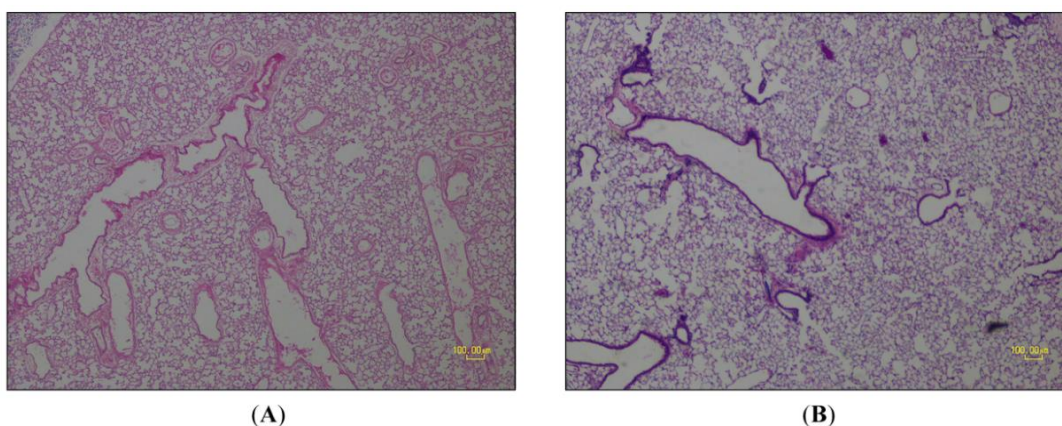


Figure IV. 5 Photomicrographs of hematoxylin-eosin stained lung mice sections of **(A)** control group and **(B)** treated group (magnification: 40x).

IV.4. DISCUSSION

As stated in the **Section IV.1**, the treatment of epilepsy, particularly drug-resistant epilepsy, remains a current challenge in medical research. The present research work aimed to assess the pharmacokinetics and toxicity of levetiracetam after its nose-to-brain delivery and compare it with IV injection. The IN delivery route will enable it to overcome the BBB and the pharmacoresistance mechanisms therein found, and to

achieve a faster brain drug delivery with enhanced targeting and reduced systemic side effects.

Since drug transport across the nasal mucosa into the CNS depends on several factors [246, 442, 483], the rational design of the nasal administration of levetiracetam had three objectives: increase the adhesion to the olfactory epithelium, thereby prolonging residence time and avoiding fast MCC; guarantee an adequate dosage for the pharmaceutical form; and provide its administration in a suitable and safe volume. Thus, the MicroSprayer® Aerosolizer coupled to the FMJ-250 High Pressure Syringe was selected to administer a precisely quantifiable air-free plume of levetiracetam aerosol directly into the nasal mucosa. This strategy advantageously allowed a larger nasal instillation volume (25 μL), without compromising animal breathing, when compared to other previously used devices to intranasally administer AEDs to mice (12 μL) [484, 485].

On the other hand, the use of a thermosensitive mucoadhesive *in situ*-gelling hydrogel avoided a fast MCC of the drug and simultaneously allowed a userfriendly and easy administration form to incorporate and deliver levetiracetam to the nasal mucosa. A major advantage of this formulation is the possibility to maintain it as a liquid solution at temperatures inferior to room temperature and change it, afterwards, to a firm gel at the physiological temperature of the nasal cavity (32-35 °C). Pluronic F-127 was used to produce the *in situ*-gelling hydrogel vehicle, because it is an amphiphilic triblock copolymer of poly(ethylene oxide) and poly(propylene oxide) units that self-aggregate as polymeric micelles. The micelles have a relatively hydrophobic core where drugs can be hosted, increasing their solubility and stability. Moreover, pluronic micellar solutions undergo a sol-to-gel transition at temperatures similar to the nasal mucosa, as a consequence of the micelle packing disorder-order transition phenomenon [484, 486, 487]. In parallel, two polymers were tested in order to provide both sufficient *in situ*-gelling properties and high mucoadhesion: Carbopol® 974P and Noveon® Polycarbophil. The former is a highly cross-linked polymer, producing highly viscous gels; it has been used in oral and mucosal contact applications such as oral liquids, bioadhesive formulations, oral care formulations and extended release tablets.

Additionally, drug release from extended-release tablets is affected by differences in the rates of hydration and swelling of the polymer hydrogel, which are largely defined by cross-linker levels. Noveon® Polycarbophil USP is a high molecular weight acrylic acid polymer cross-linked with divinyl glycol. It provides excellent bioadhesive properties and has been extensively used to enhance the delivery of active ingredients to various mucous membranes [487]. Thus, both thermoreversible gels were characterized regarding their mechanical properties (**Table IV.2**), revealing similar values of adhesiveness and, consequently, of bioadhesion at 35°C. The adhesiveness values herein obtained are considered acceptable for nasal gel administration as described by [488]. Accordingly, their 5 % and 10 % of *Ficus carica* mucilage gel formulations, with mean adhesiveness values of -2.56 and -3.628 g.s, achieved the highest values of C_{max} *in vivo* as well as a good safety profile after histological analysis of the nasal mucosa. The influence of levetiracetam inclusion in both hydrogels was assessed, revealing that the Carbopol® 974P gel (25 mg/mL) had the lowest values of compressibility and hardness at 5°C, which made the formulation easy to aspirate when maintained on ice, without losing the mucoadhesiveness required at the nasal mucosa temperature of 35°C.

Complementarily, *in vitro* cell viability studies were also performed to assess the effect of levetiracetam and gel formulations in the human nasal mucosa cell line, RPMI -2650. The *in vivo* histological analysis was hampered by the reduced area of nasal mucosa of mice, which would be easily damaged throughout its collection. Therefore, future studies should be performed in the rat. To overcome this limitation, several concentrations were tested *in vitro*, including the maximum achievable concentration in accordance with drug solubility and to use only 0.2 % of DMSO at final solutions, which is considered non-toxic for cells. According to the results displayed in **Figure IV.1**, it is evident that cell viability was not compromised by levetiracetam or by any of the gels loaded with levetiracetam.

Combining the mechanical characteristics of the different gels and their impact on the viability of nasal mucosa cells, the thermoreversible mucoadhesive gel composed by 18 % Pluronic F-127 and 0.2 % Carbopol® 974P was herein selected to incorporate and deliver levetiracetam at the dosage of 25 mg/mL by IN route. Hence, a

comprehensive characterization of the pharmacokinetic behavior of levetiracetam following IN administration to mice was performed for the first time, and compared to that observed after an IV administration of levetiracetam at the same dose (625 $\mu\text{g}/\text{animal}$, corresponding to a concentration range of 21-25 mg/kg , considering that animals weighted 25-30 g). This dose range is within the non-toxicity range of levetiracetam IV doses reported in mice (up to 750 mg/kg) [489]. The mouse was selected as an animal model because the metabolism of levetiracetam appears to be species-independent and the major metabolite observed in humans is also found in mice [489]. On the other hand, the mouse is frequently used as an animal model of epilepsy [490–493], and, as it is the most phylogenetically inferior animal species among small laboratory animals, its use is justified in accordance to ethical issues and international guidelines of the European Directive [494–496]. Although levetiracetam is currently available in oral and IV dosage forms, the IV route was chosen as a control because it ensures the highest systemic exposure of all administration routes. This creates appropriate conditions to reduce the inter-individual variability often observed during drug incorporation after oral administration. Moreover, considering that after IN administration drugs may reach the CNS either by direct nose-to-brain route or indirectly through systemic absorption, the drug fraction directly transported from nose to brain could be more accurately discriminated when compared to the IV route [484].

Similarly to IV injection, the IN administration of levetiracetam generated a rapid and extensive systemic absorption of the drug, presenting similar values of C_{max} , t_{max} , AUC_t and AUC_{inf} together with an absolute bioavailability of 107.44 % (**Table IV.3**). This phenomenon probably occurs because of the small molecular weight of levetiracetam (170.21 g/mol). Indeed, most drugs that are extensively absorbed through the nasal respiratory epithelium are highly lipophilic and cross it by transcellular mechanisms. In opposition, levetiracetam is slightly more hydrophilic than lipophilic ($\log P$ is approximately -0.60), suggesting that, in combination with its small molecular weight, its rapid systemic absorption probably takes place by paracellular mechanisms between adjacent epithelial cells, through hydrophilic pores and/or tight junctions [246, 425]. Due to the similar plasma pharmacokinetic patterns of both administration

routes, the proposed IN administration of levetiracetam in the *in situ* mucoadhesive hydrogel emerges as an innovative non-invasive and practical alternative to the IV injection. This is particularly important in acute emergency situations such as *status epilepticus*, since it does not require specialized professionals to be applied.

In addition, the brain concentrations of levetiracetam and its pharmacokinetic parameters after IN and IV administration support a direct nose-to-brain delivery of the drug. After IN administration, the brain exposure of levetiracetam almost doubled relatively to IV administration while C_{\max} increased (**Table IV.3**). Moreover, brain concentrations of levetiracetam up to 15 min are higher after IN administration ($p = 0.0024$ at 5 min post-dosing and $p = 0.033$ at 15 min post-dosing, **Figure IV.3B**) despite the similar values found in plasma after both routes of administration. These findings, together with a DTE of 182.35 % into the brain, corroborate that the IN administration of levetiracetam provides another delivery route in addition to the systemic through the BBB, given that a DTE percentage higher than 100 % indicates a more efficient brain targeting following IN administration, compared to the systemic administration [474, 497, 498]. However, DTE lacks information regarding the fraction of levetiracetam that is directly delivered from the nasal mucosa into the brain. Therefore, DTP was estimated, and revealed that 46.38 % of levetiracetam that reached the brain underwent direct nose-to-brain delivery. It is today scientifically accepted that the direct nose-to brain delivery may occur through the olfactory and/or the trigeminal neuronal pathways [499–501], with the first one being the most important direct pathway [498] and possibly the most determinant for direct nose-to-brain delivery of levetiracetam. Nonetheless, regardless of the mechanism, the fact is that, after IN instillation, almost 50 % of levetiracetam reached the biophase by circumventing the BBB and its pharmacoresistance mechanisms, such as the overexpression of ABC transporters observed in drug-resistant epilepsy. This novel strategy emerges as a new hope for the prevention and treatment of drug-resistant epilepsy.

In spite of the all the aforementioned merits, the single-dose pharmacokinetic study showed considerably higher levetiracetam concentrations in the lungs after IN administration than IV injection. Although this was found only at 5 min post administration, the effect of similar amounts of levetiracetam on Calu-3 cell viability

was assessed and a repeated dose toxicity study was performed. No decreases of Calu-3 cell viability were found *in vitro* when exposed for 24 h to levetiracetam at concentrations between 1 and 100 μM (**Figure IV.2**). These concentrations included the C_{max} achieved in lung tissues after a single IN dose (**Table IV.3**). Complementarily, the *in vivo* repeated dose study, performed during 7 consecutive days with a twice-daily administration of the mucoadhesive *in situ* gel loaded with levetiracetam, revealed no histological alterations in lung tissues (**Figure IV.5**) in accordance with [482]. Altogether, these findings suggest that, besides being promising for the treatment of drug-resistant epilepsy, the nose-to-brain delivery of levetiracetam is likely safe, taking into account the *in vitro* and *in vivo* results herein revealed.

IV.5. CONCLUSION


In the present study, an efficient and significant nose-to-brain delivery of levetiracetam was achieved after its incorporation into a thermoreversible mucoadhesive gel and administration in aerosolized form to mice. Both Pluronic F-127 and Carbopol[®] contributed to the formation of a thermogel with adequate textural characteristics, enabling its advantageous administration as a liquid aerosol that gels in the nasal mucosa. Histopathological examination of lung tissue after repeated dosing by IN route showed that the formulation caused no toxicity or structural damage. Accordingly, no reductions of cell viability were observed in nasal and lung cell lines, in the presence of the levetiracetam formulation.

The proposed *in situ* gelling mucoadhesive system carrying levetiracetam represents an alternative to invasive delivery methods by bypassing the BBB and delivering therapeutics directly to the CNS through olfactory and trigeminal nerve passages. Moreover, it is expected to not only circumvent the BBB but also avoid DDI and systemic dilution effects, thereby reducing drug delivery to non-targeted tissues and minimizing toxicity.

Despite requiring further investigations, these non-clinical investigations yield promising results that are a new hope for the treatment of drug-resistant epilepsy.

CHAPTER V

PRE-CLINICAL ASSESSMENT OF THE NOSE-TO- BRAIN DELIVERY OF ZONISAMIDE AFTER INTRANASAL ADMINISTRATION



V.1. INTRODUCTION

Since the beginning of the XXI century (2000-2005), zonisamide (1,2-benzisoxazole-3-methanesulfonamide) is licensed in the United States of America and European Union for the treatment of generalized and focal seizures, not only as monotherapy in firstly diagnosed adults but also as add-on therapy in adults and children with at least six years old [502]. Serendipitously, zonisamide also demonstrated to improve motor symptoms in patients with Parkinson's disease when co-administered with levodopa [503, 504], being currently approved in Japan as adjunctive therapy of Parkinson's disease at lower doses than those used in epilepsy [505]. In addition, zonisamide revealed to be effective in relieving chronic and episodic cluster headaches [506]. Underlying this widespread clinical use are probably the multiple mechanisms of action of zonisamide, encompassing the blockage of voltage-dependent sodium channels and T-type calcium channels, which contribute to neural membranes stabilization [507], inhibition of carbonic anhydrase [508], alteration of dopamine metabolism [503] and reduction of glutamate release [509]. Importantly, pre-clinical investigations recently highlighted that zonisamide attenuates cell death induced by seizure and/or ischemia and seems to protect the nigrostriatal dopaminergic neurons when administered to Parkinson's disease mice model [503, 510]. Moreover, zonisamide improved the treatment of dementia with Lewy bodies parkinsonism when it was added as an adjunct to levodopa [509].

However, in spite of its undeniable efficacy as antiepileptic drug, high potential as anti-parkinsonian drug and expected success as a neuroprotective drug in neurodegenerative pathologies, zonisamide exhibits a challenging safety profile, requiring careful patient selection and drug monitoring [511]. Indeed, its safety profile is currently preventing zonisamide from being used as a first-line drug for the treatment of epilepsy or other pathological conditions [511]. Among the major adverse effects of zonisamide, gastro-intestinal-related (e.g. weight loss, nausea, dizziness) and central-related (e.g. confusion, concentration difficulty, depression, somnolence) are the most prevalent. In addition, as a carbonic anhydrase inhibitor, zonisamide commonly induces nephrolithiasis, with formation of symptomatic kidney stones

[511–513]. Importantly, blood concentrations of zonisamide have demonstrated to be substantially increased in patients with adverse effects than in those without adverse effects, ascribing high blood concentration as a risk factor for urolithiasis either in monotherapy or polytherapy [502, 514]. In this regard, the ideal administration route for zonisamide would be one that would allow the drug to attain the CNS with minimal systemic exposure. However, the only currently available administration route is the oral one, which requires the systemic absorption of zonisamide followed by its passage through the BBB to attain the brain. Although zonisamide is completely and quickly absorbed after oral administration, reaching C_{max} in plasma at 2–4 h, its absorption rate is slowed with concomitant food intake, while drug absorption extent remains constant [515]. Moreover, zonisamide exhibits a long $t_{1/2}$, approximately 60 h [515], which is a limitation when if the drug needs to be quickly discontinued. Furthermore, the $t_{1/2}$ of zonisamide presents a high inter-individual variability and can be as low as 25 h [516, 517] or as high as 80 h [511]. In fact, 97 % of zonisamide excretion occurs through renal mechanisms, 30–35 % as the unchanged form, 15–20 % as *N*-acetyl-zonisamide and 50 % as the 2-sulfamoylacetylphenol glucuronide, which suffers subsequently conjugation with glucuronide [515, 518]. The major metabolite mainly results from the reduction of the parent compound by the CYP3A4 isoform, even though CYP2C19 and CYP3A5 have also demonstrated to be involved [519]. The first-pass hepatic metabolism considerably observed after oral administration not only increases inter-individual variability of its pharmacokinetic parameters particularly due to the genetic polymorphisms coupled to the CYP2C19 isoenzyme [520–522] but also the potential of zonisamide to be involved in DDI [515]. Importantly, patients co-treated with other drugs that inhibit or induce CYP3A4, are advisable to be subjected to dose adjustment, as zonisamide concentrations considerable change independently of the administered dose [515].

Bearing in mind the aforementioned limitations of oral formulations to deliver zonisamide into the brain, the exploitation of a novel administration route became of great interest and one of the most challenging research areas. Hence, the present research work aims at directly deliver zonisamide to the brain after IN administration, thereby reducing drug systemic exposure and ameliorating its safety profile. Non-

invasive nose-to-brain drug transport via olfactory epithelium has revealed to be a promising strategy for chronically given central-acting drugs with potential increasing of patient compliance [234, 258, 523–526]. For instance, we have demonstrated that the antiepileptic drug, levetiracetam, loaded in a thermoreversible gel composed of Carbopol 974P, achieved higher concentrations in the brain 5 min after IN administration than after administration by classic systemic route [523]. In theory, it has been postulated that drugs can be transported from the nasal cavity directly to CSF or brain parenchyma through two possible routes along the olfactory neurons: the olfactory nerve pathway (intracellular axonal transport) and the olfactory epithelial pathway (extracellular perineural transport). The extracellular transport, apparently a faster route of nose-to-brain delivery, allows drugs to paracellularly cross the perineural epithelium into the fluid-filled perineuronal space (within 30 min), mainly by a bulk flow transport phenomenon, along the olfactory axon up to the subarachnoid space filled with CSF. On the other hand, the intracellular mechanism has been proposed as a feasible route to transfer drugs directly to the brain via intracellular axonal transport along the olfactory sensory neurons. Accordingly, there is a slow axonal internalization of the molecule (endocytosis) and subsequent release by exocytosis into the olfactory bulb and other brain areas by the anterograde axoplasmic flow [469]. Nevertheless, due to the physiological defense mechanisms of nasal mucosa, compounds administered in nasal cavity often suffer MCC and are quickly eliminated from the nasal mucosa. This hampers the drug to remain enough time in olfactory epithelium, compromising its distribution into the brain [527].

Therefore, for the first time, the present study characterized the pharmacokinetics of zonisamide in plasma, brain, lung and kidney after IN administration, comparing them to those observed after oral and IV administrations. Due to the aforementioned principle and advantages of IN delivery route, the present study made use of a mucoadhesive formulation to reduce the clearance rate of zonisamide and increase its delivery into the brain.

V.2. MATERIAL & METHODS

V.2.1. CHEMICALS & REAGENTS

Zonisamide was acquired from Molekula SRL (Rimini, Italy) while antipyrine and Pluronic F-127 were obtained from Sigma-Aldrich (St. Louis, MO, USA) and Carbopol® 974P and Noveon® Polycarbophil were kindly provided by Lubrizol (Wickliffe, OH, USA). Quantification of zonisamide in pharmacokinetic study samples required acetonitrile of HPLC gradient grade (Fisher Scientific, Leicestershire, UK) and ultrapure water (HPLC grade, 18.2 MΩ.cm), which was prepared using a Milli-Q water apparatus from Millipore (Milford, MA, USA). Reagents used for sample homogenization and drug extraction included hydrochloric acid fuming 37 %, disodium hydrogen phosphate dihydrate and sodium dihydrogen phosphate dihydrate, from Merck KGaA (Darmstadt, Germany), and DMSO, ethyl acetate and methanol from Fisher Scientific (Leicestershire, UK). Animals were anesthetized with ketamine (Imalgene 1000®, 100 mg/mL) and xylazine (Vetaxilaze 20®, 20 mg/mL), both commercially available. All the remaining chemicals and reagents were obtained from Sigma-Aldrich (St. Louis, MO, USA) unless otherwise specified.

V.2.2. IN VITRO ASSAYS

V.2.2.1. Human Lung Adenocarcinoma Cell Line *In Vitro* Viability

The viability of human lung adenocarcinoma cells (Calu-3, ATCC® HTB-55TM) was tested by exposing them to zonisamide at various concentrations. Dulbecco's modified Eagle's medium (Sigma-Aldrich) with 0.04 M sodium bicarbonate and enriched with inactivated fetal bovine serum (10 %, v/v) and penicillin-streptomycin (1 %, v/v) was used as culture medium for Calu-3 cells. These cells were grown in T-75 flasks (Orange-

Scientific, Braine-l'Alleud, Belgium), passaged 3 times/week using a 0.25 % Trypsin-EDTA solution and cultured at 37°C in 95 % relative humidity and 5 % CO₂.

The viability of Calu-3 cells was determined applying the Alamar Blue assay, performed in accordance with [474]. Briefly, cells were seeded in 96-well plates (3.5 × 10⁴ cells/well) and incubated for 24 h at 37 °C and 5 % CO₂. After removing the culture medium, control cell group was put into contact with fresh medium without of zonisamide, while the treatment groups were incubated with zonisamide at the following concentrations: 1, 5, 10, 25, 50 and 100 μM. The incubation treatment time was 24 h. Afterwards, treatment solutions were withdrawn and fresh medium with 10 % Alamar Blue solution (125 mg/mL) was added to each well. After an incubation of 3h, fluorescence was measured (560 nm/590 nm) on the Biotek Synergy HT microplate reader (Biotek Instruments®, Winooski, VT, USA).

The Alamar Blue assay is based on the quantification of resorufin, a substance with endogenous fluorescence and that results from the reduction of resazurin by viable cells. The viability of the cells was determined in accordance with the following **Equation V.1**.

$$\text{Cell viability (\%)} = \frac{FL_{\text{Lev}} - FL_{\text{W}}}{FL_{\text{Control}} - FL_{\text{W}}} \times 100 \quad \text{Equation V.1}$$

FL refers to the mean value of fluorescence displayed after incubation with the treatment solution (FL_T), in the controls (FL_{control}) and in the wells without cells (FL_W).

V.2.2.2. Human Nasal Septum Cell Line *In Vitro* Viability

The Human nasal septum cell line (RPMI-2650, ECACC 88031602) was used to evaluate the influence of zonisamide and both gels on cell viability and, hence, select the most suitable formulation to be administered to mice.

The culture medium used for RPMI-2650 cells was the Minimum Essential Medium Eagle with Earle's salts and sodium bicarbonate, and enriched with glutamine (2 mM), nonessential amino acids (1 %, v/v), heat-inactivated fetal bovine serum (10 %, v/v) and penicillin-streptomycin mixture (1 %, v/v). Grown conditions were those aforementioned for Calu-3 cell line.

After optimization of the protocol, Alamar Blue assay was performed as described in **Section V.2.2.1**, with the exception of cell density, which was 3.0×10^5 cells/well, and the period of incubation with Alamar Blue solution which was only 2 h. The differences of incubation period and cell density were defined according to the metabolizing capacity of the cells. Metabolically viable cells convert non-fluorescent resazurin (Alamar Blue) into highly fluorescent resorufin. Thus, cell lines with higher metabolic activity require a shorter incubation time. The experimental conditions herein tested included: zonisamide in concentrations ranging from 1 to 100 μM ; Noveon® Polycarbophil or Carbopol® 974P gels unloaded; and both gels loaded with zonisamide at the concentrations of 50, 100, 150, 200, 250 and 400 μM .

V.2.3. IN VIVO PRE-CLINICAL STUDIES

V.2.3.1. Ethical Considerations and Animals

The European Directive (2010) regarding the protection of laboratory animals used for scientific purposes (2010/63/EU) (European Parliament, Council of the European Union, 2010) and the Portuguese law on animal welfare (Decreto-Lei 113/2013) were taken into account when designing and performing these investigations. In addition, the studies were authorized by the national entity, DGAV, and all efforts were made to reduce the number of used animals and their suffering.

The pre-clinical studies were carried on in adult male CD-1 mice weighing between 25-30 g. They were acquired to Charles River Laboratories (France) and acclimatized to the local bioterium for at least one week. During this period, animals were housed in groups of five animals at controlled environmental conditions (20 ± 2 °C; relative

humidity 55 ± 5 %; 12 h light/dark cycle). Standard rodent diet (4RF21, Mucedola®, Italy) and tap water were of *ad libitum* access during acclimatization and all experimental procedures.

V.2.3.2. Preparation of Zonisamide Formulations

For IN administration, the appropriate amount of zonisamide was firstly dissolved in DMSO to obtain the final concentration of 400 mg/mL; 25 μ L of this stock solution was added to 975 μ L of the thermoreversible gel, yielding a final zonisamide concentration of 10 mg/mL. Briefly, Pluronic F-127 (18 % w/v) was dissolved in 10 mL of cold Milli-Q water and stored at 4 °C overnight for complete hydration of the flakes. Subsequently, 0.02 g of Carbopol® 974P or the same amount of Noveon® Polycarbophil was added until complete dissolution as described in [523]. The gel was selected according to the results obtained during *in vitro* tests (Section V.3.1), with Carbopol® 974P being the polymer for which the results were more favorable.

In order to obtain an adequate IV solution (without suspension particles), different solvents were tested to prepare a concentrated stock solution of zonisamide. Transcutol® (Diethylene Glycol Monoethyl Ether) was selected, as it allowed zonisamide to solubilize at 10 mg/mL. This solution was, then, diluted in sodium chloride 0.9 % solution (B. Braun Medical, Queluz de Baixo, Portugal) to attain the final concentration of 4.17 mg/mL without compromising physiological pH and fluidity.

For oral administration, zonisamide was suspended in sodium chloride 0.9 % solution at the final concentration of 3.2 mg/mL.

V.2.3.3. *In vivo* pharmacokinetic study

Pharmacokinetic studies were performed to compare the pharmacokinetics of zonisamide in different biological matrices after its single-dose administration by IN, IV and oral routes.

To attain this objective, 140 the animals were randomly divided into three groups: 45 animals received zonisamide by IN route, 50 by oral route and 45 by IV route. All animal groups were pre-anesthetized with ketamine/xylazine (100/10 mg/kg, intraperitoneal) and kept in a heated environment to avoid hypothermia.

Regarding the IN administered animal group, 50 μ L of the thermoreversible gel loaded with zonisamide, corresponding to 16.7 mg/kg, were aerosolized using the high pressure system MicroSprayer[®] Aerosolizer (model IA-1B, PennCentury, Inc., Wyndmoor, PA) connected to a high pressure syringe (Model FMJ-250 from PennCentury, Inc., Wyndmoor, PA). The device was introduced approximately 1 mm into the left nostril of anesthetized mice, while anatomically positioned in right lateral decubitus.

The same dose reported for the IN route was administered intravenously via the injection of 120 μ L of the previously prepared solution with final concentration of 4.17 mg/mL. Both IN and IV administered animal groups were sacrificed at 5, 15, 30, 60, 90, 120, 240, 360 and 480 min post-administration (5 animals per time point). The group of orally treated animals was also previously anesthetized, in order to mimic the conditions of IN and IV groups. The administered single dose was 80 mg/kg and sample collection times were 5, 15, 30, 60, 90, 120, 240, 360, 480 and 780 min post-administration.

Animals were sacrificed at the defined endpoints by cervical dislocation and decapitation. Blood was quickly collected to heparinized tubes, centrifuged at 2880 *g* (4 °C, 10 min) to obtain plasma while the tissues were excised, cleaned with sodium chloride 0.9 % solution, weighted and homogenized with 0.1 M sodium phosphate buffer pH 5.0 (4 mL/g) by use of the THOMAS[®] Teflon. Homogenates were also centrifuged at 2880 *g* (4 °C, 15 min) and, similarly to plasma, the supernatant samples were collected and kept frozen at -80 °C until preparation and analysis by HPLC.

V.2.3.4. Drug Analysis

Before quantitative analysis, both plasma (100 μ L) and tissue supernatants (150 μ L) were spiked with the IS (antipyrine, 50 μ g/mL) and, then, subjected to protein precipitation with methanol and two liquid-liquid extractions with ethyl acetate in order to remove endogenous contaminants and extract zonisamide. More details of extraction and concentration procedures can be found in [523].

To quantify zonisamide in the biological samples collected from *in vivo* pharmacokinetic studies, 20 μ L of each final prepared sample was injected into the Shimadzu HPLC system (Shimadzu Corporation, Kyoto, Japan) composed of LC-20A solvent delivery model, DGU-20A5 degasser system, SIL-20AHT autosampler, CTO-10ASVP column oven (set at 40 °C) and SPD-M20A DAD (used at 220 nm and 239 nm for antipyrine and zonisamide, respectively). LCsolution software (Shimadzu Corporation, Kyoto, Japan) controlled HPLC apparatus and data acquisition. Chromatographic separation was achieved on a LiChroCART® Purospher® Star C₁₈ reverse phase column (55×4 mm, 3 μ m; Merck KGaA, Darmstadt, Germany) and using a mobile phase of water and acetonitrile with gradient elution, based on our previously validated method [476].

Before analyzing the samples, the bioanalytical method was partially validated considering the guidelines defined by the EMA [417] and FDA [418] as demonstrated in **Figure V.1** and **Table V.1**.

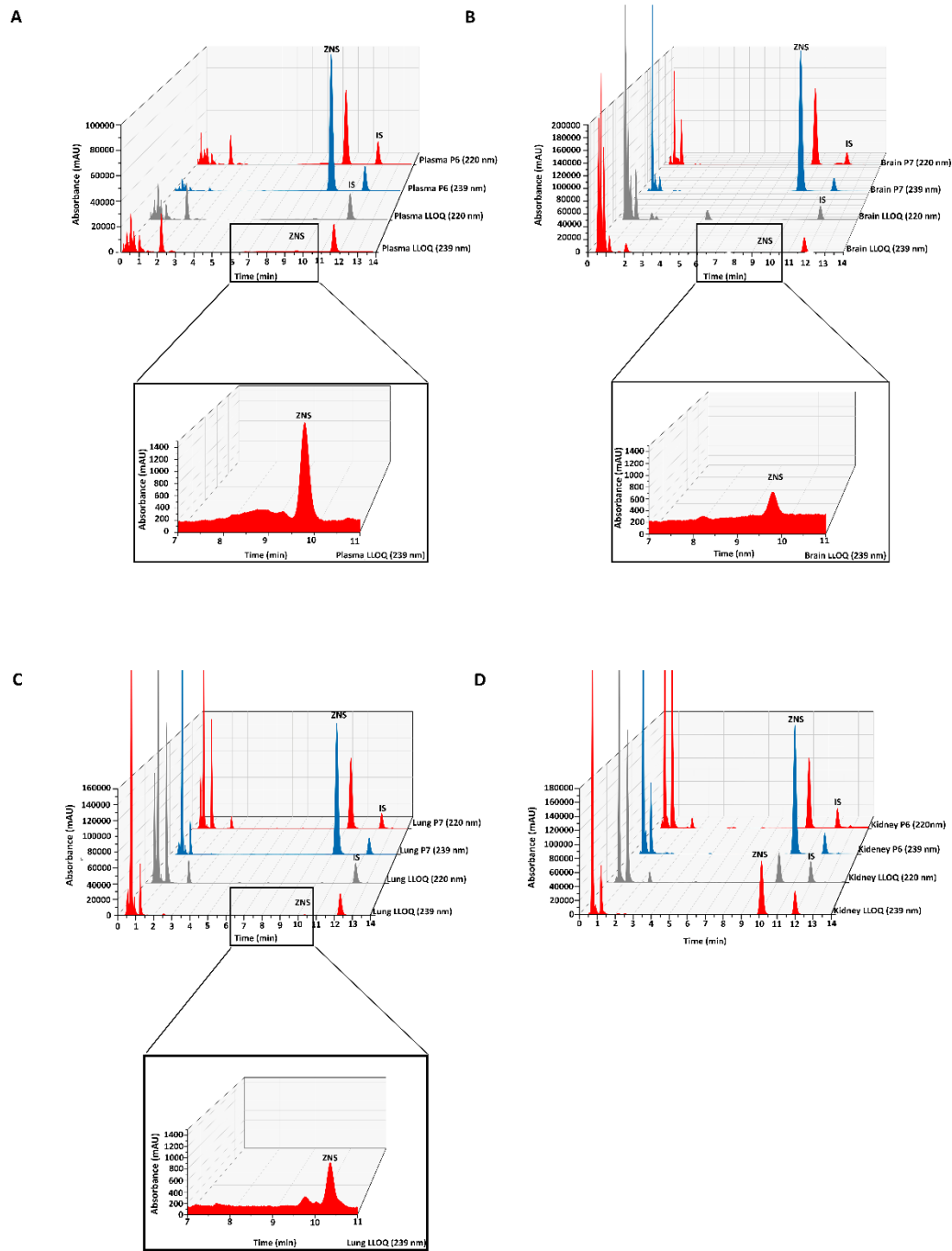


Figure V.1 Representative chromatograms achieved during validation of the analytical technique described in section 2.3.4 for mice plasma (A), brain (B), lung (C) and kidney (D) spiked at the lower limit of quantification (LLOQ) level and at the upper limit of quantification of the calibration ranges; the internal standard (IS, antypirine) was detected at 220 nm while zonisamide (ZNS) was at 239 nm.

Table V.1 Main parameters of the HPLC-DAD method validation employed to quantify zonisamide in plasma, brain, lung and kidney matrices (n = 5).

Validation Parameter	Plasma	Brain	Lungs	Kidneys
Calibration range^a (µg/mL)	0.5 – 50	0.2 – 200 ^b	0.2 – 200 ^b	4 – 200 ^b
Regression Equation^a	y=0.0566658x - 0.010688	y=0.095754x + 0.008597	y=0.116435x - 0.057024	y=0.119375x - 0.045099
Coefficient of determination (r²)	0.9958	0.9918	0.9949	0.9950
LLOQ (µg/mL)	0.5	0.2 ^b	0.2 ^b	4 ^b
Interday				
Precision (% CV)	2.88 – 9.48	4.27 – 12.24	3.23 – 7.34	9.57 – 10.86
Accuracy (% RE)	-1.52 – 13.42	-13.74 – 2.95	0.70 – 2.15	-10.16 – 9.87
Intraday				
Precision (% CV)	2.81 – 9.91	5.36 – 7.66	1.89 – 5.20	2.87 – 7.96
Accuracy (% RE)	0.60 – 8.88	-5.30 – 2.10	2.59 – 7.46	-1.04 – 1.50
Recovery (%)	68.38 – 81.45	69.10 – 87.07	64.47 – 84.59	65.93 – 90.46

^a Interday values, n = 5; ^b values expressed in µg/g

LLOQ, lower limit of quantification; CV, coefficient of variation; RE, relative error deviation from nominal value.

V.2.4. IN VIVO PHARMACOKINETIC STUDIES

The C_{max} and respective t_{max} of zonisamide in plasma and tissues were directly estimated in accordance with the temporal evolution of drug concentrations. The other pharmacokinetic parameters that were herein estimated included two related with drug exposure – the AUC from time zero to the last time with quantifiable concentration (AUC_t), from time zero to infinity (AUC_{inf}) [determined by calculating $AUC_t + (C_{last}/k_{el})$, where C_{last} is the last quantifiable concentration and k_{el} is the apparent elimination rate constant] – and other two related with drug elimination – $t_{1/2}$ and the MRT. The $t_{1/2}$ was estimated as the quotient of $\ln 2$ per k_{el} , while MRT represents the average time a molecule stays in the body and is estimated as the ratio between the area under the first moment curve or the curve of concentration *versus* time versus time and the correspondent AUC. All the aforementioned pharmacokinetic parameters were estimated by non-compartmental analysis, using the WinNonlin version 5.2 (Pharsight Co, Mountain View, CA, USA). Non-compartmental analysis was herein

selected because it considers the mean concentrations ($n = 5$) obtained at each endpoint without assuming an exponential function and, consequently, decreasing the RE of the estimated pharmacokinetic parameters. In addition, the AUC_{extrap} was calculated in percentage, corresponding to the percentage of AUC extrapolated from t_{last} to infinity. This is a relevant parameter, since AUC_{extrap} should preferably be inferior to 20 % to guarantee that samples were collected during enough time to accurately describe zonisamide pharmacokinetics.

The absolute and relative bioavailabilities were estimated according to **Equations V.2** and **V.3**, respectively.

$$F_{Abs} = \frac{AUC_{inf IN} \times Dose_{IN}}{AUC_{inf IV} \times Dose_{IV}} \times 100 \quad \text{Equation V.2}$$

$$F_{Rel} = \frac{AUC_{inf IN} \times Dose_{IN}}{AUC_{inf Oral} \times Dose_{Oral}} \times 100 \quad \text{Equation V.3}$$

$AUC_{inf IN}$, $AUC_{inf IV}$ and $AUC_{inf Oral}$ are the AUC_{inf} values observed following IN, IV and oral administration, respectively; $Dose_{IV}$, $Dose_{IN}$ and $Dose_{Oral}$ represent the drug dose (mg/kg) administered by IV, IN and oral routes.

The ratio between AUC_{tissue} and AUC_{plasma} was calculated for each tissue sample collected from three animal groups in order to assess drug distribution into the three tissues under analysis and verify whether it depends on the administration route.

In addition, the % DTE and the % DTP were calculated following **Equations V.4** and **V.5**, respectively.

$$DTE (\%) = \frac{(AUC_{brain}/AUC_{plasma})_{IN}}{(AUC_{brain}/AUC_{plasma})_{IV}} \times 100 \quad \text{Equation V.4}$$

$$DTP (\%) = \frac{AUC_{brain IN} - \left[\frac{AUC_{brain IV}}{AUC_{plasma IV}} \times AUC_{plasma IN} \right]}{AUC_{brain IN}} \times 100 \quad \text{Equation V.5}$$

AUC_{plasma} and AUC_{brain} correspond to the AUC_t observed in plasma and brain, respectively. According to literature, it is established that transport is preferential to the brain compared to the systemic pathway, when DTE is greater than 100 % [477, 497, 528]. On the other hand, DTP estimates the drug percentage that directly attained the brain after administration into the nasal cavity, without involving systemic absorption followed by the passage through the BBB. Thus, DTP values greater than 0 indicate direct drug targeting, so the lower plasma and brain exposure following IV administration, the greater the amount of drug that reaches the brain by direct transport [478]. Even though both DTE and DTP have been associated to be high variable depending on the *in vivo* protocols [529], they were herein chosen as they are the most mentioned parameters to assess nose-to-brain delivery and to compare different routes of administration [498].

The brain bioavailability of the drug has also been estimated to evaluate which pathway allows greater drug accumulation at the therapeutic target, according to the **Equation V.6**.

$$B_{\text{brain IN/IV}} = \frac{AUC_{\text{brain IN}}}{AUC_{\text{brain IV}}} \quad \text{Equation V.6}$$

V.2.5. STATISTICAL ANALYSIS

Graphpad Prism® 5.03 (San Diego, CA, USA) was used to construct graphics and perform the statistical data both from the *in vitro* cell investigations and *in vivo* pharmacokinetic study. The *in vitro* results were expressed as mean \pm standard deviation (SD) and ANOVA test was used to determine differences of cell viability (%) after incubation with zonisamide/formulations compared with untreated control cells (100 % cell viability). On the other hand, *in vivo* pharmacokinetic data was expressed as mean \pm standard error of the mean (SEM) and the two-way ANOVA test followed by the Dunnett's multiple comparison test were applied to determine statistical differences among the three administration routes of administration (dose-normalized concentrations *versus* time).

In both data types, differences were considered statistically significant when p -values were inferior to 0.05 ($p < 0.05$).

V.3. RESULTS

V.3.1. *IN VITRO* CELL VIABILITY STUDIES

The results found for Alamar Blue assay (**Figure V.2**) demonstrated no decrease on the viability of the Calu-3 and RPMI-2650 cells in the presence of zonisamide for 24 h at the tested concentrations (1-100 μ M), since no statistically significant differences were observed compared to the negative control. Indeed, cell viability was within ± 15 % compared with negative control, which is acceptable by international guidelines.

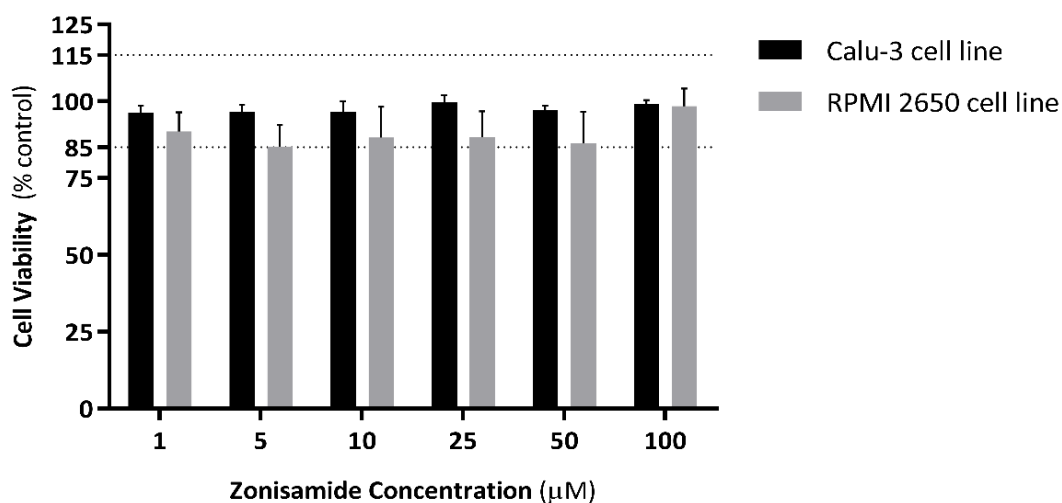


Figure V.2 Viability (%) of Calu-3 and RPMI-2650 cells after incubation with zonisamide for 24 h (1, 5, 10, 25, 50 and 100 μ M). Data represented as mean \pm standard deviation ($n = 4$, three independent replicates).

As described in **section V.2.3.2**, two thermoreversible gels were herein tested: one encompassing 0.02 g of Carbopol® 974P while the other integrated the same quantity of Noveon® Polycarbophil. The viability of RPMI 2650 cells was screened in the presence of these two gels. Empty or loaded with zonisamide, the gels did not impair cell viability within the range of 50 to 400 μ M (**Figure V.3**). Nevertheless, it is

noteworthy that the Noveon® polycarbophilic gel loading zonisamide revealed lower cell viability (ranging from 82.78 to 94.46 %) when compared to the zonisamide-loaded Carbopol® 974P gel (ranging from 99.32 to 105.16 %). For this reason, the thermoreversible gel prepared with Carbopol® 974P was selected to be administered to mice.

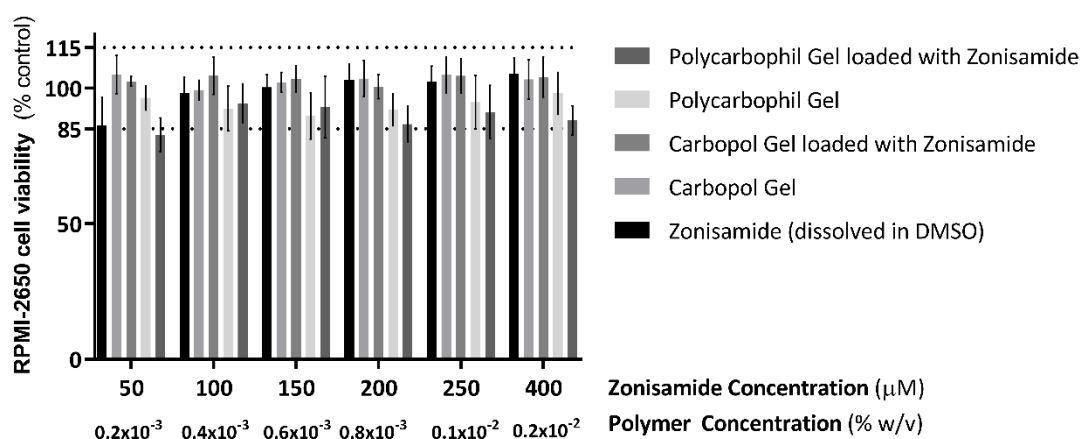


Figure V.3 Viability (%) of RPMI-2650 cells after incubation with zonisamide for 24 h (50–400 µM); empty Noveon® Polycarbophil and Carbopol® thermoreversible gels (0.02 % for both); and thermoreversible gels loaded with zonisamide at the same concentrations. Data represented as mean ± standard deviation (n = 4, three independent replicates).

V.3.2. PHARMACOKINETICS OF ZONISAMIDE

Mean concentration-time profiles (n = 5) of zonisamide in plasma, brain, lung and kidney obtained after administration of one dose of IV solution (16.7 mg/kg), IN thermoreversible *in situ* gel (16.7 mg/kg) or oral suspension (80 mg/kg) to mice are presented in **Figure V.4**. Since the administered oral dose was different from the IV and nasal ones, zonisamide concentrations were normalized according to the administered drug dose of the corresponding route (**Figure V.5**), the Dunnett's multiple comparison test results obtained for oral and IN routes using IV as the control comparator are also depicted in **Figure V.5**. The correspondent mean pharmacokinetic parameters of zonisamide in plasma, brain, lung and kidney are summarized in **Table V.2** and the dose-normalized pharmacokinetic parameters in **Table V.3**.

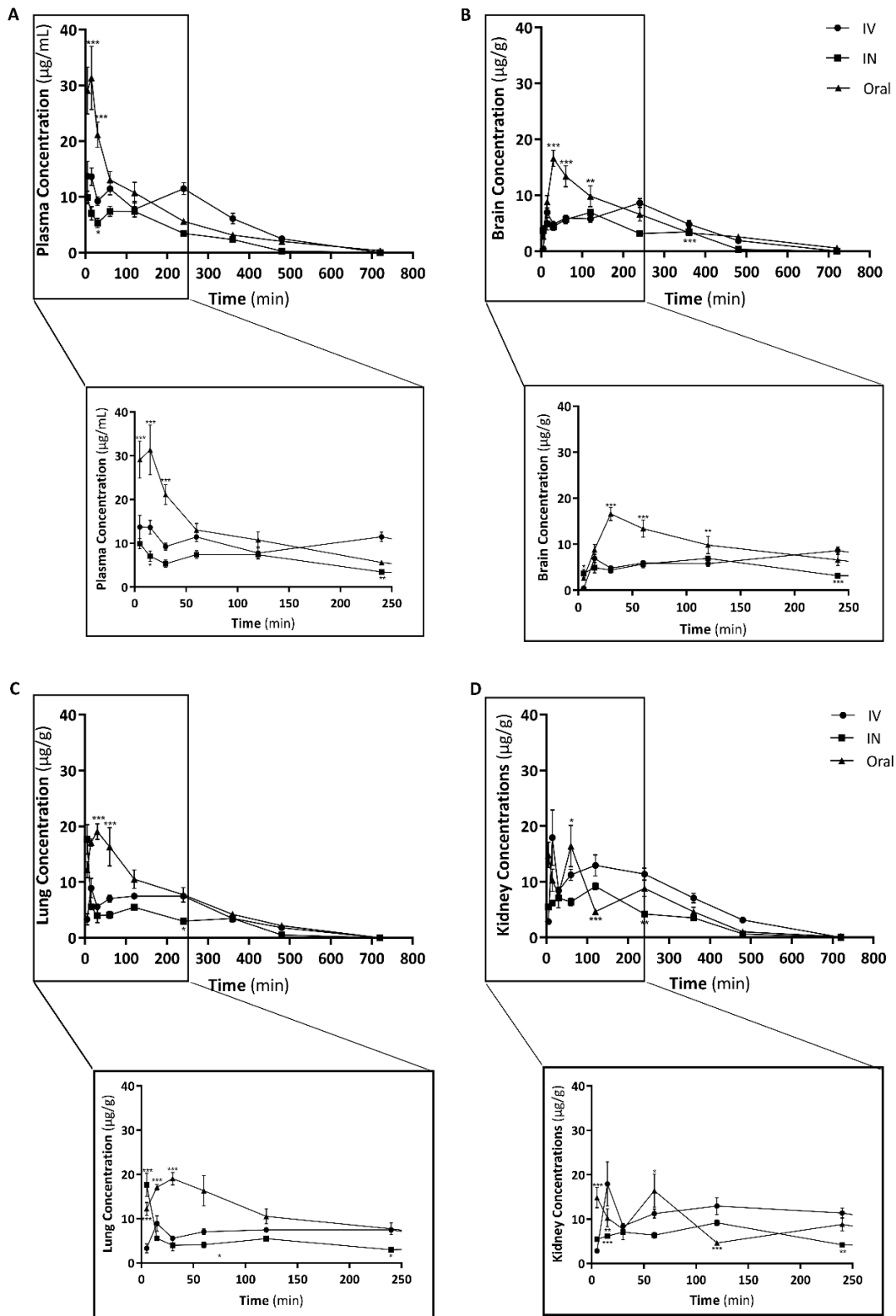


Figure V.4 Concentration-time profiles of zonisamide up to 800 min post-dosing in plasma (A), brain (B), lung (C) and kidney (D) following intranasal (IN, 16.7 mg/kg), intravenous (IV, 16.7 mg/kg) or oral administration (80 mg/kg) to mice. The figure below each profile corresponds to the respective enlargement up to 250 min post-administration. Symbols represent the mean values \pm standard error of the mean (SEM) of five determinations per time point ($n = 5$).

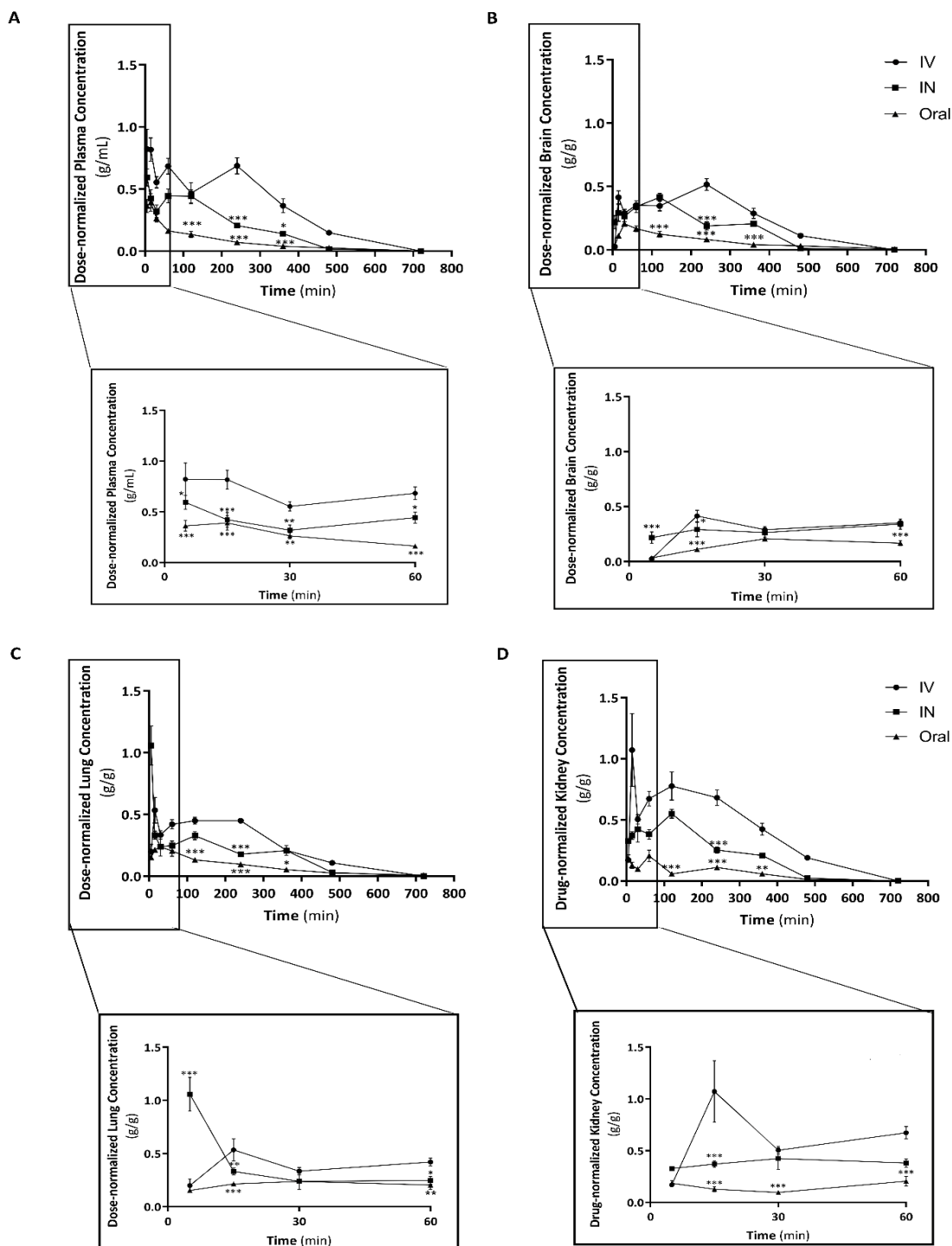


Figure V.5 Dose-normalized concentration- time profiles of zonisamide up to 800 min post-dosing in plasma (A), brain (B), lung (C) and kidney (D) following intranasal (IN, 16.7 mg/kg), intravenous (IV, 16.7 mg/kg) or oral administration (80 mg/kg) to mice. The figure below each profile corresponds to the respective enlargement up to 60 min post administration. Symbols represent the mean values \pm standard error of the mean (SEM) of five determinations per time point ($n = 5$). Statistical differences are in relation to the IV administration route as follows: * $p < 0.05$, ** $p < 0.01$, *** $p < 0.001$ assessed by two-way ANOVA followed by Dunnett's multiple comparison test.

Table V.2 Pharmacokinetic parameters of zonisamide in plasma, brain, lung and kidney tissues following its intranasal (IN, 16.7 mg/kg), intravenous (IV, 16.7 mg/kg) and oral (80 mg/kg) administration to mice.

Pharmacokinetic Parameters ^a	Plasma			Brain			Lung			Kidney		
	IV	IN	Oral	IV	IN	Oral	IV	IN	Oral	IV	IN	Oral
t_{max} (min)	5.00	5.00	15.00	240.00	120.00	30.00	15.00	5.00	30.00	15.00	120.00	60.00
C_{max} ($\mu\text{g}/\text{mL}$)	13.72	9.93	31.33	8.61 ^b	6.91 ^b	16.60 ^b	8.93 ^b	17.66 ^b	19.04 ^b	17.90 ^b	9.19 ^b	16.42 ^b
AUC_t ($\mu\text{g}\cdot\text{min}/\text{mL}$)	3955.13	1832.63	3813.40	2708.61 ^c	1876.78 ^c	3691.84 ^c	2680.70 ^c	1794.50 ^c	4315.82 ^c	4515.67 ^c	2358.06 ^c	3245.41 ^c
AUC_{inf} ($\mu\text{g}\cdot\text{min}/\text{mL}$)	4342.48	2386.23	4248.20	3003.11 ^c	1920.93 ^c	3804.93 ^c	2984.67 ^c	1980.00 ^c	4435.77 ^c	5104.55 ^c	2453.99 ^c	3358.92 ^c
AUC_{extrap} (%)	8.92	23.20	10.2350	9.81	2.30	2.97	10.18	9.37	2.70	11.53	3.91	3.38
k_{el} (min^{-1})	0.0064	0.0042	0.0046	0.0064	0.0075	0.0047	0.0059	0.0046	0.0052	0.0054	0.0068	0.0090
$t_{1/2el}$ (min)	108.48	163.92	150.17	109.04	92.17	146.53	116.79	152.32	132.18	129.46	102.30	77.14
MRT (min)	238.61	245.03	195.62	259.95	192.69	225.17	241.72	234.47	209.79	254.24	193.37	194.17
F (%)^d		54.95	20.42									
AUC_t Ratios	IV	IN	Oral									
AUC_{brain}/AUC_{plasma}	0.68	1.02	0.97									
AUC_{lung}/AUC_{plasma}	0.67	0.98	1.13									
$AUC_{kidney}/AUC_{plasma}$	1.14	0.99	0.85									

^a Parameters were estimated using the mean concentration-time profiles obtained from five different animals per time point (n = 5). ^b Values expressed in $\mu\text{g}/\text{g}$; ^c Values expressed in $\mu\text{g}\cdot\text{min}/\text{g}$;

^d Absolute intranasal bioavailability (F) was calculated based on AUC_{inf} values; AUC_{extrap} , extrapolated area under drug concentration-time curve; AUC_{inf} , area under drug concentration-time curve from time zero to infinity; AUC_t , Area under the concentration time-curve from time zero to the last quantifiable drug concentration; C_{max} , Maximum peak concentration; k_{el} , Apparent elimination rate constant; MRT, Mean residence time; $t_{1/2el}$, Apparent terminal elimination half-life; t_{max} , Time to achieve the maximum peak concentration.

Table V.3 Dose-normalized pharmacokinetic parameters of zonisamide in plasma, brain, lung and kidney tissues following its intranasal (IN, 16.7 mg/kg), intravenous (IV, 16.7 mg/kg) and oral (80 mg/kg) administration to mice.

Dose-normalized Pharmacokinetic Parameters ^a	Plasma			Brain			Lung			Kidney		
	IV	IN	Oral	IV	IN	Oral	IV	IN	Oral	IV	IN	Oral
C_{max}/Dose ($\mu\text{g}/\text{mL}$ or $\mu\text{g}/\text{g}$)/(mg/kg)	0.82	0.60	0.39	0.52	0.41	0.21	0.53	1.06	0.24	1.07	0.55	0.21
AUC_t/Dose ($\mu\text{g}\cdot\text{min}/\text{mL}$ or $\mu\text{g}\cdot\text{min}/\text{g}$)/(mg/kg)	237	110	47.7	162	112	46.1	161	107	53.9	270	141	40.6
AUC_{inf}/Dose ($\mu\text{g}\cdot\text{min}/\text{mL}$ or $\mu\text{g}\cdot\text{min}/\text{g}$)/(mg/kg)	260	143	53.1	180	115	47.6	177	119	55.4	306	147	42.0

^a Parameters were estimated using the mean concentration-time profiles obtained from five different animals per time point (n = 5). AUC_{inf}, Area under the concentration time-curve from time zero to infinite normalized per administered dose; AUC_t, Area under the concentration time-curve from time zero to the last quantifiable drug concentration; C_{max}, Maximum peak concentration.

Regarding plasma levels, zonisamide concentrations achieved after IN administration were lower than those observed after IV and oral routes, at all the collected time-points (**Figure V.4A**). Identically to IV route, IN delivery allowed zonisamide to attain the mean C_{max} in plasma at 5 min post-dosing (**Table V.2**). Furthermore, after IN dosing, zonisamide exhibited the lowest value of C_{max} (9.93 $\mu\text{g/mL}$ versus 13.72 and 31.33 $\mu\text{g/mL}$ observed for IV and oral routes, respectively) and AUC_t (1832.63 $\mu\text{g}\cdot\text{min/mL}$ versus 3955.13 and 3813.40 $\mu\text{g}\cdot\text{min/mL}$ for IV and oral routes, respectively). As these results were found with IN and IV doses that were 4.79-fold lower than the oral dose (16.7 mg/kg and 80 mg/kg, respectively), the lower plasma exposure of zonisamide is undeniable after IN delivery (as corroborated by the IN absolute bioavailability of 54.95 %). In addition, comparing the dose-normalized plasma AUC_t following IN and IV administrations, an increment of approximately 2.16-fold is detected for the IN route, confirming the advantage of its lower systemic exposure **Table V.3**. In opposition, the AUC_t/dose obtained after oral administration was 2.30-fold lower than the one of IN route. Nevertheless, in brain tissue, the AUC_t/dose observed after oral route was 2.44-fold lower than that after IN route, suggesting a decreased brain-target delivery when orally administered. Indeed, observing **Figure V.4B-D**, it is noteworthy that the concentrations achieved in brain, liver and kidney tissues are considerably higher for oral route at almost all time-points. This is not surprising, since the oral dose was considerably higher than IV or IN doses, confirming the importance of analyzing dose-normalized concentrations depicted in **Figure V.5**, when comparing with oral route. Accordingly, zonisamide concentrations presented the smallest values after oral administration in all tissues.

When comparing brain concentration-time profiles after IV and IN administration (**Figure V.4B**), it is particularly interesting to observe the anticipation of t_{max} of IN zonisamide in relation to IV formulation (120 min versus 240 min, **Table V.2**). In addition, it is noteworthy that, at 5 min post-IN-dosing, zonisamide concentration is significantly increased relatively to the IV injection (3.636 ± 0.867 and 0.420 ± 0.075 $\mu\text{g/g}$, respectively), presenting a p value of 0.021. Statistical differences were not identified at other time-points, with the exception of 240 min, when concentrations were considerably lower for IN route [11.470 versus 3.437 $\mu\text{g/g}$, respectively; $p =$

0.0065, which is in accordance with the superior k_{el} of zonisamide after IN administration than IV injection (**Table V.2**). Moreover, plasma concentration-time profiles traced for both administration routes, revealed statistical differences, not at 5 min, but at 15 min ($p = 0.0087$) and 240 min ($p = 0.0020$) post-administration, suggesting that, at 5 min, an additional route allowed zonisamide to reach the brain tissue besides the systemic one. Consistently, DTE was 149.50 % and DTP was 33.13 %. Furthermore, at 5, 15 and 30 min post-administration, the highest brain-to-plasma ratios were observed after IN administration, exhibiting significant statistical differences relatively to IV and oral routes, as detailed in **Figure V.6A**. In opposition, from 60 to 480 min, evolution of brain-to-plasma ratios after administration of the thermoreversible gel is parallel to that observed after IV injection, demonstrating that zonisamide attained the brain after systemic absorption and BBB crossing.

Since intranasally administered drugs may reach the lungs in mice, which may compromise the safety of the zonisamide IN formulation, lung tissue was also analyzed in the present study. From **Figure V.4C** and **Table V.2**, it is undeniable that, in lungs, the IN route was the fastest to attain the C_{max} , which was almost twice of that observed after IV injection (17.66 versus 8.93 $\mu\text{g/g}$). Notwithstanding, when considering lung exposure given by AUC_t and AUC_t/dose , the IV route exhibited higher values [2680.70 $\mu\text{g}\cdot\text{min/g}$ and 160.52 ($\mu\text{g/g}$)/(mg/kg)] than IN route [1794.50 $\mu\text{g}\cdot\text{min/g}$ and 107.46 ($\mu\text{g/g}$)/(mg/kg)], while the oral route stood out as the one with the lowest value of AUC_t/dose [53.95 ($\mu\text{g/g}$)/(mg/kg), **Table V.3**]. The faster C_{max} attainment coupled to the lower exposure observed after IN administration are corroborated by the ratios depicted in **Figure V.6B**. Accordingly, at 5 min post-administration, the lung-to-plasma ratio observed after IN instillation was almost 10-fold of those observed after the classical administration routes. These statistical differences were readily minimized from the 15 min post-dosing time, even though the evolution of ratios has been very distinct from IV and oral administration, suggesting that a fraction of zonisamide directly reaches the lung. Indeed, the DTE % was 144.47 %. For these reasons, the viability of Calu-3 cells was assessed *in vitro* after exposure to zonisamide, as discussed in **Section V.3.1**.

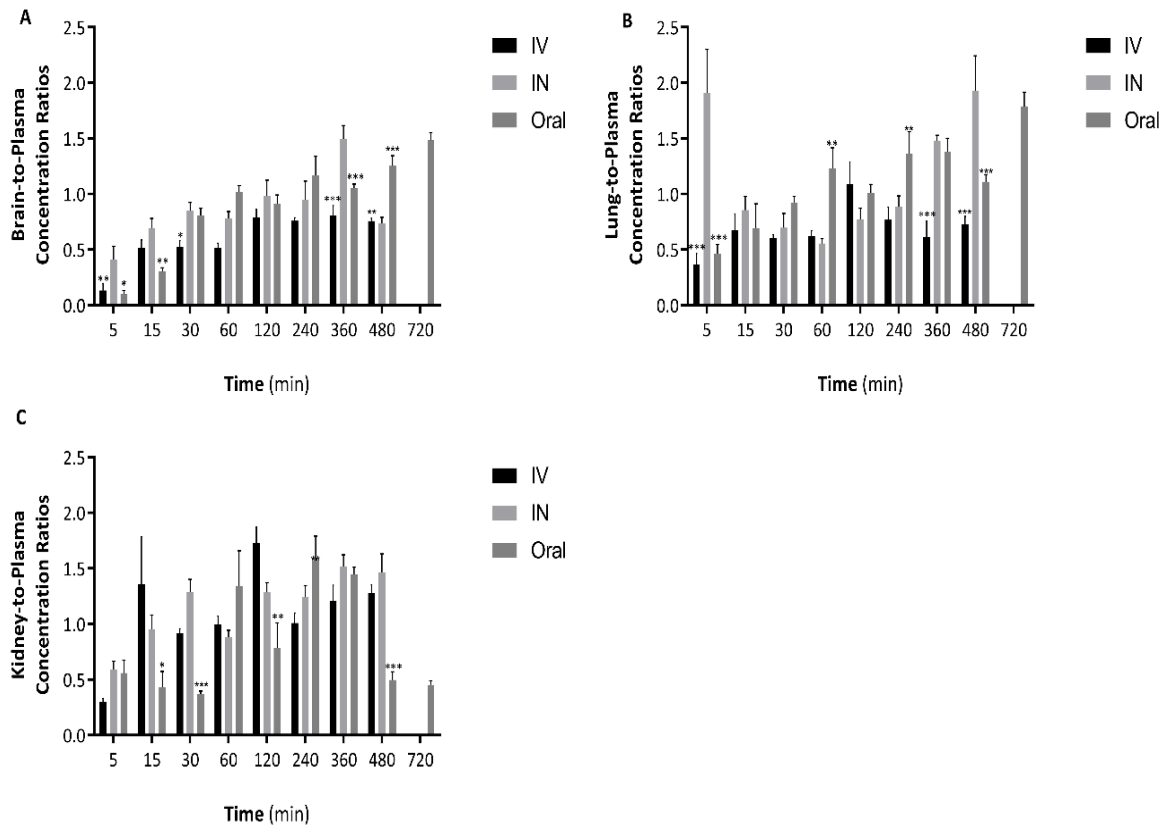


Figure V. 6 Tissue-to-plasma concentration ratios of zonisamide at 5, 15, 30, 60, 120, 240, 360, 480 and 720 min after drug administration by intranasal (IN), intravenous (IV) or oral route. **(A)** represents the variation of brain-to-plasma concentration ratios versus time; **(B)** represents the variation of lung-to-plasma concentration ratios versus time and **(C)** represents the variation of kidney-to-plasma concentration ratios versus time. Statistical differences are in relation to the IV administration route as follows: * $p < 0.05$, ** $p < 0.01$, *** $p < 0.001$ assessed by two-way ANOVA followed by Dunnett's multiple comparison test.

With respect to zonisamide concentrations found in kidney tissue up to 480 min (**Figure V.4D**), the IN route displayed the lowest values. Indeed, at all collected time-points, the concentrations were always inferior to those obtained with IV injection, as well as the C_{max} and AUC values (**Table V.3**). Complementarily, when analyzing normalized concentration-time profiles (**Figure V.5D**), both IN and oral administrations showed decreased concentrations in kidney relatively to IV injection. However, the concentrations found after IN were slightly higher than those obtained by oral route, with statistical differences at 15 min. These findings are further supported by the fact that zonisamide renal exposure (given by $C_{max}/dose$ and $AUC/dose$) was approximately half of that observed after IV injection, but twice of that found after oral administration

(**Table V.3**). Nonetheless, after IN instillation, C_{max} was attained much latter ($t_{max} = 120$ min) than after IV ($t_{max} = 15$ min) or oral ($t_{max} = 60$ min) administrations (**Table V.2**). In addition, it is also important to emphasize that the DTE observed for zonisamide in the kidney after IN administration was 1.12. This was the lowest value compared to the other tissues, suggesting that zonisamide has a decreased ability to accumulate in the kidney. Consistently, zonisamide remained in the kidney for the shortest period when intranasally administered (193.37 min *versus* 194.14 min and 254.24 min after oral and IV routes, respectively, **Table V.2**). The kidney-to-plasma ratios observed for IN zonisamide are very similar to those registered with IV and oral formulations, occasionally presenting statistically significant differences with oral zonisamide at 30, 120 and 480 min post-administration (**Figure V.6C**).

V.4. DISCUSSION

Aiming at formulating a successful and original nose-to-brain drug delivery system, but keeping it simple and achievable, the experimental design was optimized in order to warrant that zonisamide was administered in olfactory mucosa of the respiratory mucosa. The accessibility to these regions is rather difficult in mice, particularly due to their small dimensions. Although drug administration into the nose is often performed using a pipette or a polyethylene tube attached to a microsyringe/micropipette [241, 485], herein we preferred to use the MicroSprayer® Aerosolizer and to load zonisamide in an *in situ*-gelling hydrogel, the Pluronic® F-127 vehicle. This choice was based on our recent studies that demonstrated that almost 50 % of levetiracetam undergoes direct nose-to-brain delivery after its nasal administration [241, 485–487, 523, 530]. Nonetheless, to increase *in situ*-gelling properties and mucoadhesion, Carbopol® 974P and Noveon® Polycarbophil polymers were herein investigated and subjected to cellular viability tests to select the safest one for IN administration to mice. The results found in the RPMI-2640 cell line for zonisamide and the four formulations (empty and drug-loaded) are depicted in **Figures V.2** and **V.3**. Accordingly, the thermoreversible mucoadhesive gel prepared with Carbopol® 974P (0.2 %) plus Pluronic F-127 (18 %) exhibited higher values of RPMI-2650 cells viability in relation to the control and the

other tested gel, and therefore it was selected to incorporate and deliver zonisamide at the dose of 16.7 mg/kg by IN route.

Although zonisamide is only currently marketed in oral dosage forms, IV route was herein used as control because the absolute oral bioavailability of zonisamide was only 20.42 % in mice (**Table V.2**), unlike in humans, where it ranges 60-100 % [432, 531]. Moreover, when assessing the potential of a new route of administration, IV administration is recommended to be used for comparison, since intestinal absorption is avoided, decreasing the variability that may occur during incorporation. Importantly, the blood-mediated zonisamide delivery into the CNS after drug nasal instillation is estimated by IV injection and, consequently, the fraction of the drug directly transported from nose-to-brain is more accurately discriminated. Nevertheless, the pharmacokinetics of oral zonisamide was also assessed in an attempt to investigate whether systemic and brain exposures after nasal administration were within safe therapeutic ranges. This is determinant, because DTE and DTP are limited when used alone and are associated to high variability. Therefore, the orally administered dose was defined to achieve plasma concentrations within human therapeutic range of 10-40 µg/mL [432, 531]. It was established at 80 mg/kg since plasma concentrations were within it up to 120 min post-dosing (**Figure V.4**). Given that the oral dose was more than four-times higher than the nasal and IV ones (16.7 mg/kg), concentrations reached in plasma, brain, lung and kidney were dose-normalized (**Figure VI.5**), as well as the pharmacokinetic parameters which directly depended on administered doses (C_{max} and AUC, **Table VI.3**). Only applying this strategy, could oral results be compared with the remaining ones.

Pharmacokinetic results revealed that, similarly to IV injection, the IN administration of zonisamide nasal gel allowed zonisamide to be quickly absorbed into the bloodstream (t_{max} of 5 min) while oral route required 15 min to attain t_{max} . On the other hand, zonisamide concentrations attained in plasma after IN instillation were considerably lower than those observed after IV injection (**Figure VI.4A**), limiting systemic drug exposure (given by C_{max} , AUC_t and AUC_{inf}). This was supported by the absolute IN bioavailability of only 54.95 % (**Table VI.2**). Although it is undeniable that a significant amount of zonisamide was not absorbed through nasal respiratory

epithelium to bloodstream, the almost overlapping time course of plasma and brain concentrations after both routes of administration suggest that a fraction of the drug was absorbed to the systemic circulation, attaining the CNS after crossing the BBB. Nevertheless, bearing in mind that the present work intended to promote a direct nose-to-brain delivery of zonisamide, the absolute bioavailability of only 54.95 % may not hamper the drug from targeting the CNS. Moreover, it is expected to be advantageous, as fewer systemic side effects are probable to occur after IN administration. Indeed, as discussed in **Section VI.3.2**, brain concentrations of IN zonisamide at 5.00 min were 8.66-fold higher than after IV injection and DTE was 149.50 %, suggesting that a direct transport of zonisamide occurs from nasal mucosa to the brain through the olfactory and/or trigeminal nerve pathways. DTE represents the ratio between brain and plasma concentrations after IN administration in comparison to IV injection. According to Fatouh *et al.* [497] and Pires *et al.* [498], values higher than 1.0 indicate of a more efficient brain targeting following IN administration. Furthermore, the calculated DTP for zonisamide IN gel highlights that 33.13 % of the drug that reaches the brain attains it through direct nose-to-brain mechanisms, circumventing the BBB. The results found for the DTE and DTP, together with the pharmacokinetic behavior of zonisamide in plasma and brain after IN administration comparatively to classical routes are the base for the development of new mathematical pharmacokinetic/pharmacodynamic models as Ruigrok and Lange suggest [532]. Moreover, these findings are of huge clinical relevance, because 30-40 % of medicated epileptic patients develop drug-resistant epilepsy, which has been associated, among other mechanisms, to the overexpression of efflux transporters located in peripheral organs and endothelial cells of BBB. Consequently, the available concentrations to reach the CNS are reduced [144, 155]. Therefore, by circumventing BBB and enabling a direct nose-to-brain transport of zonisamide, the original strategy herein exploited may become successful for the treatment of drug-resistant epilepsy.

Bearing in mind that IV zonisamide is not available in clinical practice, oral administration was also investigated in order to compare the ability of IN administration to deliver higher zonisamide concentrations into the brain, without compromising systemic safety. Thus, the relative bioavailability of nasal

thermoreversible gel was 269.08 %, suggesting that the concentration of systemically absorbed drug through the respiratory epithelium is more than twice of that absorbed at the intestinal level. These results reinforce that the nasal first-passage effect is less relevant than the intestinal and hepatic pre-systemic effects that occur after oral administration. As explained in introduction, zonisamide is highly metabolized in humans by CYP3A4 and CYP2C19 [519, 521] which is one of the major drawbacks of the current oral forms available in clinical practice [515]. Applying the novel nose-to-brain strategy, DDI and inter-individual pharmacokinetic variability are expected to decrease or become negligible.

In addition, it is noteworthy that the brain concentrations of zonisamide after oral administration are considerably higher (**Figure VI.4B**). However, when dose-normalized concentrations are plotted against time administration (**Figure VI.5B**), it becomes clear that these differences result from the higher orally administered dose. Indeed, IN and IV routes exhibit dose-normalized C_{max} and AUC that are more than twice of those of oral administration (**Table VI.3**). In addition, IN route has the highest $AUC_{t_{brain}}/AUC_{t_{plasma}}$ ratio (1.02 *versus* 0.68 for IV and 0.98 for oral administrations, **Table VI.2**), confirming that the IN route allows a higher brain exposure, despite lower systemic drug exposure. Interestingly, since zonisamide was quantified only up to 8 h and the intracellular nose-to-brain transport implies 1.5-6 h through the olfactory route and 17-56 h through the trigeminal nerve [469, 533], it can be hypothesized that zonisamide directly attained the brain through the olfactory pathway. Despite the above conclusions, specific biodistribution and pharmacodynamic studies should be carried out in the future to clarify the issue.

In order to assess whether IN administration could compromise drug safety at pulmonary level, the pharmacokinetics of zonisamide in lungs was compared after administration by the three routes. It was clearly observed that lung concentrations of zonisamide at 5 min post-dosing were considerably superior after IN administration than intravenously (17.66 ± 2.651 and 3.33 ± 1.004 $\mu\text{g/g}$, respectively; $p = 0.007$) (**Figure VI.4C**). Nonetheless, at the remaining time-points, concentrations were always lower after IN instillation (**Figure VI.4C**). In addition, lung exposure given by AUC was lower for IN administration than for IV route (**Table VI.2**), suggesting that pulmonary

safety is expected to be maintained. These data are corroborated by the inferior value of $AUC_{\text{tlung}}/AUC_{\text{tplasma}}$ observed with IN instillation than oral administration (**Table VI.2** and **Figure VI.6B**). Additionally, zonisamide did not compromise the viability of Calu-3 cells after 24 h of exposure at concentrations between 1 and 100 μM (**Figure VI.2**), which include the concentrations found during preclinical *in vivo* investigation herein performed.


Finally, zonisamide pharmacokinetics was also assessed in kidney, particularly due to its most relevant side effect, i.e. renal lithiasis. Higher zonisamide concentrations in kidney were found after IV injection than those observed with the thermoreversible gel (**Figure VI.4D**), substantiating that the drug has enhanced renal exposure after IV injection. Comparing with oral route, kidney exposure (given by C_{max} and AUC_{t} and AUC_{inf}) after dose-normalization was higher for intranasal route (**Table VI.3**). Nevertheless, nasal route is expected to require lower doses than the oral, since the first-passage effect in the nasal cavity is less than in the intestine.

In conclusion, the present study demonstrated that the IN administration of zonisamide allowed a faster drug targeted-uptake into the brain, in relation to the IV injection. Moreover, systemic absorption through respiratory epithelium was approximately 50 % of IV route, which is considered advantageous, since fewer systemic side effects are expected to occur. The IN administration of zonisamide was also compared to the oral route, corroborating the obtained results and highlighting that drug exposure in lungs and kidneys are comparable for the three administration routes, thereby prospecting very similar pharmacological responses at those levels. Thus, the novel nose-to-brain strategy herein investigated for the first time seems to be beneficial to directly deliver the drug into the CNS, representing a suitable and promising alternative route for zonisamide administration, not only for chronic treatment of epilepsy or Parkinson's disease but also in acute emergency situations, such as *status epilepticus*. In addition to this, zonisamide is currently marketed only in oral forms, requiring novel formulations that can be used in acute situations. From this perspective, the discussed *in vitro/in vivo* results support that the aforementioned clinical needs can be met by resorting to the applied nose-to-brain strategy. It will be an economical strategy, applicable to patients with physiological or pathophysiological

swallowing restrictions (pediatrics, geriatrics, among others). Importantly, the quantitative pharmacokinetic data herein obtained for the three administration routes will be also of utmost importance to develop pharmacokinetic/pharmacodynamic mathematical models that can be, then, scaled to humans

CHAPTER VI

**IS INTRANASAL
ADMINISTRATION AN
OPPORTUNITY FOR DIRECT
BRAIN DELIVERY OF
LACOSAMIDE?**



VI.1. INTRODUCTION

Lacosamide is unique among all marketed AEDs due to its two novel mechanisms of action and favorable pharmacokinetic and safety profiles. It selectively enhances the slow inactivation of VGSCs, in opposition to classic VGSC modulators, such as carbamazepine, phenytoin and oxcarbazepine, which increase fast channel inactivation [534]. The slow inactivation of VGSCs is an endogenous mechanism by which neurons reduce ectopic hyperactivity and their modulation by lacosamide stabilizes hyper-excitable neuronal membranes in a selective manner, decreasing repetitive neuronal firing. Hence, lacosamide reduces the pathophysiological hyperactivity underlying epilepsy without affecting the physiological activity [535]. In addition, lacosamide inhibits a nervous system phosphoprotein CRMP2, attenuating the effects of neurotrophic factors on axon outgrowth and suppressing spontaneous recurrent seizures, with consequent inhibition of epileptogenesis [68]. This feature is unique to lacosamide, as the other AEDs lack it [536].

The aforementioned mechanism of action confers lacosamide fewer adverse effects and an excellent therapeutic profile, achieving patients high rates of seizure freedom, in monotherapy or as add-on treatment of partial-onset seizures, with or without secondary generalization [534, 535]. Its multifactorial mechanism of action created the possibility of using lacosamide in other pathologies, mainly due to its antinociceptive and neuroprotective functions are responsible for the use of lacosamide, specifically chronic migraine treatment [537], glioma [538], hypoxic-ischemic brain injury due to its neuroprotective effect [539] and in diabetic patients with neuropathic pain [540, 541] and inflammation [542].

Lacosamide is also distinctive among other AEDs because it exhibits many of the pharmacokinetic characteristics of an ideal AED. It displays a dose-proportional pharmacokinetic profile, rapid and complete intestinal absorption, low plasma protein binding (< 15 %) and minor first-pass hepatic metabolism. Nevertheless, it is a P-gp substrate [543], which is overexpressed in refractory epilepsy [155, 467]. Consequently, it is expected that the quantity of lacosamide that cross the BBB decreases as the disease progress and P-gp expression increases. Furthermore, only 40

% of the administered dose is excreted as the unchanged form. The remaining dose is previously metabolized to the inactive *O*-desmethyl metabolite that results primarily from CYP2C19 activity, and to other minor metabolites that result from CYP2C9 and CYP3A4 mediated metabolism. Consequently, the concomitant use of lacosamide with CYP2C19 substrates or inhibitors may decrease the formation of the major metabolite by approximately 60 %, increasing the risk of toxicity [544]. Inter-individual variability has also been observed due to the polymorphic alleles that encode CYP2C19 [534]. Accordingly, the renal excretion of *O*-desmethyl metabolite decreases 70 % in poor metabolizers relatively to extensive metabolizers [545]. Since both unchanged form and metabolites of lacosamide are excreted in urine, dose adjustment is required for patients with severe renal impairment and submitted to hemodialysis, which removes approximately 50 % of the drug from plasma [546]. Indeed, the $t_{1/2}$ of lacosamide increases up to 18-20 h in severe renal impaired patients, compromising the drug's safety profile [546, 547].

Besides the aforementioned advantages of lacosamide, it is currently available in different dosage forms, including syrup and tablets for oral administration, and solution for IV infusion; these pharmaceutical formulations are bioequivalent and directly converted without dose adjustment [534]. Parenteral administration is beneficial to patients in emergency situations or unable to take oral medications. For instance, hospitalized patients, after surgical procedures, patients with swallowing difficulty or suffering from acute gastrointestinal disorders, which is one of the most frequent adverse effect of lacosamide [535]. However, IV injection is invasive and requires qualified clinical professionals.

Since ambulatory monitoring systems are being developed to improve seizure detection, novel therapeutic systems must be able to be self-administered "at home" to improve the quality of life of patients with epilepsy and their families [548]. In this context, we developed the present work in order to administer lacosamide by non-invasive IN route. This route is characterized by a fast onset of action and direct nose-to-brain delivery, which results in lower systemic and peripheral exposure than classical drug administration routes [276, 523]. We expect to contribute to the development of a new therapeutic strategy for epilepsy and other neurological

diseases, by surpassing hepatic first-pass metabolism, DDI, inter-individual variability of the marketed formulations. Moreover, as lower plasma concentrations are expected to be attained, systemic and peripheral side effects, including the renal ones, will be probably decreased. Nevertheless, there is risk of increased drug exposure in lungs and therefore will be herein investigated. Complementarily, the direct nose-to-brain delivery is expected to decrease the development of pharmacoresistance associated to the P-gp overexpression at the endothelial cells of the BBB [549]. Therefore, a pharmacokinetic study was performed in mice to compare the biodisposition of lacosamide after IN and IV administrations. Taking into consideration the fast MCC in nasal mucosa, lacosamide was loaded into an *in situ* mucoadhesive gel system before being administered in the nasal cavity.

VI.2. MATERIAL & METHODS

VI.2.1. CHEMICALS & REAGENTS

Lacosamide (Vimpat[®] solution for infusion, 10 mg/mL), used in *in vivo* studies, as well as ketamine (Imalgene[®] 1000, 100 mg/mL) and xylazine (Vetaxilaze 20[®], 20 mg/mL) used for animal anesthesia, were commercially acquired. Antipyrine, applied as IS in the HPLC method, was obtained from Sigma-Aldrich (St. Louis, MO, USA). Lacosamide power (purity > 98 %), used for the development and validation of the HPLC method, and *in vitro* studies, was purchased from Molekula SRL (Rimini, Italy).

For the preparation of the *in situ* gel, Pluronic F-127 was purchased from Sigma-Aldrich (St. Louis, MO, USA), while Noveon[®] Polycarbophil and Carbopol[®] 974P were acquired from Lubrizol (Wickliffe, OH, USA). Sodium dihydrogen phosphate dehydrate, disodium hydrogen phosphate dehydrate and hydrochloric acid 37 %, used to prepare the 0.1 M sodium phosphate buffer pH 5.0, were purchased from Merck KGaA (Darmstadt, Germany).

The preparation of *in vivo* samples and analysis by HPLC required ethyl acetate, methanol and acetonitrile, which were purchased from Fisher Scientific

(Leicestershire, UK) and ultrapure water (HPLC grade, 18.2 M Ω .cm) prepared using a Milli-Q Millipore Water Appliance (Milford, MA, USA). DMSO used in *in vitro* assays was purchased from Fisher Scientific (Leicestershire, UK). Sodium chloride 0.9 % solution was acquired from B. Braun Medical (Queluz de Baixo, Portugal). All the remaining chemicals were obtained from Sigma-Aldrich (St. Louis, MO, USA) unless otherwise stated.

VI.2.2. PREPARATION OF LACOSAMIDE FORMULATIONS

The *in situ* nasal mucoadhesive gel system was developed by the cold method, dissolving Pluronic F-127 in 10 mL of cold Milli-Q water (22.5 %, w/v), under magnetic stirring, at a controlled temperature (5-10 °C). After mixture at 4 °C overnight, distinct mucoadhesive polymers were tested, particularly Carbopol® 974P and Noveon® Polycarbophil, at different percentages. The one with lower effect on cell viability was selected for *in vivo* pharmacokinetic studies. Therefore, to load lacosamide into the gel, 500 μ L of the Vimpat® solution for injection (10 mg/mL) were added to 500 μ L of gel, obtaining a final dosage of 5 mg/mL.

The IV solution injected to mice was prepared by diluting IV Vimpat® solution in saline solution (0.9 % NaCl), attaining a final concentration of 2.08 mg/mL.

VI.2.3. IN VITRO CELL VIABILITY ASSAYS IN RPMI-2650 AND CALU-3 CELL LINES

The Alamar Blue assay was performed on the Human nasal septum cell line (RPMI-2650, ECACC 88031602) and in human lung adenocarcinoma cell line (Calu-3, ATCC® HTB-55TM) to assess the impact of free lacosamide and distinct mucoadhesive gels on metabolic activity and cell viability. Accordingly, resazurin (7-hydroxy-10-oxophenoxazin-10-ium-3-one), which has high membrane permeability, exists in its oxidized non-fluorescent blue form. Once inside the cells, it is reduced to resorufin by the activity of mitochondrial and cytoplasmic enzymes. Resorufin is a pink substance

that emits fluorescence, allowing its quantification and further correlation with viable and metabolic active cells [550, 551].

RPMI-2650 cells were cultured in T-75 flasks with Eagle's Minimum Essential Medium, supplemented with 2 mM glutamine, 1 % nonessential amino acids and 10 % inactivated fetal bovine serum (FBS). A 1 % penicillin-streptomycin mixture was further added as recommended for bacterial contamination prophylaxis. Calu-3 cells were cultured in the same aforementioned conditions, but making use of Dulbecco's Modified Eagle Medium, supplemented with 0.04 M sodium bicarbonate, 1 % mixture penicillin-streptomycin and 10 % FBS. Three times a week, cells from both cell lines were passed with a 0.25 % trypsin-EDTA solution and cultured at 37 °C in 5 % CO₂ and 95 % relative humidity.

The Alamar Blue assay was conducted as previously described [476, 523]. Briefly, 3×10^5 cells per well (RPMI-2650) or 3.5×10^4 cells per well (Calu-3) were seeded in 96-well plates, incubated at 37 °C and 5 % CO₂ for 24 h. Once confluent, the cells were treated with 200 µL of each lacosamide solution or empty and drug loaded thermogels for 24 h. Free lacosamide was tested at several concentrations (1, 5, 10, 25, 50, 100, 150, 200, 250 and 400 µM) and distinct thermoreversible gel formulations were tested: with no lacosamide, and loading lacosamide at 50, 100, 150, 200, 250 and 400 µM. Controls corresponding to 100 % viability were performed by incubating the cells with fresh medium. Afterwards, treatment solutions were removed, 10 % resazurin solution (125 mg/mL) was added and the cells were incubated at 37 °C in 5 % CO₂. The incubation period with resazurin was 2 and 3 h for RPMI-2650 and Calu-3 cells, respectively. Finally, fluorescence was determined at 560 and 590 nm in a Biotek Synergy HT microplate reader (Biotek Instruments®, Winooski, VT, USA).

Cell viability was calculated based on the following **Equation VI.1** [276, 523].

$$\text{Cell viability (\%)} = \frac{FL_{\text{Lev}} - FL_{\text{W}}}{FL_{\text{Control}} - FL_{\text{W}}} \times 100 \quad \text{Equation VI.1}$$

FL_T refers to the mean fluorescence observed after incubation with a treatment solution, FL_{Control} is the mean fluorescence observed in non-treated cells and FL_W is the mean fluorescence observed in wells without cells (negative control) [552].

Graphpad Prism® 5.03 software (San Diego, CA, USA) was used for processing *in vitro* data, expressing them as mean \pm SD. ANOVA test was applied to determine differences in cell viability treated with lacosamide and gel formulations in relation to the control (100 % viability).

VI.2.4. IN VIVO STUDIES

VI.2.4.1. Animals and ethics

All experiments were conducted in accordance with the European Directive regarding the protection of laboratory animals used for scientific purposes (2010/63/EU) (European Parliament, Council of the European Union, 2010) and the Portuguese law on animal welfare (Decree-Law no. 113/2013). The applied experimental procedures were authorized by DGAV.

Healthy adult male CD-1 mice, weighting 25-30 g and supplied by Charles River Laboratories (France), were housed in the local animal facilities under controlled environmental conditions (temperature 20 ± 2 °C; relative humidity 55 ± 5 %; 12 h light/dark cycle) for at least 1 week before starting the experimental procedures. Before and during the experimental procedures, animals had *ad libitum* access to tap water and standard rodent diet (4RF21, Mucedola®, Italy).

VI.2.4.2. *In Vivo* Pharmacokinetic Study

Mice were randomly divided into two groups, one of which was administered with a single dose of lacosamide by IN route, and the other by IV injection. Before IN or IV administration, animals were anesthetized with a mixture of ketamine and xylazine (100 mg/kg and 10 mg/kg, respectively), by intraperitoneal route, and kept in a properly warmed environment until recovery.

The *in situ* IN gel (50 μ L) was administered with a polyurethane tube (24 G, 19 mm) coupled to a 1 mL syringe, introduced about 1 cm from the left nostril of the animal, positioned laterally. Then, 120 μ L of the sterile IV solution described in **Section VI.2.2** were injected in the lateral tail vein using an insulin syringe (27 G, 1.0 mL). Both administration routes allowed the administration of the same dose (8.33 mg/animal).

After the administration of lacosamide, animals were sacrificed by cervical dislocation followed by decapitation at predefined time points (5, 15, 30, 60, 90, 120, 240, 360 and 480 min, n = 5 per time point). Blood was immediately collected into heparinized tubes and tissues of interest (brain, lungs and kidneys) were excised, gently washed with sodium chloride 0.9 % solution and weighed. Blood was centrifuged at 4 °C and 2880 g for 10 min, followed by plasma collection for further sample treatment and drug quantification. Using a THOMAS® Teflon tissue homogenizer, tissues were homogenized with 4 mL of sodium phosphate buffer (0.1 M, pH 5.0) per g of tissue.

All samples were stored at -80°C until appropriate treatment and subsequent chromatographic analysis.

VI.2.4.3. Quantification of Lacosamide in Biological Samples

The HPLC method to quantify lacosamide in plasma and tissues was adapted from the previously developed and validated technique in human plasma, with slight changes optimized for mice plasma and tissues analysis [476].

Sample preparation consisted of adding 40 μL of methanol, 10 μL of antipyrine (50 $\mu\text{g}/\text{mL}$) and 1 mL of ethyl acetate to 100 μL of plasma or 150 μL of tissue homogenate supernatant. After vortex-mixing for 30 seconds and centrifugation at 12,045 g during 3 or 5 min for plasma or tissue homogenate, respectively, the organic phase was collected into a glass tube and the procedure was repeated. Organic phases were totally evaporated at 45 $^{\circ}\text{C}$ under a slight nitrogen stream. The solid residue was reconstituted in 100 μL of water and acetonitrile (90:10, v/v), followed by 1 min of vortex-mixing and filtration through Costar[®] Spin-X[®] (0.22 μm , Corning, Inc., NY, USA) at 12,045 g for 3 or 5 min. A final volume of 20 μL of sample was injected into the HPLC system for lacosamide quantification.

A Shimadzu HPLC system (Shimadzu Corporation, Kyoto, Japan) equipped with a solvent release model (LC-20A), a degasser (DGU-20A5), an autosampler (SIL-20AHT), a column oven (CTO-10ASVP) and a DAD (SPD-M20A) were used. Control and monitoring of the apparatus, as well as result collection were performed by LCsolution Software (Shimadzu Corporation, Kyoto, Japan).

Lacosamide and the IS were separated in a LiChroCART[®] Purospher[®] Star C18 reversed-phase column (55 \times 4 mm, 3 μm particle size; Merck KGaA, Darmstadt, Germany), at 40 $^{\circ}\text{C}$, and employing, at 1 mL/min, the same elution gradient reported in [476]. DAD was set at 220 nm.

A partial validation was performed in plasma, brain, lung and kidney according to the international guidelines of bioanalytical method validation of the EMA and the FDA [427, 428]. The validation parameters ($n = 5$) included selectivity, linearity, inter- and intraday accuracy and precision, recovery and the results are summarized in **(Table VI.1)**. Aliquots (10 μL) of the working standard solutions of lacosamide were added to blank mice plasma and tissue homogenate to obtain seven calibration standards and four QC samples. Calibration standards were used to assess linearity while the QCs were used to determine inter- and intraday accuracy and precision as well as recovery. Descriptive statistics reported for the partial validation of the HPLC bioanalytical method was performed using Microsoft Excel[®] 2016.

Table VI.1 Validation parameters of the analytical method developed in high performance liquid chromatography (HPLC-DAD) for quantification of lacosamide in plasma and brain, lung and kidney homogenate (n = 5).

Validation Parameter	Plasma	Brain	Lungs	Kidneys
Calibration range^a (µg/mL)	0.5 - 30	0.4 - 120 ^b	4 - 120 ^b	4 - 120 ^b
Regression Equation^a	y=0.0924x - 0.0353	y=0.0557x + 0.0123	y=0.0500x - 0.009	y=0.0497x + 0.0994
Coefficient of determination (r²)	0.996	0.997	0.995	0.995
LLOQ (µg/mL)	0.5	0.1	1	1
Interday				
Precision (% CV)	5.84 - 10.69	2.24 - 14.00	1.79 - 8.69	1.82 - 12.76
Accuracy (% RE)	-8.40 - 6.65	-3.03 - 10.99	-1.07 - 8.25	-1.29 - 7.18
Intraday				
Precision (% CV)	5.90 - 7.80	2.74 - 11.55	1.25 - 4.88	6.36 - 9.87
Accuracy (% RE)	-5.50 - 9.74	-9.47 - 9.69	-5.71 - 7.72	1.06 - 9.73
Recovery (%)	83.93 - 96.25	82.70 - 90.11	86.91 - 95.52	89.05 - 97.45

^a Interday values (n = 5) and the equation of the calibration curve is given by the general equation of $y = mx + b$, with m corresponding to the slope and b to the intercept. The equation represents the peak areas signals of each drug to that of the internal standard (y), versus the corresponding plasma concentration of lacosamide (x). ^b values expressed in µg/g. CV, coefficient of variation; LLOQ, lower limit of quantification; RE, relative error.

VI.2.4.4. Pharmacokinetic and Statistical Analysis

For both administration routes, mean experimental concentration *versus* time profiles were plotted in plasma, brain, lung and kidney and submitted to non-compartmental pharmacokinetic analysis, using WinNonlin software, version 5.2 (Pharsight Co, Mountain View, CA, USA). The pharmacokinetic parameters were estimated considering the mean concentrations (n = 5) obtained at each post-dose time point and included the C_{max} of lacosamide achieved in plasma and tissues, the t_{max} , the AUC_t , and AUC_{inf} . K_{el} was estimated by a log-linear regression of the terminal segment of the concentration-time profile. The AUC_{extrap} (%) was also estimated, representing the drug exposure since the last time for which the concentration was quantifiable to infinity, which should not exceed 20 %. Additionally, the apparent $t_{1/2}$, and the MRT were also determined. The aforementioned parameters allowed the

calculation of the absolute bioavailability in accordance with the equation 1 of **Table VI.2**.

Plasma-to-tissue ratios were also estimated to compare the affinity of lacosamide for each organ in relation to its systemic exposure.

In order to assess the tendency of lacosamide to reach the brain after IN administration, specific parameters regarding drug delivery were determined, namely the DTE, which predicts the drug propensity to be directly delivered from the nasal cavity to the brain and is calculated based on equation 2 of **Table VI.2**. When expressed as a percentage, a DTE value higher than 100 % suggests a preferential drug transport to the brain directly through the nasal cavity regarding the systemic route [553, 554]. In addition, DTP was calculated according to equation 3 of **Table VI.2**, which corresponds to the drug percentage that reaches the brain by direct route [477]. The brain bioavailability of lacosamide, which corresponds to the ratio between the AUC_t in brain after IN and IV administrations, was estimated applying equation 4 of **Table VI.2**.

Graphpad Prism® 5.03 software (San Diego, CA, USA) was used to express the concentrations as mean \pm SEM and determine statistical differences between both administrations (IN and IV). Unpaired two-tailed Student's t-test was performed between IN and IV administration groups. Differences were considered statistically significant for p -values lower than 0.05 ($p < 0.05$).

Table VI.2 Equations for determination of bioavailability and drug delivery parameters described in **Section VI.2.4.4**.

Equation 1	$F = \frac{AUC_{t\text{IN}} \times \text{Dose}_{\text{IN}}}{AUC_{t\text{IV}} \times \text{Dose}_{\text{IV}}} \times 100$
Equation 2	$\text{DTE (\%)} = \frac{(AUC_{\text{brain}/AUC_{\text{plasma}}})_{\text{IN}}}{(AUC_{\text{brain}/AUC_{\text{plasma}}})_{\text{IV}}} \times 100$
Equation 3	$\text{DTP (\%)} = \frac{AUC_{\text{brain IN}} - \left[\frac{AUC_{\text{brain IV}}}{AUC_{\text{plasma IV}}} \times AUC_{\text{plasma IN}} \right]}{AUC_{\text{brain IN}}} \times 100$
Equation 4	$B_{\text{brain IN/IV}} = \frac{AUC_{\text{brain IN}}}{AUC_{\text{brain IV}}}$

AUC_t , area under drug concentration-time curve from time zero to the time of last measurable concentration; $B_{\text{brainIN/IV}}$, brain bioavailability between IN and IV routes; DTE, drug targeting efficiency; DTP, direct transport percentage; F, bioavailability; IN, intranasal, IV, intravenous.

VI.3. RESULTS

VI.3.1. CELL VIABILITY OF INTRANASAL THERMOREVERSIBLE GEL

The herein used IN gel was developed based on our previous investigations [276, 485, 523], maintaining the basis of Pluronic F-127 block copolymer due to its physicochemical and biological properties, namely its thermoreversibility in water [276, 523].

Nevertheless, in an attempt to increase the mucoadhesive properties of the *in situ* gelling system, enhancing its residence time and improving the central delivery of lacosamide, two mucoadhesive polymers (Carbopol 974P and Noveon® Polycarbophil) were tested at 0.2 % (w/v) together with Pluronic F-127.

RPMI-2650 cells were incubated for 24 h with each of the gel formulations, firstly empty and then loaded with lacosamide at different concentrations. Their effects on cell viability in relation to the control group are expressed in **Figure VI.1**. Accordingly, it is evident that, although no differences have been registered, inclusion of lacosamide in Carbopol® 974P and polycarbophil gels slightly decreased cell viability in relation to the correspondent unloaded gel. Moreover, cell viability was always equal to or higher than 85 %, with exception of the Carbopol® 974P gel loaded with lacosamide at the highest concentration (mean value of 83.75 %) and polycarbophil gel loaded with lacosamide at 50, 100 and 150 μM (mean values of 82.72 %, 81.53 % and 80.31 %, respectively).

It was also observed that, at the concentration range herein investigated (1-400 μM , **Figure VI. 2**), lacosamide did not affect the viability of RPMI-2650 cells, although it decreases as concentrations increase. No statistically significant differences were observed. Similar results were also found in Calu-3 lung cells between 1 and 100 μM (**Figure VI.2**).

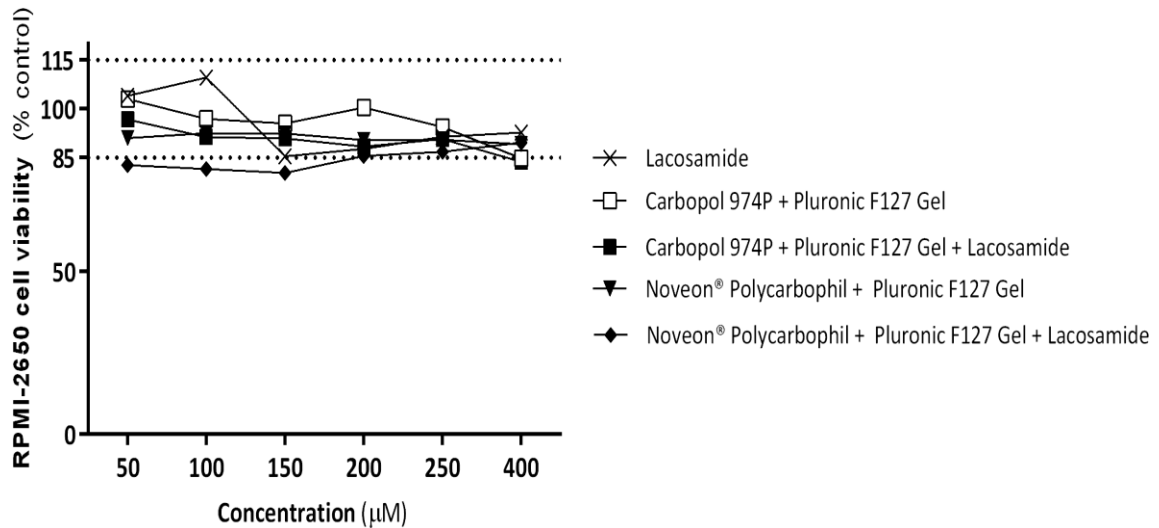


Figure VI.1 Viability (%) of RPMI-2650 cells after incubation with lacosamide, empty Noveon® Polycarbophil and Carbopol® thermoreversible gels, and thermoreversible gels loaded with lacosamide at the same concentrations, for 24 h (50, 100, 150, 200, 250 and 400 µM). Data represented as mean ± standard deviation (n = 4, three independent replicates).

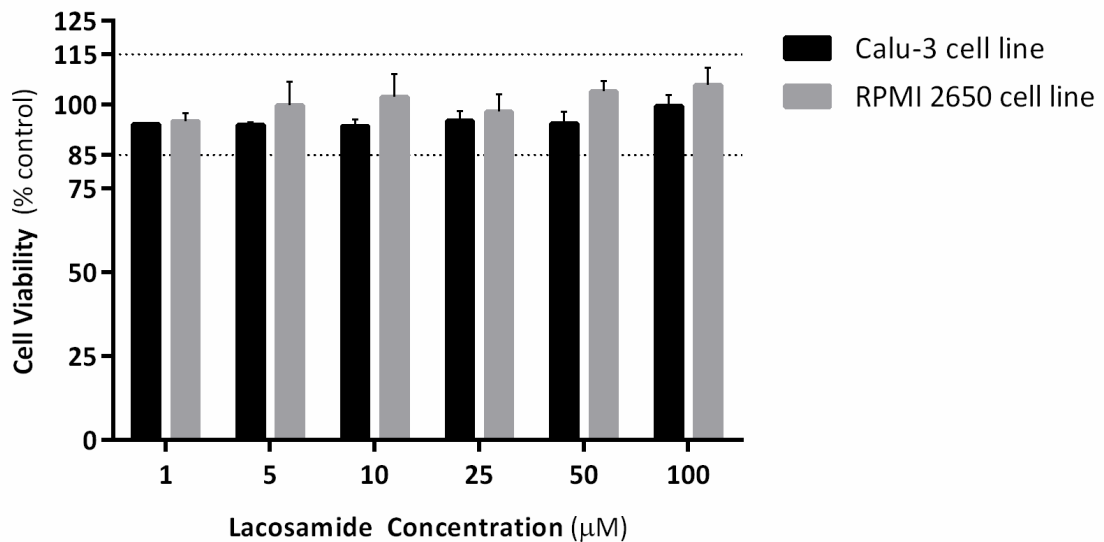


Figure VI.2 Viability (%) of Calu-3 and RPMI-2650 cells after incubation with zonisamide for 24 h (1-100 µM). Data represented as mean ± standard deviation (n = 4, three independent replicates).

VI.3.2. *IN VIVO* PHARMACOKINETIC ANALYSIS

The mean lacosamide concentrations and SEM ($n = 5$) obtained at each time-point in plasma, brain, lungs and kidneys after single dose administration of lacosamide (8.33 mg/kg) by IV and IN routes to mice are depicted in **Figure VI.3** together with the statistical differences. The correspondent pharmacokinetic parameters are presented in **Table VI.3**.

The C_{max} of lacosamide in plasma was attained at 5 min for both routes of administration even though it was significantly higher after IV injection ($12.67 \pm 1.43 \mu\text{g/mL}$) than IN instillation ($8.59 \pm 0.46 \mu\text{g/mL}$). At the remaining time-points, profiles were practically overlapped with exception of 90 and 240 min, which revealed statistically higher concentrations after IN administration ($p < 0.01$ and $p < 0.05$, respectively, **Figure VI.3A**). Nonetheless, systemic exposure was slightly higher for the IN gel ($850.33 \mu\text{g}\cdot\text{min/mL}$ vs $705.93 \mu\text{g}\cdot\text{min/mL}$), probably because its clearance was slower, as suggested by the enhanced $t_{1/2}$ (95.64 min vs 33.73 min) and MRT (139.33 min vs 60.32 min, **Table VI.3**). These facts are corroborated by the enhanced values observed for the K_{el} (0.0072 min^{-1} versus 0.0206 min^{-1} for IN and IV routes, respectively).

Regarding the biophase, C_{max} of lacosamide was attained at 15 min for both administration routes, but lower values were found after IN administration ($3.45 \mu\text{g/g}$ vs $4.79 \mu\text{g/g}$), with statistical differences ($p < 0.05$). Interestingly, the mean concentration attained at 5 min post IV dosing was approximately twice of that achieved after IN instillation ($2.35 \pm 0.28 \mu\text{g/g}$ and $1.47 \pm 0.1 \mu\text{g/g}$, **Figure VI.3B**), even though the differences were not statistically significant. The remaining time-points clearly evidence that lacosamide concentrations are higher after IN administration (**Figure VI.3B**), culminating in a considerably higher brain exposure to lacosamide (given by the AUC_{inf}) following IN administration ($471.84 \mu\text{g}\cdot\text{min/mL}$ vs $289.36 \mu\text{g}\cdot\text{min/mL}$, **Table VI.3**). Moreover, the brain-to-plasma ratios were small and similar for both routes (**Table VI.3**). Notwithstanding, DTE was 128.67 % and DTP was 22.28 %.

Table VI.3 Pharmacokinetic parameters following administration of lacosamide (8.33 mg/kg) in plasma and tissue (brain, lung and kidney) of mice through intranasal thermoreversible gel (IN) and intravenous solution (IV).

Pharmacokinetic Parameters ^a	Plasma		Brain		Lung		Kidney	
	IN	IV	IN	IV	IN	IV	IN	IV
t_{max} (min)	5.00	5.00	15.00	15.00	5.00	15.00	5.00	60.00
C_{max} ($\mu\text{g}/\text{mL}$) ^b	8.59	12.67	3.45 ^b	4.79 ^b	6.65 ^b	2.52	7.33	8.70
AUC_t ($\mu\text{g}\cdot\text{min}/\text{mL}$)	850.33	705.93	425.44 ^c	274.49 ^c	135.02 ^c	12.61	357.56	762.61
AUC_{inf} ($\mu\text{g}\cdot\text{min}/\text{mL}$)	1044.33	711.77	471.84	289.36	420.70 ^c	ND	ND	1028.18
AUC_{extrap} (%)	18.58	0.82	9.83	5.14	67.90	ND	ND	25.83
k_{el} (min^{-1})	0.0072	0.0206	0.0063	0.0134	0.0153	ND	ND	0.0141
$t_{1/2}$ (min)	95.64	33.73	109.40	51.81	45.37	ND	ND	29.23
MRT (min)	139.33	60.32	156.49	81.00	69.61	ND	ND	91.98
F (%)^d	120.46							
AUC Ratios	IN	IV	DTE (%)	DTP (%)				
AUC_{brain}/AUC_{plasma}	0.50	0.39	128.67	22.28 %				
AUC_{lung}/AUC_{plasma}	0.16	0.02	888.91					
$AUC_{kidney}/AUC_{plasma}$	0.42	0.51	38.92					

^a Parameters were estimated using the mean concentration-time profiles obtained from five different animals per time point (n = 5). ^b Values expressed in $\mu\text{g}/\text{g}$; ^c Values expressed in $\mu\text{g}\cdot\text{min}/\text{g}$; ^d Absolute intranasal bioavailability (F) was calculated based on AUC_t values; AUC_{extrap} , Extrapolated area under the drug concentration time-curve; AUC_{inf} , Area under the concentration time-curve from time zero to infinite; AUC_t , Area under the concentration time-curve from time zero to the last quantifiable drug concentration; C_{max} , Maximum concentration; DTE, Drug targeting efficiency index; DTP, direct transport percentage; k_{el} , Apparent elimination rate constant; MRT, Mean residence time; NC, not calculated; $t_{1/2}$, Apparent terminal elimination half-life; t_{max} , Time to achieve the maximum peak concentration.

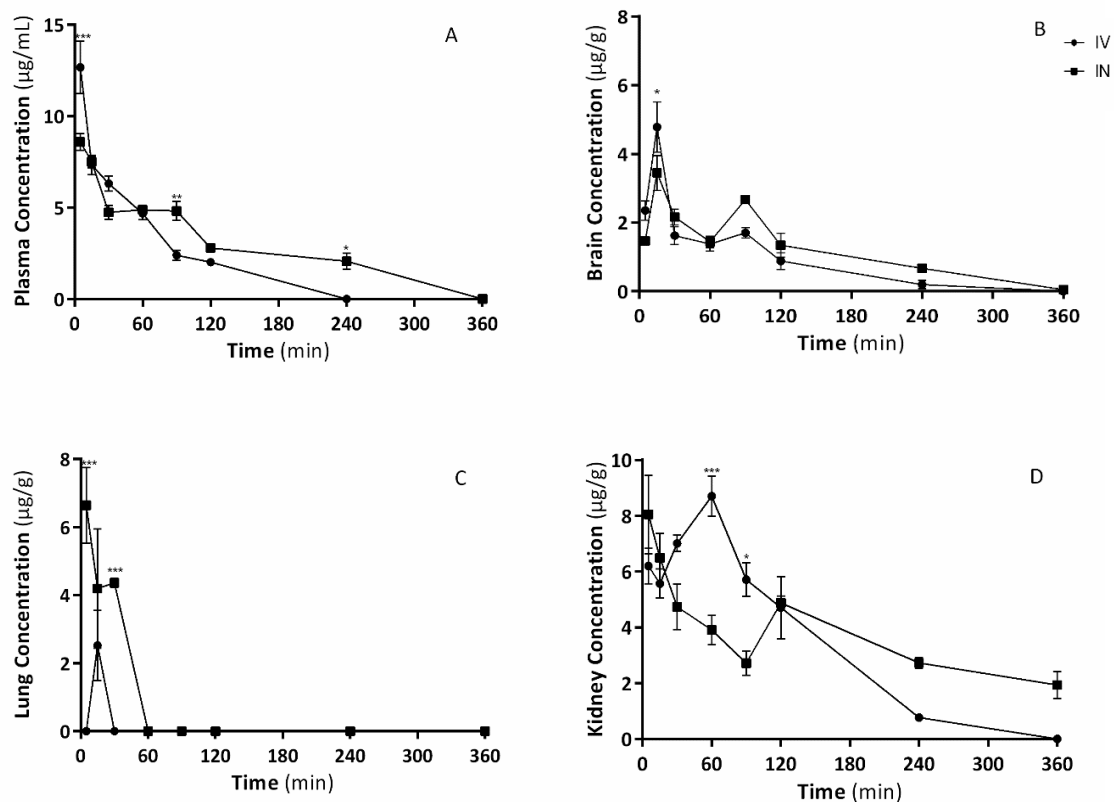


Figure VI.3 Concentration-time profiles of lacosamide after intranasal (IN) and intravenous (IV) administration (8.33 mg/kg) in plasma (A), brain (B), lung (C) and kidney (D). The symbols represent the mean \pm standard error of the mean values of five determinations per time point ($n = 5$). * $p < 0.05$.

Regarding the concentration-time profile obtained for lung tissue after IV injection (Figure VI.3C), lacosamide concentrations were always inferior to the LLOQ of the analytical technique with exception of 15 min post-administration (mean value of $2.52 \pm 1.03 \mu\text{g/g}$). After IN instillation of lacosamide loaded gel, the drug was quantified at 5, 15 and 30 min and attained a C_{max} value of $6.65 \pm 1.11 \mu\text{g/g}$. Importantly, this value is lower than those tested *in vitro* in Calu-3. In lungs, the estimated DTE value was 888.91 %, confirming that there is direct passage to the lungs even though lacosamide is quickly eliminated, presenting unquantifiable concentrations after 30 min post-administration.

In the kidney, lacosamide concentrations were also higher only at initial sample collection times (5 and 15 min) after IN dosing; thereafter, IV concentrations were higher, attaining statistically significant differences at 60 min post-dosing (Figure

VI.3D). Complementarily, kidney exposure to lacosamide was considerably higher for the IV route (762.61 $\mu\text{g}\cdot\text{min}/\text{mL}$ vs 357.56 $\mu\text{g}\cdot\text{min}/\text{mL}$), which is corroborated by the higher $\text{AUC}_{\text{kidney}}/\text{AUC}_{\text{plasma}}$ ratio (0.51 vs 0.42) and the DTE value of 38.92 %.

VI.4. DISCUSSION

Lacosamide is undeniably effective in epilepsy, particularly due to its anticonvulsant and anti-epileptogenic effects. It is also demonstrating success in other neurological diseases as antinociceptive. In addition, its IV administration is considered essential when it is not possible to use the oral route. However, IV injection is invasive and requires health care professionals to be performed. Therefore, developing a novel non-invasive therapeutic strategy to deliver lacosamide into the brain is expected to increase its clinical use, adherence to therapy and marketing potential.

Making use of our previous *know-how* in nose-to-brain delivery, this study is the first to demonstrate the potential of the IN route to deliver lacosamide into the brain.

Herein a simple *in situ* mucoadhesive gel system was used to counterbalance the anatomical and physiological characteristics of nasal mucosa, particularly the fast MCC and efflux transporters of the nasal cavity that reduce drug absorption. Therefore, Pluronic F-127 was selected at the concentration of 22.5 % (w/v). Besides its already well-documented thermoreversibility [276, 523], it is a long poly(propylene)oxide block with high hydrophobicity that allows the incorporation of lipophilic compounds such as lacosamide. Furthermore, it strongly modifies the microviscosity of plasma membranes and potentially inhibits P-gp [555], which is strongly expressed in the nasal mucosa of mice, rats and humans [249]. Bearing in mind that lacosamide is a P-gp substrate, inhibition of this efflux transporter by Pluronic F-127 is expected to increase lacosamide distribution from the nasal mucosa to the brain. Carbopol 974P and Noveon® Polycarbophil (0.2 %, w/v) were tested together with Pluronic F-127 to increase gel viscosity and avoid quick drug clearance from the nasal cavity towards the nasopharyngeal region by prolonging its retention time in the nasal cavity. Since the gel system composed of Noveon® Polycarbophil and Pluronic F-127 when loaded with

lacosamide compromised the viability of RPMI-2650 cells to values lower than 85 % (**Figure VI.1**), the Carbopol® 974P plus Pluronic F-127 combination was selected for IN administration to mice. It is important to note that maximum concentrations tested *in vitro* were defined in accordance with drug solubility in DMSO, since this should not exceed 0.5 %. Nevertheless, herein, the DMSO percentage did not exceed 0.2 %.

Herein, a comparative pharmacokinetic study was performed in mice after IN or IV administration of lacosamide at the same dose (8.33 mg/ kg). Lacosamide revealed to be effective at the dose of 1 mg/kg in a mouse model of essential tremor [556] and it completely antagonized tonic convulsions with no adverse effects at 20 mg/kg [557]. Therefore, we tested different IV doses between 1 and 20 mg/kg and selected the 8.33 mg/kg dose because it led to plasma concentrations that were within the therapeutic range suggested for lacosamide (2.2–20 µg/mL) in therapeutic drug monitoring [558].

Pharmacokinetic results demonstrated that, similarly to IV injection, the IN instillation of lacosamide *in situ* nasal gel brought an extensive but longstanding systemic absorption of the drug, attaining C_{max} at the same time, although with lower values than IV route. The absolute bioavailability value achieved for intranasally administered lacosamide was high (120.40 %). This value is superior to 100 % presumably because of the inter-individual variability among different animals since each mouse was assigned not only for one of the two administration groups but also to a unique sampling time-point. Nevertheless, it illustrates the fact that a substantial drug fraction is absorbed from the nasal cavity into the systemic circulation, gaining access to the CNS by crossing the BBB.

Moreover, the same t_{max} value was found in brain (15 min) after IN and IV administration, suggesting a fast delivery of lacosamide to the brain. The DTE was 128.67 %, indicating that lacosamide is directly delivered from the nose to the brain. Approximately 22.28 % of the drug reached the brain by direct nose-to-brain pathways, probably through the olfactory and trigeminal nerves. This means that IN delivery may be very practical and useful in emergencies. Furthermore, after the first 15 min, brain concentrations were always higher for IN administration, suggesting a sustained drug release from the nasal system and/or a slowly absorption into the systemic circulation following its passage through the BBB to the target. These findings, together with the

higher K_{el} and smaller MRT and $t_{1/2}$ of lacosamide in the brain following IV injection, suggest that a longer protective effect may occur with the IN instillation. Also, IN dosing may require a less frequent administration than IV or oral administrations.

Even though plasma concentrations were similar between both routes of administration, anticipating similar peripheral side effects, the lower drug exposure in renal tissue must be highlighted. Indeed, C_{max} is reached earlier after IN administration, but it is smaller, as well as the extent of drug exposure given by AUC_t , which is approximately 50 % of that observed after IV injection. This feature may become relevant for patients with renal failure for whom lacosamide prescription has several limitations, as described in **Section VI.1**. Since the renal concentrations achieved after IN dosing do not exceed the C_{max} reported for IV route, less toxicity is expected to occur.

Kidneys have a different pharmacokinetic profile compared to lungs. This can be justified because lacosamide is excreted by renal route and one of its major adverse effects regards the kidney. Therefore, it probably reaches the kidney earlier and at higher quantities than those attained in the lung. Moreover, to the best of our knowledge, no pulmonary adverse effects have been reported for lacosamide likely due to its low distribution to the lungs. However, the DTE is 888 %, which clearly emphasizes the direct nose-to-lung delivery of lacosamide, even though the lung-to-plasma ratio was the lowest when compared with other organs. This means that lacosamide has higher affinity to brain and kidney than to lungs. On the other hand, it is important to highlight that lacosamide was detected at all time-points but it was only quantified 15 min after its IV administration. After IN administration, lacosamide was quantifiable up to 30 min. This means that a slight increase in AUC after IN instillation comparatively to IV route is sufficient to significantly increase DTE. Moreover, the *in vitro* investigations herein performed with Calu-3 cells evidence that lacosamide does not compromise cell viability including at concentrations higher than those found *in vivo*. These results are in accordance with pharmacokinetic studies that evaluated the nose-to-brain delivery of levetiracetam [523] and zonisamide [276]. Nevertheless, the reported DTE for lacosamide (888 %) is considerably higher than those of levetiracetam (253.63 %) or zonisamide (144.47 %) [266; 519]. In opposition, the DTE into the brain

was higher for levetiracetam (182.35 % [523]) and zonisamide (149.54 % [276]) than for lacosamide (128.67 %). These findings can be justified not only because of the different physicochemical characteristics of the drugs but also because of the nasal device that was used. Herein, the catheter replaced the pulverization system used for the nasal instillation of levetiracetam and zonisamide [266; 519]. These results alert the scientific community to the importance of the physicochemical characteristics of the drug and nasal device, when designing future nasal formulations.

Moreover, the *in vitro* investigations herein performed with Calu-3 cells evidence that lacosamide does not compromise cell viability including at concentrations higher than those found *in vivo*. These results are unsurprising and in accordance with other pharmacokinetic studies that evaluated the nose-to-brain delivery of levetiracetam [523] and zonisamide [276]. Nevertheless, the reported DTE (888 %) is considerably higher than those of levetiracetam (253.63 %) or zonisamide (144.47 %)[276, 523], probably because a catheter was used for the administration of the *in situ* gel into the nasal cavity, instead of a pulverization system such as the one used in [276, 523]. These results alert the scientific community for the importance of the selection of an appropriate device for nasal administration.

VI.5. CONCLUSION

To the best of our knowledge, a comprehensive characterization of the pharmacokinetic profiles of lacosamide in plasma, brain, lungs and kidneys following IN instillation to mice was herein reported for the first time.


Altogether, IN and IV administrations of lacosamide exhibited similar concentration–time profiles, suggesting similar pharmacological responses. However, brain drug exposure was enhanced after IN instillation, demonstrating, together with a DTE of 128.67 % and a DTP of 22.28 %, the direct drug delivery from the nasal cavity to the brain. Moreover, t_{max} in brain was similar for both administration routes (15 min), highlighting the potential of IN delivery for acute convulsive emergencies. The

MRT value of lacosamide in the brain supports the sustained concentrations and the usefulness of IN administration during chronic treatments with lacosamide.

The IN instillation of lacosamide is practical and adequate to be used outside the hospital setting. Herein, evidence was gathered accounting for a direct transport of lacosamide from the nose to the brain, circumventing the BBB, which may render the IN route as a promising and valuable drug delivery strategy for a prospective management of pharmacoresistance.

CHAPTER VII

**A COMBO-STRATEGY TO
IMPROVE BRAIN DELIVERY OF
ANTIEPILEPTIC DRUGS: FOCUS
ON BCRP AND INTRANASAL
ADMINISTRATION**



VII.1. INTRODUCTION

Prophylactic seizure control has been the primary focus of researchers since 1983, when only 7 to 8 antiepileptic drugs (AEDs) were available, until the current days, with more than 18 new molecules. Clinically available AEDs, administered in monotherapy or in combination, have different pharmacokinetics, therapeutic indications and safety profiles. Nevertheless, effects against epileptogenesis are registered only for a few of them [560, 561]. Lacosamide, levetiracetam and zonisamide stand out due to their neuroprotective and anti-inflammatory effects observed in rodents and humans [562–564].

The poor anti-epileptogenic effects of most AEDs may contribute to the development of drug resistance. One third of epileptic patients do not respond to more than three AEDs administered at the maximal dose, which prompted the investigation of the underlying mechanisms [565]. One of the most studied mechanisms that have been proposed to justify the occurrence of pharmacoresistance involves the expression of ABC efflux transporters. These transporters appear to be overexpressed in patients with refractory neurological diseases, including epilepsy [566]. Since ABC transporters are expressed in enterocytes, endothelial cells of the BBB and renal tubule cells, the plasma and tissue exposure of a drug strongly depends on their activity. For instance, plasma and brain concentrations tend to decrease, as their activity increases. This theory has a solid basis because it explains resistance to AEDs with distinct mechanisms of action [567]. Several studies have already demonstrated that the expression of P-gp is higher in the brain of refractory epileptic patients and the uptake of AEDs into the brain increases with the co-administration of verapamil, a well-known P-gp inhibitor. Additionally, recent investigations evidenced an increased BCRP expression in brain tissue from patients with mesial temporal sclerosis, focal cortical dysplasia and mesial temporal lobe epilepsy, compared to brain tissue from healthy humans [566].

The protective role of BCRP at the BBB also compromises the delivery of AEDs to the biophase, particularly if they are BCRP substrates. This had already been demonstrated for other ABC transporters, namely P-gp. However, possible interactions

between BCRP and most of the AEDs remain scarcely investigated, probably because its relevance at the human BBB has been described more recently. Therefore, as recommended by the International Transporter Consortium, FDA and EMA [354, 568, 569] the interaction between lacosamide, levetiracetam and zonisamide with BCRP was herein assessed *in vitro* for the first time. The identification of BCRP substrates and/or inhibitors is particularly important to understand their brain exposure and investigate their potential to develop pharmacoresistance and drug-drug interactions that may compromise their clinical efficacy and safety.

Complementarily, we intended to investigate whether the IN administration of AEDs can not only surpass the BBB but also avoid BCRP-mediated efflux transport. This is based on our previous observations regarding the direct nose-to-brain delivery of levetiracetam [523] and zonisamide [276]. Despite the few transporters that were investigated until now concerning nasal drug absorption, it is known that P-gp is expressed in murine and bovine nasal mucosa, hampering drug transfer into the brain [235]. In addition, BCRP is also expressed in the olfactory and respiratory epithelia of rodents and, consequently, it can also compromise the absorption and the distribution of BCRP substrates into the brain [257, 271]. Therefore, the present study was designed to characterize the interaction between lacosamide, levetiracetam and zonisamide and the BCRP efflux transport. After *in vitro* studies, the AEDs identified as BCRP substrates were administered to mice by IN and IV routes in the presence or absence of elacridar, a P-gp and BCRP inhibitor.

VII.2. MATERIAL & METHODS

VII.2.1. CHEMICALS & REAGENTS

Lacosamide, levetiracetam and zonisamide were purchased from Molekula SRL (Rimini, Italy). Antipyrine, used as IS in the chromatographic technique employed to quantify zonisamide in plasma and brain samples, and sulfasalazine, used as a reference BCRP substrate in *in vitro* studies, were both obtained from Sigma-Aldrich

(St. Louis, MO, USA). The excipients used to prepare the thermoreversible nasal gel were purchased from Sigma-Aldrich (Pluronic F-127) and Lubrizol, Wickliffe, OH, USA (Carbopol 974P and Noveon® polycarbophil).

The analysis of *in vitro* and *in vivo* sample was performed by HPLC methods that required acetonitrile, purchased from Fisher Scientific (Leicestershire, United Kingdom), and ultra-purified water (HPLC grade, 18.2 MΩ.cm) produced by a Milli-Q water device from Millipore (Milford, MA, USA). Reagents used for *in vivo* sample homogenization and drug extraction included hydrochloric acid 37 %, disodium hydrogen phosphate dihydrate and sodium dihydrogen phosphate dihydrate, all from Merck KGaA (Darmstadt, Germany), as well as DMSO, ethyl acetate and methanol from Fisher Scientific (Leicestershire, UK).

Ketamine (Imalgene® 1000®, 100 mg/mL) and xylazine (Vetaxilaze®, 20 mg/mL) are both commercially available and were acquired for animal anesthesia.

All remaining chemicals and reagents were obtained from Sigma-Aldrich (St. Louis, MO, USA), unless otherwise specified.

VII.2.2. *IN VITRO* STUDIES

VII.2.2.1. Cell Culture

Parental MDCK-II and the respective cell line transfected with the human ABCG2 gene (MDCK-BCRP) were provided by the Netherlands Cancer Institute (NKI-AVL, Amsterdam, Netherlands). Both cell lines were grown in T-75 flasks (Orange-Scientific, Braine-l'Alleud, Belgium), in Dulbecco's modified Eagle's medium (Sigma-Aldrich), supplemented with 0.04 M sodium bicarbonate, a mixture of 1 % penicillin-streptomycin and 10 % inactivated fetal bovine serum.

The RPMI 2650 cell line (ATCC® CCL-30™) was purchased from Sigma-Aldrich, grown in T-75 flasks with Eagle's Minimum Essential Medium and supplemented with

2 mM glutamine, 1 % of non-essential amino acids and 10 % of bovine fetal serum, as instructed by the provider.

VII.2.2.2. Cell Viability Assays

The colorimetric Alamar Blue assay was herein used for the quantitative analysis of the viability of MDCK-II, MDCK-BCRP and RPMI-2650 cells in the presence of different concentrations of each AED under investigation. The results of this assay were used to define the drug concentrations to be applied for intracellular accumulation and bidirectional transport assays in both MDCK cell lines and RPMI-2650 cells. The Alamar Blue is a metabolic test, based on the reduction of blue-colored resazurin to resorufin, a pink compound that emits fluorescence, allowing its easy quantification [474]. Thus, this method determines viable cells indirectly, as it depends on their intracellular mitochondrial activity.

The cells were seeded in 96-well plates (Orange Scientific, Belgium), at the density of 1×10^4 for MDCK-II and MDCK-BCRP and at 5×10^5 cells per well for RPMI-2650, for 24 h, under controlled conditions (37 °C and 5 % CO₂ atmosphere). Afterwards, various concentrations of lacosamide, levetiracetam and zonisamide were tested, namely 1, 5, 10, 25, 50 and 100 μM for the MDCK-II and MDCK-BCRP cell line. Two additional concentrations (200 and 300 μM) were tested for levetiracetam and zonisamide in MDCK-BCRP cell line in order to investigate their BCRP inhibitory effect in accumulation studies (**Section VII.2.2.3**). Lacosamide was not tested at 200 or 300 μM, because it was not within its therapeutic window. The effect of lacosamide in RPMI-2650 cells viability was tested at 1, 5, 10, 25, 50 and 100 μM. Levetiracetam and zonisamide have already demonstrated to have no effect on the viability of RPMI-2650 cells under the same concentration range [265, 523].

The culture medium was removed and 200 μL of each drug solution was added at the concentrations mentioned above. The positive control was carried out in parallel by adding fresh blank medium, instead of drug solution, to each well. The solutions were incubated for 24 h, under the same conditions. The negative control consisted of

performing the test in wells without cells. Then, the solutions or culture medium were removed and 200 μ L of a 10 % resazurin solution was added to each well and incubated at 37 °C, 5 % CO₂ for 2 h. Finally, fluorescence was quantified at 560 and 590 nm in a Biotek Synergy HT microplate reader (Biotek Instruments®, Winooski, VT, USA). Cell viability is calculated in accordance to **Equation VII.1**.

$$\text{Cell viability (\%)} = \frac{F_{\text{Lev}} - F_{\text{LW}}}{F_{\text{Control}} - F_{\text{LW}}} \times 100 \quad \text{Equation VII.1}$$

FL_T corresponds to the mean fluorescence value obtained in the wells after cell incubation with drug solutions, FL_W corresponds to the fluorescence emitted in wells without cells and FL_{control} corresponds to the mean fluorescence obtained in positive control wells.

VII.2.2.3. Intracellular Accumulation Assays

In order to investigate whether lacosamide, levetiracetam and zonisamide are BCRP inhibitors, MDCK-BCRP cells were seeded at the density of 3.0 x 10⁵ cells/well, in 12-well plates (Corning Costar, NY, USA) for 48 h. Hoechst 33342 is a fluorescent BCRP substrate used to assess the impact of test compounds on its intracellular concentrations. Ko143 is a specific BCRP inhibitor, selected as positive control.

Firstly, cells were submitted to a double pre-washing step with Hanks balanced salt solution (HBSS) supplemented with 10 mM HEPES pH 7.4. The Ko143 solution (0.50 μ M) or test drug solutions at the concentrations that revealed no effect on cell viability. Each drug was dissolved in DMSO, diluted to 0.1 % with HBSS/HEPES and then added to the cells for 30 min of incubation. The negative control was performed by adding 0.1 % DMSO to the cells. Subsequently, these solutions were replaced by Hoechst 33342 (10 μ M), and the cells were incubated at 37 °C for 1 h. Lastly, the cells were washed three times with ice-cold phosphate buffered saline and lysed with Triton X-100 (0.1 %, v/v) for 30 min, at room temperature. The cell lysate was collected, and

200 μL were transferred into black 96-well plates to read the fluorescence emitted by intracellularly accumulated Hoechst 33342. The Biotek Synergy HT microplate reader (Biotek Instruments, VT, USA) was used in fluorescence mode (excitation wavelength 360 nm and 460 nm emission).

The protein content of cell lysates was assessed using the Bio-Rad Protein Assay Kit II (Bio-Rad Laboratories, California, USA) to normalize Hoechst 33342 concentrations.

VII.2.2.4. Bidirectional Transport Studies: MDCK-II and MDCK-BCRP Cells

To identify BCRP substrates among the set of test drugs, MDCK-II and MDCK-BCRP cells were seeded in 12-well Transwell inserts of microporous polycarbonate (1.12 cm^2 , 0.4 μm pore size; Corning Costar®, NY, USA) at a density of 6.0×10^5 cells per well. During the 7 days required to form the cell monolayer, the cells were maintained at 37 °C and 5 % CO_2 , and the medium was replaced every 2 days. The integrity of the cell monolayer was monitored by measuring the electrical transepithelial resistance (TEER) with an Evom® STX2 voltohmmeter (WPI, Sarasota, Florida, USA). Sodium fluorescein (Na-F) was used to assess the paracellular integrity of the cell monolayer. Sulfasalazine was herein selected as positive control, as it is a specific BCRP substrate. Acceptable cell monolayers must present TEER values greater than $90 \Omega \cdot \text{cm}^2$, a representative value of the movement of ions through the pores, and therefore allows to determine the degree of confluence and development of tight junctions [570, 571].

Bidirectional studies were performed for 2 h from apical to basolateral (AP-BL) and basolateral to apical (BL-AP) sides, under gentle agitation (45 rpm) at 37 °C. In the apical compartment, 0.5 mL of each AED solution (100 μM) were added, while 1.5 mL of HBSS buffer with 10 mM HEPES were placed in the basolateral compartment. Samples were harvested every 30 min and replaced with fresh HBSS/HEPES. In order to ensure an equal dilution in each compartment, the same volume percentage was collected (16 %), specifically 240 μL of the basolateral compartment and 80 μL of the

apical compartment. The samples collected from the donor side at the end of the assay were used to calculate mass balance, according to the **Equation VII.2**.

$$\text{Mass balance (\%)} = \frac{C_f^D V^D + C_f^R V^R}{C_0^D V^D} \times 100 \quad \text{Equation VII.2}$$

C_f represents the final concentration of the compound in the donor (C_f^D) or receptor compartment (C_f^R), C_0 corresponds to the initial concentration in the donor compartment, and V^D and V^R are the volumes of the donor and receptor compartments, respectively.

The AEDs and sulfasalazine were quantified in the collected samples by a validated HPLC-DAD. Chromatographic conditions and validation parameters are summarized in **Table VII.1**. The apparent permeability coefficient (P_{app}) was determined by applying **Equation VII.3**.

$$P_{app} \text{ (cm/s)} = \frac{(dQ/dt)}{A \times C_0} \quad \text{Equation VII.3}$$

dQ/dt indicates the change in the amount of compound (dQ) in the receptor compartment as a function of time (dt), A is the surface area of the membrane (cm^2) and C_0 is the initial drug concentration in the donor compartment.

Subsequently, the efflux ratio (ER) was determined for each cell line. It is calculated through the quotient between the $P_{app_{BL-AP}}$ and the $P_{app_{AP-BL}}$. In turn, the net flux ratio was determined from the ratio between the ER observed in MDCK-BCRP cells and that of the parental line MDCK-II.

When the net flux ratio was greater than 2, the bidirectional studies were also performed in the presence of the BCRP inhibitor, Ko143 0.5 μM , which was added 1 h before donor solutions to both compartments to prove the specificity of BCRP mediated efflux.

VII.2.2.5. RPMI-2650 Cell Permeability Studies

The experimental conditions of this study were similar to those described in **section VII.2.2.4**, with slight differences. RPMI-2650 cells were seeded in 12-well polycarbonate microporous Transwell inserts (1.12 cm², 0.4 μm pore size; Corning Costar®, NY, USA) at a density of 4x10⁵ cells/well. During the first 4 days, the cells were submerged in Minimum Essential Medium Eagle with Earle's salts and sodium bicarbonate, and enriched with glutamine (2 mM), nonessential amino acids (1 %, v/v), heat-inactivated fetal bovine serum (10 %, v/v) and penicillin-streptomycin mixture (1 %, v/v). On the 4th day, culture medium of the apical compartment was removed to allow cells to differentiate in contact with the air. The culture medium from basolateral side was renewed every 2 days for 21 days. Membrane integrity was assessed by the apparent permeability of Na-F and TEER monitoring.

During the assay, aliquots of 200 μL were collected every 30 min up to 120 min from the basolateral compartment, and 200 μL were collected from apical compartment at the end of the assay. The corresponding volume was replaced with fresh medium to keep the final volume in the basolateral compartment at 1.5 mL.

The samples were analyzed by HPLC-DAD according to **Table VII.1**. Mass balance and the P_{app} were estimated according to **Equations VII.2** and **VII.3**, respectively.

VII.2.3. PLASMA AND BRAIN DISPOSITION OF ZONISAMIDE IN MICE

Healthy male CD-1 mice were purchased from Charles River Laboratories (France) and housed for one week in local facilities at a controlled environment (12 h cycle light/dark, 20 ± 2°C, relative humidity 55 ± 5 %). During this period and in all the experiments, mice had *ad libitum* access to standard rodent diet (4RF21, Mucedola®, Italy) and tap water.

Table VII.1 Chromatographic conditions and partial validation parameters obtained for the high performance liquid chromatography-diode array (HPLC-DAD) assays applied for the quantification of the antiepileptic drugs, lacosamide, levetiracetam and zonisamide, and the reference BCRP substrate (sulfasalazine) in *in vitro* samples.

Drug	Mobile Phase	Detection Wavelength (nm)	Injection Volume (μL)	Retention Time (min)	Calibration Range (μM)	r^2 ^c	LLOQ (μM)	Precision (% CV) ^c	Accuracy (% RE) ^c
Lacosamide	H ₂ O/ACN (90:10, V/V)	220 nm	50 μL ^a	5.4	0.5 - 100	0.9992	0.5	-7.6 to 5.2	-9.1 to 4.4
Levetiracetam	H ₂ O/ACN (97:3, V/V)	220 nm	20 μL ^b	4.1	1 - 100	0.9985	1	0.4 to 4.5	-3.4 to 5.1
Sulfasalazine	50 mM phosphate buffer pH 2.5/ACN (70:30, V/V)	360 nm	50 μL	2.3	0.01 - 0.4	0.9996	0.01	1.2 to 4.3	7.4 to 12.0
Zonisamide	H ₂ O/ACN (90:10, V/V)	239 nm	50 μL ^a 20 μL ^b	4.2	0.5 - 100	0.9987	0.5	-4.8 to 10.0	-5.0 to 4.4

^a Samples collected from MDCK-II and MDCK-BCRP assays; ^b Samples collected from RPMI-2650 permeability assay; ^c Interday values (n = 3). ACN, acetonitrile; LLOQ, lower limit of quantification; CV, coefficient of variation; RE, relative error, deviation from nominal value.

The experimental procedures were conducted in accordance with the European Directive (2010/63/EU) on the protection of laboratory animals and the Portuguese animal welfare law [475]. The experimental procedures were reviewed and approved by DGAV. The previous *in vitro* studies allowed the reduction of the number of animals required in agreement with the 3Rs rule.

Based on the results described in **Section VII.3.3**, zonisamide revealed to be a BCRP substrate. Therefore, it was selected for *in vivo* studies in order to investigate the impact of BCRP on its pharmacokinetics after IV and IN administration.

Mice were randomly sorted into two groups (32 animals each), according to the administration route: zonisamide was administered to one group by IV route and to another group by IN route. Each group was then sub-divided into other two subgroups (16 animals each). Elacridar (2.5 mg/kg) was intravenously administered to one subgroup, while vehicle was administered to the other. Before treatment, all animals were anesthetized with a mixture of xylazine and ketamine (100/10 mg/kg) by intraperitoneal route. The animals were kept in a warm environment during and after the experimental procedure until full recovery, due to the decrease of body temperature caused by anesthesia.

For IN administration of zonisamide (16.7 mg/kg), the drug was dissolved in the thermoreversible gel composed of Pluronic-F127 (18 %) and Carbopol® 974P polymer (0.2 %) [276] and 50 µL with a polyurethane tube (24 G, 19 mm) coupled to a 1 mL syringe. The tube was introduced approximately 1 mm into the left nostril of anesthetized mice which was anatomically positioned in right lateral decubitus. Before IN administration, both animal groups received an IV bolus (4 mL/kg) of vehicle (Transcutol®, Diethylene Glycol Monoethyl Ether) or elacridar (dissolved in Transcutol®) into the lateral tail vein. The IV administration of zonisamide was performed together with vehicle or elacridar, using an insulin syringe (27 G, 1.0 mL).

Based on our previous study [276], the animals were sacrificed (n = 4 per time point) by cervical dislocation and subsequent decapitation at 5, 15, 30 and 60 min post-administration. Blood was immediately centrifuged at 4 °C and 2880 g for 10 min, while the brain was collected, weighted and homogenized with 0.1 M sodium phosphate buffer pH 5.0 (4 mL buffer per g of tissue), using a THOMAS® Teflon tissue

homogenizer. It was subsequently centrifuged at 4147 *g* for 15 min at 4 °C. Zonisamide was quantified in plasma and brain homogenate samples by a validated HPLC-DAD method [276].

The concentration-time profiles of zonisamide in plasma and brain were plotted based on the average concentration at each time point (*n* = 4). Pharmacokinetic parameters were estimated by non-compartmental analysis using the software WinNonlin® version 5.2 (Pharsight Co, Mountain View, CA, USA) and included the *C*_{max}, *t*_{max}, AUC_t and AUC_{inf}. The MRT was also estimated.

To evaluate whether zonisamide was preferentially distributed to the brain, the quotient between the AUC_t in the brain and plasma was calculated, as well as the DTE that determines the tendency of zonisamide to reach the brain. DTE was calculated when zonisamide was administered by IN and IV routes in the absence of the co-administration with elacridar, following **Equation VII.4**.

$$\text{DTE (\%)} = \frac{(\text{AUC}_{\text{brain}}/\text{AUC}_{\text{plasma}})_{\text{IN}}}{(\text{AUC}_{\text{brain}}/\text{AUC}_{\text{plasma}})_{\text{IV}}} \times 100 \quad \text{Equation VII.4}$$

AUC_{brain} and AUC_{plasma} are given by AUC_t in brain tissue and plasma. According to the literature, DTE values greater than 100 % suggest a direct transport of zonisamide from the nasal mucosa to the CNS [547, 554].

The DTP was estimated in accordance with **Equation VII.5**. It indicates the drug percentage that reaches the brain by direct transport.

$$\text{DTP (\%)} = \frac{\text{AUC}_{\text{brain IN}} - \left[\frac{\text{AUC}_{\text{brain IV}}}{\text{AUC}_{\text{plasma IV}}} \times \text{AUC}_{\text{plasma IN}} \right]}{\text{AUC}_{\text{brain IN}}} \times 100 \quad \text{Equation VII.5}$$

VII.2.4. Statistical Data Analysis

The data obtained from *in vitro* studies were processed using Graphpad Prism® 8 (San Diego, CA, USA) and expressed as mean ± SD. Two-way analysis of variance

(ANOVA) with Dunnett's Multiple Comparison Test was used to determine differences in viability studies in comparison to untreated control cells (cell viability of 100 %). This test was also applied to the intracellular accumulation of Hoechst 33342 in comparison to the negative control. Differences were considered statistically significant when $p < 0.05$ (*), $p < 0.01$ (**) and $p < 0.001$ (***)).

At each time-point, concentrations determined in samples collected from *in vivo* studies were presented as mean \pm SEM. Statistical analysis to identify differences between the concentrations obtained with elacridar and vehicle was performed as aforementioned.

VII.3. RESULTS

VII.3.1. CELLULAR VIABILITY OF MDCK-II, MDCK-BCRP AND RPMI-2650 CELLS

The viability of MDCK-II and MDCK-BCRP cells did not significantly change after incubation for 24 h with lacosamide, levetiracetam or zonisamide, independently of drug concentrations tested. For the MDCK-BCRP, levetiracetam and zonisamide were also tested at 200 and 300 μ M to assess whether these concentrations could be used in accumulation studies. At these concentrations, lacosamide precipitated and hence it could not be tested. At these concentrations, viability of MDCK-BCRP cells were not compromised, revealing no statistically significant differences ($p > 0.05$) with the untreated control group.

Since levetiracetam and zonisamide have already demonstrated not to determine the viability of RPMI-2650 cell within the concentration range of 1-100 μ M [276, 523], we herein investigated the effect of lacosamide in RPMI-2650 cell viability. At 1, 5, 10, 25, 50 and 100 μ M, cell viability was, comparatively to the control, 95.20 ± 2.25 %, 99.86 ± 6.96 %, 102.41 ± 6.68 %, 97.99 ± 5.23 %, 104.04 ± 3.04 % and 105.96 ± 5.16 %, respectively.

VII.3.2. *IN VITRO* IDENTIFICATION OF BCRP INHIBITORS

MDCK-BCRP cells were incubated with lacosamide, levetiracetam or zonisamide, at the concentrations defined in **Section VII.2.2.3**, in order to quantify the intracellular accumulation of Hoechst 33342 and infer whether the AEDs had an inhibitory effect on BCRP-mediated efflux.

Figure VII.1A demonstrates statistical increment of Hoechst 33342 concentrations in MDCK-BCRP cells when incubated with Ko143 ($p < 0.001$) compared with those incubated without BCRP inhibitor, confirming the functionality of the BCRP transporter. The intracellular accumulation of Hoechst 33342 in MDCK-BCRP cells also increased substantially after incubation with all the tested concentrations of lacosamide (2.5 to 75 μM) (**Figure VII.1B**), suggesting that lacosamide inhibits BCRP independently of its concentration. On the other hand, zonisamide inhibited BCRP only at the highest concentrations (200 and 300 μM , **Figure VII.1D**). These results suggest a weaker BCRP inhibitory effect for zonisamide compared with lacosamide. In opposition, incubation of MDCK-BCRP cells with levetiracetam did not reveal statistically significant differences relatively to the negative control (**Figure VII.1C**) throughout the whole concentration range, suggesting no inhibitory effect on the BCRP protein.

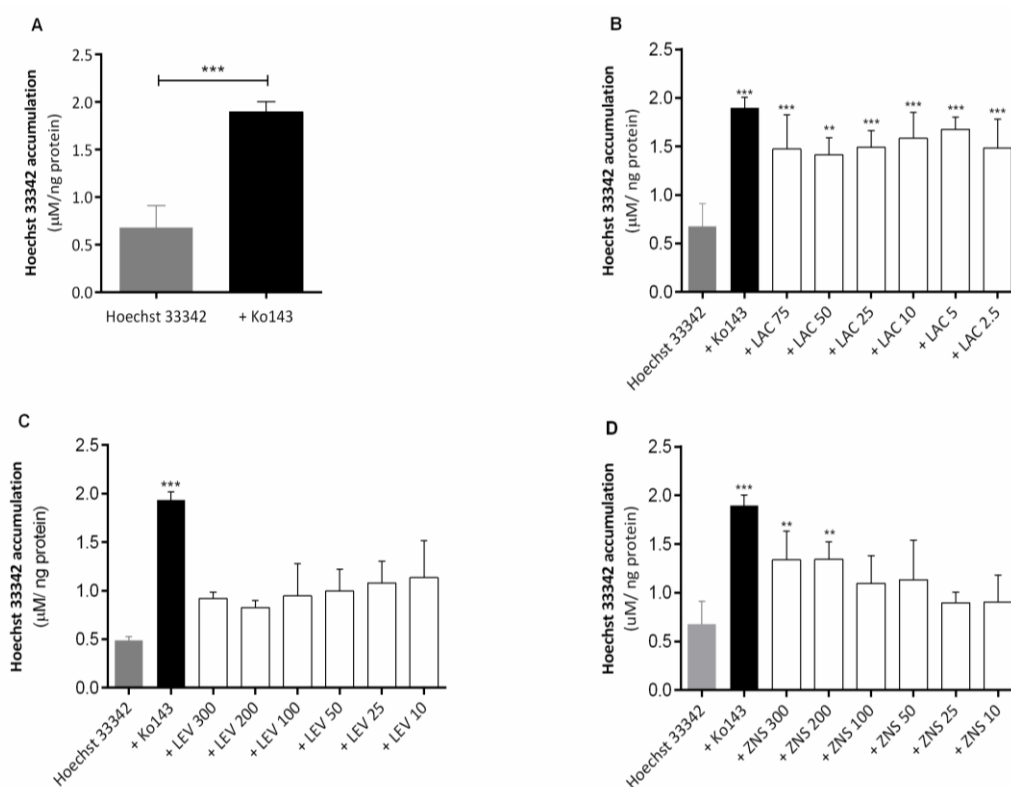


Figure VII.1 (A) Hoechst 33342 intracellular accumulation in MDCK-BCRP cells, in the presence and absence of 0.5 µM Ko143 (positive control). (B) Intracellular accumulation of Hoechst 33342, after incubation with lacosamide (LAC), (C) levetiracetam (LEV) and (D) zonisamide (ZNS) for 30 min. Data compared with negative control cells (without inhibitor) and expressed as mean ± standard deviation (n = 4). * $p < 0.05$, ** $p < 0.01$ and *** $p < 0.001$.

VII.3.3. IN VITRO IDENTIFICATION OF BCRP SUBSTRATES

The values of Papp obtained in AP-BL and BL-AP directions as well as the efflux ratios and net flux ratios of lacosamide, levetiracetam, zonisamide and sulfasalazine (positive control) are shown in **Table VII.2**.

Sulfasalazine was herein used as a classic reference BCRP substrate [313] in order to assess the functionality of the ABC transporter. Its efflux ratio in MDCK-BCRP cells was higher than 2.0 as well as the net flux ratio (**Table VII.2**) in the absence of Ko143. In addition, the efflux ratio decreased 71.08 % (from 3.25 to 0.94) after incubation with Ko143 while the net flux ratio decreased 61.30 % (from 2.30 to 0.89).

Observing **Table VII.2**, lacosamide was the only AED that presented an efflux ratio higher than 2.0 in MDCK-II and MDCK-BCRP cells. On the other hand, its net flux ratio

was lower than 2.0, suggesting that lacosamide is effluxed by canine endogenous transporters, but not by human BCRP. Levetiracetam was the compound with the lowest value of net flux ratio, which was lower than 2.0 (**Table VII.2**). Thus, according to the guidelines [343; 556], levetiracetam is unlikely to be a BCRP substrate. It is noteworthy that zonisamide revealed a behavior completely distinct from that of the other two AEDs but similar to that of sulfasalazine (**Table VII.2**). In the transfected cell line, zonisamide $P_{appAB-BL}$ was lower than $P_{appBL-AP}$ (7.64 and 26.49 $\times 10^{-6}$ cm/s, respectively) in the absence of Ko143, while similar results were registered between both directions when considering MDCK-II (15.42 and 19.60 $\times 10^{-6}$ cm/s). Indeed, the net flux ratio was 2.73 in the absence of BCRP inhibition, decreasing 53.85 % after incubation with Ko143, evidencing that zonisamide is a BCRP substrate under these experimental conditions.

Table VII.2 Bidirectional apparent permeability coefficient (P_{app}) from apical to basolateral (AP-BL) and basolateral to apical (BL-AP) compartments, efflux ratio (ER) and net flux ratio in MCDKII and MDCK-BCRP cells for lacosamide, levetiracetam, zonisamide. Sulfasalazine was used as reference BCRP substrate. P_{app} values are expressed as mean (standard deviation) (n = 3).

Test Compound	Donor Solution (μM)	MDCK-II						MDCK-BCRP						Net Flux Ratio	
		Without Ko143			With Ko143			Without Ko143			With Ko143			Without Ko143	With Ko143
		$P_{app(\text{AP-BL})} \times 10^{-6}$ cm/s	$P_{app(\text{BL-AP})} \times 10^{-6}$ cm/s	ER	$P_{app(\text{AP-BL})} \times 10^{-6}$ cm/s	$P_{app(\text{BL-AP})} \times 10^{-6}$ cm/s	ER	$P_{app(\text{AP-BL})} \times 10^{-6}$ cm/s	$P_{app(\text{BL-AP})} \times 10^{-6}$ cm/s	ER	$P_{app(\text{AP-BL})} \times 10^{-6}$ cm/s	$P_{app(\text{BL-AP})} \times 10^{-6}$ cm/s	ER		
Lacosamide	100	7.24 (0.62)	17.32 (1.85)	2.39	-	-	-	6.97 (0.42)	23.94 (5.58)	3.43	-	-	-	1.44	-
Levetiracetam	100	9.29 (1.59)	7.02 (0.83)	0.76	-	-	-	11.20 (6.62)	2.71 (0.63)	0.24	-	-	-	0.32	-
Zonisamide	100	15.42 (3.98)	19.60 (6.35)	1.27	16.72 (1.92)	16.81 (1.95)	1.01	7.64 (4.04)	26.49 (8.24)	3.47	18.62 (3.44)	23.61 (0.66)	1.27	2.73	1.26
Sulfasalazine	60	0.22 (0.13)	0.31 (0.10)	1.41	0.89 (0.58)	0.94 (0.37)	1.06	0.12 (0.05)	0.39 (0.16)	3.25	0.54 (0.23)	0.51 (0.11)	0.94	2.30	0.89

ER, efflux ratio; $P_{app(\text{AP-BL})}$, apparent permeability coefficient from apical to basolateral compartment; $P_{app(\text{BL-AP})}$, apparent permeability coefficient from basolateral to apical compartment.

VII.3.4. PERMEABILITY OF AEDs THROUGH RPMI-2650 CELLS

Investigating drug permeability in nasal epithelium has become important to predict their behavior in future *in vivo* studies. To achieve this, the RPMI-2650 cell line was selected, because it is described as a reliable model of the human nasal mucosa [573, 574]. According to cell viability tests, the concentration of 100 μ M was defined for the donor solution of the three AEDs, since it did not decrease cell viability.

Obtained P_{app} values were $4.32 \times 10^{-6} \pm 2.11 \times 10^{-6}$ cm/s, $5.32 \times 10^{-6} \pm 1.75 \times 10^{-6}$ cm/s and $7.46 \times 10^{-6} \pm 0.86 \times 10^{-6}$ cm/s for levetiracetam, lacosamide and zonisamide, respectively. It is observed that the apparent permeability increases with the lipophilicity of the compounds [$\log D(\text{pH } 7.4)$: -0.5, 0.18 and 0.5 for levetiracetam, lacosamide and zonisamide, respectively] [575].

Mass balance was approximately 80.16 ± 0.61 % for the most lipophilic compound (zonisamide), while lacosamide presented 90.50 ± 2.37 % and levetiracetam with more than 89.91 ± 4.82 %.

VII.3.5. *IN VIVO* PLASMA AND BRAIN DISPOSITION OF ZONISAMIDE

The average concentration-time profiles of zonisamide in plasma and brain after single-dose administration by IV and IN route (16.7 mg/kg), with co-administration of vehicle or elacridar (2.5 mg/kg, IV), are presented in **Figure VII.2**. The main pharmacokinetic parameters estimated by non-compartmental analysis are summarized in **Table VII.3**.

Considering the co-administration of zonisamide with the vehicle, plasma exposure attained after IN administration was inferior to that achieved with IV route (AUC_t 59.74 % lower, **Table VII.3**), despite t_{max} having been 5 min for both routes. As expected, brain concentrations were also lower after IN administration, but AUC_t decrease was only 31.72 % (194.24 *versus* 284.47 $\mu\text{g}\cdot\text{min}/\text{mL}$). This indicates that, despite the reduced systemic exposure after IN instillation, brain exposure did not

decrease in the same proportion. Indeed, the brain-to-plasma ratios were 0.70 and 0.41 for IN and IV routes respectively, suggesting that another route of brain delivery is involved besides the systemic one. The DTE was 169.60 % and DTP was 41.04 %, corroborating that zonisamide reaches the brain through direct nose-to-brain mechanisms when BCRP is not inhibited.

Regarding the experimental results found after co-administration of elacridar, it is noteworthy that plasma (**Figure VII.2A**) and brain concentrations (**Figure VII.2B**) after IN administration were very similar to those described for the vehicle group, with no statistical differences at any time-point ($p > 0.05$). In opposition, the co-administration of zonisamide with elacridar by IV route led to considerably higher drug concentrations in the brain (**Figure VII.2B**) than those found without elacridar. Brain exposure, given by AUC_t , was 2.37-fold higher when elacridar was co-administered (**Table VII.3**).

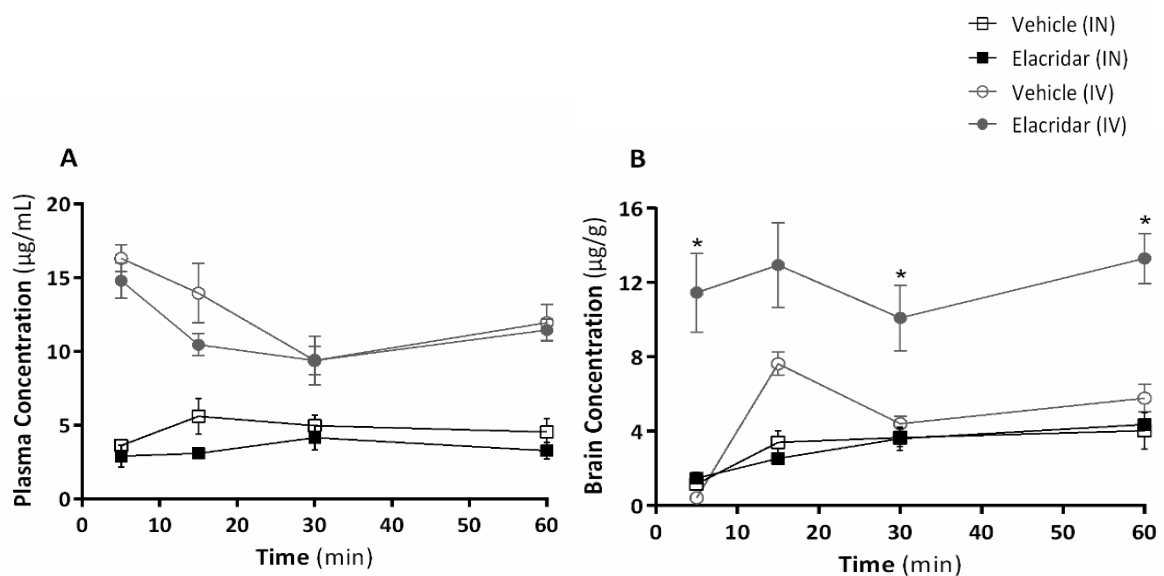


Figure VII.2 Mean concentration-time profiles of zonisamide after its intranasal (IN) or intravenous (IV) administrations with and without the co-administration of elacridar (2.5 mg/kg, intravenous), depicted in plasma (**A**) and brain (**B**). Each data point is presented as mean \pm standard error of the mean (SEM) ($n = 4$ animals per group) and significant differences between group concentrations at specific time-points were assessed by the two-way analysis of variance (ANOVA) with Dunnett's Multiple Comparison Test. * $p < 0.05$ In relation to vehicle after IV administration.

Table VII.3 Plasma and brain pharmacokinetic parameters after intranasal (IN) and intravenous (IV) administration of zonisamide (16.7 mg/kg) with vehicle (transcutol, 4 mL/kg, IV) or BCRP inhibitor, elacridar (2.5 mg/kg, IV).

Pharmacokinetic Parameters ^a	Plasma				Brain			
	IN with vehicle	IN with elacridar	IV with vehicle	IV with elacridar	IN with vehicle	IN with elacridar	IV with vehicle	IV with elacridar
t_{max} (min)	15	30	5	5	60	60	15	60
C_{max} (µg/mL)	5.59	4.14	16.31	14.80	4.03 ^b	4.37 ^b	7.63 ^b	13.29 ^b
AUC_t (µg.min/mL)	276.33	202.06	686.35	624.19	194.24 ^c	189.29 ^c	284.47 ^c	674.12 ^c
MRT (min)	31.14	31.71	29.56	30.66	34.91	36.40	33.84	32.09

^a Parameters were estimated using the mean concentration-time profiles obtained from four different animals per time point (n = 4). ^b Values expressed in µg/g; ^c Values expressed in µg.min/g; AUC_t, area under the concentration time-curve from time zero to the last quantifiable drug concentration; C_{max}, maximum concentration; MRT, mean residence time; t_{max}, time to reach the C_{max}.

Furthermore, statistical differences were always detected with exception of the 15 min time-point (**Figure VII.2B**). A slightly decreasing trend was observed in plasma concentrations at 5 and 15 min post-administration, but no statistical significance was observed. Altogether, the results obtained after IV administration of zonisamide suggest that this drug is a BCRP substrate, corroborating the *in vitro* results described in **Section VII.3.3**.

Interestingly, when BCRP is inhibited, DTE decreased to 86.74 %, mainly due to changes in AUC_t values in brain after zonisamide IV administration and not due to IN pharmacokinetic parameters, which were very similar to those without elacridar.

Brain/plasma ratios were calculated for each time-point and summarized in **Table VII.4**. Accordingly, statistical differences were observed at 5, 15 and 60 min after zonisamide IV administration, exhibiting higher values when co-administered with elacridar. In opposition, IN administration of zonisamide only reflected statistical differences at 5 min (0.32 vs 0.61 with vehicle and elacridar, respectively).

Table VII. 4 Brain/plasma ratios obtained after the intranasal (IN) or intravenous (IV) administration of zonisamide to mice (16.7 mg/kg) with vehicle (transcutol, 4 mL/kg, IV) or BCRP inhibitor, elacridar (2.5 mg/kg, IV) (n = 4). Statistical differences are reported in relation to the correspondent vehicle group.

Time	Intranasal		Intravenous	
	Vehicle	Elacridar	Vehicle	Elacridar
5 min	0.32 ± 0.14	0.61 ± 0.43	0.03 ± 0.01	0.79 ± 0.34***
15 min	0.64 ± 0.09	0.8 ± 0.08*	0.57 ± 0.14	1.23 ± 0.40**
30 min	0.75 ± 0.12	0.91 ± 0.24	0.48 ± 0.08	1.29 ± 0.84
60 min	1.05 ± 0.68	1.46 ± 0.52	0.49 ± 0.09	1.18 ± 0.28***

* $p < 0.05$; ** $p < 0.02$ *** $p < 0.001$

VII.4. DISCUSSION

The BBB has been associated with pharmacological resistance to AEDs, attributed to the overexpression of ABC efflux transporters, namely P-gp and BCRP. These transporters work synergistically to prevent AEDs from exerting their therapeutic effect on the CNS [576]. Hence, it becomes essential to investigate whether AEDs are BCRP substrates or inhibitors.

Herein, parental and BCRP transfected MDCK cell models were selected for *in vitro* assays, as they have already been validated to identify BCRP substrates and inhibitors using a set of reference compounds [313]. Brain endothelial cell lines generate leaky monolayers with excessive paracellular permeability that compromises the assessment of transporter function [308], while the isolation process underlying primary cultures is challenging, and has a low yield that demands a high number of animals to obtain sufficient cells [577, 578]. Despite their canine and renal origin, MDCK-II cells can be transfected with the human *ABCG2* gene that encodes human BCRP and are considered by international guidelines as a reference model to identify substrates of ABC transporters [343; 556]. The main advantage of MDCK-BCRP cells is that the transporter has human origin, avoiding inter-species differences obtained for substrates and inhibitors of ABC transporters [579, 580]. In addition, bidirectional studies were also performed in the respective MDCK-II parental cell line, in order to normalize the results and neutralize the influence of endogenous transporters of canine origin.

Before testing the AEDs, both accumulation and bidirectional transport assays were performed with reference BCRP substrates (Hoechst 33342 and sulfasalazine, respectively) and reference BCRP inhibitor (Ko143). The results presented in **Figure VII.1A** and **Table VII.2** are in accordance to the literature [313] and undoubtedly demonstrate the functionality of the BCRP transporter in this cell model.

In accumulation studies, Ko143 inhibited the BCRP-mediated transport of Hoechst 33342, by increasing its intracellular accumulation ($p < 0.001$). Similarly, lacosamide and zonisamide exhibited the same pattern, suggesting that they are BCRP inhibitors,

in opposition to levetiracetam. Lacosamide increased the intracellular accumulation of Hoechst 33342 at all concentrations under investigation while zonisamide only inhibited at 200 and 300 μM . Care was taken when selecting the concentration range, in order to include the therapeutic range reported in humans (lacosamide: 5-10 $\mu\text{g}/\text{mL}$ or 20-40 μM ; zonisamide: 10-40 $\mu\text{g}/\text{mL}$ or 47-188 μM) [414, 432]. Therefore, our results highlight that, even at sub-therapeutic concentrations (2.5 μM), lacosamide may inhibit BCRP *in vivo*. On the other hand, zonisamide was also able to inhibit BCRP but only at non-therapeutic concentrations (200 and 300 μM , $p < 0.01$). These findings suggest that zonisamide is unlikely to inhibit BCRP when administered in clinical practice at the therapeutic doses. The concentrations were also similar to those reported for P-gp. Indeed, the IC_{50} of zonisamide regarding P-gp was 267 μM , which is also superior to the minimal toxic concentration (40 $\mu\text{g}/\text{mL}$) [581]. Herein, it was not possible to estimate the IC_{50} for zonisamide or lacosamide because it would require higher concentrations to be tested, which was compromised by the lack of drug solubility in cell medium. Nevertheless, since equimolar concentrations were investigated, it appears that lacosamide is more potent than zonisamide, as it inhibits BCRP at lower concentrations. This makes lacosamide a clinically interesting drug for refractory epilepsy associated with the overexpression of BCRP.

In the bidirectional transport study, zonisamide was the only compound that demonstrated to be a BCRP substrate, because its net flux ratio was higher than 2.0 and decreased 53.85 % after BCRP inhibition with Ko143 (from 3.47 to 1.27, **Table VII.2**). This is interesting because zonisamide is the most lipophilic compound among the tested AEDs, and substrates of ABC transporters are often lipophilic compounds. In addition, zonisamide was the AED with the highest P_{app} in RPMI-2650 cells, probably also due to its lipophilicity.

However, the contribution of the BCRP-mediated efflux to the overall distribution of compounds across the BBB must be combined with information regarding to other aspects that affect CNS exposure and/or activity *in vivo*. For instance, our results did not identify levetiracetam as a BCRP substrate, which was also reported following an *in vitro* concentration equilibrium transport assay performed with MDCK-BCRP [410]. In opposition, an *in vivo* non-clinical study suggested that levetiracetam was a double

P-gp and BCRP substrate, because the brain-to-plasma ratios were higher in Mdr1a/1b(-/-)/Bcrp(-/-) mice than in Mdr1a/1b(-/-) mice [582]. However, the synergistic role of ABC transporters observed *in vivo* is not applicable to the *in vitro* cell model herein used. Moreover, Nakanishi *et al.* did not describe the pharmacokinetics in Bcrp(-/-) mice to assess the influence of BCRP alone, and therefore it should not be compared to our results [582].

Therefore, the present *in vivo* studies were performed to increase the robustness of the *in vitro* studies and assess the distribution of zonisamide to the brain after its administration to CD-1 mice by IV and IN routes, with elacridar or vehicle. To reduce the number of animals, in agreement with the 3R principles, we opted to only test *in vivo* the AED that revealed to be a BCRP substrate in *in vitro* conditions. In addition, pharmacokinetics was assessed up to 1 h post-administration because our previous investigations demonstrated that the effect of elacridar is noted in the first hour post-administration [313] and because the major differences between both administration routes have been identified during this period of time in our previous work [276]. First, IN administration was compared with IV route in the absence of elacridar, in order to investigate the nose-to-brain delivery of zonisamide. Then, IV administration with and without elacridar was used to assess whether BCRP inhibition influenced the access of zonisamide to the brain, validating the *in vitro* bidirectional test. Finally, the impact of BCRP inhibition was tested after IN administration. Thus, the direct nose-to-brain delivery was evaluated in the absence of elacridar, and approximately 28 % of zonisamide reached the brain by direct route, as it was anticipated [276].

Elacridar was herein selected to inhibit BCRP *in vivo*, because the metabolic instability of Ko143 would compromise its inhibitory function in *in vivo* assays [583, 584]. Moreover, elacridar is, together with tariquidar, the most potent BCRP inhibitor [585, 586] even though they must be administered intravenously due to a very low oral bioavailability [587].

In the presence of elacridar, C_{max} of zonisamide in the brain more than doubled that achieved when vehicle was co-administered. Similarly, brain AUC_t increased 3-fold, although the plasma pharmacokinetic parameters were comparable to those

found with the administration of the vehicle (**Table VII.2**). These findings attest that zonisamide is a BCRP substrate, corroborating the results reported *in vitro*.

Interestingly, when zonisamide was instilled to the nasal cavity, brain exposure (as assessed by C_{max} and AUC_t) seemed independent of the administration of elacridar. Moreover, plasma profiles were not affected by BCRP inhibition. This can be explained by the contribution of the direct nose-to-brain transport of zonisamide, diminishing the impact of BCRP-mediated efflux at the BBB. Importantly, the results herein found corroborate our previous studies [276] and demonstrate that systemic/pulmonary absorption occurs simultaneously with direct brain delivery and it should not be ignored, even though the BCRP influence seems to be residual. It is noteworthy that zonisamide presented a higher permeation through RPMI-2650 cells than levetiracetam or lacosamide, and its high permeability through the nasal mucosa may compensate eventual BCRP efflux on this tissue [257].

The administration of elacridar clearly influenced brain concentrations after IV dosing of zonisamide, in opposition to IN administration. This reinforces that the IN route may be a novel strategy for zonisamide administration. Besides being painless and non-invasive, it offers a quick onset of action and enhances bioavailability by avoiding gastrointestinal and hepatic first-pass metabolism. Furthermore, it may also avoid the development of refractory epilepsy associated with BCRP overexpression.

VII.5. CONCLUSION

To this day, there is still little information about BCRP and its impact on AEDs pharmacokinetics. Our study demonstrated for the first time that lacosamide is a BCRP inhibitor at therapeutic concentrations. This may be useful in clinical practice to avoid potential DDI in the presence of BCRP substrates. Despite controversy in literature regarding the identification of levetiracetam as a BCRP substrate, this study contributed to increase the consistency of pre-existing results that it is not significantly effluxed by BCRP.

Conversely, zonisamide was the only herein investigated AEDs identified as BCRP substrate both *in vitro* and *in vivo* non-clinical studies. We demonstrated that elacridar (and consequently BCRP inhibition) significantly increased the brain exposure of zonisamide after IV administration to mice. Noteworthy, the IN administration of zonisamide was unaffected by the presence of BCRP inhibitor. This was the first time that the influence of BCRP inhibition in the pharmacokinetics of IN drugs was reported, suggesting that nose-to-brain delivery is not modulated by BCRP, and it can be, hence, used as a new strategy to overcome the overexpression of BCRP in refractory epilepsy.

CHAPTER VIII

GENERAL DISCUSSION



GENERAL DISCUSSION

This chapter presents an integrative approach on the various issues discussed within previous sections, by critically overviewing the developed research activities and their respective findings.

Firstly, the importance of the defined objectives for the scientific community will be thoroughly discussed, as well as the rationale applied to the selection of lacosamide, levetiracetam and zonisamide.

The bioanalytical HPLC-DAD methodologies herein developed and validated will be commented, demonstrating their essential role to accurately quantify the AEDs in a wide variety of biological samples, encompassing those from patients as well as from *in vitro* cell models and *in vivo* pharmacokinetic studies.

The usefulness of performing *in vitro* cell assays to identify BCRP substrates and inhibitors, and investigate the P_{app} of the AEDs through human nasal cells will be also summarized. *In vitro* results will be critically compared with those from the *in vivo* studies, which were carried out to investigate the nose-to-brain delivery of lacosamide, levetiracetam and zonisamide and compare the systemic/peripheral drug disposition following IN administration and classical routes.

The final remarks will focus the feasibility of using the IN route to avoid BCRP activity at the BBB.

Despite the introduction of dozens of new AEDs into clinical practice during the last two decades, the proportion of patients with drug-resistant epilepsy has remained unchanged (\approx 30-40 %). Nevertheless, the pathophysiological mechanisms underlying the onset and recurrence of epileptic seizures advanced in the last decade, with several hypotheses being outlined. Among them is the overexpression of ABC transporters (e.g. P-gp and BCRP) in biological barriers of refractory epileptic patients, including the intestinal membrane and the BBB. Since several AEDs are currently recognized as P-gp and/or BCRP substrates, their systemic and brain exposures, when orally or intravenously administered, decrease as pharmacoresistance mechanisms progress. The inhibition of P-gp-mediated efflux has already revealed to enhance the brain

concentrations of AEDs, but it may not be feasible in clinical practice, since other xenobiotics and neurotoxic endogenous compounds may also attain cerebral tissue, compromising its vital functions. Therefore, avoiding P-gp and/or BCRP-mediated efflux transport can be a disease-modifying therapy with expected benefits in epilepsy.

The increasing scientific evidence regarding direct drug delivery into the brain after IN administration was the basis of the present PhD thesis. In this context, our aim was to assess whether the IN administration of new-generation AEDs allowed their direct nose-to-brain transport in mice and investigate if the underlying mechanisms effectively avoided the BCRP expressed at the BBB. Moreover, bearing in mind that 80 % of patients with epilepsy report adverse events related to AEDs and that 30–40 % have impaired quality of life that promote non-adherence, IN administration is expected to require lower drug doses, reduce drug systemic exposure and decrease side effects. Therefore, comparative non-clinical pharmacokinetic studies were herein performed in order to explore the systemic, brain, lung and renal exposures of the AEDs after their IN, IV and oral administration.

It was recently demonstrated that BCRP expression and activity are higher than those of P-gp in the human BBB [588]. This finding, as well as the scarce data concerning potential interactions between AEDs and BCRP, prompted the investigation of BCRP as an additional target of pharmacoresistance mechanisms that should be avoided. Thus, the AEDs were selected as those for which no information regarding their interaction with BCRP was available in literature or it was contradictory. Moreover, as their inhibitory effect on BCRP could hamper the interpretation of results and the evaluation of BCRP influence on brain delivery through IN administration, some AEDs were screened regarding their *in vitro* inhibitory effect on BCRP activity. These preliminary cellular screening assays are described in **Appendix A** and revealed that carbamazepine, levetiracetam and zonisamide did not inhibit BCRP-mediated transport at 25 μ M. However, since carbamazepine had already been administered by IN route and it did not evidence direct nose-to-brain delivery [484], we opted not to test it. On the other hand, oxcarbazepine, licarbazepine and lacosamide inhibited BCRP *in vitro*, but we chose lacosamide because it has stronger pharmacokinetics drawbacks

and DDI potential when orally administered than licarbazepine and oxcarbazepine [589–592].

The first aim of the present PhD thesis consisted of the development and full validation of a bioanalytical method to accurately quantify lacosamide, levetiracetam and zonisamide in different biological matrices. This method was essential to support subsequent *in vivo* pharmacokinetic studies. A reversed phase HPLC method was chosen because it is the gold standard for the quantification of substances in complex samples, such as biological matrices. It allows the separation, identification, and selective quantification of several analytes.

This objective was attained in two steps, starting with the development of chromatographic conditions and the acquisition of know-how in the bioanalytical field using human plasma. The technique was subsequently transposed to the bioanalysis of the AEDs in mouse matrices (plasma, brain, lung and kidney). The selection of human plasma for this purpose was based on the fact that the development of analytical techniques requires considerable volumes of biological sample and human plasma is easily accessible, available in larger quantities and ethically more acceptable than mice plasma. Consequently, the number of sacrificed animals required for technique development/validation was substantially reduced, as demanded by 3Rs rules, ethical principles and legislation [475].

No less important than the aforementioned justification is the usefulness of the HPLC-DAD technique using human plasma for clinical therapeutic drug monitoring. The relevance of therapeutic monitoring of AEDs was firstly reported in the 60s [146]. Diphenylhydantoin and phenobarbital were the first AEDs to be monitored, using serum from epileptic patients [593], but nowadays it continues to be required for drugs with narrow therapeutic ranges, pharmacokinetic limitations, considerable inter- and intra-individual variability and propensity to develop DDIs [561]. Although 2nd and 3rd generations of AEDs (namely lacosamide, levetiracetam and zonisamide) are safer and exhibit better pharmacokinetic profiles, their therapeutic drug monitoring is advisable, particularly in subpopulations such as pregnant women, pediatrics, geriatrics, ultra-rapid or poor metabolizers, and refractory epileptic patients [432, 459, 558, 559, 594]. The herein developed HPLC-DAD method could hence be applied not only for

therapeutic drug monitoring of lacosamide, levetiracetam and zonisamide, but also for assessing patient compliance to AEDs pharmacotherapy [595].

As described in *Chapter III*, isocratic and gradient conditions, as well as distinct organic solvents and aqueous solutions (e.g. water and buffers) were tested. Due to the distinct lipophilic-hydrophilic properties of levetiracetam, lacosamide and zonisamide [$\log D$ (pH 7.4): -0.5, 0.18 and 0.5, respectively], a gradient elution method was preferable, and the final mobile phase was composed of water and a very small percentage of acetonitrile that ranged from 3 % to 10 %. This economic and eco-friendly mobile phase, together with the DAD detection set at 220 and 239 nm, made it possible to separate and quantify the three investigated AEDs in only 14 minutes. Importantly, the double LLE removed various biological constituents and concentrated the AEDs allowing the definition of LLOQ values that were lower than the therapeutic range defined in literature [596]. This technique fulfilled the international validation requirements for the reliable quantification of aforementioned AEDs in a wide plasma concentration range, with good selectivity, sensitivity, and feasibility of sample dilution. Moreover, it was successfully applied to analyze 651 samples collected from 321 patients admitted in the *Centro de Epilepsia Refratária, Centro Hospitalar e Universitário de Coimbra* (CHUC, EPE). This highlights that the technique is practical, fast and easy to execute in clinical context. In fact, its application allowed a recent publication identifying new factors that compromise the clearance and volume of distribution of levetiracetam [559].

Based on the knowledge acquired during the optimization of the analytical technique in human plasma, the method was straightforward applied to biological matrices of mice. HPLC-DAD conditions were kept the same for all the matrices, while the sample preparation procedure was slightly optimized in tissue homogenates. Minor changes were introduced in the extraction technique for tissue homogenates, namely sample volume, 150 μL for homogenates (*versus* 100 μL for plasma) and centrifugation time (5 min *versus* 3 min in plasma). Validation parameters were within those defined by international guidelines and, at the end, all methodologies comprised several favorable aspects, including an inexpensive and highly reproducible sample preparation procedure, which is extremely relevant when a large number of samples

derived from pharmacokinetic studies need to be analyzed. Additionally, the small sample volumes required (100 μL and 150 μL for plasma and tissue homogenates, respectively) were compatible with animal size and volume of biological fluids collected during *in vivo* pharmacokinetic studies presented in *Chapters IV, V, VI and VII*.

In parallel, and because AED quantification by HPLC-DAD is not required, cellular accumulation assays were carried out to identify BCRP inhibitors. This model consists of investigating the impact of each AED in the transport of Hoechst 33342 into the cell. Hoechst 33342 is a specific BCRP substrate and it is fluorescent, allowing its quantification in intracellular content by fluorescence. The immortalized MDCK-BCRP cell line was herein used because primary cultures are too laborious to prepare and maintain, while BBB-specific cell lines form excessively leaky monolayers that would be indiscriminating in the bidirectional transport assay performed to identify BCRP substrates. Therefore, in an attempt to maintain the same cell line throughout *in vitro* tasks, we opted to use the MDCK-BCRP cells. This is a commercially available cell line that results from the transfection of MDCK-II cells with the human *ABCG2* gene. It presents rapid growth and differentiation, and the ability to develop tight junctions that restrict paracellular transport, forming tight monolayers [155]. In addition, this cell line has already been properly validated in previous studies through its application to various reference compounds [313]. In comparison with the classic Caco-2 cell line, the MDCK-BCRP cell line is preferable because it takes approximately 7 days to develop a restrictive membrane, instead of 21 days. Although parental and transfected MDCK cells have different morphological characteristics comparatively to BBB endothelial cells, they have been widely used in transport-interaction studies [155]. Even though MDCK cells are canine kidney cells, the transfected *ABCG2* gene is human, minimizing variability between species.

After demonstrating that several concentrations of AEDs, encompassing their therapeutic concentration ranges, did not influence the viability of MDCK-II and MDCK-BCRP cells in the Alamar Blue Assay, potential BCRP inhibitors were identified resorting to intracellular accumulation studies. BCRP functionality was always demonstrated, making use of a reference BCRP substrate and inhibitor (Hoechst 33342 and Ko143,

respectively). Levetiracetam did not inhibit BCRP within the concentration range of 10-300 μM , in opposition to zonisamide, which inhibited BCRP at 200 and 300 μM , and lacosamide, which inhibited BCRP function independently of the concentration.

In addition to accumulation assays, BCRP substrates were identified in bidirectional transport assays that require an HPLC technique to quantify the AEDs that cross cell line monolayer from apical to basolateral side and *vice versa*. Following the line of work defined for HPLC technique development in biological samples (**Section III.3.1**), new HPLC-DAD techniques were defined to quantify lacosamide, levetiracetam and zonisamide in samples collected from the *in vitro* transport assays (**Table VII.1**). Their quantification was achieved in less than 6 min. Despite being more arduous than intracellular accumulation assays, bidirectional studies accurately predict efflux liabilities, correlate well with *in vivo* results and are relevant to evaluate CNS distribution [597, 598]. Thus, following the recommended international criteria [591, 599] the net flux ratio was determined for the three AEDs under investigation, and also for a BCRP specific substrate (sulfasalazine) as control. Mass balance was estimated for all compounds, attaining values higher than 80 %. This is somehow expected, since mass balance is lower for highly lipophilic compounds that can be adsorbed onto the plastic or membrane support, preventing the attainment of meaningful and reliable P_{app} values. In addition, TEER was monitored, varying between 38.90 and 32.78 $\Omega\cdot\text{cm}^2$, before starting transport assay and at the end, respectively. Recorded TEER values could indicate monolayer leakiness, however the MDCK-II cell line is commonly associated with low TEER [600], related to the ion movement between pores [598]. The P_{app} of the paracellular fluorescent marker, Na-F, was lower than 1×10^{-6} cm/s , guarantying that the monolayers were free from leakiness when used for experiments. Sulfasalazine was correctly identified as BCRP substrate, exhibiting a net flux ratio superior to 2 that decreased more than 50 % after pre-incubation with Ko143. Regarding the AEDs under investigation, only zonisamide undoubtedly presented a similar pattern, evidencing that it is a BCRP substrate.

The combination of the aforementioned *in vitro* cell-based assays allowed the acquisition of new information regarding the interaction of lacosamide, levetiracetam and zonisamide with human BCRP. Since levetiracetam was neither an inhibitor nor a

substrate of BCRP, under the experimental conditions herein applied, it was the first AED to proceed to *in vivo* studies. It is also important to emphasize that zonisamide was a BCRP substrate but it only inhibited the efflux transporter at concentrations considerably higher than those of the therapeutic range. Therefore, zonisamide passage through the intestinal membrane and BBB is expected to decrease as the expression of the efflux transporter increases, but its inhibitory effect is unlikely to occur within the therapeutic range. For that reason, zonisamide was subjected to comparative pharmacokinetic *in vivo* pharmacokinetic studies, but its biodisposition was also compared with that observed when co-administered with elacridar, a BCRP inhibitor.

Before performing *in vivo* studies, the permeability of the AEDs under investigation was also assessed through a monolayer of nasal mucosa RPMI-2650 cells. This model has been used to predict nasal absorption but, until now, there are no findings reporting that it accurately predicts the nose-to-brain drug delivery. With this purpose, P_{app} (AP-BL) was determined for the three AEDs and a direct relationship was found between drug permeability and its lipophilicity. Zonisamide, the most lipophilic AED [$\log D(\text{pH } 7.4) = 0.5$], showed the greatest P_{app} through RPMI-2650 cell monolayer ($7.46 \times 10^{-6} \pm 0.86 \times 10^{-6}$ cm/s), followed by lacosamide [$\log D(\text{pH } 7.4) = 0.18$; $P_{app} = 5.32 \times 10^{-6} \pm 1.75 \times 10^{-6}$ cm/s] and levetiracetam, the least lipophilic compound [$\log D(\text{pH } 7.4) = -0.5$; $P_{app} = 4.32 \times 10^{-6} \pm 2.11 \times 10^{-6}$ cm/s].

In vivo pharmacokinetic studies were performed in male CD-1 mice to investigate the potential of the IN route, BCRP impact on AEDs biodisposition and whether RPMI-2650 cell line can be used as a reliable model to accurately predict drug nasal absorption and/or nose-to-brain delivery. The mouse and rat are the animal models most frequently used for assessing the profile of new chemical compounds or therapeutic approaches, including the IN administration of AEDs. Particularly regarding the aims of the present thesis, the mouse was the preferred animal species because the AEDs pharmacokinetics was intended to be described not only in plasma but also in tissues (brain, lung and kidney), requiring animal sacrifice. According to ethical principles, investigations should be initiated in species phylogenetically more distant from humans and therefore the mouse was selected instead of the rat. Adult male CD-

1 mice with 25-30 g were used to avoid the interference of the hormonal female cycle on pharmacokinetic profiles.

Given the limitations of the IN administration route, namely the reduced volume that can be administered and the very fast MCC, an *in situ* thermoreversible gel was used to increase mucoadhesiveness, decrease the rapid post-nasal drainage and enhance residence time in the nasal cavity, particularly in olfactory epithelium, without compromising drug biodegradability. Two polymers were tested in order to provide both sufficient *in situ*-gelling properties and high mucoadhesion: Carbopol® 974P and Noveon® Polycarbophil. The former is a cross-linked polymer, producing highly viscous gels, while Noveon® Polycarbophil USP is a high molecular weight acrylic acid polymer cross-linked with divinyl glycol, which provides excellent bioadhesive properties and has been extensively used to enhance the delivery of active ingredients to various mucous membranes [487]. Although both polymers were liquid at 5 °C, and hence syringeable, and jellified at 34 °C (nasal cavity temperature), Carbopol® 974P was selected since the formulation had no impact on *in vitro* Calu-3 and RPMI-2650 cells viability. Thus, the thermoreversible gel of Carbopol® 974P at 0.2 % (w/v) and Pluronic F-127 at 18 % (w/v) was loaded with each of the three AEDs and then individually administered to mice.

Since nose-to-brain drug delivery requires the passage through the olfactory mucosa, by either neuronal or epithelial route, it is very important the drug to attain the upper part of the nasal cavity. Moreover, lung-delivery must be avoided due to the risk of death by asphyxiation. Significant progress has been made regarding the development of efficient nasal delivery devices that direct the flow and optimize drug deposition in the olfactory epithelium [251, 601–605].

In this context, three distinct nasal devices were tested in an attempt to increase the volume of drug formulation that could be safely administered, reduce systemic and pulmonary absorption and promote nose-to-brain delivery:

- Gel administration to awake mice using a pipette: the filled tip of the pipette is placed near the mouse's left nostril, at a 45°C angle; the droplet is placed sufficiently close to the mouse's nostril so that the mouse inhales it; the procedure is repeated until all the volume is administered [245].

- Gel administration to anesthetized mice using a polyurethane tube: a polyurethane tube (24 G, 19 mm) coupled to a 1 mL syringe, introduced about 1 cm from the left nostril of the animal, positioned laterally [485].
- Gel administration to anesthetized mice using a MicroSprayer® aerosolizer attached to a FMJ-250 high pressure syringe: instillation takes place unilaterally into the left nostril using a MicroSprayer® Aerosolizer (Model IA-1B, Penn-Century) coupled to a high pressure syringe (Model FMJ-250 from Penn-Century); together, both devices produce a highly concentrated, air-free aerosol from the end of the small diameter delivery tube to aerosolize the thermoreversible gel; the tip of the delivery tube is inserted 1 mm into the nostril.

The design and results of the preliminary study that was developed to evaluate the potential of each device to directly deliver the thermoreversible gel loading levetiracetam are presented in **Appendix B**. Comparing them with the results described in *Chapter V*, it is evident that the aerosolization of the drug formulation provides a more significant direct nose-to-brain transport than that attained with the pipette and the polyurethane tube. The pipette did not even conduct the drug to the brain within the first 5 min and some animals revealed liquid in the mouth, suggesting that the drop did not make it fully into the nose. These animals were excluded from the analysis. Lower concentrations of levetiracetam were also found in lung tissues after the aerosolization of the drug formulation, rather than with the other two methodologies. These findings were a breakthrough to identify the MicroSprayer® Aerosolizer coupled to the high-pressure syringe as the best device to administer the AEDs by IN route. Importantly, as this device requires the administration of fixed-volumes (multiple of 25 μ L), animal weight was defined between 25 and 30 g in order to reduce inter-individual variability.

It is relevant to point out that the preliminary study carried out to assess the pharmacokinetics of lacosamide after its aerosolization in nasal cavity revealed a considerable mortality rate (53.84 %), which was higher than those found for levetiracetam (9.01 %) and zonisamide (9.01 %). This observation prevented the pharmacokinetic pre-clinical study with the MicroSprayer® Aerosolizer for lacosamide.

Probably due to its physico-chemical characteristics, lacosamide modified the jellification of the formulation slightly and drips into the lungs with greater speed and extension. Since the animals are anesthetized, respiratory function may be impaired, leading to animal death. Hence, lacosamide hydrogel was herein intranasally administered using the polyurethane tube, despite its aforementioned limitations.

Once study design protocols were optimized, pharmacokinetic studies were performed for the three AEDs in order to evaluate drug concentration-time profiles in plasma, brain (biophase), lung and kidney (the major excretory organ). Consequently, the pharmacokinetic behavior of lacosamide, levetiracetam and zonisamide was characterized, following their IN delivery to mice. When investigating the potential of a new administration route, the obtained experimental results must be compared with those derived from conventional delivery alternatives. In accordance with international guidelines, all administration routes, including IN administration, can result in systemic absorption and, therefore, the systemic exposure obtained with a proposed new formulation must be compared with that observed with an approved administration route. Hence, the adequate non-clinical evaluation of the absorption, distribution, metabolism, and excretion of the drug when administered as new formulation must be compared with classical ones. Moreover, if systemic exposure by a new route of administration is equivalent to or less than that of the approved route, histological evaluation may be limited to locally exposed tissues. For these reasons, the histological evaluation of the lung was herein performed after multiple-dose administration of levetiracetam by IN route (*Chapter V*). AEDs are usually available as oral and IV formulations, which can be used as reference administration routes. At this point, it is important to remember that one of the main objectives outlined for this thesis consisted in investigating the direct nose-to-brain delivery of the AEDs. Considering that IN drugs also attain the CNS via systemic circulation, upon nasal vasculature absorption and subsequent BBB crossing, the exact contribution of this pathway can only be inferred using IV injection, which enables a complete systemic bioavailability ($\approx 100\%$), requiring drug passage across the BBB to reach the brain. Therefore, the IV route was used as reference for all AEDs, providing an accurate discrimination between the drug fraction that attained the brain by systemic pathway

and that transported directly by nose-to-brain pathways. Both lacosamide and levetiracetam are available in clinical practice as injectable formulations, however zonisamide is only available as oral dosage forms. For this reason, zonisamide was herein investigated after IN, IV and oral administrations. We opted not to administer lacosamide or levetiracetam by oral gavage in an attempt of reducing the number of animals to be used. We expect that the evidence of similar pharmacokinetic behavior of drugs administered by IN route comparatively to the IV injection will reflect its potential as a promising alternative approach, implicitly confirming its superiority over oral delivery.

To facilitate the comparison of drug concentration-time profiles after IN and IV administrations and attenuate error sources, the same dose was administered and defined in order to achieve plasma concentrations within the human therapeutic range reported in literature [596]. Importantly, higher doses of orally administered zonisamide were required to attain quantifiable concentrations in tissues, probably because of its gastrointestinal degradation and hepatic first-pass metabolism. Indeed, the absolute bioavailability of zonisamide was only 20.42 % in mice (**Table V.2**). Therefore, the oral dose of zonisamide was 80 mg/kg as defined in previous *in vivo* studies [581].

The pharmacokinetic behavior of levetiracetam after administration of 625 µg per animal through IN instillation resulted in a bioavailability of 107.44 %, with rapid and extensive systemic absorption. The similar t_{max} values (5 min) reported after IN and IV administrations, as well as the higher values found in brain after IN administration suggest the advantageous use of the IN route for the delivery of levetiracetam in emergency situations, bypassing the invasive IV technique and allowing the self-administration by patients or caregivers. Noteworthy, brain exposure of levetiracetam after IN administration almost doubled comparatively to IV injection (742.41 vs 381.93 µg.min/mL) and the DTE was 182.35 %. These findings evidence the direct nose-to-brain delivery of levetiracetam and create a new hope in the treatment of refractory epilepsy.

After IN instillation, zonisamide was not completely absorbed (bioavailability of 54.95 %), but quickly attained the systemic bloodstream, specifically compared with

oral administration (t_{\max} was 5 min vs 15 min). When focusing on brain tissue, it is relevant that the concentrations achieved at 5 min post-nasal-administration were 8 times higher than those achieved by IV administration. Indeed, the DTE of 149.54 % and the DTP of 33.13 % undoubtedly emphasize the direct nose-to-brain delivery of the drug. Approximately 33.13 % of the drug that reached the brain made it through direct pathways. In contrast, renal exposure of zonisamide after IN administration was considerably reduced in relation to IV or oral routes. This is of utmost importance, because it decreases the likelihood of renal lithiasis, which is the adverse effect most often associated with zonisamide. These findings are not only promising for the treatment of refractory epilepsy, but also as a more tolerable treatment of seizures and epilepsy.

Lacosamide was the investigated AED with highest absolute IN bioavailability (mean value of 120.46 %), but the lowest values of DTE (128.67 %) and DTP (22.28 %), clearly standing out as the AED that attained the brain mainly by systemic pathways. Moreover, the MRT of lacosamide in plasma and tissues were considerably superior after IN administration than IV injection (**Table VI.3**), in opposition to zonisamide and levetiracetam. This makes the IN administration of lacosamide very interesting for prolonged and sustained release. It is probable that the use of a different administration device (polyurethane tube instead of the MicroSprayer® Aerosolizer) can be responsible by the prolonged absorption of lacosamide and consequently its prolonged MRT in brain. Importantly, and probably due to the same reason, lacosamide presented a large value of DTE regarding the lungs (888.91 %), which is considerably superior to those reported for levetiracetam (240.44 %) and zonisamide (144.47 %). These findings suggest that the polyurethane tube does not reach the olfactory epithelium as effectively as the aerosolizer, which delivers the drug formulation across a more extensive area, thereby promoting nose-to-brain delivery.

The aforementioned comparison between the *in vivo* pharmacokinetics and biodisposition of the three AEDs after IN administration is also interesting to correlate with *in vitro* permeability investigations herein carried out on RPMI-2650 cells, described in **section IV.3.4**. Accordingly, it is evident that the P_{app} (AP-BL) through the RPMI-2650 cell monolayer does not correlate with direct nose-to-brain delivery given

by DTE or DTP. Indeed, levetiracetam was the AED with highest values of DTE or DTP *in vivo*, but it was the least permeable compound *in vitro*. However, it was possible to establish a relationship between *in vitro* P_{app} through RPMI-2650 cell monolayers and *in vivo* brain-plasma ratios. Zonisamide was the AED with highest value of brain-to-plasma ratio, as well as the one with the highest P_{app} , suggesting that P_{app} can be used as a biomarker to predict the ability of the drug to reach the brain, in detriment of the bloodstream levels.

Table VIII. 1 Summary of *in vitro* and *in vivo* results. Apparent permeability (P_{app}) from apical to basolateral side (AP-BL) obtained across RPMI-2650 cell monolayers, drug targeting efficiency (DTE), direct transport percentage (DTP) and ratios between area under the curve (AUC) of tissues and plasma for the three investigated AEDs.

	Lacosamide	Levetiracetam	Zonisamide
<i>In vitro permeability assays</i>			
P_{app} (AP-BL) ($\times 10^{-6}$ cm/s) RPMI-2650	5.32	4.30	7.46
<i>In vivo pharmacokinetic studies</i>			
DTE	128.67 %	182.35 %	149.54 %
DTP	22.28 %	46.38 %	33.13 %
Tissue-plasma ratios			
Brain-to-plasma	0.50	0.31	1.02
Lung-to-Plasma	0.16	0.48	0.98
Kidney-to-Plasma	0.42	1.02	0.99

$P_{app(AP-BL)}$, apparent permeability coefficient from apical to basolateral compartment.

To finalize, the effect of BCRP on zonisamide biodisposition after IN and IV administrations was investigated *in vivo*. As aforementioned, zonisamide was herein identified *in vitro* as a BCRP substrate and, therefore, the final aim of the present thesis was to investigate whether BCRP in the BBB was avoided when zonisamide is administered intranasally. Thus, zonisamide was intravenously or intranasally administered to CD-1 mice, in order to determine its extent of brain penetration, in the presence and absence of elacridar. Elacridar was administered by IV route to attest the involvement of BCRP in the transport of zonisamide across the BBB. This way, it was guaranteed that BBB passage was being analyzed without interference of other

biological barriers (e.g., intestinal membrane, if elacridar was orally administered). Elacridar inhibits BCRP and P-gp, but previous studies showed that zonisamide is not a P-gp substrate, and thus its contribution to zonisamide efflux is negligible [599, 606].

In relation to the animals administered with vehicle, the co-administration of zonisamide and elacridar by IV route increased the C_{max} and AUC by 2- and 3-fold, respectively. These findings corroborate the *in vitro* results that identified zonisamide as a BCRP substrate. Interestingly, after the IN administration of zonisamide, its pharmacokinetics remained comparable between elacridar and vehicle groups, suggesting that the impact of BCRP at the BBB is not as significant as that observed after systemic administration of the AED. Moreover, IN administration seems to contribute to the direct transport, while efflux transport at the BBB seems to have less impact. Even so, from previous pharmacokinetic studies described in **Chapter V**, systemic absorption should not be overlooked.

By completing the proposed project, it is possible to verify that BCRP influences the cerebral concentration of its substrates, such as zonisamide. In this context, IN administration may be an efficient alternative in refractory patients due to direct nose-to-brain drug delivery, but also because the overexpression of BCRP may be circumvented. Furthermore, the IN route is non-invasive, enables self-administration and may contribute to the reduction of systemic drug exposure and, consequently, undesirable side effects.

Therefore, through the association of the several experimental models herein applied, it was demonstrated that investigating the interaction between AEDs and BCRP, together with the potential of the IN administration of AEDs, may be a successful strategy to develop new pharmacological treatments with fewer side effects and a higher success rate in refractory epilepsy.

The advances herein reported increased the knowledge about the limitations of CNS penetration involving BCRP and may contribute to a major shift in epilepsy treatment.

CHAPTER IX

CONCLUSION



CONCLUSION

Epilepsy and pharmaco-resistant epilepsy remain untreated diseases despite the wide variety of AEDs available in clinical practice. This makes the research of new drugs and therapeutic approaches an unmet clinical need in current days. AEDs are an undeniably efficient prophylactic treatment but their peripheral administration requires passage through the BBB into the brain. Moreover, scientific investigations evidence that efflux transporters compromise the therapeutic effect of some AEDs. Therefore, it was herein hypothesized that the IN administration of lacosamide, levetiracetam and zonisamide could overcome the BBB and efflux transporters, increasing drug access into the brain and avoiding some of the pharmaco-resistance mechanisms underlying epilepsy.

In brief, the main relevant findings brought from the experimental work developed under the scope of the present thesis are as follows:

- An HPLC-DAD analytical technique was developed and fully validated to simultaneously quantify lacosamide, levetiracetam and zonisamide in human plasma. The method revealed to be accurate, precise, linear, selective and reproducible in agreement with international guidelines. The attainment of this objective allowed the acquisition of know-how to develop and validate a similar method in mice biological samples, reducing the number of animals required. Importantly, the HPLC-DAD technique was, and is still being, implemented in routine therapeutic drug monitoring of refractory epileptic patients due to its feasible use in hospitals.
- The aforementioned analytical technique was successfully implemented and validated to quantify lacosamide, levetiracetam and zonisamide in plasma, brain, lung and kidney homogenates from mice, demonstrating its accuracy, precision and linearity through wide calibration ranges that allowed their application in the pharmacokinetic studies herein executed.

- The impact of lacosamide, levetiracetam, zonisamide and the thermoreversible gel on nasal and lung cell lines (RPMI-2560 and Calu-3) was assessed in a broad range that included the therapeutic windows and allowed the definition of concentrations for further *in vitro* investigations.
- The identification of human BCRP substrates and/or inhibitors was performed in cell-based assays with MDCK-II and MDCK-BCRP cells. Firstly, cell viability was investigated through the Alamar blue assay for the three AEDs under investigation. Thereafter, intracellular accumulation assays were performed, demonstrating that only lacosamide inhibited BCRP within therapeutic concentrations, while zonisamide inhibited the same ABC transporter only at concentrations higher than those reported as therapeutics.
- The bidirectional permeability assay performed on MDCK-II and MDCK-BCRP cells identified zonisamide as the only BCRP substrate. It presented a net flux ratio of 2.73 that decreased more than 50 % in the presence of the BCRP inhibitor, Ko143.
- Screening of the apparent permeability of the AEDs through the RPMI-2650 cell monolayer classified zonisamide as the most permeable compound through the nasal mucosa, followed by lacosamide and levetiracetam. The results evidenced that the apparent permeability increases with drug lipophilicity.
- For pharmacokinetic studies, AEDs were incorporated into a thermoreversible gel and aerosolized with the MicroSprayer® Aerosolizer connected to a high-pressure syringe. The device revealed a good accuracy, precision and reproducible administration of a higher volume than those attained with other devices. Importantly, the administration of the thermoreversible gel loading lacosamide required the use of a polyurethane tube, because its aerosolization led to an increased animal death rate.

- The concentration-time profiles obtained in plasma, brain and kidney after IN and IV administration of levetiracetam were quite similar. Nonetheless, the high values of DTE and DTP emphasize that a considerable part of the drug reaches the brain by direct transport after IN administration. Moreover, the multiple dosing study evidenced no histological differences between treated and non-treated animals. In opposition, plasma concentrations attained for zonisamide after IN administration were considerably lower than those observed after IV injection ($F = 54.95\%$). However, direct nose-to-brain distribution was demonstrated (DTE = 144.47 % and DTP = 33.13 %), although in lower extent than levetiracetam. Interestingly, pulmonary and renal exposures were lower after IN administration, corroborating that this may represent an alternative to the administration of oral formulations, which are the only clinically available option. Lacosamide was the investigated AED with highest absolute IN bioavailability (mean value of 120.46 %), but the lowest values of DTE (128.67 %) and DTP (22.28 %), clearly standing out as the AED that attained the brain mainly by systemic pathways.
- The aforementioned results enabled the investigation of *in vitro/in vivo* relationships, evidencing that although the P_{app} through the RPMI-2650 cell monolayer did not correlate with direct nose-to-brain delivery, given by DTE or DTP, it could predict the ability of the drug to reach the brain through the BBB.
- Lastly, *in vivo* pharmacokinetic studies carried out with the co-administration of elacridar demonstrated that the brain concentrations of zonisamide increased after IV administration, confirming the involvement of BCRP in its passage across the BBB. Interesting results were found when the AED was administered by IN route. The plasma and brain concentrations of intranasally administered zonisamide remained similar when it was co-administered with elacridar or with vehicle. These findings suggest that the influence of BCRP has a greater impact if the drug is administered by IV route that inevitably implies the passage through the BBB.

Altogether, the results herein described support the importance of investigating the interaction between AEDs and BCRP, as well as the high potential of the IN route to not only deliver the AEDs directly into the brain but also reduce the impact of BCRP on drug access to the biophase.

In the future, it would be interesting to investigate the pharmacological effects of lacosamide, levetiracetam and zonisamide after their IN administration, in order to estimate the correlation between the pharmacokinetics of the AEDs and their potency/toxicity. It would also be important to co-administrate zonisamide and lacosamide and investigate whether lacosamide decreases the development of drug-resistant epilepsy.

REFERENCES



REFERENCES

- [1] **FISHER, R.; CROSS, J.; FRENCH, J. *et al.*** - Operational classification of seizure types by the International League Against Epilepsy: Position Paper of the ILAE Commission for Classification and Terminology. *Epilepsia*. 58:4 (2017) 522–530. doi: 10.1111/epi.13670.
- [2] **FISHER, R.; ACEVEDO, C.; ARZIMANOGLU, A. *et al.*** - ILAE official report: a practical clinical definition of epilepsy. *Epilepsia*. 55:4 (2014) 475–482. doi: 10.1111/epi.12550.
- [3] **HESDORFFER, D.; BENN, E.; CASCINO, G. *et al.*** - Is a first acute symptomatic seizure epilepsy? Mortality and risk for recurrent seizure. *Epilepsia*. 50:5 (2009) 1102–1108. doi: 10.1111/j.1528-1167.2008.01945.x.
- [4] **BEGHI, E.; CARPIO, A.; FORSGREN, L. *et al.*** - Recommendation for a definition of acute symptomatic seizure. *Epilepsia*. 51:4 (2010) 671–675. doi: 10.1111/j.1528-1167.2009.02285.x.
- [5] **BEGHI, E.** - The epidemiology of epilepsy. *Neuroepidemiology*. 54:2 (2019) 185–191. doi: 10.1159/000503831.
- [6] **WILSON, K.; REYNOLDS, E.** - Translation and analysis of a cuneiform text forming part of a babylonian treatise on epilepsy. *Medical History*. 34:2 (1990) 185–198. doi: 10.1017/S0025727300050651.
- [7] **BOTTING, C.; KUHN, R.** - Novel approaches to flavivirus drug discovery. *Expert Opinion on Drug Discovery*. 7:5 (2012) 417–428. doi: 10.1517/17460441.2012.673579.
- [8] **VAJDA, F.; EADIE, M.** - The clinical pharmacology of traditional antiepileptic drugs. *Epileptic Disorders*. 16:4 (2014) 395–408. doi: 10.1684/epd.2014.0704.
- [9] **EADIE, M.** - Epilepsy-from the Sakikku to hughlings Jackson. *Journal of Clinical Neuroscience*. 2:2 (1995) 156–162. doi: 10.1016/0967-5868(95)90010-1.
- [10] **GROSS, R.** - A brief history of epilepsy and its therapy in the western hemisphere. *Epilepsy Research*. 12:2 (1992) 65–74. doi: 10.1016/0920-1211(92)90028-R.
- [11] **NORN, S.; PERMIN, H.; KRUSE, E. *et al.*** - [On the history of barbiturates]. *Dan Medicinhist Arbog*. 43:(2015) 133–151.
- [12] **MAGIORKINIS, E.; DIAMANTIS, A.; SIDIROPOULOU, K. *et al.*** - Highlights in the

- History of Epilepsy: The Last 200 Years. *Epilepsy Research and Treatment*. (2014) 582039. doi: 10.1155/2014/582039.
- [13] **LÖSCHER, W.; KLITGAARD, H.; TWYMAN, R. *et al.*** - New avenues for anti-epileptic drug discovery and development. *Nature Reviews Drug Discovery*. 12:10 (2013) 757–776. doi: 10.1038/nrd4126.
- [14] **LÖSCHER, W.; BRANDT, C.** - Prevention or modification of epileptogenesis after brain insults: Experimental approaches and translational research. *Pharmacological Reviews*. 62:4 (2010) 668–700. doi: 10.1124/pr.110.003046.
- [15] **KLEIN, B.; JACOBSON, C.; METCALF, C. *et al.*** - Evaluation of Cannabidiol in Animal Seizure Models by the Epilepsy Therapy Screening Program (ETSP). *Neurochemical Research*. 42:7 (2017) 1939–1948. doi: 10.1007/s11064-017-2287-8.
- [16] **TRINKA, E.; KWAN, P.; LEE, B. *et al.*** - Epilepsy in Asia: Disease burden, management barriers, and challenges. *Epilepsia*. 60:1 (2019) 7–21. doi: 10.1111/epi.14458.
- [17] **THIJS, R.; SURGES, R.; O'BRIEN, T. *et al.*** - Epilepsy in adults. *The Lancet*. 393:10172 (2019) 689–701. doi: 10.1016/S0140-6736(18)32596-0.
- [18] **MIZIAK, B.; KONARZEWSKA, A.; UŁAMEK-KOZIOŁ, M. *et al.*** - Anti-Epileptogenic Effects of Antiepileptic Drugs. *Internacional Journal Molecular Sciences*. 21:7 (2020) 2340. doi: 10.3390/ijms21072340.
- [19] **VEZZANI, A.; FUJINAMI, R.; WHITE, H. *et al.*** - Infections, inflammation and epilepsy. *Acta Neuropathol*. 131:2 (2016) 211–234. doi: 10.1007/s00401-015-1481-5. Infections.
- [20] **WIRRELL, E.; GROSSARDT, B.; WONG-KISIEL, L. *et al.*** - Incidence and Classification of New-Onset Epilepsy and Epilepsy Syndromes in Children in Olmsted County, Minnesota from 1980–2004: A population-based study. *Epilepsy Res*. 95:1–2 (2011) 110–118. doi: 10.1016/j.eplepsyres.2011.03.009.
- [21] **SINGH, A.; TREVICK, S.** - The Epidemiology of Global Epilepsy. *Neurologic Clinics*. 34:4 (2016) 837–847. doi: 10.1016/j.ncl.2016.06.015.
- [22] **NELIGAN, A.; HAUSER, W.; SANDER, J.** - The epidemiology of the epilepsies. *Handb Clin Neurol*. 107:(2012) 113–133. doi: 10.1016/B978-0-444-52898-8.00006-9.
- [23] **SÁNCHEZ, S.; RINCON, F.** - Status Epilepticus: Epidemiology and Public Health Needs. *Journal of Clinical Medicine*. 5:8 (2016) 71. doi: 10.3390/jcm5080071.
- [24] **THURMAN, D.; BEGHI, E.; BEGLEY, C.; *et al.*** - Standards for epidemiologic studies and surveillance of epilepsy. *Epilepsia*. 52:7 (2011) 2–26. doi: 10.1111/j.1528-

- 1167.2011.03121.x.
- [25] **WORLD HEALTH ORGANIZATION** - Epilepsy - A Public Health Imperative. (2019) 1–171.
- [26] **BEGHI, E.; HESDORFFER, D.** - Prevalence of epilepsy - An unknown quantity. *Epilepsia*. 55:7 (2014) 963–967. doi: 10.1111/epi.12579.
- [27] **THURMAN, D.; LOGROSCINO, G.; BEGHI, E. et al.** - The burden of premature mortality of epilepsy in high-income countries: A systematic review from the Mortality Task Force of the International League Against Epilepsy. *Epilepsia*. 58:1 (2017) 17–26. doi: 10.1111/epi.13604.
- [28] **GASTAUT, H.** - Clinical and Electroencephalographical Classification of Epileptic Seizures. *Epilepsia*. 11:1 (1970) 102–112. doi: 10.1111/j.1528-1157.1970.tb03871.x.
- [29] **COMMISSION ON CLASSIFICATION AND TERMINOLOGY OF THE ILAE** - Proposal for revised clinical and electroencephalographic classification of epileptic seizures. *Epilepsia*. 30:4 (1981) 489–501. doi: 10.1111/j.1528-1157.1981.tb06159.x.
- [30] **PANTELIADIS, C.; VASSILYADI, P.; FEHLERT, J. et al.** - Historical documents on epilepsy: From antiquity through the 20th century. *Brain and Development*. 39:6 (2017) 457–463. doi: 10.1016/j.braindev.2017.02.002.
- [31] **MILLETT, D.** - A history of seizures and epilepsies. From the falling disease to dysrhythmias of the brain. *Handb Clin Neurol*. 95:(2010) 387–400. doi: 10.1016/S0072-9752(08)02126-X.
- [32] **FISHER, R.** - The New Classification of Seizures by the International League Against Epilepsy 2017. *Current Neurology and Neuroscience Reports*. 17:6 (2017) 48. doi: 10.1007/s11910-017-0758-6.
- [33] **FISHER, R.** - An overview of the 2017 ILAE operational classification of seizure types. *Epilepsy and Behavior*. 70:(2017) 271–273. doi: 10.1016/j.yebeh.2017.03.022.
- [34] **SCHEFFER, I.; BERKOVIC, S.; CAPOVILLA, G. et al.** - ILAE classification of the epilepsies: Position paper of the ILAE Commission for Classification and Terminology. *Epilepsia*. 58:4 (2017) 512–521. doi: 10.1111/epi.13709.
- [35] **TRINKA, E.; COCK, H.; HESDORFFER, D. et al.** - A definition and classification of status epilepticus - Report of the ILAE Task Force on Classification of Status Epilepticus. *Epilepsia*. 56:10 (2015) 1515–1523. doi: 10.1111/epi.13121.
- [36] **PATEL, P.; MOSHÉ, S.** - The evolution of the concepts of seizures and epilepsy: What's in a name? *Epilepsia Open*. 5:1 (2020) 22–35. doi: 10.1002/epi4.12375.

- [37] **ZHU, L.; CHEN, L.; XU, P. *et al.*** - Genetic and molecular basis of epilepsy-related cognitive dysfunction. *Epilepsy and Behavior*. 104:(2020) 106848. doi: 10.1016/j.yebeh.2019.106848.
- [38] **ENDE, T. VAN DEN; SHARIFI, S.; SALM, S. VAN DER *et al.*** - Familial cortical myoclonic tremor and epilepsy, an enigmatic disorder: From phenotypes to pathophysiology and genetics. A systematic review. *Tremor and Other Hyperkinetic Movements*. 23:8 (2018) 503. doi: 10.7916/D85155WJ.
- [39] **GOLDIN, A.; ESCAYG, A.** - Sodium channel SCN1A and epilepsy: mutations and mechanisms. *Epilepsia*. 51:9 (2010) 1650–1658. doi: 10.1111/j.1528-1167.2010.02640.x.
- [40] **KANG, J.; MACDONALD, R.** - GABRG2 Mutations Associated with a spectrum of epilepsy syndromes from Generalized Absence Epilepsy to Dravet syndrome. *AMA Neurol*. 73:8 (2016) 1009–1016. doi: 10.1001/jamaneurol.2016.0449.GABRG2.
- [41] **SHARMA, S.; PRASAD, A.** - Inborn errors of metabolism and epilepsy: Current understanding, diagnosis, and treatment approaches. *International Journal of Molecular Sciences*. 18:7 (2017) 1384. doi: 10.3390/ijms18071384.
- [42] **GARCIA, H.; BRUTTO, O.** - Infection and inflammation. *Handbook of Clinical Neurology*. 108:(2012) 601–620. doi: 10.1016/B978-0-444-52899-5.00018-6.
- [43] **LERCHE, H.** - Drug-resistant epilepsy — time to target mechanisms. *Nature Reviews Neurology*. 16:11 (2020) 595–596. doi: 10.1038/s41582-020-00419-y.
- [44] **CLOSSEN, B.; REDDY, D.** - Novel therapeutic approaches for disease-modification of epileptogenesis for curing epilepsy. *Biochim Biophys Acta*. 1863:6 (2017) 1519–1538. doi: 10.1016/j.bbadis.2017.02.003.
- [45] **WELLS, B.; DIPIRO, J.; SCHWINGHAMMER, T. *et al.*** - *Pharmacotherapy Handbook*. 10th. ed. New York : [s.n.]
- [46] **WEAVER, D.** - Epileptogenesis, ictogenesis and the design of future antiepileptic drugs. *Canadian Journal of Neurological Sciences*. 30:1 (2003) 4–7. doi: 10.1017/S0317167100002353.
- [47] **ENGELBORGH, S.; D’HOOGHE, R.; DEYN, P.** - Pathophysiology of epilepsy. *Acta neurol. belg*. 100:4 (2000) 201–213.
- [48] **GUERRIERO, R.; GIZA, C.; ROTENBERG, A.** - Glutamate and GABA Imbalance Following Traumatic Brain Injury. *Current Neurology and Neuroscience Reports*. 15:5 (2015) 27. doi: 10.1007/s11910-015-0545-1.

- [49] **CHARSOUEI, S.; JABALAMELI, M.; KARIMI, A.** - Molecular insights into the role of AMPA receptors in the synaptic plasticity , pathogenesis and treatment of epilepsy : therapeutic potentials of perampanel and antisense oligonucleotide (ASO) technology. *Acta Neurologica Belgica*. 120:3 (2020) 531–544. doi: 10.1007/s13760-020-01318-1.
- [50] **ÇAVUŞ, I.; ROMANYSHYN, J.; KENNARD, J. et al.** - Elevated basal glutamate and unchanged glutamine and GABA in refractory epilepsy: Microdialysis study of 79 patients at the yale epilepsy surgery program. *Annals of Neurology*. 80:1 (2016) 35–45. doi: 10.1002/ana.24673.
- [51] **ARUNDINE, M.; TYMIANSKI, M.** - Molecular mechanisms of glutamate-dependent neurodegeneration in ischemia and traumatic brain injury. *Cellular and Molecular Life Sciences*. 61:6 (2004) 657–668. doi: 10.1007/s00018-003-3319-x.
- [52] **NICOLO, J.; O’BRIEN, T.; KWAN, P.** - Role of cerebral glutamate in post-stroke epileptogenesis. *NeuroImage: Clinical*. 24:(2019) 102069. doi: 10.1016/j.nicl.2019.102069.
- [53] **VEZZANI, A.; BALOSSO, S.; RAVIZZA, T.** - Neuroinflammatory pathways as treatment targets and biomarkers in epilepsy. *Nature Reviews Neurology*. 15:8 (2019) 459–472. doi: 10.1038/s41582-019-0217-x.
- [54] **DISABATO, D.; QUAN, N.; GODBOUT, J.** - Neuroinflammation: the devil is in the details. *Journal of Neurochemistry*. 139:(2016) 136–153. doi: 10.1111/jnc.13607.
- [55] **VLIET, E. VAN; ARONICA, E.; GORTER, J.** - Blood-brain barrier dysfunction, seizures and epilepsy. *Seminars in Cell and Developmental Biology*. 38:(2015) 26–34. doi: 10.1016/j.semcd.2014.10.003.
- [56] **VACCAREZZA, M.; SILVA, W.** - Dietary therapy is not the best option for refractory nonsurgical epilepsy. *Epilepsia*. 56:9 (2015) 1330–1334. doi: 10.1111/epi.13074.
- [57] **MCGOVERN, R.; BANKS, G.; MCKHANN, G.** - New Techniques and Progress in Epilepsy Surgery. *Current Neurology and Neuroscience Reports*. 16:7 (2016) 1–9. doi: 10.1007/s11910-016-0661-6.
- [58] **KOPPEL, S.; SWERDLOW, R.** - Neuroketotherapeutics: A modern review of a century-old therapy. *Neurochemistry International*. 117:(2018) 114–125. doi: 10.1016/j.neuint.2017.05.019.
- [59] **ŁUKAWSKI, K.; GRZYTA, P.; ŁUSZCZKI, J. et al.** - Exploring the latest avenues for antiepileptic drug discovery and development. *Expert Opinion on Drug Discovery*. 11:4 (2016) 369–382. doi: 10.1517/17460441.2016.1154840.

- [60] **FRENCH, J.** - Refractory Epilepsy: One Size Does Not Fit All. *Epilepsy Curr.* 6:6 (2006) 177–180.
- [61] **SILLS, G.; ROGAWSKI, M.** - Mechanisms of action of currently used antiseizure drugs. *Neuropharmacology.* 168:(2020) 107966. doi: 10.1016/j.neuropharm.2020.107966.
- [62] **SHORVON, S.** - Drug treatment of epilepsy in the century of the ILAE: The second 50 years, 1959-2009. *Epilepsia.* 50:3 (2009) 93–130. doi: 10.1111/j.1528-1167.2009.02042.x.
- [63] **GSCHWIND, M.; SEECK, M.** - Modern management of seizures and epilepsy. *Swiss medical weekly.* 146:(2016) w14310. doi: 10.4414/sm.w.2016.14310.
- [64] **MARGOLIS, J.; CHU, B.; WANG, Z. et al.** - Effectiveness of antiepileptic drug combination therapy for partial-onset seizures based on mechanisms of action. *JAMA Neurology.* 71:8 (2014) 985–993. doi: 10.1001/jamaneurol.2014.808.
- [65] **REDDY, A.; ZHANG, V.** - Polypharmacology: Drug discovery for the future. *Expert Review of Clinical Pharmacology.* 6:1 (2013) 41–47.
- [66] **NAKAMURA, M.; CHO, J.; SHIN, H. et al.** - Effects of cenobamate (YKP3089), a newly developed anti-epileptic drug, on voltage-gated sodium channels in rat hippocampal CA3 neurons. *European Journal of Pharmacology.* 855:(2019) 175–182. doi: 10.1016/j.ejphar.2019.05.007.
- [67] **RUFFOLO, G.; BONAVENTURA, C.; CIFELLI, P. et al.** - A novel action of lacosamide on GABAA currents sets the ground for a synergic interaction with levetiracetam in treatment of epilepsy. *Neurobiology of Disease.* 115:(2018) 59–68. doi: 10.1016/j.nbd.2018.03.015.
- [68] **WANG, X.; YU, Y.; MA, R. et al.** - Lacosamide modulates collapsin response mediator protein 2 and inhibits mossy fiber sprouting after kainic acid-induced status epilepticus. *NeuroReport.* 29:16 (2018) 1384–1390. doi: 10.1097/WNR.0000000000001123.
- [69] **BEN-MENACHEM, E.** - Medical management of refractory epilepsy-Practical treatment with novel antiepileptic drugs. *Epilepsia.* 55:1 (2014) 3–8. doi: 10.1111/epi.12494.
- [70] **GHANNAD-REZAIE, M.; EIMON, P.; WU, Y. et al.** - Engineering brain activity patterns by neuromodulator polytherapy for treatment of disorders. *Nature Communications.* 10:1 (2019). doi: 10.1038/s41467-019-10541-1.

- [71] **YASIRY, Z.; SHORVON, S.** - How phenobarbital revolutionized epilepsy therapy: The story of phenobarbital therapy in epilepsy in the last 100 years. *Epilepsia*. 53:(2012) 26–39. doi: 10.1111/epi.12026.
- [72] **PERUCCA, E.** - Antiepileptic drugs : evolution of our knowledge and changes in drug trials. 21:4 (2019) 319–329. doi: 10.1684/epd.2019.1083.
- [73] **PUTNAM, T.; MERRITT, H.** - Experimental determination of the anticonvulsant properties of some phenyl derivatives. *Science*. 85:(1937) 525–526.
- [74] **PERUCCA, E.** - Clinical pharmacology and therapeutic use of the new antiepileptic drugs. *Fundamental and Clinical Pharmacology*. 15:6 (2001) 405–417. doi: 10.1046/j.1472-8206.2001.00055.x.
- [75] **WAHAB, A.** - Difficulties in treatment and management of epilepsy and challenges in new drug development. *Pharmaceuticals*. 3:7 (2010) 2090–2110. doi: 10.3390/ph3072090.
- [76] **LAPENNA, P.; TORMOEHLEN, L.** - The Pharmacology and Toxicology of Third-Generation Anticonvulsant Drugs. *Journal of Medical Toxicology*. 13:4 (2017) 329–342. doi: 10.1007/s13181-017-0626-4.
- [77] **LÖSCHER, W.; SCHMIDT, D.** - Modern antiepileptic drug development has failed to deliver: Ways out of the current dilemma. *Epilepsia*. 52:4 (2011) 657–678. doi: 10.1111/j.1528-1167.2011.03024.x.
- [78] **BRODIE, M.** - Pharmacological Treatment of Drug-Resistant Epilepsy in Adults: a Practical Guide. *Current Neurology and Neuroscience Reports*. 16:9 (2016) 82. doi: 10.1007/s11910-016-0678-x.
- [79] **NATIONAL INSTITUTE FOR HEALTH AND CARE EXCELLENCE** - The epilepsies: the diagnosis and management of the epilepsies in adults and children in primary and secondary care. 137:(2012) 25340221.
- [80] **ROGAWSKI, M.; LÖSCHER, W.; RHO, J. et al.** - Mechanisms of action of Antiseizure Drugs and the Ketogenic diet. *Cold Spring Harbor Perspectives in Medicine*. 6:5 (2016) 28. doi: 10.1101/cshperspect.a022780.
- [81] **ROGAWSKI, M.; CAVAZOS, J.** - MECHANISMS OF ACTION OF ANTISEIZURE MEDICATION. *Neuropharmacology*. 168:(2020) 107966. doi: 10.1016/j.neuropharm.2020.107966.
- [82] **O'MALLEY, H.; ISOM, L.** - Sodium channel β subunits: emerging targets in channelopathies. *Physiology & behavior*. 77:(2015) 481–504. doi: 10.1146/annurev-

- physiol-021014-071846.Sodium.
- [83] **HEMMINGS, H.** - Sodium channels and the synaptic mechanisms of inhaled anaesthetics. *British Journal of Anaesthesia*. 103:1 (2009) 61–69. doi: 10.1093/bja/aep144.
- [84] **KAPLAN, D.; ISOM, L.; PETROU, S.** - Role of sodium channels in epilepsy. *Cold Spring Harbor Perspectives in Medicine*. 6:6 (2016) 1–17. doi: 10.1101/cshperspect.a022814.
- [85] **STAFSTROM, C.** - Persistent Sodium Current and Its Role in Epilepsy. *Epilepsy Currents*. 7:1 (2007) 15–22.
- [86] **MANTEGAZZA, M.; CURIA, G.; BIAGINI, G. et al.** - Voltage-gated sodium channels as therapeutic targets in epilepsy and other neurological disorders. *The Lancet Neurology*. 9:4 (2010) 413–424. doi: 10.1016/S1474-4422(10)70059-4.
- [87] **RAGSDALE, D.; AVOLI, M.** - Sodium channels as molecular targets for antiepileptic drugs. *Brain Research Reviews*. 26:1 (1998) 16–28. doi: 10.1016/S0165-0173(97)00054-4.
- [88] **LUCAS, P.; MEADOWS, L.; NICHOLLS, J. et al.** - An epilepsy mutation in the β 1 subunit of the voltage-gated sodium channel results in reduced channel sensitivity to phenytoin. *Epilepsy Research*. 64:3 (2005) 77–84. doi: 10.1016/j.eplepsyres.2005.03.003.
- [89] **NAIMO, G.; GUARNACCIA, M.; SPROVIERI, T. et al.** - A systems biology approach for personalized medicine in refractory epilepsy. *International Journal of Molecular Sciences*. 20:15 (2019) 1–15. doi: 10.3390/ijms20153717.
- [90] **HEBEISEN, Simon; PIRES, Nuno; LOUREIRO, Ana I. et al.** - Eslicarbazepine and the enhancement of slow inactivation of voltage-gated sodium channels: A comparison with carbamazepine, oxcarbazepine and lacosamide. *Neuropharmacology*. 89:(2015) 122–135. doi: 10.1016/j.neuropharm.2014.09.008.
- [91] **JO, S.; BEAN, B.** - Lacosamide inhibition of Nav1.7 voltage-gated sodium channels: Slow binding to fast-inactivated states. *Molecular Pharmacology*. 91:4 (2017) 331–338. doi: 10.1124/mol.116.106401.
- [92] **SHANK, R.; MARYANOFF, B.** - Molecular pharmacodynamics, clinical therapeutics, and pharmacokinetics of topiramate. *CNS Neuroscience and Therapeutics*. 14:2 (2008) 120–142. doi: 10.1111/j.1527-3458.2008.00041.x.
- [93] **CÉLINE M., Hugues A.** - Cardiac Sodium Current Under Sympathetic - Control Protein

- Phosphatase 2A Regulates Cardiac Na⁺ Channels. *Circ Res* . 124:15 (2019) 674–676. doi: 10.1161/CIRCRESAHA.119.314680.
- [94] **DOLPHIN, A.** - Calcium channel $\alpha_2\delta$ subunits in epilepsy and as targets for antiepileptic drugs. *Epilepsia*. 51:5 (2010) 82. doi: 10.1111/j.1528-1167.2010.02868.x.
- [95] **COLE, R.; LECHNER, S.; WILLIAMS, M. et al.** - Differential Distribution of VoltageGated Calcium Channel Alpha-2 Delta (α_2) Subunit mRNA-Containing Cells in the Rat Central Nervous System and the Dorsal Root Ganglia. *The Journal of Comparative Neurology*. 269:(2005) 246–269. doi: 10.1002/cne.20693.
- [96] **CELLI, R.; SANTOLINI, I.; GUIDUCCI, M. et al.** - The $\alpha_2\delta$ Subunit and Absence Epilepsy: Beyond Calcium Channels? *Current Neuropharmacology*. 15:6 (2017) 918–925. doi: 10.2174/1570159x15666170309105451.
- [97] **HOPPA, M.; LANA, B.; MARGAS, W. et al.** - A2 Δ Expression Sets Presynaptic Calcium Channel Abundance and Release Probability. *Nature*. 486:7401 (2012) 122–125. doi: 10.1038/nature11033.
- [98] **CHEN, J.; LI, L.; CHEN, S. et al.** - The $\alpha_2\delta$ -1-NMDA Receptor Complex Is Critically Involved in Neuropathic Pain Development and Gabapentin Therapeutic Actions. *Cell Reports*. 22:9 (2018) 2307–2321. doi: 10.1016/j.celrep.2018.02.021.
- [99] **HUGUENARD, J.** - Block of T-Type Ca²⁺ Channels Is an Important Action of Succinimide Antiabsence Drugs. *Epilepsy Currents*. 2:2 (2002) 49–52.
- [100] **LAMBERT, R.; BESSAÏH, T.; CRUNELLI, V. et al.** - The many faces of T-type calcium channels. *Pflugers Archiv European Journal of Physiology*. 466:3 (2014) 415–423. doi: 10.1007/s00424-013-1353-6.
- [101] **GAMBARDELLA, A.; LABATE, A.** - The role of calcium channel mutations in human epilepsy. *Progress in Brain Research*. 213:C (2014) 87–96. doi: 10.1016/B978-0-444-63326-2.00004-1.
- [102] **GÖREN, M.; ONAT, F.** - Ethosuximide: From bench to bedside. *CNS Drug Reviews*. 13:2 (2007) 224–239. doi: 10.1111/j.1527-3458.2007.00009.x.
- [103] **POWELL, K.; CAIN, S.; SNUTCH, T. et al.** - Low threshold T-type calcium channels as targets for novel epilepsy treatments. *British Journal of Clinical Pharmacology*. 77:5 (2014) 729–739. doi: 10.1111/bcp.12205.
- [104] **BROICHER, T.; SEIDENBECHER, T.; MEUTH, P. et al.** - T-current related effects of antiepileptic drugs and a Ca²⁺ channel antagonist on thalamic relay and local circuit

- interneurons in a rat model of absence epilepsy. *Neuropharmacology*. 53:3 (2007) 431–446. doi: 10.1016/j.neuropharm.2007.05.030.
- [105] **CORBIN-LEFTWICH, A.; MOSSADEQ, S.; HA, J. *et al.*** - Retigabine holds KV7 channels open and stabilizes the resting potential. *Journal of General Physiology*. 147:3 (2016) 229–241. doi: 10.1085/jgp.201511517.
- [106] **MILLIGAN, C.; LI, M.; GAZINA, E. *et al.*** - KCNT1 gain of function in 2 epilepsy phenotypes is reversed by quinidine. *Annals of Neurology*. 75:4 (2014) 581–590. doi: 10.1002/ana.24128.
- [107] **BOONSTRA, E.; KLEIJN, R.; COLZATO, L. *et al.*** - Neurotransmitters as food supplements: The effects of GABA on brain and behavior. *Frontiers in Psychology*. 6:(2015) 6–11. doi: 10.3389/fpsyg.2015.01520.
- [108] **SMART, T.; PAOLETTI, P.** - Synaptic Neurotransmitter-Gated Receptors. 4:3 (2012) a009662.
- [109] **SAHARA, S.; YANAGAWA, Y.; O'LEARY, D. *et al.*** - The fraction of cortical GABAergic neurons is constant from near the start of cortical neurogenesis to adulthood. *Journal of Neuroscience*. 32:14 (2012) 4755–4761. doi: 10.1523/JNEUROSCI.6412-11.2012.
- [110] **CHUANG, S.; REDDY, D.** - Genetic and molecular regulation of extrasynaptic GABA-A receptors in the brain: Therapeutic insights for epilepsy. *Journal of Pharmacology and Experimental Therapeutics*. 364:2 (2018) 180–197. doi: 10.1124/jpet.117.244673.
- [111] **FOGERSON, P.; HUGUENARD, J.** - Tapping the Brakes: Cellular and Synaptic Mechanisms that Regulate Thalamic Oscillations. *Neuron*. 92:4 (2016) 687–704. doi: 10.1016/j.neuron.2016.10.024.
- [112] **FRENCH-MULLEN, J.; BARKER, J.; ROGAWSKI, M.** - Calcium current block by (-)-pentobarbital, phenobarbital, and CHEB but not (+)-pentobarbital in acutely isolated hippocampal CA1 neurons: Comparison with effects on GABA-activated Cl⁻ current. *Journal of Neuroscience*. 13:8 (1993) 3211–3221. doi: 10.1523/jneurosci.13-08-03211.1993.
- [113] **WHITE, H.; BROWN, S.; WOODHEAD, J. *et al.*** - Topiramate enhances GABA-mediated chloride flux and GABA-evoked chloride currents in murine brain neurons and increases seizure threshold. *Epilepsy Research*. 28:3 (1997) 167–179. doi: 10.1016/S0920-1211(97)00045-4.
- [114] **KHAZIPOV, R.** - GABAergic Synchronization in Epilepsy. *Cold Spring Harb Perspect*

- Med. 6:2 (2016) 1–13.
- [115] **FRITSCH, B.; REIS, J.; GASIOR, M. *et al.*** - Role of GluK1 kainate receptors in seizures, epileptic discharges, and epileptogenesis. *Journal of Neuroscience*. 34:17 (2014) 5765–5775. doi: 10.1523/JNEUROSCI.5307-13.2014.
- [116] **ROGAWSKI, M.** - The intrinsic severity hypothesis of pharmacoresistance to antiepileptic drugs. *Epilepsia*. 54:2 (2013) 33–40. doi: 10.1111/epi.12182.
- [117] **GREENWOOD, J.; VALDES, J.** - Perampanel (Fycompa): A review of clinical efficacy and safety in epilepsy. *Pharm. Ther.* 41:11 (2016) 683–688.
- [118] **DUPUIS, N.; ENDERLIN, J.; THOMAS, J. *et al.*** - Anti-ictogenic and antiepileptogenic properties of perampanel in mature and immature rats. *Epilepsia*. 58:11 (2017) 1985–1992. doi: 10.1111/epi.13894.
- [119] **ZHANG, X.; VELUMIAN, A.; JONES, O. *et al.*** - Modulation of High-Voltage-Activated Calcium Channels in Dentate Granule Cells by Topiramate. *Epilepsia*. 41:1 (2000) 52–60. doi: 10.1111/j.1528-1157.2000.tb02173.x.
- [120] **HANSEN, C.; LJUNG, H.; BRODTKORB, E. *et al.*** - Mechanisms underlying aggressive behavior induced by antiepileptic drugs: Focus on topiramate, levetiracetam, and perampanel. *Behavioural Neurology*. (2018). doi: 10.1155/2018/2064027.
- [121] **GARCÍA-PÉREZ, E.; MAHFOOZ, K.; COVITA, J. *et al.*** - Levetiracetam accelerates the onset of supply rate depression in synaptic vesicle trafficking. *Epilepsia*. 56:4 (2015) 535–545. doi: 10.1111/epi.12930.
- [122] **KAMINSKI, R.; GILLARD, M.; LECLERCQ, K. *et al.*** - Proepileptic phenotype of SV2A-deficient mice is associated with reduced anticonvulsant efficacy of levetiracetam. *Epilepsia*. 50:7 (2009) 1729–1740. doi: 10.1111/j.1528-1167.2009.02089.x.
- [123] **LYSENG-WILLIAMSON, K. A.** - Levetiracetam: A review of its use in epilepsy. *Drugs*. 71:4 (2011) 489–514.
- [124] **ROWLEY, N.; MADSEN, K.; SCHOUSBOE, A. *et al.*** - Glutamate and GABA synthesis, release, transport and metabolism as targets for seizure control. *Neurochemistry International*. 61:4 (2012) 546–558. doi: 10.1016/j.neuint.2012.02.013.
- [125] **KLITGAARD, H.; MATAGNE, A.; NICOLAS, J. *et al.*** - Brivaracetam: Rationale for discovery and preclinical profile of a selective SV2A ligand for epilepsy treatment. *Epilepsia*. 57:4 (2016) 538–548. doi: 10.1111/epi.13340.
- [126] **MATAGNE, A.; MARGINEANU, D. G.; KENDA, B. *et al.*** - Anti-convulsive and anti-epileptic properties of brivaracetam (ucb 34714), a high-affinity ligand for the

- synaptic vesicle protein, SV2A. *British Journal of Pharmacology*. 154:8 (2008) 1662–1671. doi: 10.1038/bjp.2008.198.
- [127] **ROGAWSKI, M.** - Brivaracetam: A rational drug discovery success story. *British Journal of Pharmacology*. 154:8 (2008) 1555–1557. doi: 10.1038/bjp.2008.221.
- [128] **NGUYEN, L.; MAHADEO, T.; BORDEY, A.** - mTOR Hyperactivity Levels Influence the Severity of Epilepsy and Associated Neuropathology in an Experimental Model of Tuberous Sclerosis Complex and Focal Cortical Dysplasia. *Journal Neurosci*. 39:14 (2019) 2762–2773.
- [129] **GRIFFITH, J.; WONG, M.** - The mTOR pathway in treatment of epilepsy: A clinical update. *Future Neurology*. 13:2 (2018) 49–58. doi: 10.2217/fnl-2018-0001.
- [130] **JEONG, A.; WONG, M.** - Targeting the Mammalian Target of Rapamycin for Epileptic Encephalopathies and Malformations of Cortical Development. *Journal of Child Neurology*. 33:1 (2018) 55–63. doi: 10.1177/0883073817696814.
- [131] **HESS, E.; MOODY, K.; GEFREY, A. et al.** - Cannabidiol as a new treatment for drug-resistant epilepsy in tuberous sclerosis complex. *Epilepsia*. 57:10 (2016) 1617–1624. doi: 10.1111/epi.13499.
- [132] **CHEN, J.; BORGELT, L.; BLACKMER, A.** - Cannabidiol: A New Hope for Patients With Dravet or Lennox-Gastaut Syndromes. *Annals of Pharmacotherapy*. 53:6 (2019) 603–611. doi: 10.1177/1060028018822124.
- [133] **FRANCO, V.; PERUCCA, E.** - Pharmacological and Therapeutic Properties of Cannabidiol for Epilepsy. *Drugs*. 79:13 (2019) 1435–1454. doi: 10.1007/s40265-019-01171-4.
- [134] **JONES, N.; HILL, A.; SMITH, I. et al.** - Cannabidiol displays antiepileptiform and antiseizure properties in vitro and in vivo. *Journal of Pharmacology and Experimental Therapeutics*. 332:2 (2010) 569–577. doi: 10.1124/jpet.109.159145.
- [135] **IANNOTTI, F.; HILL, C.; LEO, A. et al.** - Nonpsychotropic plant cannabinoids, Cannabidivarin (CBDV) and Cannabidiol (CBD), activate and desensitize Transient Receptor Potential Vanilloid 1 (TRPV1) channels in vitro: Potential for the treatment of neuronal hyperexcitability. *ACS Chemical Neuroscience*. 5:11 (2014) 1131–1141. doi: 10.1021/cn5000524.
- [136] **BRUNI, N.; PEPA, C.; OLIARO-BOSSO, S. et al.** - Cannabinoid delivery systems for pain and inflammation treatment. *Molecules*. 23:10 (2018). doi: 10.3390/molecules23102478.

- [137] **NAZIROGLU, M.** - TRPV1 Channel: A Potential Drug Target for Treating Epilepsy. *Current Neuropharmacology*. 13:2 (2015) 239–247. doi: 10.2174/1570159x13666150216222543.
- [138] **GHOVANLOO, M.; SHUART, N.; MEZEYOVA, J. et al.** - Inhibitory effects of cannabidiol on voltage-dependent sodium currents. *Journal of Biological Chemistry*. 293:43 (2019) 16546–16558. doi: 10.1074/jbc.RA118.004929.
- [139] **SYLANTYEV, S.; JENSEN, T.; ROSS, R. et al.** - Cannabinoid- and lysophosphatidylinositol-sensitive receptor GPR55 boosts neurotransmitter release at central synapses. *Proceedings of the National Academy of Sciences of the United States of America*. 110:13 (2013) 5193–5198. doi: 10.1073/pnas.1211204110.
- [140] **MORANO, A.; FANELLA, M.; ALBINI, M. et al.** - Cannabinoids in the treatment of epilepsy: Current status and future prospects. *Neuropsychiatric Disease and Treatment*. 16:(2020) 381–396. doi: 10.2147/NDT.S203782.
- [141] **ENGLUND, M.; HYLLIENMARK, L.; BRISMAR, T.** - Effect of valproate, lamotrigine and levetiracetam on excitability and firing properties of CA1 neurons in rat brain slices. *Cellular and Molecular Neurobiology*. 31:4 (2011) 645–652. doi: 10.1007/s10571-011-9660-y.
- [142] **SORIA-CASTRO, R.; SCHCOLNIK-CABRERA, A.; RODRÍGUEZ-LÓPEZ, G. et al.** - Exploring the drug repurposing versatility of valproic acid as a multifunctional regulator of innate and adaptive immune cells. *Journal of Immunology Research*. (2019) 9678098. doi: 10.1155/2019/9678098.
- [143] **MISHAL, N.; ARKILO, D.; TANG, J. et al.** - A Potential Role for Felbamate in TSC- and NF1-Related Epilepsy: A Case Report and Review of the Literature. *Case Reports in Neurological Medicine*. 2015:(2015) 1–8. doi: 10.1155/2015/960746.
- [144] **KWAN, P.; ARZIMANOGLU, A.; BERG, A. et al.** - Definition of drug resistant epilepsy: Consensus proposal by the ad hoc Task Force of the ILAE Commission on Therapeutic Strategies. *Epilepsia*. 51:6 (2010) 1069–1077. doi: 10.1111/j.1528-1167.2009.02397.x.
- [145] **LENCK-SANTINI, P.** - Cognitive and behavioral comorbidities in epilepsy: The treacherous nature of animal models. *Epilepsy Currents*. 13:4 (2013) 182–183. doi: 10.5698/1535-7597-13.4.182.
- [146] **SCHILLER, Y.; NAJJAR, Y.** - Quantifying the response to antiepileptic drugs: Effect of past treatment history. *Neurology*. 70:1 (2008) 54–65. doi: 10.1212/01.wnl.0000286959.22040.6e.

- [147] **MOHANRAJ, R.; BRODIE, M.** - Early predictors of outcome in newly diagnosed epilepsy. *Seizure*. 22:5 (2013) 333–344. doi: 10.1016/j.seizure.2013.02.002.
- [148] **SANTULLI, L.; COPPOLA, A.; BALESTRINI, S. et al.** - The challenges of treating epilepsy with 25 antiepileptic drugs. *Pharmacological Research*. 107:(2016) 211–219. doi: 10.1016/j.phrs.2016.03.016.
- [149] **LAXER, K.; TRINKA, E.; HIRSCH, L. et al.** - The consequences of refractory epilepsy and its treatment. *Epilepsy and Behavior*. 37:(2014) 59–70. doi: 10.1016/j.yebeh.2014.05.031.
- [150] **TANG, F.; HARTZ, A.; BAUER, B.** - Drug-resistant epilepsy: Multiple hypotheses, few answers. *Frontiers in Neurology*. 8:JUL (2017) 1–19. doi: 10.3389/fneur.2017.00301.
- [151] **BELEZA, P.** - Refractory epilepsy: A clinically oriented review. *European Neurology*. 62:2 (2009) 65–71. doi: 10.1159/000222775.
- [152] **JANMOHAMED, M.; BRODIE, M.; KWAN, P.** - Pharmacoresistance – Epidemiology, mechanisms, and impact on epilepsy treatment. *Neuropharmacology*. 168:(2020). doi: 10.1016/j.neuropharm.2019.107790.
- [153] **CALATOZZOLO, C.; POLLO, B.; BOTTURI, A. et al.** - Multidrug resistance proteins expression in glioma patients with epilepsy. *Journal of Neuro-Oncology*. 110:1 (2012) 129–135. doi: 10.1007/s11060-012-0946-9.
- [154] **KWAN, P.; LI, H.; AL-JUFAIRI, E. et al.** - Association between temporal lobe P-glycoprotein expression and seizure recurrence after surgery for pharmacoresistant temporal lobe epilepsy. *Neurobiology of Disease*. 39:2 (2010) 192–197. doi: 10.1016/j.nbd.2010.04.006.
- [155] **LEANDRO, K.; BICKER, J.; ALVES, G. et al.** - ABC transporters in drug-resistant epilepsy: mechanisms of upregulation and therapeutic approaches. *Pharmacological Research*. 144:(2019) 357–376. doi: 10.1016/j.phrs.2019.04.031.
- [156] **TISHLER, D.; WEINBERG, K.; HINTON, D. et al.** - MDR1 Gene Expression in Brain of Patients with Medically Intractable Epilepsy. *Epilepsia*. 36:1 (1995) 1–6. doi: 10.1111/j.1528-1157.1995.tb01657.x.
- [157] **LÖSCHER, W.; POTSCHKA, H.; SISODIYA, S. et al.** - Drug resistance in epilepsy: Clinical impact, potential mechanisms, and new innovative treatment options. *Pharmacological Reviews*. 72:3 (2020) 606–638. doi: 10.1124/pr.120.019539.
- [158] **SISODIYA, S.; LIN, W.; HARDING, B. et al.** - Drug resistance in epilepsy: expression

- of drug resistance proteins in common causes of refractory epilepsy. *Brain : a journal of neurology*. 125:1 (2002) 22–31. doi: 10.1093/brain/awf002.
- [159] **FELDMANN, M.; ASSELIN, M.; LIU, J. *et al.*** - P-glycoprotein expression and function in patients with temporal lobe epilepsy: A case-control study. *The Lancet Neurology*. 12:8 (2013) 777–785. doi: 10.1016/S1474-4422(13)70109-1.
- [160] **Ji, J.; LI, G.; MA, Y. *et al.*** - Expression of multidrug resistance genes in peripheral blood of patients with refractory epilepsy and the reverse effect of oxcarbazepine on its expression. *Iranian Journal of Public Health*. 47:1 (2018) 40–48.
- [161] **TATE, S.; SISODIYA, S.** - Multidrug resistance in epilepsy: A pharmacogenomic update. *Expert Opinion on Pharmacotherapy*. 8:10 (2007) 1441–1449. doi: 10.1517/14656566.8.10.1441.
- [162] **CHANTEUX, H.; KERVYN, S.; GERIN, B. *et al.*** - In Vitro Pharmacokinetic Profile of Brivaracetam (BRV) Reveals Low Risk of Drug-Drug Interaction (DDI) and Unrestricted Brain Permeability. *Epilepsy Curr*. 15:(2015) 333.
- [163] **ROGAWSKI, M.; HANADA, T.** - Preclinical pharmacology of perampanel, a selective non-competitive AMPA receptor antagonist. *Acta Neurologica Scandinavica*. 127:197 (2013) 19–24. doi: 10.1111/ane.12100.
- [164] **FANG, M.; XI, Z.; WU, Y. *et al.*** - A new hypothesis of drug refractory epilepsy: Neural network hypothesis. *Medical Hypotheses*. 76:6 (2011) 871–876. doi: 10.1016/j.mehy.2011.02.039.
- [165] **MEFFORD, H.; MUHLE, H.; OSTERTAG, P. *et al.*** - Genome-wide copy number variation in epilepsy: novel susceptibility loci in idiopathic generalized and focal epilepsies. *PLoS genetics*. 6:5 (2010) 1–9. doi: 10.1371/journal.pgen.1000962.
- [166] **HELBIG, I.; MEFFORD, H.; SHARP, A. *et al.*** - Epilepsy. *Nat. Genet*. 41:2 (2011) 160–162. doi: 10.1038/ng.292.15q13.3.
- [167] **KOVEL, C. DE; TRUCKS, H.; HELBIG, I. *et al.*** - Recurrent microdeletions at 15q11.2 and 16p13.11 predispose to idiopathic generalized epilepsies. *Brain*. 133:1 (2010) 23–32. doi: 10.1093/brain/awp262.
- [168] **PONG, A.; GEARY, B.; ENGELSTAD, K. *et al.*** - Glucose transporter type i deficiency syndrome: Epilepsy phenotypes and outcomes. *Epilepsia*. 53:9 (2012) 1503–1510. doi: 10.1111/j.1528-1167.2012.03592.x.
- [169] **LAKHAN, R.; KUMARI, R.; SINGH, K. *et al.*** - Possible role of CYP2C9 & CYP2C19 single nucleotide polymorphisms in drug refractory epilepsy. *Indian Journal of Medical*

- Research. 134:9 (2011) 295–301.
- [170] **LÓPEZ-GARCÍA, M.; FERIA-ROMERO, I.; SERRANO, H. *et al.*** - Influence of genetic variants of CYP2D6, CYP2C9, CYP2C19 and CYP3A4 on antiepileptic drug metabolism in pediatric patients with refractory epilepsy. *Pharmacological Reports*. 69:3 (2017) 504–511. doi: 10.1016/j.pharep.2017.01.007.
- [171] **TALWAR, P.; KANOJIA, N.; MAHENDRU, S. *et al.*** - Genetic contribution of CYP1A1 variant on treatment outcome in epilepsy patients: A functional and interethnic perspective. *Pharmacogenomics Journal*. 17:3 (2017) 242–251. doi: 10.1038/tpj.2016.1.
- [172] **GOLDSTEIN, D.; NEED, A.; SINGH, R. *et al.*** - Potential Genetic Causes of Heterogeneity of Treatment Effects. *American Journal of Medicine*. 120:4 (2007) 21–25. doi: 10.1016/j.amjmed.2007.02.004.
- [173] **SEVEN, M.; BATAR, B.; UNAL, S. *et al.*** - The effect of genetic polymorphisms of cytochrome P450 CYP2C9, CYP2C19, and CYP2D6 on drug-resistant epilepsy in Turkish children. *Molecular Diagnosis and Therapy*. 18:2 (2014) 229–236. doi: 10.1007/s40291-013-0078-8.
- [174] **COLE, A.; WIEBE, S.** - Should antiepileptic drugs be stopped after successful epilepsy surgery? *Epilepsia*. 49:9 (2008) 29–34. doi: 10.1111/j.1528-1167.2008.01924.x.
- [175] **BAUMGARTNER, C.; KOREN, J.; BRITTO-ARIAS, M. *et al.*** - Presurgical epilepsy evaluation and epilepsy surgery. *F1000Research*. 8:(2019). doi: 10.12688/f1000research.17714.1.
- [176] **GOLYALA, A.; KWAN, P.** - Drug development for refractory epilepsy: The past 25 years and beyond. *Seizure*. 44:(2017) 147–156. doi: 10.1016/j.seizure.2016.11.022.
- [177] **FRANCO, V.; FRENCH, J.; PERUCCA, E.** - Challenges in the clinical development of new antiepileptic drugs. *Pharmacological Research*. 103:(2016) 95–104. doi: 10.1016/j.phrs.2015.11.007.
- [178] **ŁUSZCZKI, J.** - Third-generation antiepileptic drugs: Mechanisms of action, pharmacokinetics and interactions. *Pharmacological Reports*. 61:2 (2009) 197–216. doi: 10.1016/S1734-1140(09)70024-6.
- [179] **PERUCCA, E.; FRENCH, J.; BIALER, M.** - Development of new antiepileptic drugs: challenges, incentives, and recent advances. *Lancet Neurology*. 6:9 (2007) 793–804. doi: 10.1016/S1474-4422(07)70215-6.
- [180] **QADEER, M.; WAQAS, M.; RASHID, M. *et al.*** - Preventive gabapentin versus

- pregabalin to decrease postoperative pain after lumbar microdiscectomy: A randomized controlled trial. *Asian Spine Journal*. 11:1 (2017) 93–98. doi: 10.4184/asj.2017.11.1.93.
- [181] **COPPOLA, G.; LAPADRE, G.; OPERTO, F.** - New developments in the management of partial-onset epilepsy: role of brivaracetam *Review*. 6:11 (2017) 643–657. doi: 10.2147/DDDT.S103468.
- [182] **PITKÄNEN, A.; LUKASIUK, K.** - Mechanisms of epileptogenesis and potential treatment targets. *The Lancet Neurology*. 10:2 (2011) 173–186. doi: 10.1016/S1474-4422(10)70310-0.
- [183] **KLEIN, P.; HERR, D.; PEARL, P. et al.** - Results of phase 2 safety and feasibility study of treatment with levetiracetam for prevention of posttraumatic epilepsy. *Archives of Neurology*. 69:10 (2012) 1290–1295. doi: 10.1001/archneurol.2012.445.
- [184] **DOESER, A.; DICKHOF, G.; REITZE, M. et al.** - Targeting pharmaco-resistant epilepsy and epileptogenesis with Eslicarbazepine acetate. *Brain*. 138:2 (2014) 371–387. doi: 10.1093/awu.
- [185] **YOSHIMURA, T.; KAWANO, Y.; ARIMURA, N. et al.** - GSK-3 β regulates phosphorylation of CRMP-2 and neuronal polarity. *Cell*. 120:1 (2005) 137–149. doi: 10.1016/j.cell.2004.11.012.
- [186] **WILSON, S.; YEON, S.; YANG, X. et al.** - Differential regulation of collapsin response mediator protein 2 (CRMP2) phosphorylation by GSK3 β and CDK5 following traumatic brain injury. *Frontiers in Cellular Neuroscience*. 8:(2014) 1–14. doi: 10.3389/fncel.2014.00135.
- [187] **LEE, C.; JAW, T.; TSENG, H. et al.** - Lovastatin modulates glycogen synthase kinase-3 β pathway and inhibits mossy fiber sprouting after pilocarpine-induced status epilepticus. *PLoS ONE*. 7:6 (2012) 1–8. doi: 10.1371/journal.pone.0038789.
- [188] **KHANNA, R.; WILSON, S.; BRITAIN, J. et al.** - Opening Pandoras jar: A primer on the putative roles of CRMP2 in a panoply of neurodegenerative, sensory and motor neuron, and central disorders. *Future Neurology*. 7:6 (2012) 749–771. doi: 10.2217/fnl.12.68.
- [189] **LÖSCHER, W.** - Critical review of current animal models of seizures and epilepsy used in the discovery and development of new antiepileptic drugs. *Seizure*. 20:5 (2011) 359–368. doi: 10.1016/j.seizure.2011.01.003.
- [190] **SUDHA, K.; RAO, A.; RAO, A.** - Oxidative stress and antioxidants in epilepsy. *Clinica Chimica Acta*. 303:1–2 (2001) 19–24. doi: 10.1016/S0009-8981(00)00337-5.

- [191] **KAMIŃSKI, K.; RAPACZ, A.; ŁUSZCZKI, J. *et al.*** - Design, synthesis and biological evaluation of new hybrid anticonvulsants derived from N-benzyl-2-(2,5-dioxopyrrolidin-1-yl)propanamide and 2-(2,5-dioxopyrrolidin-1-yl)butanamide derivatives. *Bioorganic and Medicinal Chemistry*. 23:10 (2015) 2548–2561. doi: 10.1016/j.bmc.2015.03.038.
- [192] **ARONICA, E.; BAUER, S.; BOZZI, Y. *et al.*** - Neuroinflammatory targets and treatments for epilepsy validated in experimental models. *Epilepsia*. 58:(2017) 27–38. doi: 10.1111/epi.13783.
- [193] **GRECO, M.; VARRIALE, G.; COPPOLA, G. *et al.*** - Investigational small molecules in phase II clinical trials for the treatment of epilepsy. *Expert Opinion on Investigational Drugs*. 27:12 (2018) 971–979. doi: 10.1080/13543784.2018.1543398.
- [194] **ELGER, C.; HONG, S.; BRANDT, C. *et al.*** - BGG492 as an adjunctive treatment in patients with partial-onset seizures: A 12-week, randomized, double-blind, placebo-controlled, phase II dose-titration study with an open-label extension. *Epilepsia*. 58:7 (2017) 1217–1226. doi: 10.1111/epi.13771.
- [195] **KASTELEIJN-NOLST TRENITÉ, D.; BITON, V.; FRENCH, J. *et al.*** - Kv7 potassium channel activation with ICA-105665 reduces photoparoxysmal EEG responses in patients with epilepsy. *Epilepsia*. 54:8 (2013) 1437–1443. doi: 10.1111/epi.12224.
- [196] **STERIADE, C.; FRENCH, J.; DEVINSKY, O.** - Epilepsy: key experimental therapeutics in early clinical development. *Expert Opinion on Investigational Drugs*. 29:4 (2020) 373–383. doi: 10.1080/13543784.2020.1743678.
- [197] **BIALER, M.; JOHANNESSEN, S.; LEVY, R. *et al.*** - Progress report on new antiepileptic drugs: A summary of the Twelfth Eilat Conference (EILAT XII). *Epilepsy Research*. 111:(2015) 85–141. doi: 10.1016/j.eplepsyres.2015.01.001.
- [198] **FRENCH, J.; LAWSON, J.; YAPICI, Z. *et al.*** - Adjunctive everolimus therapy for treatment-resistant focal-onset seizures associated with tuberous sclerosis (EXIST-3): a phase 3, randomised, double-blind, placebo-controlled study. *The Lancet*. 388:10056 (2016) 2153–2163. doi: 10.1016/S0140-6736(16)31419-2.
- [199] **MULA, M.** - Investigational new drugs for focal epilepsy. *Expert Opinion on Investigational Drugs*. 25:1 (2016) 1–5. doi: 10.1517/13543784.2016.1110144.
- [200] **JIA, Y.; LIN, Y.; LI, J. *et al.*** - Quinidine therapy for Lennox-Gastaut syndrome with KCNT1 mutation. A case report and literature review. *Frontiers in Neurology*. 10:64 (2019) 1–7. doi: 10.3389/fneur.2019.00064.

- [201] **MODI, H.; KAIZONG, M.; CHANG, L. *et al.*** - Valnoctamide, which reduces rat brain arachidonic acid turnover, is a potential non-teratogenic valproate substitute to treat bipolar disorder. *Psychiatry Res.* 254:(2017) 279–283. doi: 10.1016/j.psychres.2017.04.048.
- [202] **PROSPERO, N. DI; GAMBALE, J.; PANDINA, G. *et al.*** - Evaluation of JNJ-26489112 in patients with photosensitive epilepsy: A placebo-controlled, exploratory study. *Epilepsy Research.* 108:4 (2014) 709–716. doi: 10.1016/j.eplepsyres.2014.01.018.
- [203] **PAULI, C.; CONROY, M.; HEUVEL, B. VANDEN *et al.*** - Cannabidiol Drugs Clinical Trial Outcomes and Adverse Effects. *Frontiers in Pharmacology.* 11:63 (2020) 1–6. doi: 10.3389/fphar.2020.00063.
- [204] **KADRY, H.; NOORANI, B.; CUCULLO, L.** - A blood–brain barrier overview on structure, function, impairment, and biomarkers of integrity. *Fluids and Barriers of the CNS.* 17:1 (2020) 1–24. doi: 10.1186/s12987-020-00230-3.
- [205] **YADAV, K.; KAPSE-MISTRY, S.; PETERS, G. *et al.*** - E-drug delivery: a futuristic approach. *Drug Discovery Today.* 24:4 (2019) 1023–1030. doi: 10.1016/j.drudis.2019.02.005.
- [206] **ANDERSON, G.; SANETO, R.** - Current oral and non-oral routes of antiepileptic drug delivery. *Advanced Drug Delivery Reviews.* 64:10 (2012) 911–918. doi: 10.1016/j.addr.2012.01.017.
- [207] **WHELESS, J.; PHELPS, S.** - A clinician’s guide to oral extended-release drug delivery systems in epilepsy. *Journal of Pediatric Pharmacology and Therapeutics.* 23:4 (2018) 277–292. doi: 10.5863/1551-6776-23.4.277.
- [208] **DULAC, O.; ALVAREZ, J.** - Bioequivalence of a new sustained-release formulation of sodium valproate, valproate modified-release granules, compared with existing sustained-release formulations after once- or twice-daily administration. *Pharmacotherapy.* 25:1 (2005) 35–41. doi: 10.1592/phco.25.1.35.55626.
- [209] **HOMAYUN, B.; LIN, X.; CHOI, H.** - Challenges and recent progress in oral drug delivery systems for biopharmaceuticals. *Pharmaceutics.* 11:3 (2019). doi: 10.3390/pharmaceutics11030129.
- [210] **AZIZI, A.; KUMAR, A.; DIAZ-MITOMA, F. *et al.*** - Enhancing oral vaccine potency by targeting intestinal M cells. *PLoS Pathogens.* 6:11 (2010). doi: 10.1371/journal.ppat.1001147.
- [211] **BIASE, S. DE; VALENTE, M.; GIGLI, G. *et al.*** - Pharmacokinetic drug evaluation of lacosamide for the treatment of partial-onset seizures. *Expert Opinion on Drug*

- Metabolism and Toxicology. 13:9 (2017) 997–1005. doi: 10.1080/17425255.2017.1360278.
- [212] **KWAN, S.; CHUANG, Y.; HUANG, C. *et al.*** - Zonisamide: Review of Recent Clinical Evidence for Treatment of Epilepsy. *CNS Neuroscience and Therapeutics*. 21:9 (2015) 683–691. doi: 10.1111/cns.12418.
- [213] **SARMA, A.; KHANDKER, N.; KURCZEWSKI, L. *et al.*** - Medical management of epileptic seizures: Challenges and solutions. *Neuropsychiatric Disease and Treatment*. 12:(2016) 467–485. doi: 10.2147/NDT.S80586.
- [214] **MAGLALANG, P.; RAUTIOLA, D.; SIEGEL, R. *et al.*** - Rescue therapies for seizure emergencies: New modes of administration. *Epilepsia*. 59:(2018) 207–215. doi: 10.1111/epi.14479.
- [215] **XIONG, J.; MAO, D.; LIU, L.** - Research Progress on the Role of ABC Transporters in the Drug Resistance Mechanism of Intractable Epilepsy. *BioMed Research International*. 2015:(2015) 1–10. doi: 10.1155/2015/194541.
- [216] **AGARWAL, S.; CLOYD, J.** - Development of benzodiazepines for out-of-hospital management of seizure emergencies. *Neurology: Clinical Practice*. 5:1 (2015) 80–85. doi: 10.1212/CPJ.0000000000000099.
- [217] **GERNERT, M.; FEJA, M.** - Bypassing the blood–brain barrier: Direct intracranial drug delivery in epilepsies. *Pharmaceutics*. 12:12 (2020) 1–39. doi: 10.3390/pharmaceutics12121134.
- [218] **KUMAR, H.; MISHRA, G.; SHARMA, A. *et al.*** - Intranasal Drug Delivery: A Non-Invasive Approach for the Better Delivery of Neurotherapeutics. *Pharm Nanotechnol*. 5:3 (2017) 203–214.
- [219] **MORANO, A.; IANNONE, L.; PALLERIA, C. *et al.*** - Pharmacology of new and developing intravenous therapies for the management of seizures and epilepsy. *Expert Opinion on Pharmacotherapy*. 20:1 (2019) 25–39. doi: 10.1080/14656566.2018.1541349.
- [220] **RIEBESEHL, B.** - Drug Delivery with Organic Solvents or Colloidal Dispersed Systems. *The Practice of Medicinal Chemistry: fourth edition*. 4 (2015) 699–722. doi: 10.1016/B978-0-12-417205-0.00029-8.
- [221] **HUA, S.** - Advances in nanoparticulate drug delivery approaches for sublingual and buccal administration. *Frontiers in Pharmacology*. 10:(2019) 1–9. doi: 10.3389/fphar.2019.01328.

- [222] **NAKKEN, K.; LOSSIUS, M.** - Buccal midazolam or rectal diazepam for treatment of residential adult patients with serial seizures or status epilepticus. *Acta Neurologica Scandinavica*. 124:2 (2011) 99–103. doi: 10.1111/j.1600-0404.2010.01474.x.
- [223] **GARNETT, W.; BARR, W.; EDINBORO, L. et al.** - Diazepam autoinjector intramuscular delivery system versus diazepam rectal gel: A pharmacokinetic comparison. *Epilepsy Research*. 93:1 (2011) 11–16. doi: 10.1016/j.eplepsyres.2010.10.001.
- [224] **LAMSON, M.; SITKI-GREEN, D.; WANNARKA, G. et al.** - Pharmacokinetics of Diazepam Administered Intramuscularly by Autoinjector versus Rectal Gel in Healthy Subjects. *Clinical Drug Investigation*. 31:8 (2011) 585–597. doi: 10.2165/11590250-000000000-00000.
- [225] **VERROTTI, A.; AMBROSI, M.; PAVONE, P. et al.** - Pediatric status epilepticus: improved management with new drug therapies? *Expert Opinion on Pharmacotherapy*. 18:8 (2017) 789–798. doi: 10.1080/14656566.2017.1323873.
- [226] **LOIACONO, G.; MASCI, M.; ZACCARA, G. et al.** - The treatment of neonatal seizures: Focus on Levetiracetam. *Journal of Maternal-Fetal and Neonatal Medicine*. 29:1 (2016) 69–74. doi: 10.3109/14767058.2014.986651.
- [227] **LEPPIK, I.; PATEL, S.** - Intramuscular and rectal therapies of acute seizures. *Epilepsy and Behavior*. 49:(2015) 307–312. doi: 10.1016/j.yebeh.2015.05.001.
- [228] **PAULUHN, J.** - Inhalation toxicology: Methodological and regulatory challenges. *Experimental and Toxicologic Pathology*. 60:2–3 (2008) 111–124. doi: 10.1016/j.etp.2008.01.013.
- [229] **PORTER, Roger J.; DHIR, Ashish; MACDONALD, Robert L. et al.** - Mechanisms of action of antiseizure drugs. 1th. ed. [S.l.] : Elsevier B.V., 2012 in <http://dx.doi.org/10.1016/B978-0-444-52899-5.00021-6>
- [230] **SELVARAJ, K.; GOWTHAMARAJAN, K.; KARRI, V.** - Nose to brain transport pathways an overview: potential of nanostructured lipid carriers in nose to brain targeting. *Artificial Cells, Nanomedicine and Biotechnology*. 46:8 (2018) 2088–2095. doi: 10.1080/21691401.2017.1420073.
- [231] **SAMARIDOU, E.; ALONSO, M.** - Nose-to-brain peptide delivery – The potential of nanotechnology. *Bioorganic and Medicinal Chemistry*. 26:10 (2018) 2888–2905. doi: 10.1016/j.bmc.2017.11.001.
- [232] **GIUNCHEDI, P.; GAVINI, E.** - Nose-to-Brain Delivery. *Pharmaceutics*. 12:2 (2020) 138.

- [233] **FREY, W.** - Neurologic Agents for Nasal Administration to the Brain, atual. 1991.
- [234] **AGRAWAL, M.; SARAF, S.; SARAF, S. et al.** - Nose-to-brain drug delivery: An update on clinical challenges and progress towards approval of anti-Alzheimer drugs. *Journal of Controlled Release*. 281:May (2018) 139–177. doi: 10.1016/j.jconrel.2018.05.011.
- [235] **BORS, L.; BAJZA, Á.; MÁNDOKI, M. et al.** - Modulation of nose-to-brain delivery of a P-glycoprotein (MDR1) substrate model drug (quinidine) in rats. *Brain Research Bulletin*. 160:(2020) 65–73. doi: 10.1016/j.brainresbull.2020.04.012.
- [236] **SHARMA, D.; AGARWAL, S.** - Nasal anatomy and absorption through nasal route. *International Journal of Current Research*. 10:5 (2018) 69121–69132.
- [237] **GÄNGER, S.; SCHINDOWSKI, K.** - Tailoring formulations for intranasal nose-to-brain delivery: A review on architecture, physico-chemical characteristics and mucociliary clearance of the nasal olfactory mucosa. *Pharmaceutics*. 10:3 (2018) 116. doi: 10.3390/pharmaceutics10030116.
- [238] **BITTER, C.; SUTER-ZIMMERMANN, K.** - Topical Treatment of Impaired Mucosal Membranes Nasal Drug Delivery in Humans. *Curr Probl Dermatol*. 40:(2011) 20–35.
- [239] **MARTIN, E.; SCHIPPER, N.; COOS VERHOEF, J.; et al.** - Nasal mucociliary clearance as a factor in nasal drug delivery. *Advanced Drug Delivery Reviews*. 29:1–2 (1998) 13–38. doi: 10.1016/S0169-409X(97)00059-8.
- [240] **GHORI, M. U.; MAHDI, M. H.; SMITH, A. M.** - Nasal drug delivery: An overview. *American Journal of Pharmacological Sciences*. 3:5 (2015) 110–119.
- [241] **FORTUNA, A.; ALVES, G.; SERRALHEIRO, A. et al.** - Intranasal delivery of systemic-acting drugs: Small-molecules and biomacromolecules. *European Journal of Pharmaceutics and Biopharmaceutics*. 8:1 (2014) 8–27. doi: 10.1016/j.ejpb.2014.03.004.
- [242] **DHURIA, S.; HANSON, L.; FREY, W.** - Molecular Nanomedicine Towards Cancer : *Journal of pharmaceutical sciences*. 101:7 (2012) 2271–2280. doi: 10.1002/jps.
- [243] **MISTRY, A.; STOLNIK, S.; ILLUM, L.** - Nanoparticles for direct nose-to-brain delivery of drugs. *International Journal of Pharmaceutics*. 379:1–2 (2009) 146–157. doi: 10.1016/j.ijpharm.2009.06.019.
- [244] **JOHNSON, N.; HANSON, L.; FREY, W.** - Trigeminal pathways deliver a low molecular weight drug from the nose to the brain and orofacial structures. *Molecular Pharmaceutics*. 7:3 (2010) 884–893. doi: 10.1021/mp100029t.

- [245] **HANSON, L.; FINE, J.; SVITAK, A. *et al.*** - Intranasal administration of CNS therapeutics to awake mice. *Journal of visualized experiments*. 74 (2013) 1–7. doi: 10.3791/4440.
- [246] **PIRES, A.; FORTUNA, A.; ALVES, G. *et al.*** - Intranasal drug delivery: How, why and what for? *Journal of Pharmacy and Pharmaceutical Sciences*. 12:3 (2009) 288–311. doi: 10.18433/J3NC79.
- [247] **VYAS, T.; SHAHIWALA, A.; MARATHE, S. *et al.*** - Intranasal Drug Delivery for Brain Targeting. *Current Drug Delivery*. 2:2 (2005) 165–175. doi: 10.2174/1567201053586047.
- [248] **MORAN, D.; R., Carter; JAFEK, B.** - Electron microscopy of human olfactory epithelium reveals a new cell type: The microvillar cell. *Brain Research*. 253:1–2 (1982) 39–46. doi: 10.1016/0006-8993(82)90671-0.
- [249] **OLIVEIRA, P.; FORTUNA, A.; ALVES, G. *et al.*** - Drug-metabolizing Enzymes and Efflux Transporters in Nasal Epithelium: Influence on the Bioavailability of Intranasally Administered Drugs. *Curr Drug Metab*. 17:7 (2016) 628–647.
- [250] **LI, Y.; FIELD, P.; RAISMAN, G.** - Olfactory ensheathing cells and olfactory nerve fibroblasts maintain continuous open channels for regrowth of olfactory nerve fibres. *Glia*. 52:3 (2005) 245–251. doi: 10.1002/glia.20241.
- [251] **DJUPESLAND, P.; MESSINA, J.; MAHMOUD, R.** - The nasal approach to delivering treatment for brain diseases: An anatomic, physiologic, and delivery technology overview. *Therapeutic Delivery*. 5:6 (2014) 709–733. doi: 10.4155/tde.14.41.
- [252] **SCHWAB, R.; KUNA, S.; REMMERS, J.** - Anatomy and Physiology of Upper Airway Obstruction. *Principles and Practice of Sleep Medicine*. 20:(2005) 983–1000. doi: 10.1016/B0-72-160797-7/50089-6.
- [253] **BEULE, A.** - Funktionen und Funktionsstörungen der respiratorischen Schleimhaut der Nase und der Nasennebenhöhlen. *Laryngo-Rhino-Otologie*. 89:1 (2010) 1–24. doi: 10.1055/s-0029-1246124.
- [254] **BUSTAMANTE-MARIN, X.; OSTROWSKI, L.** - Cilia and mucociliary clearance. *Cold Spring Harbor Perspectives in Biology*. 9:4 (2017) 1–18. doi: 10.1101/cshperspect.a028241.
- [255] **ALI, A.; WAHLGREN, M.; REMBRATT-SVENSSON, B. *et al.*** - Dehydration affects drug transport over nasal mucosa. *Drug Delivery*. 26:1 (2019) 831–840. doi: 10.1080/10717544.2019.1650848.

- [256] **OSTROWSKI, L. E.; BENNETT, W. D.** - Cilia and Mucociliary Clearance. Encyclopedia of Respiratory Medicine, Four-Volume Set. (2006) 466–470. doi: 10.1016/B0-12-370879-6/00079-X.
- [257] **MERCIER, C.; JACQUEROUX, E.; HE, Z. et al.** - Pharmacological characterization of the 3D MucilAir™ nasal model. European Journal of Pharmaceutics and Biopharmaceutics. 139:March (2019) 186–196. doi: 10.1016/j.ejpb.2019.04.002.
- [258] **VITORINO, C.; SILVA, S.; BICKER, J. et al.** - Antidepressants and nose-to-brain delivery: drivers, restraints, opportunities and challenges. Drug Discovery Today. 24:9 (2019) 1911–1923. doi: 10.1016/j.drudis.2019.06.001.
- [259] **ALAGUSUNDARAM, M.; CHENGAI AH, B.; GNANAPRAKASH, K.; et al.** - Nasal drug delivery: An overview. Int J Res Pharm Sci. 1:4 (2010) 454–465.
- [260] **CHUN, J.; HAN, J.; SEO, D.** - Molybdenum-doped zinc oxide electrodes for organic light-emitting devices. Electrochemical and Solid-State Letters. 12:4 (2009) 1–21. doi: 10.1149/1.3078491.
- [261] **WIJESURIYA, H.; BULLOCK, J.; FAULL, R. et al.** - ABC efflux transporters in brain vasculature of Alzheimer's subjects. Brain Research. 1358:(2010) 228–238. doi: 10.1016/j.brainres.2010.08.034.
- [262] **DOLBERG, A.; REICHL, S.** - Expression of P-glycoprotein in excised human nasal mucosa and optimized models of RPMI 2650 cells. International Journal of Pharmaceutics. 508:1–2 (2016) 22–33. doi: 10.1016/j.ijpharm.2016.05.010.
- [263] **KANDIMALLA, Karunya K.; DONOVAN, Maureen D.** - Localization and differential activity of P-glycoprotein in the bovine olfactory and nasal respiratory mucosae. Pharmaceutical Research. 22:7 (2005) 1121–1128. doi: 10.1007/s11095-005-5420-3.
- [264] **GAMEIRO, M.; SILVA, R.; ROCHA-PEREIRA, C. et al.** - Cellular models and in vitro assays for the screening of modulators of P-gp, MRP1 and BCRP. Molecules. 22:4 (2017) 4–6. doi: 10.3390/molecules22040600.
- [265] **WIOLAND, M.; FLEURY-FEITH, J.; CORLIEU, P. et al.** - CFTR, MDR1, and MRP1 immunolocalization in normal human nasal respiratory mucosa. Journal of Histochemistry and Cytochemistry. 48:9 (2000) 1215–1222. doi: 10.1177/002215540004800905.
- [266] **BREMER, S.; HOOF, T.; WILKE, M. et al.** - Quantitative expression patterns of multidrug-resistance P-glycoprotein (MDR1) and differentially spliced cystic-fibrosis transmembrane-conductance regulator mRNA transcripts in human epithelia.

- European Journal of Biochemistry. 206:1 (1992) 137–149. doi: 10.1111/j.1432-1033.1992.tb16911.x.
- [267] **CHO, H.; CHOI, M.; LIN, H. *et al.*** - Expression and functional activity of P-glycoprotein in passaged primary human nasal epithelial cell monolayers cultured by the air-liquid interface method for nasal drug transport study. *Journal of Pharmacy and Pharmacology*. 63:3 (2011) 385–391. doi: 10.1111/j.2042-7158.2010.01221.x.
- [268] **SHILLING, R.; VENTER, H.; VELAMAKANNI, S. *et al.*** - New light on multidrug binding by an ATP-binding-cassette transporter. *Trends in Pharmacological Sciences*. 27:4 (2006) 195–203. doi: 10.1016/j.tips.2006.02.008.
- [269] **BLEIER, B.** - Regional expression of epithelial MDR1/P-glycoprotein in chronic rhinosinusitis with and without nasal polyposis. *International Forum of Allergy and Rhinology*. 2:2 (2012) 122–125. doi: 10.1002/alr.21004.
- [270] **GRAFF, C.; ZHAO, R.; POLLACK, G.** - Pharmacokinetics of substrate uptake and distribution in murine brain after nasal instillation. *Pharmaceutical Research*. 22:2 (2005) 235–244. doi: 10.1007/s11095-004-1191-5.
- [271] **AL-GHABEISH, M.; SCHEETZ, T.; ASSEM, M. *et al.*** - Microarray Determination of the Expression of Drug Transporters in Humans and Animal Species Used for the Investigation of Nasal Absorption. *Molecular Pharmaceutics*. 12:8 (2015) 2742–2754. doi: 10.1021/acs.molpharmaceut.5b00103.
- [272] **GELERNTER, J.; VANDENBERGH, D.; KRUGER, S. *et al.*** - The dopamine transporter protein gene (SLC6A3): Primary linkage mapping and linkage studies in tourette syndrome. *Genomics*. 30:3 (1995) 459–463. doi: 10.1006/geno.1995.1265.
- [273] **HARVEY, R.** - Pharmacokinetics. In: *Lippincott's Illustrated Reviews: Pharmacology*. Harvey R, Champe P. (Eds). Lippincott, Williams & Wilkins, PA, USA. (2008) 6–7.
- [274] **KUDO, H.; DOI, Y.; FUJIMOTO, S.** - Expressions of the multidrug resistance-related proteins in the rat olfactory epithelium: A possible role in the phase III xenobiotic metabolizing function. *Neuroscience Letters*. 468:2 (2010) 98–101. doi: 10.1016/j.neulet.2009.10.073.
- [275] **ALEXANDER, A.; AGRAWAL, M.; BHUPAL CHOUGULE, M. *et al.*** - Nose-to-brain drug delivery: An alternative approach for effective brain drug targeting. an alternative approach for effective brain drug targeting. *Nanopharmaceuticals*. 1:(2020) 175–200. doi: 10.1016/B978-0-12-817778-5.00009-9.
- [276] **GONÇALVES, J.; ALVES, G.; CARONA, A. *et al.*** - Pre-Clinical Assessment of the Nose-

- to-Brain Delivery of Zonisamide After Intranasal Administration. *Pharmaceutical Research*. 37:4 (2020). doi: 10.1007/s11095-020-02786-z.
- [277] **COOK, I.; ABRAMS, M.; LEUCHTER, A.** - Trigeminal Nerve Stimulation for Comorbid Posttraumatic Stress Disorder and Major Depressive Disorder. *Neuromodulation*. 19:3 (2016) 299–305. doi: 10.1111/ner.12399.
- [278] **ROSS, T.; MARTINEZ, P.; RENNER, J. et al.** - Intranasal administration of interferon beta bypasses the blood-brain barrier to target the central nervous system and cervical lymph nodes: A non-invasive treatment strategy for multiple sclerosis. *Journal of Neuroimmunology*. 151:1–2 (2004) 66–77. doi: 10.1016/j.jneuroim.2004.02.011.
- [279] **GARTZIANDIA, O.; HERRAN, E.; PEDRAZ, J. et al.** - Chitosan coated nanostructured lipid carriers for brain delivery of proteins by intranasal administration. *Colloids and Surfaces B: Biointerfaces*. 134:(2015) 304–313. doi: 10.1016/j.colsurfb.2015.06.054.
- [280] **LOCHHEAD, J.; THORNE, R.** - Intranasal delivery of biologics to the central nervous system. *Advanced Drug Delivery Reviews*. 64:7 (2012) 614–628. doi: 10.1016/j.addr.2011.11.002.
- [281] **SEKERDAG, E.** - Nasal Physiology and Drug Transport. *Nanotechnology Methods for Neurological Diseases and Brain Tumors*. (2017) 93–102. doi: 10.1016/B978-0-12-803796-6.00005-8.
- [282] **CHEN, X.; FAWCETT, J.; RAHMAN, Y. et al.** - Delivery of nerve growth factor to the brain via the olfactory pathway. *Journal of Alzheimer's Disease*. 1:1 (1998) 35–44. doi: 10.3233/JAD-1998-1102.
- [283] **FREY, W.; LIU, J.; CHEN, X. et al.** - Delivery of Route I-NGF to the Brain via the Olfactory Delivery of 125I-NGF to the Brain via the Olfactory Route. *Drug Delivery*. 4:2 (2008) 87–92.
- [284] **KANAYAMA, Y.; ENOMOTO, S.; IRIE, T. et al.** - Axonal transport of rubidium and thallium in the olfactory nerve of mice. *Nuclear Medicine and Biology*. 32:5 (2005) 505–512. doi: 10.1016/j.nucmedbio.2005.03.009.
- [285] **STRIEPENS, N.; KENDRICK, K.; HANKING, V. et al.** - Elevated cerebrospinal fluid and blood concentrations of oxytocin following its intranasal administration in humans. *Scientific Reports*. 3:(2013) 1–5. doi: 10.1038/srep03440.
- [286] **PARDESHI, C.; BELGAMWAR, V.** - Direct nose to brain drug delivery via integrated nerve pathways bypassing the blood-brain barrier: An excellent platform for brain targeting. *Expert Opinion on Drug Delivery*. 10:7 (2013) 957–972. doi:

- 10.1517/17425247.2013.790887.
- [287] **DI, L.; ARTURSSON, P.; AVDEEF, A. *et al.*** - Evidence-based approach to assess passive diffusion and carrier-mediated drug transport. *Drug Discovery Today*. 17:15–16 (2012) 905–912. doi: 10.1016/j.drudis.2012.03.015.
- [288] **MATSSON, P.; DOAK, B.; OVER, B. *et al.*** - Cell permeability beyond the rule of 5. *Advanced Drug Delivery Reviews*. 101:(2016) 42–61. doi: 10.1016/j.addr.2016.03.013.
- [289] **ROBEY, R.; POLGAR, O.; DEEKEN, J. *et al.*** - ABCG2: Determining its relevance in clinical drug resistance. *Cancer and Metastasis Reviews*. 26:1 (2007) 39–57. doi: 10.1007/s10555-007-9042-6.
- [290] **PICK, A.; KLINKHAMMER, W.; WIESE, M.** - Specific inhibitors of the breast cancer resistance protein (BCRP). *ChemMedChem*. 5:9 (2010) 1498–1505. doi: 10.1002/cmdc.201000216.
- [291] **FERREIRA, R.; BONITO, C.; CORDEIRO, M. *et al.*** - Structure-function relationships in ABCG2: Insights from molecular dynamics simulations and molecular docking studies. *Scientific Reports*. 7:1 (2017) 1–17. doi: 10.1038/s41598-017-15452-z.
- [292] **XU, J.; LIU, Y.; YANG, Y. *et al.*** - Characterization of Oligomeric Human Half-ABC Transporter ATP-binding Cassette G2. *Journal of Biological Chemistry*. 279:19 (2004) 19781–19789. doi: 10.1074/jbc.M310785200.
- [293] **HAZAI, E.; BIKÁDI, Z.** - Homology modeling of breast cancer resistance protein (ABCG2). *Journal of Structural Biology*. 162:1 (2008) 63–74. doi: 10.1016/j.jsb.2007.12.001.
- [294] **KHUNWEERAPHONG, N.; STOCKNER, T.; KUCHLER, K.** - The structure of the human ABC transporter ABCG2 reveals a novel mechanism for drug extrusion. *Scientific Reports*. 7:1 (2017) 1–15. doi: 10.1038/s41598-017-11794-w.
- [295] **MAO, Q.; UNADKAT, J.** - Role of the Breast Cancer Resistance Protein (BCRP/ABCG2) in Drug Transport—an Update. *AAPS Journal*. 17:1 (2015) 65–82. doi: 10.1208/s12248-014-9668-6.
- [296] **MALIEPAARD, M.; SCHEFFER, G.; FANEYTE, I. *et al.*** - Subcellular localization and distribution of the Breast Resistance Protein Transporter in normal human tissues. *Cancer Research*. 61:8 (2001) 3458–3464.
- [297] **JONKER, J.** - Role of Breast Cancer Resistance Protein in the Bioavailability and Fetal Penetration of Topotecan. *Journal of the National Cancer Institute*. 92:20 (2000)

- 1651–1656. doi: 10.1093/jnci/92.20.1651.
- [298] **PULIDO, M.; MOLINA, A.; MERINO, G. *et al.*** - Interaction of enrofloxacin with breast cancer resistance protein (BCRP/ABCG2): Influence of flavonoids and role in milk secretion in sheep. *Journal of Veterinary Pharmacology and Therapeutics*. 29:4 (2006) 279–287. doi: 10.1111/j.1365-2885.2006.00744.x.
- [299] **HERWAARDEN, A. VAN; WAGENAAR, E.; MERINO, G. *et al.*** - Multidrug Transporter ABCG2/Breast Cancer Resistance Protein Secretes Riboflavin (Vitamin B2) into Milk. *Molecular and Cellular Biology*. 27:4 (2007) 1247–1253. doi: 10.1128/mcb.01621-06.
- [300] **BRACKMAN, D.; GIACOMINI, K.** - Reverse Translational Research of ABCG2 (BCRP) in Human Disease and Drug Response. *Clin.Pharmacol. Ther.* 103:(2018) 233–242.
- [301] **HULS, M.; BROWN, C.; WINDASS, A. *et al.*** - The breast cancer resistance protein transporter ABCG2 is expressed in the human kidney proximal tubule apical membrane. *Kidney International*. 73:2 (2008) 220–225. doi: 10.1038/sj.ki.5002645.
- [302] **FETSCH, P.; ABATI, A.; LITMAN, T. *et al.*** - Localization of the ABCG2 mitoxantrone resistance-associated protein in normal tissues. *Cancer Letters*. 235:1 (2006) 84–92. doi: 10.1016/j.canlet.2005.04.024.
- [303] **MILLER, D.** - ABC transporter regulation by signaling at the blood-brain barrier: Relevance to pharmacology. *Advances in Pharmacology*. 71:(2014) 1–24. doi: 10.1016/bs.apha.2014.06.008.
- [304] **JABLONSKI, M.; JACOB, D.; CAMPOS, C. *et al.*** - Selective increase of two ABC drug efflux transporters at the blood-spinal cord barrier suggests induced pharmacoresistance in ALS. *Neurobiology of Disease*. 47:2 (2012) 194–200. doi: 10.1016/j.nbd.2012.03.040.
- [305] **JANI, M.; AMBRUS, C.; MAGNAN, R. *et al.*** - Structure and function of BCRP, a broad specificity transporter of xenobiotics and endobiotics. *Archives of Toxicology*. 88:6 (2014) 1205–1248. doi: 10.1007/s00204-014-1224-8.
- [306] **BROUWER, K.; KEPPLER, D.; HOFFMASTER, K. *et al.*** - In vitro methods to support transporter evaluation in drug discovery and development. *Clinical Pharmacology and Therapeutics*. 94:1 (2013) 95–112. doi: 10.1038/clpt.2013.81.
- [307] **FENG, B.; VARMA, M.; COSTALES, C. *et al.*** - In vitro and in vivo approaches to characterize transporter-mediated disposition in drug discovery. *Expert Opinion on Drug Discovery*. 9:8 (2014) 873–890. doi: 10.1517/17460441.2014.922540.

- [308] **BICKER, J.; ALVES, G.; FORTUNA, A. et al.** - Blood-brain barrier models and their relevance for a successful development of CNS drug delivery systems: A review. *European Journal of Pharmaceutics and Biopharmaceutics*. 87:3 (2014) 409–432. doi: 10.1016/j.ejpb.2014.03.012.
- [309] **WANG, J.; GAN, C.; SPARIDANS, R. et al.** - P-glycoprotein (MDR1/ABCB1) and Breast Cancer Resistance Protein (BCRP/ABCG2) affect brain accumulation and intestinal disposition of encorafenib in mice. *Pharmacological Research*. 129:(2018) 414–423. doi: 10.1016/j.phrs.2017.11.006.
- [310] **POIRIER, A.; PORTMANN, R.; CASCAIS, A.; et al.** - The need for human breast cancer resistance protein substrate and inhibition evaluation in drug discovery and development: Why, when, and how? *Drug Metabolism and Disposition*. 42:9 (2014) 1466–1477. doi: 10.1124/dmd.114.058248.
- [311] **HODIN, S.; BASSET, T.; JACQUEROUX, E. et al.** - In Vitro Comparison of the Role of P-Glycoprotein and Breast Cancer Resistance Protein on Direct Oral Anticoagulants Disposition. *European Journal of Drug Metabolism and Pharmacokinetics*. 43:2 (2018) 183–191. doi: 10.1007/s13318-017-0434-x.
- [312] **ZHANG, D.; FROST, C.; HE, K. et al.** - Investigating the enteroenteric recirculation of apixaban, a factor Xa inhibitor: Administration of activated charcoal to bile duct-cannulated rats and dogs receiving an intravenous dose and use of drug transporter knockout rats. *Drug Metabolism and Disposition*. 41:4 (2013) 906–915. doi: 10.1124/dmd.112.050575.
- [313] **BICKER, J.; FORTUNA, A.; ALVES, G. et al.** - Elucidation of the impact of P-glycoprotein and breast cancer resistance protein on the brain distribution of catechol-O-methyltransferase inhibitors. *Drug Metabolism and Disposition*. 45:12 (2017) 1282–1291. doi: 10.1124/dmd.117.077883.
- [314] **HASLAM, I.; WRIGHT, J.; O'REILLY, D. et al.** - Intestinal ciprofloxacin efflux: The role of breast cancer resistance protein (ABCG2). *Drug Metabolism and Disposition*. 39:12 (2011) 2321–2328. doi: 10.1124/dmd.111.038323.
- [315] **MERINO, G.; ÁLVAREZ, A.; PULIDO, M. et al.** - Breast cancer resistance protein (BCRP/ABCG2) transports fluoroquinolone antibiotics and affects their oral availability, pharmacokinetics, and milk secretion. *Drug Metabolism and Disposition*. 34:4 (2006) 690–695. doi: 10.1124/dmd.105.008219.
- [316] **MITTAPALLI, R.; VAIDHYANATHAN, S.; DUDEK, A. et al.** - Mechanisms limiting distribution of the threonine-protein kinase B-RaF V600E inhibitor dabrafenib to the brain: Implications for the treatment of melanoma brain metastases. *Journal of*

- Pharmacology and Experimental Therapeutics. 344:3 (2013) 655–664. doi: 10.1124/jpet.112.201475.
- [317] **CHEN, Y.; AGARWAL, S.; SHAIK, N. *et al.*** - P-glycoprotein and breast cancer resistance protein influence brain distribution of dasatinib. *Journal of Pharmacology and Experimental Therapeutics*. 330:3 (2009) 956–963. doi: 10.1124/jpet.109.154781.
- [318] **TAKEUCHI, R.; SHINOZAKI, K.; NAKANISHI, T. *et al.*** - Local drug-drug interaction of donepezil with cilostazol at breast cancer resistance protein (ABCG2) increases drug accumulation in heart. *Drug Metabolism and Disposition*. 44:1 (2016) 68–74. doi: 10.1124/dmd.115.066654.
- [319] **VLAMING, M.; LÄPPCHEN, T.; JANSEN, H. *et al.*** - PET-CT imaging with [18F]-gefitinib to measure Abcb1a/1b (P-gp) and Abcg2 (Bcrp1) mediated drug-drug interactions at the murine blood-brain barrier. *Nuclear Medicine and Biology*. 42:11 (2015) 833–841. doi: 10.1016/j.nucmedbio.2015.07.004.
- [320] **BIHOREL, S.; CAMENISCH, G.; LEMAIRE, M. *et al.*** - Influence of breast cancer resistance protein (Abcg2) and p-glycoprotein (Abcb1a) on the transport of imatinib mesylate (Gleevec®) across the mouse blood-brain barrier. *Journal of Neurochemistry*. 102:6 (2007) 1749–1757. doi: 10.1111/j.1471-4159.2007.04808.x.
- [321] **BREEDVELD, P.; PLUIM, D.; CIPRIANI, G. *et al.*** - The effect of Bcrp1 (Abcg2) on the in vivo pharmacokinetics and brain penetration of imatinib mesylate (Gleevec): Implications for the use of breast cancer resistance protein and P-glycoprotein inhibitors to enable the brain penetration of imatinib in pat. *Cancer Research*. 65:7 (2005) 2577–2582. doi: 10.1158/0008-5472.CAN-04-2416.
- [322] **RÖMERMANN, K.; BANKSTAHL, J.; LÖSCHER, W. *et al.*** - Pilocarpine-induced convulsive activity is limited by multidrug transporters at the rodent blood-brain barrier. *Journal of Pharmacology and Experimental Therapeutics*. 353:2 (2015) 351–359. doi: 10.1124/jpet.114.221952.
- [323] **LI, J.; WANG, Y.; ZHANG, W. *et al.*** - The role of a basolateral transporter in rosuvastatin transport and its interplay with apical breast cancer resistance protein in polarized cell monolayer systems. *Drug Metabolism and Disposition*. 40:11 (2012) 2102–2108. doi: 10.1124/dmd.112.045666.
- [324] **FUJITA, K.; MASUO, Y.; YAMAZAKI, E. *et al.*** - Involvement of the Transporters P-Glycoprotein and Breast Cancer Resistance Protein in Dermal Distribution of the Multikinase Inhibitor Regorafenib and Its Active Metabolites. *Journal of Pharmaceutical Sciences*. 106:9 (2017) 2632–2641. doi:

- 10.1016/j.xphs.2017.04.064.
- [325] **MILANE, A.; VAUTIER, S.; CHACUN, H. *et al.*** - Interactions between riluzole and ABCG2/BCRP transporter. *Neuroscience Letters*. 452:1 (2009) 12–16. doi: 10.1016/j.neulet.2008.12.061.
- [326] **GONG, I.; MANSELL, S.; KIM, R.** - Absence of both MDR1 (ABCB1) and Breast Cancer Resistance Protein (ABCG2) Transporters Significantly Alters Rivaroxaban Disposition and Central Nervous System Entry. *Basic and Clinical Pharmacology and Toxicology*. 112:3 (2013) 164–170. doi: 10.1111/bcpt.12005.
- [327] **KITAMURA, S.; MAEDA, K.; WANG, Y. *et al.*** - Involvement of multiple transporters in the hepatobiliary transport of rosuvastatin. *Drug Metabolism and Disposition*. 36:10 (2008) 2014–2023. doi: 10.1124/dmd.108.021410.
- [328] **DURMUS, Selvi; SPARIDANS, Rolf W.; ESCH, Anita VAN *et al.*** - Breast cancer resistance protein (BCRP/ABCG2) and P-glycoprotein (P-GP/ABCB1) restrict oral availability and brain accumulation of the PARP inhibitor rucaparib (AG-014699). *Pharmaceutical Research*. 32:1 (2015) 37–46. doi: 10.1007/s11095-014-1442-z.
- [329] **LIN, F.; HOOGENDIJK, L.; BUIL, L.; *et al.*** - Sildenafil is not a useful modulator of ABCB1 and ABCG2 mediated drug resistance in vivo. *European Journal of Cancer*. 49:8 (2013) 2059–2064. doi: 10.1016/j.ejca.2012.12.028.
- [330] **YUAN, Z.; LI, Y.; LIU, Z. *et al.*** - Role of tangeretin as a potential bioavailability enhancer for silybin: Pharmacokinetic and pharmacological studies. *Pharmacological Research*. 128:(2018) 153–166. doi: 10.1016/j.phrs.2017.09.019.
- [331] **AGAWAL, S.; SANE, R.; OHLFEST, J. *et al.*** - The Role of the Breast Cancer Resistance Protein (ABCG2) in the Distribution of Sorafenib to the Brain. *J. Pharmacol. Exp. Ther.* 336:1 (2011) 223–233. doi: 10.1124/jpet.110.175034.
- [332] **WANG, Q.; STRAB, R.; KARDOS, P. *et al.*** - Application and limitation of inhibitors in drug-transporter interactions studies. *International Journal of Pharmaceutics*. 356:1–2 (2008) 12–18. doi: 10.1016/j.ijpharm.2007.12.024.
- [333] **ZAHER, H.; KHAN, A.; PALANDRA, J. *et al.*** - Breast Cancer Resistance Protein (Bcrp/abcg2) Is a Major Determinant of Sulfasalazine Absorption and Elimination in the Mouse. *Mol. Pharm.* 3:(2006) 55–61.
- [334] **LI, H.; JIN, H.; KIM, W. *et al.*** - Involvement of P-glycoprotein, multidrug resistance protein 2 and breast cancer resistance protein in the transport of belotecan and topotecan in Caco-2 and MDCKII cells. *Pharmaceutical Research*. 25:11 (2008) 2601–2612. doi: 10.1007/s11095-008-9678-0.

- [335] **MINOCHA, M.; KHURANA, V.; QIN, B. *et al.*** - Co-administration strategy to enhance brain accumulation of vandetanib by modulating P-glycoprotein (P-gp/Abcb1) and breast cancer resistance protein (Bcrp1/Abcg2) mediated efflux with m-TOR inhibitors. *International Journal of Pharmaceutics*. 434:1–2 (2012) 306–314. doi: 10.1016/j.ijpharm.2012.05.028.
- [336] **XIA, C.; LIU, N.; MIWA, G. *et al.*** - Interactions of cyclosporin A with breast cancer resistance protein. *Drug Metabolism and Disposition*. 35:4 (2007) 576–582. doi: 10.1124/dmd.106.011866.
- [337] **SHUKLA, S.; ZAHER, H.; HARTZ, A. *et al.*** - Curcumin inhibits the activity of ABCG2/BCRP1, a multidrug resistance-linked ABC drug transporter in mice. *Pharmaceutical Research*. 26:2 (2009) 480–487. doi: 10.1007/s11095-008-9735-8.
- [338] **KUSUHARA, H.; FURUIE, H.; INANO, A. *et al.*** - Pharmacokinetic interaction study of sulphasalazine in healthy subjects and the impact of curcumin as an in vivo inhibitor of BCRP. *British Journal of Pharmacology*. 166:6 (2012) 1793–1803. doi: 10.1111/j.1476-5381.2012.01887.x.
- [339] **WEISS, J.; ROSE, J.; STORCH, C. *et al.*** - Modulation of human BCRP (ABCG2) activity by anti-HIV drugs. *Journal of Antimicrobial Chemotherapy*. 59:2 (2007) 238–245. doi: 10.1093/jac/dkl474.
- [340] **NOGUCHI, K.; KAWAHARA, H.; KAJI, A. *et al.*** - Substrate-dependent bidirectional modulation of P-glycoprotein-mediated drug resistance by erlotinib. *Cancer Science*. 100:9 (2009) 1701–1707. doi: 10.1111/j.1349-7006.2009.01213.x.
- [341] **GONZÁLEZ-LOBATO, L.; REAL, R.; PRIETO, J. *et al.*** - Differential inhibition of murine Bcrp1/Abcg2 and human BCRP/ABCG2 by the mycotoxin fumitremorgin C. *European Journal of Pharmacology*. 644:1–3 (2010) 41–48. doi: 10.1016/j.ejphar.2010.07.016.
- [342] **ALLEN, J.; LOEVEZIEN, A. VAN; LAKHAI, J. *et al.*** - Potent and specific inhibition of the breast cancer resistance protein multidrug transporter in vitro and in mouse intestine by a novel analogue of fumitremorgin C. *Molecular Cancer Therapeutics*. 1:6 (2002) 417–425.
- [343] **SUZUKI, K.; DOKI, K.; HOMMA, M. *et al.*** - Co-administration of proton pump inhibitors delays elimination of plasma methotrexate in high-dose methotrexate therapy. *British Journal of Clinical Pharmacology*. 67:1 (2009) 44–49. doi: 10.1111/j.1365-2125.2008.03303.x.
- [344] **SU, Y.; HU, P.; LEE, S. *et al.*** - Using novobiocin as a specific inhibitor of breast cancer resistant protein to assess the role of transporter in the absorption and disposition

- of topotecan. *Journal of pharmacy & pharmaceutical sciences* : a publication of the Canadian Society for Pharmaceutical Sciences, Société canadienne des sciences pharmaceutiques. 10:4 (2007) 519–536. doi: 10.18433/j3qp4w.
- [345] **WANG, J.; ZHU, H.; MARKOWITZ, J. *et al.*** - Antipsychotic drugs inhibit the function of breast cancer resistance protein. *Basic and Clinical Pharmacology and Toxicology*. 103:4 (2008) 336–341. doi: 10.1111/j.1742-7843.2008.00298.x.
- [346] **GUPTA, A.; DAI, Y.; VETHANAYAGAM, R. *et al.*** - Cyclosporin A, tacrolimus and sirolimus are potent inhibitors of the human breast cancer resistance protein (ABCG2) and reverse resistance to mitoxantrone and topotecan. *Cancer Chemotherapy and Pharmacology*. 58:3 (2006) 374–383. doi: 10.1007/s00280-005-0173-6.
- [347] **WEI, Y.; MA, Y.; ZHAO, Q. *et al.*** - New use for an old drug: Inhibiting ABCG2 with sorafenib. *Molecular Cancer Therapeutics*. 11:8 (2012) 1693–1702. doi: 10.1158/1535-7163.MCT-12-0215.
- [348] **HERWAARDEN, A. VAN; JONKER, J.; WAGENAAR, E. *et al.*** - The breast cancer resistance protein (Bcrp1/Abcg2) restricts exposure to the dietary carcinogen 2-amino-1-methyl-6-phenylimidazo[4,5-b]pyridine. *Cancer Research*. 63:19 (2003) 6447–6452.
- [349] **KRUIJTZER, C.; BEIJNEN, J.; ROSING, H. *et al.*** - Increased oral bioavailability of topotecan in combination with the breast cancer resistance protein and P-glycoprotein inhibitor GF120918. *Journal of Clinical Oncology*. 20:13 (2002) 2943–2950. doi: 10.1200/JCO.2002.12.116.
- [350] **SINNAEVE, P.; BRUECKMANN, M.; CLEMENS, A. *et al.*** - Stroke prevention in elderly patients with atrial fibrillation: Challenges for anticoagulation. *Journal of Internal Medicine*. 271:1 (2012) 15–24. doi: 10.1111/j.1365-2796.2011.02464.x.
- [351] **FOX, K.; PICCINI, J.; WOJDYLA, D. *et al.*** - Prevention of stroke and systemic embolism with rivaroxaban compared with warfarin in patients with non-valvular atrial fibrillation and moderate renal impairment. *European Heart Journal*. 32:19 (2011) 2387–2394. doi: 10.1093/eurheartj/ehr342.
- [352] **AGAWAL, S.; SANE, R.; OHLFEST, J. *et al.*** - The Role of the Breast Cancer Resistance Protein (ABCG2) in the Distribution of Sorafenib to the Brain. *J. Pharmacol. Exp. Ther.* 336:(2011) 223–233. doi: 10.1124/jpet.110.175034.
- [353] **BIHOREL, S.; CAMENISCH, G.; LEMAIRE, M. *et al.*** - Modulation of the brain distribution of imatinib and its metabolites in mice by valsopodar, zosuquidar and elacridar. *Pharmaceutical Research*. 24:9 (2007) 1720–1728. doi: 10.1007/s11095-

007-9278-4.

- [354] **FOOD AND DRUG ADMINISTRATION** - Guidance for Industry: in vitro Metabolism and Transporter Mediated Drug-Drug Interaction Studies. FDA Guidelines. (2017) 10–24.
- [355] **LIU, H.; HUANG, L.; LI, Y. *et al.*** - Correlation between membrane protein expression levels and transcellular transport activity for breast cancer resistance protein. *Drug Metabolism and Disposition*. 45:5 (2017) 449–456. doi: 10.1124/dmd.116.074245.
- [356] **SCHNEPF, R.; ZOLK, O.** - Effect of the ATP-binding cassette transporter ABCG2 on pharmacokinetics: Experimental findings and clinical implications. *Expert Opinion on Drug Metabolism and Toxicology*. 9:3 (2013) 287–306. doi: 10.1517/17425255.2013.742063.
- [357] **DAVIDSON, M.** - Rosuvastatin safety: Lessons from the FDA review and post-approval surveillance. *Expert Opinion on Drug Safety*. 3:6 (2004) 547–557. doi: 10.1517/14740338.3.6.547.
- [358] **ELSBY, R.; HILGENDORF, C.; FENNER, K.** - Understanding the critical disposition pathways of statins to assess drugdrug interaction risk during drug development: It's not just about OATP1B1. *Clinical Pharmacology and Therapeutics*. 92:5 (2012) 584–598. doi: 10.1038/clpt.2012.163.
- [359] **LI, R.; BI, Y.; LAI, Y. *et al.*** - Permeability comparison between hepatocyte and low efflux MDCKII cell monolayer. *AAPS Journal*. 16:4 (2014) 802–809. doi: 10.1208/s12248-014-9616-5.
- [360] **ZHANG, W.; YU, B.; HE, Y. *et al.*** - Role of BCRP 421C>A polymorphism on rosuvastatin pharmacokinetics in healthy Chinese males. *Clinica Chimica Acta*. 373:1–2 (2006) 99–103. doi: 10.1016/j.cca.2006.05.010.
- [361] **KESKITALO, J.; ZOLK, O.; FROMM, M. *et al.*** - ABCG2 polymorphism markedly affects the pharmacokinetics of atorvastatin and rosuvastatin. *Clinical Pharmacology and Therapeutics*. 86:2 (2009) 197–203. doi: 10.1038/clpt.2009.79.
- [362] **LEE, H.; HU, M.; HO, C. *et al.*** - Effects of polymorphisms in ABCG2, SLCO1B1, SLC10A1 and CYP2C9/19 on plasma concentrations of rosuvastatin and lipid response in Chinese patients. *Pharmacogenomics*. 14:11 (2013) 1283–1294.
- [363] **TANAKA, M.; KAMADA, I.; TAKAHASHI, J. *et al.*** - Defining the Jr(a-) phenotype in the Japanese population. *Transfusion*. 54:2 (2014) 412–417. doi: 10.1111/trf.12277.
- [364] **ALLRED, A.; BOWEN, C.; PARK, J. *et al.*** - Eltrombopag increases plasma rosuvastatin

- exposure in healthy volunteers. *British Journal of Clinical Pharmacology*. 72:2 (2011) 321–329. doi: 10.1111/j.1365-2125.2011.03972.x.
- [365] **VINET, L.; ZHEDANOV, A.** - A 'missing' family of classical orthogonal polynomials. *Journal of Physics A: Mathematical and Theoretical*. 44:8 (2011). doi: 10.1088/1751-8113/44/8/085201.
- [366] **FOOD AND DRUG ADMINISTRATION** - Drug Development and Drug Interactions: Table of Substrates, inhibitors and Inducers. in <https://www.fda.gov/drugs/drug-interactions-labeling/drug-development-and-drug-interactions-table-substrates-inhibitors-and-inducers>
- [367] **YAMASAKI, Y.; IEIRI, I.; KUSUHARA, H. et al.** - Pharmacogenetic characterization of sulfasalazine disposition based on NAT2 and ABCG2 (BCRP) gene polymorphisms in humans. *Clinical Pharmacology and Therapeutics*. 84:1 (2008) 95–103. doi: 10.1038/sj.clpt.6100459.
- [368] **URQUHART, B.; WARE, J.; TIRONA, R. et al.** - Breast cancer resistance protein (ABCG2) and drug disposition: Intestinal expression, polymorphisms and sulfasalazine as an in vivo probe. *Pharmacogenetics and Genomics*. 18:5 (2008) 439–448. doi: 10.1097/FPC.0b013e3282f974dc.
- [369] **TOMARU, A.; MORIMOTO, N.; MORISHITA, M. et al.** - Studies on the intestinal absorption characteristics of sulfasalazine, a breast cancer resistance protein (BCRP) substrate. *Drug Metabolism and Pharmacokinetics*. 28:1 (2013) 71–74. doi: 10.2133/dmpk.DMPK-12-NT-024.
- [370] **SPARREBOOM, A.; LOOS, W.; BURGER, H. et al.** - Effect of ABCG2 genotype on the oral bioavailability of topotecan. *Cancer Biology and Therapy*. 4:6 (2005). doi: 10.4161/cbt.4.6.1731.
- [371] **LI, N.; SONG, Y.; DU, P. et al.** - Oral topotecan: Bioavailability, pharmacokinetics and impact of ABCG2 genotyping in Chinese patients with advanced cancers. *Biomedicine and Pharmacotherapy*. 67:8 (2013) 801–806. doi: 10.1016/j.biopha.2013.08.002.
- [372] **LEE, C.; O'CONNOR, M.; RITCHIE, T. et al.** - Breast Cancer Resistance Protein (ABCG2) in Clinical Pharmacokinetics and Drug Interactions: Practical Recommendations for Clinical Victim and Perpetrator Drug-Drug Interaction Study Design. *Drug Metabolism and Disposition*. 43:4 (2015) 490–509. doi: 10.1124/dmd.114.062174.
- [373] **WEIDNER, L.; ZOGHBI, S.; LU, S. et al.** - The inhibitor Ko143 is not specific for ABCG2. *Journal of Pharmacology and Experimental Therapeutics*. 354:3 (2015) 384–393.

- doi: 10.1124/jpet.115.225482.
- [374] **KALVASS, J.; POLLI, J.; BOURDET, D. *et al.*** - Why clinical modulation of efflux transport at the human blood-brain barrier is unlikely: The ITC evidence-based position. *Clinical Pharmacology and Therapeutics*. 94:1 (2013) 80–94. doi: 10.1038/clpt.2013.34.
- [375] **KUPPENS, I.; WITTEVEEN, E.; JEWELL, R. *et al.*** - A phase I, randomized, open-label, parallel-cohort, dose-finding study of elacridar (GF120918) and oral topotecan in cancer patients. *Clinical Cancer Research*. 13:11 (2007) 3276–3285. doi: 10.1158/1078-0432.CCR-06-2414.
- [376] **KANNAN, P.; TELU, S.; SHUKLA, S. *et al.*** - The «specific» P-glycoprotein inhibitor tariquidar is also a substrate and an inhibitor for Breast Cancer Resistance Protein (BCRP/ABCG2). *ACS Chemical Neuroscience*. 2:2 (2011) 82–89. doi: 10.1021/cn100078a.
- [377] **HEGEDUS, C.; TRUTA-FELES, K.; ANTALFFY, G *et al.*** - Interaction of the EGFR inhibitors gefitinib, vandetanib, pelitinib and neratinib with the ABCG2 multidrug transporter: Implications for the emergence and reversal of cancer drug resistance. *Biochem. Pharmacol.* 84:(2012) 260–267.
- [378] **PEÑA-SOLÓRZANO, D.; STARK, S.; KÖNIG, B. *et al.*** - ABCG2/BCRP: Specific and Nonspecific Modulators. *Medicinal Research Reviews*. 37:(2017) 987–1050. doi: 10.1002/med.
- [379] **KÜHNLE, M.; EGGER, M.; MÜLLER, C. *et al.*** - Potent and selective inhibitors of breast cancer resistance protein (ABCG2) derived from the p-glycoprotein (ABCB1) modulator tariquidar. *Journal of Medicinal Chemistry*. 52:4 (2009) 1190–1197. doi: 10.1021/jm8013822.
- [380] **SODANI, K.; PATEL, A.; ANREDDY, N. *et al.*** - Telatinib reverses chemotherapeutic multidrug resistance mediated by ABCG2 efflux transporter in vitro and in vivo. *Biochemical Pharmacology*. 89:1 (2014) 52–61. doi: 10.1016/j.bcp.2014.02.012.
- [381] **KIS, O.; SANKARAN-WALTERS, S.; HOQUE, M. T. *et al.*** - HIV-1 alters intestinal expression of drug transporters and metabolic enzymes: Implications for antiretroviral drug disposition. *Antimicrobial Agents and Chemotherapy*. 60:5 (2016) 2771–2781. doi: 10.1128/AAC.02278-15.
- [382] **GUPTA, A.; ZHANG, Y.; UNADKAT, J. *et al.*** - HIV protease inhibitors are inhibitors but not substrates of the human breast cancer resistance protein (BCRP/ABCG2). *Journal of Pharmacology and Experimental Therapeutics*. 310:1 (2004) 334–341. doi: 10.1124/jpet.104.065342.

- [383] **WANG, X.; BABA, M.** - The role of breast cancer resistance protein (BCRP/ABCG2) in cellular resistance to HIV-1 nucleoside reverse transcriptase inhibitors. *Antiviral Chemistry and Chemotherapy*. 16:4 (2005) 213–216. doi: 10.1177/095632020501600401.
- [384] **NAGASAKA, Y.; ODA, K.; IWATSUBO, T. et al.** - Effects of aripiprazole and its active metabolite dehydroaripiprazole on the activities of drug efflux transporters expressed both in the intestine and at the blood–brain barrier. *Biopharm. & Drug Dispos.* 33:(2012) 304–315. doi: 10.1002/bdd.
- [385] **BREEDVELD, P.; ZELCER, N.; PLUIM, D. et al.** - Mechanism of the pharmacokinetic interaction between methotrexate and benzimidazoles: Potential role for breast cancer resistance protein in clinical drug-drug interactions. *Cancer Research*. 64:16 (2004) 5804–5811. doi: 10.1158/0008-5472.CAN-03-4062.
- [386] **TAKEUCHI, K.; SUGIURA, T.; MATSUBARA, K. et al.** - Interaction of novel platelet-increasing agent eltrombopag with rosuvastatin via breast cancer resistance protein in humans. *Drug Metabolism and Disposition*. 42:4 (2014) 726–734. doi: 10.1124/dmd.113.054767.
- [387] **ADIWIDJAJA, J.; MCLACHLAN, A.; BODDY, A.** - Curcumin as a clinically-promising anti-cancer agent: pharmacokinetics and drug interactions. *Expert Opinion on Drug Metabolism and Toxicology*. 13:9 (2017) 953–972. doi: 10.1080/17425255.2017.1360279.
- [388] **GE, S.; YIN, T.; XU, B. et al.** - Curcumin Affects Phase II Disposition of Resveratrol Through Inhibiting Efflux Transporters MRP2 and BCRP. *Pharmaceutical Research*. 33:3 (2016) 590–602. doi: 10.1007/s11095-015-1812-1.
- [389] **WIESE, M.** - BCRP/ABCG2 inhibitors: A patent review (2009 - present). *Expert Opinion on Therapeutic Patents*. 25:11 (2015) 1229–1237. doi: 10.1517/13543776.2015.1076796.
- [390] **DEGHAN, A.; KÖTTGEN, A.; YANG, Q. et al.** - Association of three genetic loci with uric acid concentration and risk of gout: a genome-wide association study. *The Lancet*. 372:9654 (2008) 1953–1961. doi: 10.1016/S0140-6736(08)61343-4.
- [391] **WOODWARD, O.; KÖTTGEN, A.; CORESH, J. et al.** - Identification of a urate transporter, ABCG2, with a common functional polymorphism causing gout. *Proceedings of the National Academy of Sciences of the United States of America*. 106:25 (2009) 10338–10342. doi: 10.1073/pnas.0901249106.
- [392] **ZHANG, L.; SPENCER, K.; VORUGANTI, V.; et al.** - Association of functional polymorphism rs2231142 (Q141K) in the ABCG2 gene with serum uric acid and gout

- in 4 US populations. *American Journal of Epidemiology*. 177:9 (2013) 923–932. doi: 10.1093/aje/kws330.
- [393] **DONG, Z.; GUO, S.; YANG, Y. *et al.*** - Association between ABCG2 Q141K polymorphism and gout risk affected by ethnicity and gender: A systematic review and meta-analysis. *International Journal of Rheumatic Diseases*. 18:4 (2015) 382–391. doi: 10.1111/1756-185X.12519.
- [394] **BURGER, H.; TOL, H. VAN; BROK, M. *et al.*** - Chronic imatinib mesylate exposure leads to reduced intracellular drug accumulation by induction of the ABCG2 (BCRP) and ABCB1 (MDR1) drug transport pumps. *Cancer Biology and Therapy*. 4:7 (2005) 747–752. doi: 10.4161/cbt.4.7.1826.
- [395] **BURGER, H.; NOOTER, K.** - Pharmacokinetic resistance to imatinib mesylate: Role of the ABC drug pumps ABCG2 (BCRP) and ABCB1 (MDR1) in the oral bioavailability of imatinib. *Cell Cycle*. 3:12 (2004) 1502–1505. doi: 10.4161/cc.3.12.1331.
- [396] **YOTSUMOTO, K.; AKIYOSHI, T.; WADA, N. *et al.*** - 5-Fluorouracil treatment alters the expression of intestinal transporters in rats. *Biopharmaceutics and Drug Disposition*. 38:9 (2017) 509–516. doi: 10.1002/bdd.2102.
- [397] **ZEMBRUSKI, N.; BÜCHEL, G.; JÖDICKE, L. *et al.*** - Potential of novel antiretrovirals to modulate expression and function of drug transporters in vitro. *Journal of Antimicrobial Chemotherapy*. 66:4 (2011) 802–812. doi: 10.1093/jac/dkq501.
- [398] **ZEMBRUSKI, N.; HAEFELI, W.; WEISS, J.** - Interaction potential of etravirine with drug transporters assessed in vitro. *Antimicrobial Agents and Chemotherapy*. 55:3 (2011) 1282–1284. doi: 10.1128/AAC.01527-10.
- [399] **JIGOREL, E.; VEE, M. LE; BOURSIER-NEYRET, C. *et al.*** - Differential regulation of sinusoidal and canalicular hepatic drug transporter expression by xenobiotics activating drug-sensing receptors in primary human hepatocytes. *Drug Metabolism and Disposition*. 34:10 (2006) 1756–1763. doi: 10.1124/dmd.106.010033.
- [400] **BADOLO, L.; JENSEN, B.; SÄLL, C. *et al.*** - Evaluation of 309 molecules as inducers of CYP3A4, CYP2B6, CYP1A2, OATP1B1, OCT1, MDR1, MRP2, MRP3 and BCRP in cryopreserved human hepatocytes in sandwich culture. *Xenobiotica*. 45:2 (2015) 177–187. doi: 10.3109/00498254.2014.955831.
- [401] **WEISS, J.; BECKER, J.; HAEFELI, W.** - Telaprevir is a substrate and moderate inhibitor of P-glycoprotein, a strong inducer of ABCG2, but not an activator of PXR in vitro. *International Journal of Antimicrobial Agents*. 43:2 (2014) 184–188. doi: 10.1016/j.ijantimicag.2013.10.003.

- [402] **REMY, S.; BECK, H.** - Molecular and cellular mechanisms of pharmacoresistance in epilepsy. *Brain*. 129:1 (2006) 18–35. doi: 10.1093/brain/awh682.
- [403] **LASOÑ, W.; CHLEBICKA, M.; REJDAK, K.** - Research advances in basic mechanisms of seizures and antiepileptic drug action. *Pharmacological Reports*. 65:4 (2013) 787–801. doi: 10.1016/S1734-1140(13)71060-0.
- [404] **ARONICA, E.; GORTER, J.; REDEKER, S. et al.** - Localization of breast cancer resistance protein (BCRP) in microvessel endothelium of human control and epileptic brain. *Epilepsia*. 46:6 (2005) 849–857. doi: 10.1111/j.1528-1167.2005.66604.x.
- [405] **ARONICA, E.; SISODIYA, S.; GORTER, J.** - Cerebral expression of drug transporters in epilepsy. *Advanced Drug Delivery Reviews*. 64:10 (2012) 919–929. doi: 10.1016/j.addr.2011.11.008.
- [406] **SISODIYA, S.; MARTINIAN, L.; SCHEFFER, G. et al.** - Vascular colocalization of P-glycoprotein, multidrug-resistance associated protein 1, breast cancer resistance protein and major vault protein in human epileptogenic pathologies. *Neuropathology and Applied Neurobiology*. 32:1 (2006) 51–63. doi: 10.1111/j.1365-2990.2005.00699.x.
- [407] **HUGHES, J.** - One of the hottest topics in epileptology: ABC proteins. Their inhibition may be the future for patients with intractable seizures. *Neurological Research*. 30:9 (2008) 920–925. doi: 10.1179/174313208X319116.
- [408] **FELDMANN, M.; KOEPP, M.** - ABC Transporters and Drug Resistance in Patients with Epilepsy. *Current Pharmaceutical Design*. 22:38 (2016) 5793–5807. doi: 10.2174/1381612822666160810150416.
- [409] **BANERJEE DIXIT, A.; SHARMA, D.; SRIVASTAVA, A. et al.** - Upregulation of breast cancer resistance protein and major vault protein in drug resistant epilepsy. *Seizure*. 47:(2017) 9–12. doi: 10.1016/j.seizure.2017.02.014.
- [410] **RÖMERMANN, K.; HELMER, R.; LÖSCHER, W.** - The antiepileptic drug lamotrigine is a substrate of mouse and human breast cancer resistance protein (ABCG2). *Neuropharmacology*. 93:(2015) 7–14. doi: 10.1016/j.neuropharm.2015.01.015.
- [411] **JENNUM, P.; SABERS, A.; CHRISTENSEN, J. et al.** - Socioeconomic outcome of epilepsy surgery: A controlled national study. *Seizure*. 42:(2016) 52–56. doi: 10.1016/j.seizure.2016.09.016.
- [412] **BEGLEY, C.; DURGIN, T.** - The direct cost of epilepsy in the United States: A systematic review of estimates. *Epilepsia*. 56:9 (2015) 1376–1387. doi:

- 10.1111/epi.13084.
- [413] **ALEXOPOULOS, A.** - Pharmacoresistant epilepsy: Definition and explanation. *Epileptology*. 1:1 (2013) 38–42.
- [414] **PATSALOS, P.; BERRY, D.; BOURGEOIS, B. et al.** - Antiepileptic drugs - Best practice guidelines for therapeutic drug monitoring: A position paper by the subcommission on therapeutic drug monitoring, ILAE Commission on Therapeutic Strategies. *Epilepsia*. 49:7 (2008) 1239–1276. doi: 10.1111/j.1528-1167.2008.01561.x.
- [415] **STRIANO, S.; CAPONE, D.; PISANI, F.** - Limited place for plasma monitoring of new antiepileptic drugs in clinical practice. *Med Sci Monit*. 10:14 (2008) 173–178.
- [416] **RHEE, S.; SHIN, J.; LEE, S. et al.** - Population pharmacokinetics and dose-response relationship of levetiracetam in adult patients with epilepsy. *Epilepsy Research*. 132:(2017) 8–14. doi: 10.1016/j.eplepsyres.2017.02.011.
- [417] **TOMSON, T.; LANDMARK, C.; BATTINO, D.** - Antiepileptic drug treatment in pregnancy: Changes in drug disposition and their clinical implications. *Epilepsia*. 54:3 (2013) 405–414. doi: 10.1111/epi.12109.
- [418] **REIMERS, A.; BRODTKORB, E.** - Second-generation antiepileptic drugs and pregnancy: A guide for clinicians. *Expert Review of Neurotherapeutics*. 12:6 (2012) 707–717. doi: 10.1586/ern.12.32.
- [419] **MOAVERO, R.; SANTARONE, M.; GALASSO, C. et al.** - Cognitive and behavioral effects of new antiepileptic drugs in pediatric epilepsy. *Brain and Development*. 39:6 (2017) 464–469. doi: 10.1016/j.braindev.2017.01.006.
- [420] **CROSS, J.** - Epilepsy (generalised seizures). *BMJ Clin. Evid.* (2015) 1201.
- [421] **CONTIN, M.; ALBANI, F.; RIVA, R. et al.** - Lacosamide therapeutic monitoring in patients with epilepsy: Effect of concomitant antiepileptic drugs. *Therapeutic Drug Monitoring*. 35:6 (2013) 849–852. doi: 10.1097/FTD.0b013e318290eacc.
- [422] **KUHN, J.; KNABBE, C.** - Fully validated method for rapid and simultaneous measurement of six antiepileptic drugs in serum and plasma using ultra-performance liquid chromatography-electrospray ionization tandem mass spectrometry. *Talanta*. 110:(2013) 71–80. doi: 10.1016/j.talanta.2013.02.010.
- [423] **DEEB, S.; MCKEOWN, D.; TORRANCE, H. et al.** - Simultaneous analysis of 22 antiepileptic drugs in postmortem blood, serum and plasma using LC-MS-MS with a focus on their role in forensic cases. *Journal of Analytical Toxicology*. 38:8 (2014) 485–494. doi: 10.1093/jat/bku070.

- [424] **JIMENEZ, M.** - How Pitfalls during Drug Quantitation by Mass Spectrometry May Affect the Variability of Pharmacokinetic Data during a Bioequivalence Trial. *Journal of Bioequivalence & Bioavailability*. 09:04 (2017) 430–431. doi: 10.4172/jbb.1000337.
- [425] **FORTUNA, A.; ALVES, G.; FALCÃO, A.** - Chiral chromatographic resolution of antiepileptic drugs and their metabolites: A challenge from the optimization to the application. *Biomedical Chromatography*. 28:1 (2014) 27–58. doi: 10.1002/bmc.3004.
- [426] **GONZÁLEZ, O.; BLANCO, M.; IRIARTE, G.; et al.** - Bioanalytical chromatographic method validation according to current regulations, with a special focus on the non-well defined parameters limit of quantification, robustness and matrix effect. *Journal of Chromatography A*. 1353:(2014) 10–27. doi: 10.1016/j.chroma.2014.03.077.
- [427] **EUROPEAN MEDICINES AGENCY** - Guideline on Bioanalytical Method Validation. EMEA/CHMP/EWP/192217/2009 Rev. 1 Corr. 2**. (2011) 1–23.
- [428] **FOOD AND DRUG ADMINISTRATION** - Guidance for Industry: Bioanalytical Method Validation. *Bioanalytical Method Validation*. (2013) 1–44.
- [429] **TIWARI, G.; TIWARI, R.** - Bioanalytical method validation: An updated review. *Pharmaceutical Methods*. 1:1 (2010) 25–38. doi: 10.1016/s2229-4708(10)11004-8.
- [430] **LANCELIN, F.; FRANCHON, E.; KRAOUL, L. et al.** - Therapeutic drug monitoring of levetiracetam by high-performance liquid chromatography with photodiode array ultraviolet detection: Preliminary observations on correlation between plasma concentration and clinical response in patients with refractory epil. *Therapeutic Drug Monitoring*. 29:5 (2007) 576–583. doi: 10.1097/FTD.0b013e318157032d.
- [431] **STEPANOVA, D.; BERAN, R.** - Measurement of levetiracetam drug levels to assist with seizure control and monitoring of drug interactions with other anti-epileptic medications (AEMs). *Seizure*. 23:5 (2014) 371–376. doi: 10.1016/j.seizure.2014.02.003.
- [432] **JACOB, S.; NAIR, A.** - An Updated Overview on Therapeutic Drug Monitoring of Recent Antiepileptic Drugs. *Drugs in R and D*. 16:4 (2016) 303–316. doi: 10.1007/s40268-016-0148-6.
- [433] **ALMEIDA, A.; CASTEL-BRANCO, M.; FALCÃO, A.** - Linear regression for calibration lines revisited: Weighting schemes for bioanalytical methods. *Journal of Chromatography B: Analytical Technologies in the Biomedical and Life Sciences*. 774:2 (2002) 215–222. doi: 10.1016/S1570-0232(02)00244-1.

- [434] **CONTIN, M.; MOHAMED, S.; ALBANI, F. *et al.*** - Simple and validated HPLC-UV analysis of levetiracetam in deproteinized plasma of patients with epilepsy. *Journal of Chromatography B: Analytical Technologies in the Biomedical and Life Sciences*. 873:1 (2008) 129–132. doi: 10.1016/j.jchromb.2008.08.007.
- [435] **CONTIN, M.; MOHAMED, S.; CANDELA, C. *et al.*** - Simultaneous HPLC-UV analysis of rufinamide, zonisamide, lamotrigine, oxcarbazepine monohydroxy derivative and felbamate in deproteinized plasma of patients with epilepsy. *Journal of Chromatography B: Analytical Technologies in the Biomedical and Life Sciences*. 878:3–4 (2010) 461–465. doi: 10.1016/j.jchromb.2009.11.039.
- [436] **GREINER-SOSANKO, E.; LOWER, D.; VIRJI, M. *et al.*** - Simultaneous determination of lamotrigine, zonisamide, and carbamazepine in human plasma by high-performance liquid chromatography. *Biomedical Chromatography*. 21:3 (2007) 225–228. doi: 10.1002/bmc.
- [437] **OLÁH, E.; BACSÓI, G.; FEKETE, J. *et al.*** - Determination of ng/mL levetiracetam using ultra-high-performance liquid chromatography-photodiode absorbance. *Journal of Chromatographic Science*. 50:3 (2012) 253–258. doi: 10.1093/chromsci/bmr053.
- [438] **SHAH, S.; VASANTHARAJU, S.; ARUMUGAM, K. *et al.*** - Development of a sensitive bioanalytical method for the quantification of lacosamide in rat plasma application to preclinical pharmacokinetics studies in rats. *Arzneimittel-Forschung/Drug Research*. 62:5 (2012) 243–246. doi: 10.1055/s-0032-1301911.
- [439] **MAJNOONI, M.; MOHAMMADI, B.; JALILI, R. *et al.*** - Rapid and sensitive high performance liquid chromatographic determination of zonisamide in human serum application to a pharmacokinetic study. *Indian J. Pharm. Sci.* 74:4 (2012) 360–364.
- [440] **JAIN, D.; SUBBAIA, G.; SANYA, M. *et al.*** - Determination of levetiracetam in human plasma by liquid chromatography/electrospray tandem mass spectrometry and its application to bioequivalence studies. *Rapid Communications in Mass Spectrometry*. 20:17 (2006) 2539–2547. doi: 10.1002/rcm.
- [441] **SOUSA, J.; ALVES, G.; FORTUNA, A. *et al.*** - Analytical methods for determination of new fluoroquinolones in biological matrices and pharmaceutical formulations by liquid chromatography: A review. *Analytical and Bioanalytical Chemistry*. 403:1 (2012) 93–129. doi: 10.1007/s00216-011-5706-8.
- [442] **SERRALHEIRO, A.; ALVES, G.; FORTUNA, A. *et al.*** - First HPLC-UV method for rapid and simultaneous quantification of phenobarbital, primidone, phenytoin, carbamazepine, carbamazepine-10,11-epoxide, 10,11-trans-dihydroxy-10,11-dihydrocarbamazepine, lamotrigine, oxcarbazepine and licarbazepine in human

- plas. *Journal of Chromatography B: Analytical Technologies in the Biomedical and Life Sciences*. 925:(2013) 1–9. doi: 10.1016/j.jchromb.2013.02.026.
- [443] **FORTUNA, A.; SOUSA, J.; ALVES, G. *et al.*** - Development and validation of an HPLC-UV method for the simultaneous quantification of carbamazepine, oxcarbazepine, eslicarbazepine acetate and their main metabolites in human plasma. *Analytical and Bioanalytical Chemistry*. 397:4 (2010) 1605–1615. doi: 10.1007/s00216-010-3673-0.
- [444] **FORTUNA, A.; ALVES, G.; ALMEIDA, A. *et al.*** - A chiral liquid chromatography method for the simultaneous determination of oxcarbazepine, eslicarbazepine, R-licarbazepine and other new chemical derivatives BIA 2-024, BIA 2-059 and BIA 2-265, in mouse plasma and brain. *Biomedical Chromatography*. 26:3 (2012) 384–392. doi: 10.1002/bmc.1670.
- [445] **FERREIRA, A.; RODRIGUES, M.; OLIVEIRA, P. *et al.*** - Liquid chromatographic assay based on microextraction by packed sorbent for therapeutic drug monitoring of carbamazepine, lamotrigine, oxcarbazepine, phenobarbital, phenytoin and the active metabolites carbamazepine-10,11-epoxide and licarbazepine. *Journal of Chromatography B: Analytical Technologies in the Biomedical and Life Sciences*. 971:(2014) 20–29. doi: 10.1016/j.jchromb.2014.09.010.
- [446] **YENICELI, D.** - Development and validation of a simple and efficient HPLC method for the determination of zonisamide in pharmaceuticals and human plasma. *J. Anal. Chem.* 68:5 (2013) 436–443.
- [447] **KESTELYN, C.; LASTELLE, M.; HIGUET, N. *et al.*** - A simple HPLC-UV method for the determination of lacosamide in human plasma. *Bioanalysis*. 3:22 (2011) 2515–2522. doi: 10.4155/bio.11.261.
- [448] **DEVI, M.; VARMA, D.; RANI, G. *et al.*** - Liquid chromatographic assay of lacosamide in human plasma using liquidliquid extraction. *International Journal of Pharmacy and Pharmaceutical Sciences*. 6:1 (2014) 530–533.
- [449] **MARTENS-LOBENHOFFER, J.; BODE-BÖGER, S.** - Determination of levetiracetam in human plasma with minimal sample pretreatment. *Journal of Chromatography B: Analytical Technologies in the Biomedical and Life Sciences*. 819:1 (2005) 197–200. doi: 10.1016/j.jchromb.2005.01.040.
- [450] **VERMEIJ, T.; EDELBROEK, P.** - Robust isocratic high performance liquid chromatographic method for simultaneous determination of seven antiepileptic drugs including lamotrigine, oxcarbazepine and zonisamide in serum after solid-phase extraction. *Journal of Chromatography B: Analytical Technologies in the*

- Biomedical and Life Sciences. 857:1 (2007) 40–46. doi: 10.1016/j.jchromb.2007.06.023.
- [451] **ZUFÍA, L.; ALDAZ, A.; IBÁÑEZ, N. *et al.*** - LC method for therapeutic drug monitoring of levetiracetam: Evaluation of the assay performance and validation of its application in the routine area. *Clinical Biochemistry*. 43:4–5 (2010) 473–482. doi: 10.1016/j.clinbiochem.2009.10.014.
- [452] **BOSAK, M.; CYRANKA, K.; DUDEK, D. *et al.*** - Psychiatric comedication in patients with epilepsy. *Epilepsy and Behavior*. 83:(2018) 207–211. doi: 10.1016/j.yebeh.2018.03.033.
- [453] **LIGUORI, C.; IZZI, F.; MANFREDI, N. *et al.*** - Efficacy and tolerability of perampanel and levetiracetam as first add-on therapy in patients with epilepsy: A retrospective single center study. *Epilepsy and Behavior*. 80:(2018) 173–176. doi: 10.1016/j.yebeh.2018.01.001.
- [454] **SHORVON, S.; BERMEJO, P.; GIBBS, A. *et al.*** - Antiepileptic drug treatment of generalized tonic–clonic seizures: An evaluation of regulatory data and five criteria for drug selection. *Epilepsy and Behavior*. 82:(2018) 91–103. doi: 10.1016/j.yebeh.2018.01.039.
- [455] **MCHUGH, D.; LANCASTER, S.; MANGANAS, L.** - A Systematic Review of the Efficacy of Levetiracetam in Neonatal Seizures. *Neuropediatrics*. 49:1 (2018) 12–17. doi: 10.1055/s-0037-1608653.
- [456] **ABOU-KHALIL, B.** - Levetiracetam in the treatment of epilepsy. *Neuropsychiatric Disease and Treatment*. 4:3 (2008) 507–523. doi: 10.2147/NDT.S2937.
- [457] **TAN, J.; PAQUETTE, V.; LEVINE, M.; *et al.*** - Levetiracetam Clinical Pharmacokinetic Monitoring in Pediatric Patients with Epilepsy. *Clinical Pharmacokinetics*. (2017). doi: 10.1007/s40262-017-0537-1.
- [458] **WRIGHT, C.; DOWNING, J.; MUNGALL, D. *et al.*** - Clinical pharmacology and pharmacokinetics of levetiracetam. *Frontiers in Neurology*. 4:(2013) 1–6. doi: 10.3389/fneur.2013.00192.
- [459] **SOURBRON, J.; CHAN, H.; WAMMES-VAN DER HEIJDEN, E. *et al.*** - Review on the relevance of therapeutic drug monitoring of levetiracetam. *Seizure*. 62:(2018) 131–135. doi: 10.1016/j.seizure.2018.09.004.
- [460] **BEUCHAT, I.; NOVY, J.; ROSSETTI, A.** - Newer Antiepileptic Drugs in Status Epilepticus: Prescription Trends and Outcomes in Comparison with Traditional Agents. *CNS Drugs*. 31:4 (2017) 327–334. doi: 10.1007/s40263-017-0424-1.

- [461] **BEUCHAT, I.; NOVY, J.; ROSSETTI, A.** - Newer Antiepileptic Drugs for Status Epilepticus in Adults: What's the Evidence? *CNS Drugs*. 32:3 (2018) 259–267. doi: 10.1007/s40263-018-0509-5.
- [462] **JARVIE, D.; MAHMOUD, S.** - Therapeutic Drug Monitoring of Levetiracetam in Select Populations. *J Pharm Pharm Sci*. 21:1 (2018) 149–176.
- [463] **ALDAZ, A.; ALZUETA, N.; VITERI, C.** - Influence of comedication on levetiracetam pharmacokinetics. *Therapeutic Drug Monitoring*. 40:1 (2018) 130–134. doi: 10.1097/FTD.0000000000000470.
- [464] **LANDMARK, C.; BAFTIU, A.; TYSSE, I. et al.** - Pharmacokinetic variability of four newer antiepileptic drugs, lamotrigine, levetiracetam, oxcarbazepine, and topiramate: A comparison of the impact of age and comedication. *Therapeutic Drug Monitoring*. 34:4 (2012) 440–445. doi: 10.1097/FTD.0b013e31825ee389.
- [465] **GALGANI, A.; PALLERIA, C.; IANNONE, L. et al.** - Pharmacokinetic interactions of clinical interest between direct oral anticoagulants and antiepileptic drugs. *Frontiers in Neurology*. 9:(2018) 1–10. doi: 10.3389/fneur.2018.01067.
- [466] **FALCO-WALTER, J.; SCHEFFER, I.; FISHER, R.** - The new definition and classification of seizures and epilepsy. *Epilepsy Research*. 139:2017 (2018) 73–79. doi: 10.1016/j.eplepsyres.2017.11.015.
- [467] **LAZAROWSKI, A.; CZORNYJ, L.; LUBIENIEKI, F. et al.** - ABC transporters during epilepsy and mechanisms underlying multidrug resistance in refractory epilepsy. *Epilepsia*. 48:SUPPL. 5 (2007) 140–149. doi: 10.1111/j.1528-1167.2007.01302.x.
- [468] **POTSCHKA, H.** - Transporter hypothesis of drug-resistant epilepsy: Challenges for pharmacogenetic approaches. *Pharmacogenomics*. 11:10 (2010) 1427–1438. doi: 10.2217/pgs.10.126.
- [469] **CROWE, T.; GREENLEE, M.; KANTHASAMY, A. et al.** - Mechanism of intranasal drug delivery directly to the brain. *Life Sciences*. 195:(2018) 44–52. doi: 10.1016/j.lfs.2017.12.025.
- [470] **GUENNOUN, R.; FRÉCHOU, M.; GAIGNARD, P. et al.** - Intranasal administration of progesterone: A potential efficient route of delivery for cerebroprotection after acute brain injuries. *Neuropharmacology*. 145:(2019) 283–291. doi: 10.1016/j.neuropharm.2018.06.006.
- [471] **SCHMOLKA, I.** - Artificial skin I. Preparation and properties of pluronic F-127 gels for treatment of burns. *Journal of Biomedical Materials Research*. 6:6 (1972) 571–582. doi: 10.1002/jbm.820060609.

- [472] **SWAMY, N.; ABBAS, Z.** - Mucoadhesive in situ gels as nasal drug delivery systems: an overview. *Asian J Pharm Sci.* 73:(2012) 168–180.
- [473] **VITORINO, C.; ALVES, L.; ANTUNES, F. et al.** - Design of a dual nanostructured lipid carrier formulation based on physicochemical, rheological, and mechanical properties. *Journal of Nanoparticle Research.* 15:10 (2013). doi: 10.1007/s11051-013-1993-7.
- [474] **O'BRIEN, J.; WILSON, I.; ORTON, T. et al.** - Investigation of the Alamar Blue (resazurin) fluorescent dye for the assessment of mammalian cell cytotoxicity. *European Journal of Biochemistry.* 267:17 (2000) 5421–5426. doi: 10.1046/j.1432-1327.2000.01606.x.
- [475] **EUROPEAN PARLIAMENT, COUNCIL OF THE EUROPEAN UNION** - (2010) - Directive 2010/63/EU of the European Parliament and of the Council of 22 September 2010 on the protection of animals used for scientific purposes. *Off J Eur Union.* 276:(2010) 33–79.
- [476] **GONÇALVES, J.; ALVES, G.; BICKER, J. et al.** - Development and full validation of an innovative HPLC-diode array detection technique to simultaneously quantify lacosamide, levetiracetam and zonisamide in human plasma. *Bioanalysis.* 10:8 (2018) 541–547.
- [477] **FATOUH, A.; ELSHAFFEY, A.; ABDELBAR, A.** - Intranasal agomelatine solid lipid nanoparticles to enhance brain delivery: Formulation, optimization and in vivo pharmacokinetics. *Drug Design, Development and Therapy.* 11:(2017) 1815–1825. doi: 10.2147/DDDT.S102500.
- [478] **KATARE, Y.; PIAZZA, J.; BHANDARI, J. et al.** - Intranasal delivery of antipsychotic drugs. *Schizophrenia Research.* 184:(2017) 2–13. doi: 10.1016/j.schres.2016.11.027.
- [479] **HAQUE, S.; MD, S.; FAZIL, M. et al.** - Venlafaxine loaded chitosan NPs for brain targeting: Pharmacokinetic and pharmacodynamic evaluation. *Carbohydrate Polymers.* 89:1 (2012) 72–79. doi: 10.1016/j.carbpol.2012.02.051.
- [480] **MORTON, J.; SNIDER, T.** - Guidelines for collection and processing of lungs from aged mice for histological studies. *Pathobiology of Aging & Age-related Diseases.* 7:1 (2017) 1313676. doi: 10.1080/20010001.2017.1313676.
- [481] **QU, W.; YIN, J.; WANG, H. et al.** - A simple method for the formalin fixation of lungs in toxicological pathology studies. *Experimental and Toxicologic Pathology.* 67:10 (2015) 533–538. doi: 10.1016/j.etp.2015.08.002.

- [482] **RENNE, R.; BRIX, A.; HARKEMA, J. *et al.*** - Proliferative and Nonproliferative Lesions of the Rat and Mouse Respiratory Tract. *Toxicologic Pathology*. 37:7 (2009) 55–73. doi: 10.1177/0192623309353423.
- [483] **COSTA, C.; MOREIRA, J. N.; AMARAL, M. H. *et al.*** - Nose-to-brain delivery of lipid-based nanosystems for epileptic seizures and anxiety crisis. *Journal of Controlled Release*. 295:January (2019) 187–200. doi: 10.1016/j.jconrel.2018.12.049.
- [484] **SERRALHEIRO, A.; ALVES, G.; FORTUNA, A. *et al.*** - Intranasal administration of carbamazepine to mice: A direct delivery pathway for brain targeting. *European Journal of Pharmaceutical Sciences*. 60:May (2014) 32–39. doi: 10.1016/j.ejps.2014.04.019.
- [485] **SERRALHEIRO, A.; ALVES, G.; FORTUNA, A. *et al.*** - Direct nose-to-brain delivery of lamotrigine following intranasal administration to mice. *International Journal of Pharmaceutics*. 490:1–2 (2015) 39–46. doi: 10.1016/j.ijpharm.2015.05.021.
- [486] **CUNHA-FILHO, M.; ALVAREZ-LORENZO, C.; MARTÍNEZ-PACHECO, R. *et al.*** - Temperature-sensitive gels for intratumoral delivery of β -lapachone: Effect of cyclodextrins and ethanol. *The Scientific World Journal*. (2012) 126723. doi: 10.1100/2012/126723.
- [487] **ZAHIR-JOUZDANI, F.; WOLF, J.; ATYABI, F. *et al.*** - In situ gelling and mucoadhesive polymers: why do they need each other? *Expert Opinion on Drug Delivery*. 15:10 (2018) 1007–1019. doi: 10.1080/17425247.2018.1517741.
- [488] **BASU, S.; BANDYOPADHYAY, A.** - Development and characterization of mucoadhesive in situ nasal gel of midazolam prepared with ficus carica mucilage. *AAPS PharmSciTech*. 11:3 (2010) 1223–1231.
- [489] **EUROPEAN MEDICINES AGENCY** - Keppra -. EMA/163052/2013. (2010).
- [490] **LÖSCHER, W.** - Animal Models of Seizures and Epilepsy: Past, Present, and Future Role for the Discovery of Antiseizure Drugs. *Neurochemical Research*. 42:7 (2017) 1873–1888. doi: 10.1007/s11064-017-2222-z.
- [491] **LÖSCHER, W.** - The Search for New Screening Models of Pharmacoresistant Epilepsy: Is Induction of Acute Seizures in Epileptic Rodents a Suitable Approach? *Neurochemical Research*. 42:7 (2017) 1926–1938. doi: 10.1007/s11064-016-2025-7.
- [492] **LÖSCHER, W.** - Fit for purpose application of currently existing animal models in the discovery of novel epilepsy therapies. *Epilepsy Research*. 126:(2016) 157–184. doi: 10.1016/j.eplepsyres.2016.05.016.

- [493] **CAMPOS, G.; FORTUNA, A.; FALCÃO, A. *et al.*** - In vitro and in vivo experimental models employed in the discovery and development of antiepileptic drugs for pharmacoresistant epilepsy. *Epilepsy Research*. 146:(2018) 63–86. doi: 10.1016/j.eplepsyres.2018.07.008.
- [494] **CHLEBUS, M.; GUILLEN, J.; PRINS, J.** - Directive 2010/63/EU: Facilitating full and correct implementation. *Laboratory Animals*. 50:2 (2016) 151. doi: 10.1177/0023677216639470.
- [495] **OLSSON, I.; SILVA, S.; TOWNEND, D. *et al.*** - Protecting animals and enabling research in the European Union: An overview of development and implementation of directive 2010/63/EU. *ILAR Journal*. 57:3 (2016) 347–357. doi: 10.1093/ilar/ilw029.
- [496] **EUROPEAN PARLIAMENT, COUNCIL OF THE EUROPEAN UNION** - Directive 2010/63/EU of the European Parliament and of the Council of 22 September 2010 on the protection of animals used for scientific purposes. *Official Journal of the European Union*. 276:(2010) 33–79.
- [497] **FATOUH, A.; ELSHAFFEY, A.; ABDELBAR, A.** - Agomelatine-based in situ gels for brain targeting via the nasal route: Statistical optimization, in vitro, and in vivo evaluation. *Drug Delivery*. 24:1 (2017) 1077–1085. doi: 10.1080/10717544.2017.1357148.
- [498] **PIRES, P.; SANTOS, A.** - Nanosystems in nose-to-brain drug delivery: A review of non-clinical brain targeting studies. *Journal of Controlled Release*. 270:(2018) 89–100. doi: 10.1016/j.jconrel.2017.11.047.
- [499] **BOURGANIS, V.; KAMMONA, O.; ALEXOPOULOS, A. *et al.*** - Recent advances in carrier mediated nose-to-brain delivery of pharmaceuticals. *European Journal of Pharmaceutics and Biopharmaceutics*. 128:(2018) 337–362. doi: 10.1016/j.ejpb.2018.05.009.
- [500] **FENG, Y.; HE, H.; LI, F. *et al.*** - An update on the role of nanovehicles in nose-to-brain drug delivery. *Drug Discovery Today*. 23:5 (2018) 1079–1088. doi: 10.1016/j.drudis.2018.01.005.
- [501] **MITTAL, D.; ALI, A.; MD, S. *et al.*** - Insights into direct nose to brain delivery: Current status and future perspective. *Drug Delivery*. 21:2 (2014) 75–86. doi: 10.3109/10717544.2013.838713.
- [502] **PARK, K.; LEE, B.; SHIN, K. *et al.*** - Efficacy, tolerability, and blood concentration of zonisamide in daily clinical practice. *Journal of Clinical Neuroscience*. 61:(2019) 44–47. doi: 10.1016/j.jocn.2018.11.012.

- [503] **SANO, H.; NAMBU, A.** - The effects of zonisamide on L-DOPA–induced dyskinesia in Parkinson’s disease model mice. *Neurochemistry International*. 124:(2019) 171–180. doi: 10.1016/j.neuint.2019.01.011.
- [504] **IWAKI, H.; TAGAWA, M.; IWASAKI, K. et al.** - Comparison of zonisamide with non-levodopa, anti-Parkinson’s disease drugs in the incidence of Parkinson’s disease-relevant symptoms. *Journal of the Neurological Sciences*. 402:(2019) 145–152. doi: 10.1016/j.jns.2019.05.028.
- [505] **NISHIJIMA, H.; MIKI, Y.; UENO, S. et al.** - Zonisamide Enhances Motor Effects of Levodopa, Not of Apomorphine, in a Rat Model of Parkinson’s Disease. *Parkinson’s Disease*. (2018). doi: 10.1155/2018/8626783.
- [506] **LIMMER, A.; HOLLAND, L.; LOFTUS, B.** - Zonisamide for Cluster Headache Prophylaxis: A Case Series. *Headache*. 59:6 (2019) 924–929. doi: 10.1111/head.13546.
- [507] **MARTÍNEZ-ÁVILA, J.; GARCÍA BARTOLOMÉ, A.; GARCÍA, I. et al.** - Pharmacometabolomics applied to zonisamide pharmacokinetic parameter prediction. *Metabolomics*. 14:5 (2018). doi: 10.1007/s11306-018-1365-5.
- [508] **KANNER, A.; ASHMAN, E.; GLOSS, D.; et al.** - Practice guideline update summary: Efficacy and tolerability of the new antiepileptic drugs I: Treatment of new-onset epilepsy: Report of the Guideline Development, Dissemination, and Implementation Subcommittee of the American Acade. *Neurology*. 91:2 (2018) 74–81. doi: 10.1212/WNL.0000000000005755.
- [509] **HERSHEY, L.; COLEMAN-JACKSON, R.** - Pharmacological Management of Dementia with Lewy Bodies. *Drugs and Aging*. 36:4 (2019) 309–319. doi: 10.1007/s40266-018-00636-7.
- [510] **SANO, H.; MURATA, M.; NAMBU, A.** - Zonisamide reduces nigrostriatal dopaminergic neurodegeneration in a mouse genetic model of Parkinson’s disease. *Journal of Neurochemistry*. 134:2 (2015) 371–381. doi: 10.1111/jnc.13116.
- [511] **REIMERS, A.; LJUNG, H.** - An evaluation of zonisamide, including its long-term efficacy, for the treatment of focal epilepsy. *Expert Opinion on Pharmacotherapy*. 20:8 (2019) 909–915. doi: 10.1080/14656566.2019.1595584.
- [512] **KUBOTA, M.; NISHI-NAGASE, M.; SAKAKIHARA, Y. et al.** - Zonisamide - Induced urinary lithiasis in patients with intractable epilepsy. *Brain and Development*. 22:4 (2000) 230–233. doi: 10.1016/S0387-7604(00)00118-2.
- [513] **JION, Y.; RAFF, A.; GROSBERG, B. et al.** - The risk and management of kidney stones

- from the use of topiramate and zonisamide in migraine and idiopathic intracranial hypertension. *Headache*. 55:1 (2015) 161–166. doi: 10.1111/head.12480.
- [514] **BEJANKI, H.; BIRD, V.; RUCHI, R.** - Letter to the editor regarding the manuscript “Efficacy, tolerability, and blood concentration of zonisamide in daily clinical practice”. *Journal of Clinical Neuroscience*. 63:(2019) 283. doi: 10.1016/j.jocn.2019.01.035.
- [515] **SILLS, G.; BRODIE, M.** - Pharmacokinetics and drug interactions with zonisamide. *Epilepsia*. 48:3 (2007) 435–441. doi: 10.1111/j.1528-1167.2007.00983.x.
- [516] **MCCLEANE, G.** - Pharmacological management of neuropathic pain. *Therapie*. 74:6 (2019) 633–643. doi: 10.1016/j.therap.2019.04.003.
- [517] **LEVY, R.; RAGUENEAU-MAJLESSI, I.; GARNETT, W. et al.** - Lack of a clinically significant effect of zonisamide on phenytoin steady-state pharmacokinetics in patients with epilepsy. *Journal of Clinical Pharmacology*. 44:11 (2004) 1230–1234. doi: 10.1177/0091270004268045.
- [518] **FRAMPTON, J.; SCOTT, L.** - Zonisamide: A review of its use in the management of partial seizures in epilepsy. *CNS Drugs*. 19:4 (2005) 347–367. doi: 10.2165/00023210-200519040-00010.
- [519] **NAKASA, H.; NAKAMURA, H.; ONO, S. et al.** - Prediction of drug-drug interactions of zonisamide metabolism in humans from in vitro data. *European Journal of Clinical Pharmacology*. 54:2 (1998) 177–183. doi: 10.1007/s002280050442.
- [520] **LÖSCHER, W.; KLOTZ, U.; ZIMPRICH, F. et al.** - The clinical impact of pharmacogenetics on the treatment of epilepsy. *Epilepsia*. 50:1 (2009) 1–23. doi: 10.1111/j.1528-1167.2008.01716.x.
- [521] **SARUWATARI, J.; ISHITSU, T.; NAKAGAWA, K.** - Update on the genetic polymorphisms of drug-metabolizing enzymes in antiepileptic drug therapy. *Pharmaceuticals*. 3:8 (2010) 2709–2732. doi: 10.3390/ph3082709.
- [522] **GOTO, S.; SEO, T.; MURATA, T. et al.** - Population Estimation of the Effects of Cytochrome P450 2C9 and 2C19 Polymorphisms on Phenobarbital Clearance in Japanese. 29:1 (2007) 118–121.
- [523] **GONÇALVES, J.; BICKER, J.; GOUVEIA, F. et al.** - Nose-to-brain delivery of levetiracetam after intranasal administration to mice. *International Journal of Pharmaceutics*. 564:(2019) 329–339. doi: 10.1016/j.ijpharm.2019.04.047.
- [524] **SABIR, F.; ISMAIL, R.; CSOKA, I.** - Nose-to-brain delivery of anti-glioblastoma drugs

- embedded into lipid nanocarrier systems: status quo and outlook. *Drug Discovery Today*. 25:1 (2020) 185–194. doi: 10.1016/j.drudis.2019.10.005.
- [525] **MARTINS, P.; SMYTH, H.; CUI, Z.** - Strategies to facilitate or block nose-to-brain drug delivery. *International Journal of Pharmaceutics*. 570:May (2019) 118635. doi: 10.1016/j.ijpharm.2019.118635.
- [526] **WANG, Z.; XIONG, G.; TSANG, W. et al.** - Special Section on Drug Delivery Technologies-Minireview Nose-to-Brain Delivery. *J Pharmacol Exp Ther*. 370:(2019) 593–601.
- [527] **ROMANELLI, M.; GELARDI, M.; FIORELLA, M. et al.** - Nasal ciliary motility: A new tool in estimating the time of death. *International Journal of Legal Medicine*. 126:3 (2012) 427–433. doi: 10.1007/s00414-012-0682-x.
- [528] **RAVAL, N.; BARAI, P.; ACHARYA, N. et al.** - Fabrication of peptide-linked albumin nanoconstructs for receptor-mediated delivery of asiatic acid to the brain as a preventive measure in cognitive impairment: optimization, in-vitro and in-vivo evaluation. *Artificial Cells, Nanomedicine and Biotechnology*. 46:3 (2018) 832–846. doi: 10.1080/21691401.2018.1513942.
- [529] **KOZLOVSKAYA, L.; ABOU-KAoud, M.; STEPENSKY, D.** - Quantitative analysis of drug delivery to the brain via nasal route. *Journal of Controlled Release*. 189:(2014) 133–140. doi: 10.1016/j.jconrel.2014.06.053.
- [530] **SOUSA, J.; ALVES, G.; FORTUNA, A. et al.** - Intranasal Delivery of Topically-Acting Levofloxacin to Rats: a Proof-of-Concept Pharmacokinetic Study. *Pharmaceutical Research*. 34:11 (2017) 2260–2269. doi: 10.1007/s11095-017-2232-1.
- [531] **HIEMKE, C.; BERGEMANN, N.; CLEMENT, H. W. et al.** - Consensus Guidelines for Therapeutic Drug Monitoring in Neuropsychopharmacology: Update 2017. *Pharmacopsychiatry*. 51:1–2 (2018) 9–62. doi: 10.1055/s-0043-116492.
- [532] **RUIGROK, M.; LANGE, E. DE** - Emerging Insights for Translational Pharmacokinetic and Pharmacokinetic-Pharmacodynamic Studies: Towards Prediction of Nose-to-Brain Transport in Humans. *AAPS Journal*. 17:3 (2015) 493–505. doi: 10.1208/s12248-015-9724-x.
- [533] **LOCHHEAD, J.; WOLAK, D.; PIZZO, M. et al.** - Rapid transport within cerebral perivascular spaces underlies widespread tracer distribution in the brain after intranasal administration. *Journal of Perinatology*. 35:3 (2015) 371–381. doi: 10.1038/jcbfm.2014.215.
- [534] **BIASE, S.; GIGLI, G.; VALENTE, M. et al.** - Lacosamide for the treatment of epilepsy.

- Expert Opinion on Drug Metabolism and Toxicology. 10:3 (2014) 459–468. doi: 10.1517/17425255.2014.883378.
- [535] **HALFORD, J.; LAPOINTE, M.** - Clinical Perspectives on Lacosamide. *Epilepsy Curr.* 9:(2009) 1–9.
- [536] **ENGEL, J.; PITKÄNEN, A.** - Biomarkers for epileptogenesis and its treatment. *Neuropharmacology.* 167:(2020) 107735. doi: 10.1016/j.neuropharm.2019.107735.
- [537] **LIONETTO, L.; NEGRO, A.; PALMISANI, S. et al.** - Emerging treatment for chronic migraine and refractory chronic migraine. *Expert Opinion on Emerging Drugs.* 17:3 (2012) 393–406. doi: 10.1517/14728214.2012.709846.
- [538] **RIZZO, A.; DONZELLI, S.; GIRGENTI, V. et al.** - In vitro antineoplastic effects of brivaracetam and lacosamide on human glioma cells. *Journal of Experimental and Clinical Cancer Research.* 36:1 (2017) 1–13. doi: 10.1186/s13046-017-0546-9.
- [539] **KIM, G.; BYEON, J.; EUN, B.** - Neuroprotective effect of lacosamide on hypoxic-ischemic brain injury in neonatal rats. *Journal of Clinical Neurology (Korea).* 13:2 (2017) 138–143. doi: 10.3988/jcn.2017.13.2.138.
- [540] **CARMLAND, M.; KREUTZFELDT, M.; HOLBECH, J. et al.** - Effect of lacosamide in peripheral neuropathic pain: Study protocol for a randomized, placebo-controlled, phenotype-stratified trial. *Trials.* 20:1 (2019) 1–8. doi: 10.1186/s13063-019-3695-7.
- [541] **CHEW, L.; YANG, X.; WANG, Y. et al.** - (S)-lacosamide inhibition of CRMP2 phosphorylation reduces postoperative and neuropathic pain behaviors through distinct classes of sensory neurons identified by constellation pharmacology. *Pain.* 157:7 (2016) 1448–1463. doi: 10.1097/j.pain.0000000000000555.
- [542] **AL-MASSRI, K.; AHMED, L.; EL-ABHAR, H.** - Pregabalin and lacosamide ameliorate paclitaxel-induced peripheral neuropathy via inhibition of JAK/STAT signaling pathway and Notch-1 receptor. *Neurochemistry International.* 120:July (2018) 164–171. doi: 10.1016/j.neuint.2018.08.007.
- [543] **ZHANG, C.; CHANTEUX, H.; ZUO, Z. et al.** - Potential role for human P-glycoprotein in the transport of lacosamide. *Epilepsia.* 54:7 (2013) 1154–1160. doi: 10.1111/epi.12158.
- [544] **CAWELLO, W.; MUELLER-VOESSING, C.; FICHTNER, A.** - Pharmacokinetics of lacosamide and omeprazole coadministration in healthy volunteers: Results from a phase I, randomized, crossover trial. *Clinical Drug Investigation.* 34:5 (2014) 317–325. doi: 10.1007/s40261-014-0177-2.

- [545] **DEAN, L.** - Lacosamide Therapy and CYP2C19 Genotype. *Medical Genetics Summaries*. (2018) 1–4.
- [546] **CAWELLO, W.; FUHR, U.; HERING, U. et al.** - Impact of impaired renal function on the pharmacokinetics of the antiepileptic drug lacosamide. *Clinical Pharmacokinetics*. 52:10 (2013) 897–906. doi: 10.1007/s40262-013-0080-7.
- [547] **KUMAR, B.; MODI, M.; SAIKIA, B. et al.** - Evaluation of Brain Pharmacokinetic and Neuropharmacodynamic Attributes of an Antiepileptic Drug, Lacosamide, in Hepatic and Renal Impairment: Preclinical Evidence. *ACS Chemical Neuroscience*. 8:7 (2017) 1589–1597. doi: 10.1021/acscemneuro.7b00084.
- [548] **AMENGUAL-GUAL, M.; ULATE-CAMPOS, A.; LODDENKEMPER, T.** - Status epilepticus prevention, ambulatory monitoring, early seizure detection and prediction in at-risk patients. *Seizure*. 68:(2019) 31–37. doi: 10.1016/j.seizure.2018.09.013.
- [549] **WANG, G.; WANG, D.; LIU, Y.; et al.** - Intractable epilepsy and the P-glycoprotein hypothesis. *International Journal of Neuroscience*. 126:5 (2016) 385–392. doi: 10.3109/00207454.2015.1038710.
- [550] **PAGE, B.; PAGE, M.; NOEL, C.** - A new fluorometric assay for cytotoxicity measurements in vitro. *International Journal of Oncology*. 3:3 (1993) 473–476. doi: 10.3892/ijo.3.3.473.
- [551] **RAMPERSAD, S.** - Multiple applications of alamar blue as an indicator of metabolic function and cellular health in cell viability bioassays. *Sensors (Switzerland)*. 12:9 (2012) 12347–12360. doi: 10.3390/s120912347.
- [552] **ZACHARI, M.; CHONDROU, P.; POULILIOU, S. et al.** - Evaluation of the alamarblue assay for adherent cell irradiation experiments. *Dose-Response*. 12:2 (2014) 246–258. doi: 10.2203/dose-response.13-024.Koukourakis.
- [553] **KUMAR, M.; MISRA, A.; BABBAR, A. et al.** - Intranasal nanoemulsion based brain targeting drug delivery system of risperidone. *International Journal of Pharmaceutics*. 358:1–2 (2008) 285–291. doi: 10.1016/j.ijpharm.2008.03.029.
- [554] **NIGAM, K.; KAUR, A.; TYAGI, A. et al.** - Nose-to-brain delivery of lamotrigine-loaded PLGA nanoparticles. *Drug Delivery and Translational Research*. 9:5 (2019) 879–890. doi: 10.1007/s13346-019-00622-5.
- [555] **PITTO-BARRY, A.; BARRY, N.** - Pluronic® block-copolymers in medicine: From chemical and biological versatility to rationalisation and clinical advances. *Polymer Chemistry*. 5:10 (2014) 3291–3297. doi: 10.1039/c4py00039k.

- [556] **STÖHR, T.; LEKIEFFRE, D.; FREITAG, J.** - Lacosamide, the new anticonvulsant, effectively reduces harmaline-induced tremors in rats. *European Journal of Pharmacology*. 589:1–3 (2008) 114–116. doi: 10.1016/j.ejphar.2008.06.038.
- [557] **CHUNG, S.** - New treatment option for partial-onset seizures: Efficacy and safety of lacosamide. *Therapeutic Advances in Neurological Disorders*. 3:2 (2010) 77–83. doi: 10.1177/1756285609355850.
- [558] **SCHULTZ, L.; MAHMOUD, S.** - Is Therapeutic Drug Monitoring of Lacosamide Needed in Patients with Seizures and Epilepsy? *European Journal of Drug Metabolism and Pharmacokinetics*. (2020). doi: 10.1007/s13318-019-00601-8.
- [559] **SILVA, R.; ALMEIDA, A.; BICKER, J. et al.** - Pharmacokinetic monitoring of levetiracetam in portuguese refractory epileptic patients: Effect of gender, weight and concomitant therapy. *Pharmaceutics*. 12:10 (2020) 1–15. doi: 10.3390/pharmaceutics12100943.
- [560] **ARFMAN, I.; WAMMES-VAN DER HEIJDEN, E.; HORST, P. et al.** - Therapeutic Drug Monitoring of Antiepileptic Drugs in Women with Epilepsy Before, During, and After Pregnancy. *Clinical Pharmacokinetics*. 59:4 (2020) 427–445. doi: 10.1007/s40262-019-00845-2.
- [561] **PATSALOS, P.; SPENCER, E.; BERRY, D.** - Therapeutic drug monitoring of antiepileptic drugs in epilepsy: A 2018 update. *Therapeutic Drug Monitoring*. 40:5 (2018) 526–548. doi: 10.1097/FTD.0000000000000546.
- [562] **KLITGAARD, H.; PITKÄNEN, A.** - Antiepileptogenesis, neuroprotection, and disease modification in the treatment of epilepsy: Focus on levetiracetam. *Epileptic Disorders*. 5:1 (2003) 9–16.
- [563] **KUMAR, B.; MEDHI, B.; MODI, M. et al.** - A mechanistic approach to explore the neuroprotective potential of zonisamide in seizures. *Inflammopharmacology*. 26:4 (2018) 1125–1131. doi: 10.1007/s10787-018-0478-9.
- [564] **POLAT, I.; CILAKER, M.; ÇALIŞIR, M. et al.** - Neuroprotective Effects of Lacosamide and Memantine on Hyperoxic Brain Injury in Rats. *Neurochemical Research*. 45:8 (2020) 1920–1929. doi: 10.1007/s11064-020-03056-5.
- [565] **ENRIQUE, A.; IANNI, M.; GOICOECHEA, S. et al.** - New anticonvulsant candidates prevent P-glycoprotein (P-gp) overexpression in a pharmaco-resistant seizure model in mice. *Epilepsy and Behavior*. (2019). doi: 10.1016/j.yebeh.2019.106451.
- [566] **WEIDNER, L.; KANNAN, P.; MITSIOS, N. et al.** - The expression of inflammatory markers and their potential influence on efflux transporters in drug-resistant mesial

- temporal lobe epilepsy tissue. *Epilepsia*. 59:8 (2018) 1507–1517. doi: 10.1111/epi.14505.
- [567] **HEINRICH, A.; ZHONG, X.; RASMUSSEN, T.** - Variability in expression of the human MDR1 drug efflux transporter and genetic variation of the ABCB1 gene: implications for drug-resistant epilepsy. *Current Opinion in Toxicology*. 11–12:(2018) 35–42. doi: 10.1016/j.cotox.2018.12.004.
- [568] **MAEDA, K.; SUGIYAMA, Y.** - Transporter biology in drug approval: Regulatory aspects. *Molecular Aspects of Medicine*. 34:2–3 (2013) 711–718. doi: 10.1016/j.mam.2012.10.012.
- [569] **EUROPEAN MEDICINES AGENCY** - Guideline on the investigation of drug interactions. CPMP/EWP/560/95/Rev. 1 Corr. 2**. (2012) 1–59.
- [570] **FENG, B.; WEST, M.; PATEL, N. et al.** - Validation of Human MDR1-MDCK and BCRP-MDCK Cell Lines to Improve the Prediction of Brain Penetration. *Journal of Pharmaceutical Sciences*. 108:7 (2019) 2476–2483. doi: 10.1016/j.xphs.2019.02.005.
- [571] **IRVINE, J.; TAKAHASHI, L.; LOCKHART, K. et al.** - MDCK (Madin-Darby canine kidney) cells: A tool for membrane permeability screening. *Journal of Pharmaceutical Sciences*. 88:1 (1999) 28–33. doi: 10.1021/js9803205.
- [572] **FOOD AND DRUG ADMINISTRATION** - Guidance for industry: drug interaction studies study design, data analysis, implications for dosing, and labeling recommendations. Guidance Document. (2012) 1–79.
- [573] **MERCIER, C.; HODIN, S.; HE, Z.; et al.** - Pharmacological Characterization of the RPMI 2650 Model as a Relevant Tool for Assessing the Permeability of Intranasal Drugs. *Molecular Pharmaceutics*. 15:6 (2018) 2246–2256. doi: 10.1021/acs.molpharmaceut.8b00087.
- [574] **SIBINOVSKA, N.; ŽAKELJ, S.; KRISTAN, K.** - Suitability of RPMI 2650 cell models for nasal drug permeability prediction. *European Journal of Pharmaceutics and Biopharmaceutics*. 145:(2019) 85–95. doi: 10.1016/j.ejpb.2019.10.008.
- [575] **DAVE, R.; MORRIS, M.** - A quantitative threshold for high/low extent of urinary excretion of compounds in humans. *Biopharmaceutics and Drug Disposition*. (2016) 287–309. doi: 10.1002/bdd.2013.
- [576] **SOARES, R.; DO, T.** - Ontogeny of ABC and SLC transporters in the microvessels of developing rat brain. (2016) 107–116. doi: 10.1111/fcp.12175.

- [577] HE, Y.; YAO, Y.; TSIRKA, S. *et al.* - Cell-culture models of the blood-brain barrier. *Stroke*. 45:8 (2014) 2514–2526. doi: 10.1161/STROKEAHA.114.005427.
- [578] NAKAGAWA, S.; DELI, M.; KAWAGUCHI, H. *et al.* - A new blood-brain barrier model using primary rat brain endothelial cells, pericytes and astrocytes. *Neurochemistry International*. 54:3–4 (2009) 253–263. doi: 10.1016/j.neuint.2008.12.002.
- [579] DICKENS, D.; YUSOF, S.; ABBOTT, N. *et al.* - A Multi-System Approach Assessing the Interaction of Anticonvulsants with P-gp. *PLoS ONE*. 8:5 (2013). doi: 10.1371/journal.pone.0064854.
- [580] ZHANG, C.; ZUO, Z.; KWAN, P. *et al.* - In vitro transport profile of carbamazepine, oxcarbazepine, eslicarbazepine acetate, and their active metabolites by human P-glycoprotein. *Epilepsia*. 52:10 (2011) 1894–1904. doi: 10.1111/j.1528-1167.2011.03140.x.
- [581] EUROPEAN MEDICINES AGENCY - Zonégren -. EMA/CHMP/345694/2012. (2012).
- [582] NAKANISHI, H.; YONEZAWA, A.; MATSUBARA, K. *et al.* - Impact of P-glycoprotein and breast cancer resistance protein on the brain distribution of antiepileptic drugs in knockout mouse models. *European Journal of Pharmacology*. 710:1–3 (2013) 20–28. doi: 10.1016/j.ejphar.2013.03.049.
- [583] ANTONI, F.; BAUSE, M.; SCHOLLER, M. *et al.* - Tariquidar-related triazoles as potent, selective and stable inhibitors of ABCG2 (BCRP). *European Journal of Medicinal Chemistry*. 191:(2020) 1–16. doi: 10.1016/j.ejmech.2020.112133.
- [584] VERHEIJEN, R.; YAQUB, M.; SAWICKI, E. *et al.* - Molecular imaging of ABCB1 and ABCG2 inhibition at the human blood–brain barrier using elacridar and 11 C-Erlotinib PET. *Journal of Nuclear Medicine*. 59:6 (2018) 973–979. doi: 10.2967/jnumed.117.195800.
- [585] DURMUS, S.; HENDRIKX, J.; SCHINKEL, A. - Apical ABC Transporters and Cancer Chemotherapeutic Drug Disposition. *Advances in Cancer Research*. 125:(2015) 1–41. doi: 10.1016/bs.acr.2014.10.001.
- [586] TOURNIER, N.; GOUTAL, S.; AUVITY, S. *et al.* - Strategies to inhibit ABCB1-and ABCG2-mediated efflux transport of Erlotinib at the blood-brain barrier: A PET study on nonhuman primates. *Journal of Nuclear Medicine*. 58:1 (2017) 117–122. doi: 10.2967/jnumed.116.178665.
- [587] SANE, R.; AGARWAL, S.; ELMQUIST, W. - Brain distribution and bioavailability of elacridar after different routes of administration in the mouse. *Drug Metabolism and Disposition*. 40:8 (2012) 1612–1619. doi: 10.1124/dmd.112.045930.

- [588] **UCHIDA, Y.; OHTSUKI, S.; KATSUKURA, Y. *et al.*** - Quantitative targeted absolute proteomics of human blood-brain barrier transporters and receptors. *Journal of Neurochemistry*. 117:2 (2011) 333–345. doi: 10.1111/j.1471-4159.2011.07208.x.
- [589] **EUROPEAN MEDICINES AGENCY** - Vimpat -. EMEA/H/C/000863. (2008).
- [590] **BIALER, M.; JOHANNESSEN, S.; LEVY, R. *et al.*** - Progress report on new antiepileptic drugs: A summary of the Ninth Eilat Conference (EILAT IX). *Epilepsy Research*. 83:1 (2009) 1–43. doi: 10.1016/j.eplepsyres.2008.09.005.
- [591] **PATSALOS, P.; BERRY, D.** - Pharmacotherapy of the third-generation AEDs: Lacosamide, retigabine and eslicarbazepine acetate. *Expert Opinion on Pharmacotherapy*. 13:5 (2012) 699–715. doi: 10.1517/14656566.2012.667803.
- [592] **SVENDSEN, T.; BRODTKORB, E.; BAFTIU, A. *et al.*** - Therapeutic Drug Monitoring of Lacosamide in Norway: Focus on Pharmacokinetic Variability, Efficacy and Tolerability. *Neurochemical Research*. 42:7 (2017) 2077–2083. doi: 10.1007/s11064-017-2234-8.
- [593] **STROMGREN, E.** - Mental Health Service planning in Denmark. *Dan Med Bull*. 5:1 (1958) 1–17.
- [594] **MENDOZA, M.; BELLÉS, M.; ÁLVAREZ, T. *et al.*** - Therapeutic drug monitoring of levetiracetam in daily clinical practice: High-performance liquid chromatography versus immunoassay. *European Journal of Hospital Pharmacy*. (2018) 1–5. doi: 10.1136/ejhpharm-2018-001616.
- [595] **BRANDT, C.** - Pharmacodynamic monitoring of antiepileptic drug therapy. *Therapeutic Drug Monitoring*. 41:2 (2019) 168–173. doi: 10.1097/FTD.0000000000000623.
- [596] **KRASOWSKI, M.** - Therapeutic drug monitoring of the newer anti-epilepsy medications. *Pharmaceuticals*. 3:6 (2010) 1909–1935. doi: 10.3390/ph3061908.
- [597] **WANG, Q.; RAGER, J.; WEINSTEIN, K. *et al.*** - Evaluation of the MDR-MDCK cell line as a permeability screen for the blood-brain barrier. *International Journal of Pharmaceutics*. 288:2 (2005) 349–359. doi: 10.1016/j.ijpharm.2004.10.007.
- [598] **HELLINGER, É.; VESZELKA, S.; TÓTH, A. *et al.*** - Comparison of brain capillary endothelial cell-based and epithelial (MDCK-MDR1, Caco-2, and VB-Caco-2) cell-based surrogate blood-brain barrier penetration models. *European Journal of Pharmaceutics and Biopharmaceutics*. 82:2 (2012) 340–351. doi: 10.1016/j.ejpb.2012.07.020.

- [599] **WEST, C.; MEALEY, K.** - Assessment of antiepileptic drugs as substrates for canine P-glycoprotein. *American Journal of Veterinary Research*. 68:10 (2007) 1106–1110. doi: 10.2460/ajvr.68.10.1106.
- [600] **DUKES, J.; WHITLEY, P.; CHALMERS, A.** - The MDCK variety pack: Choosing the right strain. *BMC Cell Biology*. 12:(2011) 2–5. doi: 10.1186/1471-2121-12-43.
- [601] **DJUPESLAND, P.** - Nasal drug delivery devices: Characteristics and performance in a clinical perspective-a review. *Drug Delivery and Translational Research*. 3:1 (2013) 42–62. doi: 10.1007/s13346-012-0108-9.
- [602] **MYSTIC PHARMACEUTICALS** - Nose to Brain Delivery systems in <http://mysticpharmaceuticals.com/nose-to-brain-delivery/>.
- [603] **IMPEL NEUROPHARMA INC.** - POD Technology, atual. 2017. in <http://impelnp.com/pod-technology>
- [604] **SIPNOSE** - Nasal Delivery Systems in <https://www.sipnose.com>.
- [605] **DJUPESLAND, P. G.** - Who nose how far nasal delivery can go?, atual. 2003. in http://www.optinose.com/wpcontent/%0Auploads/2003/10/20040915172955_Who_nose_how_far.pdf.
- [606] **CHAN, P.; ZHANG, C.; ZUO, Z. et al.** - In vitro transport assays of rufinamide, pregabalin, and zonisamide by human P-glycoprotein. *Epilepsy Research*. 108:3 (2014) 359–366. doi: 10.1016/j.eplepsyres.2014.01.011.
- [607] **WANG, Yi; CHEN, Z.** - An update for epilepsy research and antiepileptic drug development: Toward precise circuit therapy. *Pharmacology and Therapeutics*. 201:(2019) 77–93. doi: 10.1016/j.pharmthera.2019.05.010.

APPENDIX A

Preliminary *in vitro* accumulation studies

Summary

It is essential to determine the interaction of ADEs and the BCRP protein to predict the kinetics of drugs after *in vivo* administration. Among several ADEs widely used in clinical practice, preliminary *in vitro* assays, allowed to identify BCRP inhibitors, and to select the various factors, drugs and to administer to mice, in order to determine the ability to deliver nose to the brain of the IN pathway.

Assays of intracellular accumulation of the substrate BCRP, Hoechst, allowed to investigate whether carbamazepine, oxcarbazepine, licarbazepine, levetiracetam, lacosamide and zonisamide are BCRP inhibitors.

BCRP-mediated efflux transport was not affected by carbamazepine, levetiracetam and zonisamide, unlike oxcarbazepine, licarbazepine and lacosamide, BCRP inhibitors according to market results.

Among the molecules of interest, levetiracetam, zonisamide and lacosamide were selected for *in vivo* administration, since carbamazepine has previously been tested, and among the inhibitors, lacosamide has more favorable pharmacokinetic characteristics, compared to oxcarbazepine and licarbazepine.

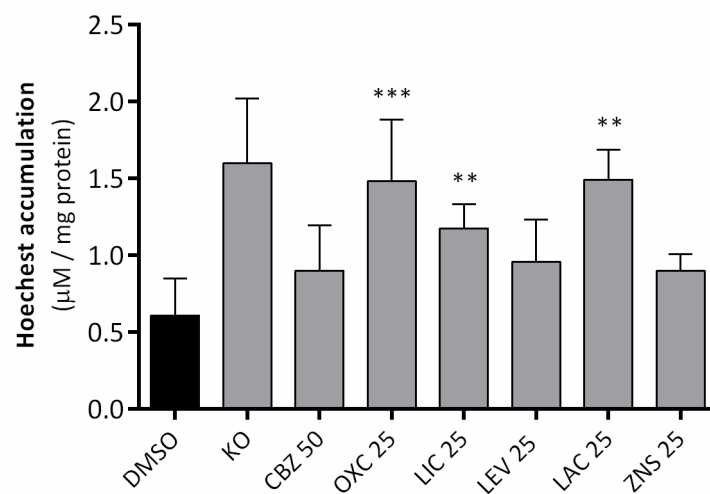
Preliminary *in vitro* accumulation studies

Figure A. 1 Accumulation of Hoechst 33342 in MDCK-BCRP cells. Demonstration of BCRP functionality after incubation with 0.5 µM KO143. Intracellular uptake observed following an incubation period with test compounds at indicated concentrations (µM). Data expressed as mean ± SD (n = 9, 3 independent assays). $p < 0.01$ (**) and $p < 0.001$ (***)

APPENDIX B

This work was presented as a poster in Drug Delivery to the Lungs 2019 and the extended abstract published in Journal of Aerosol Medicine and Pulmonary Drug Delivery, 33 (2) A4-A5

How does the device determine nose-to-brain drug delivery to mice?

Joana Gonçalves^{1,2}, Soraia Silva^{1,2}, Carla Vitorino^{1,3,4}, Gilberto Alves⁵, Ana Fortuna^{1,2}

¹ Faculty of Pharmacy of University of Coimbra, Pólo das Ciências da Saúde, Azinhaga de Santa Comba, Coimbra, 3000-548, Portugal

² CIBIT/ICNAS – Coimbra Institute for Biomedical Imaging and Translational Research of University of Coimbra, Edifício do ICNAS, Pólo das Ciências da Saúde, Azinhaga de Santa Comba, Coimbra, 3000-548, Portugal

³ Centre for Neurosciences and Cell Biology (CNC), University of Coimbra, Faculty of Medicine, Rua Larga, Pólo I, 1st floor, 3004-504 Coimbra, Portugal

⁴ Coimbra Chemistry Centre, Department of Chemistry, University of Coimbra, Rua Larga, 3004-535 Coimbra, Portugal

⁵ CICS-UBI – Health Sciences Research Centre, University of Beira Interior, Av. Infante D. Henrique, Covilhã, 6201-506 Portugal

Summary

Owing to the unique anatomical connection between the nasal cavity and central nervous system, a great deal of interest has been focused on the exploitation of the intranasal route for direct drug delivery to the brain by circumventing the blood-brain barrier. Particularly, nose-to-brain delivery of aerosolized levetiracetam was recently demonstrated in mice, emerging as a new hope for epilepsy treatment.

However, it is not yet clear whether the extent of nose-to-brain drug delivery depends on the device utilized for intranasal administration.

Therefore, a thermoreversible gel loaded with levetiracetam was intranasally administered to CD-1 male mice with a micropipette or a polyurethane tube inserted 1 cm into the nasal cavity. At 5 and 15 min post-administration, concentrations were determined in plasma, brain and lungs and plasma-tissue ratios were calculated.

Results showed that when administered with the micropipette, levetiracetam was not detected in the brain, and its concentrations in plasma and lungs were only 17 % and 6 % of those observed with the polyurethane tube. Moreover, plasma-brain ratio observed with the polyurethane tube was lower than that reported for aerosolized levetiracetam, suggesting that a direct delivery into the brain may occur but at less

extent. Moreover, lung concentrations reached with the polyurethane tube were much higher at 5 min (151.36 µg/g).

This study highlights the importance of selecting the adequate device for intranasal administration that does not compromise the direct passage into the brain. We propose the use of an aerosolizer to attain this objective during pre-clinical studies in order to prompt a correct translation to humans.

Key Message

Direct nose-to-brain drug delivery is not attained when the drug is administered as a pipette nasal gel in opposition to drug nasal gel instillation with a polyurethane tube inserted 1 cm deep into nasal cavity into the nasal cavity. This must be considered when designing pre-clinical studies during intranasal central drugs development.

Introduction

Nose-to-brain drug delivery is a mainstream of the current investigations performed to treat central diseases, including psychiatric and neurological disorders, such as neurodegenerative diseases. The olfactory region is the unique site in the human body where the nervous system is in direct contact with the surrounding environment, providing a great opportunity for intranasally administered drugs to gain a quick and easy access to the brain, while minimising their systemic exposure.

Following intranasal delivery, the deposition of the drug within the nasal chamber should be appropriately optimised for the intended therapeutic goal, whether it may be highly concentrated at the olfactory mucosa for a central effect or low deposited in that area when a systemic outcome is desired. The distance from the nostril to the olfactory epithelium is very short; however, its location in the slit-like olfactory cleft behind the narrow nasal vestibule and at the end of a complex labyrinth of respiratory turbinates severely hinder the access ^[1]. As expected, deposition in adequate innervated regions of the nasal cavity can therefore be a critical component of the overall approach towards obtaining the full potential of nose-to-brain drug delivery.

Due to methodological and ethical limitations, very few investigations providing evidence for nose-to-brain drug delivery in humans have been reported. In contrast, rodents are undeniably the laboratory animals most frequently used to assess the potential of new formulations to directly deliver the drug from the nose into the brain.

With the intent of formulating a successful novel nose-to-brain drug delivery system, the experimental design must be optimized in order to warrant that the drug is administered in the olfactory mucosa and dorsal part of the respiratory mucosa, which have a difficult accessibility in mice, due to their small dimensions. Typically, the administration of drugs into the nose is most often performed by using either a pipettor for delivering drops to alternating nostrils, a piece of tubing attached to a microsyringe/micropipette for inserting within the nasal cavity, or a nasal spray device. But is it really indifferent?

In this context, this study aimed at assessing the potential of different devices to directly deliver a thermoreversible gel loading levetiracetam into the brain. This formulation was selected as a model since it was recently demonstrated that almost 50 % of levetiracetam undergoes direct nose-to-brain delivery after its administration with a MicroSprayer® Aerosolizer [2]. We intend to define the best experimental methodology to apply when testing the pharmacokinetics and pharmacological effects of new central drug formulations administered into the nasal cavity, in order to decrease the error associated when extrapolating data from pre-clinical studies to humans. Therefore, two classic devices were tested (pipetted nasal drops and a polyurethane tube attached to a microsyringe for inserting within the nasal cavity) and compared with the aerosolizer.

Main Body of Text

Materials and Experimental Methods

CD-1 male mice, weighting between 25-30 g, were housed under controlled environmental conditions (temperature 20 ± 2 °C; relative humidity 55 ± 5 %; 12 h

light/dark cycle), with *ad libitum* access to tap water and standard rodent diet (4RF21, Mucedola®, Italy) during all experimental procedures.

All the experiments were conducted in conformity with the international regulations of the European Directive (2010) regarding the protection of laboratory animals used for scientific purposes (2010/63/EU) (European Parliament, Council of the European Union, 2010) and the Portuguese law on animal welfare (Decreto-Lei 113/2013). The applied experimental procedures were authorized by the *Direção-Geral de Alimentação e Veterinária*.

The animals were randomly divided into 2 groups in accordance to the nasal device used for the administration of levetiracetam (625 µg/animal): one group was administered with a micropipette while the other was administered applying a polyurethane tube coupled to a graduated microsyringe. In both groups, the administered volume was set at 25 µL and levetiracetam was dissolved in a thermoreversible gel, prepared according to the method described by Gonçalves and collaborators [2]. Animals were pre-anesthetized by intraperitoneal injection of a mixture of ketamine (100 mg / kg) e xylazine (10 mg / kg), and kept in a heated environment to maintain the body temperature.

At two pre-defined time points (5 and 15 min, n = 3 / time point), animals were sacrificed, blood (to obtain plasma) and tissues (brain and lungs) were collected and properly treated for further quantification of levetiracetam by High Performance Liquid Chromatography (HPLC) with diode array detector (DAD) [4]. Experimental concentrations were calculated and tissue-plasma ratios were determined for each device tested. Data from levetiracetam concentrations and tissue-plasma ratios were processed using Graphpad Prism® 5.03 (San Diego, CA, USA) and expressed as mean ± standard deviation or standard error of the mean (SEM). At each time point, statistical comparisons were performed between both groups using the unpaired two-tailed Student's t-test.

Results

The mean plasma, brain and lung concentrations of levetiracetam 5 and 15 min after intranasal administration with the micropipette or the polyurethane tube are summarized in **(Table 1)**. Accordingly, plasma concentrations are considerably lower when using the micropipette in comparison to the polyurethane tube, as well as brain concentrations. Indeed, at 5 min post-dosing, no levetiracetam was detected after administration with the micropipette discarding the hypothesis of direct nose-to-brain delivery with this device.

However, levetiracetam concentrations in the lung were considerably higher after drug administration with the polyurethane tube 1 cm inserted in the nostril, achieving a mean value of 151.357 $\mu\text{g/g}$ at the first time-point, which quickly decreased to 20.068 $\mu\text{g/g}$ up to 15 min.

Table B. 1 Concentrations of levetiracetam in plasma, brain and lung after its nasal administration with two distinct devices to mice (625 $\mu\text{g}/\text{animal}$). Data is represented as mean \pm standard deviation.

Post-dosing time (min)	Micropipette			Polyurethane tube		
	Plasma ^a	Brain ^b	Lungs ^b	Plasma ^a	Brain ^b	Lungs ^b
5 min	7.19 \pm 6.36	0	9.24 \pm 3.87	42.02 \pm 8.48	2.96 \pm 0.30	151.36 \pm 12.85
15 min	0.52 \pm 0.13	0.03 \pm 0.05	ND	23.86 \pm 0.30	2.77 \pm 0.59	20.07 \pm 3.60

ND, not determined

^a concentrations expressed at $\mu\text{g}/\text{mL}$

^b concentrations expressed at $\mu\text{g}/\text{g}$

Similarly, the brain-to-plasma concentration ratios (**Figure 1A**) are higher after instillation of the gel than the corresponding micropipette (mean values at 5 min: 0,071 versus 0; at 15 min: 0.116 *versus* 0.033), as well as in the lung (**Figure 1B**).

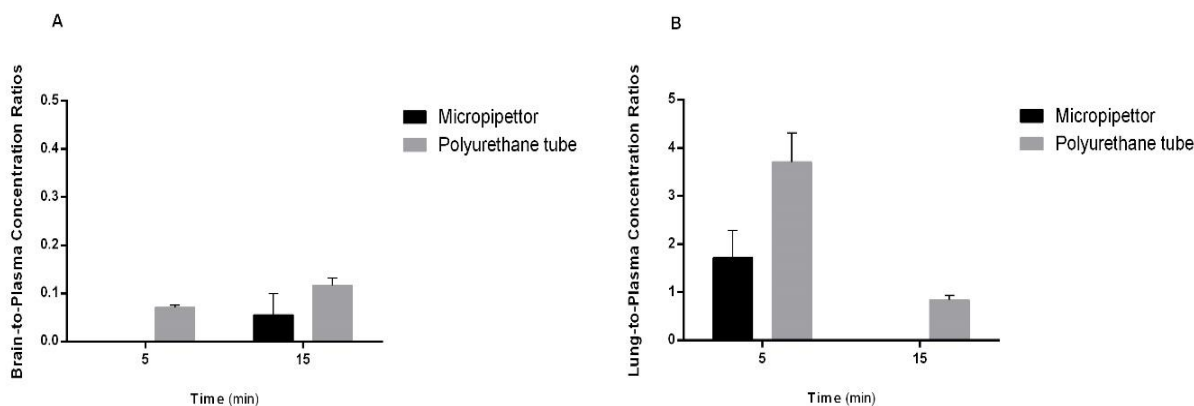


Figure B. 1 Tissue-to-plasma concentration ratios of levetiracetam at 5 and 15 min after administration of levetiracetam (625 $\mu\text{g}/\text{animal}$) with the micropipette and the polyurethane tube. **(A)** represents the brain-to-plasma concentration ratios variation *versus* time; **(B)** represents the lung-to-plasma concentration ratios variation *versus* time. Data is represented as mean \pm standard error of mean (SEM).

Discussion

The study herein presented compared the concentrations and tissue-plasma ratios found for levetiracetam after its nasal administration in a thermoreversible gel through a micropipette and a polyurethane tube inserted into the nasal cavity. The 5 and 15 min post-dosing times were selected, because the direct nose-to-brain transport of levetiracetam was found at those time points after the same formulation had been administered with the MicroSprayer[®] Aerosolizer [2].

Analyzing **Table B.1**, it is evident that the lowest quantity of levetiracetam systemically absorbed was achieved when using the micropipette. Indeed, placing the nasal gel drops at the opening of the nostrils allows the animal to sniff them into the nasal cavity but the tendency is probably to deposit on the nasal floor and be subjected to a rapid MCC [5]. These facts reduce the mean residence time of the drug to be absorbed in the respiratory epithelium or to be directly delivered into the brain in olfactory epithelium.

On the other hand, the nasal thermoreversible gel administered with the polyurethane tube inserted into the nasal cavity provided higher reproducibility in terms of the emitted dose and allowed a higher systemic absorption in relation to the micropipette (**Table B.1**). Moreover, comparing the brain-plasma ratios herein found

with those reported with the MicroSprayer® Aerosolizer^{1qwsae} it is noteworthy that the nasal spray achieved higher values, probably because of the widespread distribution of the drug within the nasal cavity. Conversely, levetiracetam deposition in lungs was considerably augmented with the polyurethane tube, suggesting that the spray will develop fewer systemic and pulmonary side effects. It is however important to emphasize that the brain-tissue ratio herein calculated for levetiracetam 5 min after its administration with the polyurethane tube was slightly higher than that observed 5 min after intravenous administration of levetiracetam^[2], suggesting that nose-to-brain delivery may exist but in less extent than with the spray.

Conclusion

The results herein reported demonstrate that aerosolization of drug formulations is preferable to attain a direct nose-to-brain delivery in detriment of pulmonary exposure. Moreover, none of the herein tested devices provided a direct nose-to-brain transport as significant as that with the aerosolizer^[2]. It is, hence, extremely important to be aware that the device may hamper nose-to-brain delivery, and whenever possible, aerosolizers are advised.

References

Djupesland P G, Messina J C, Mahmoud R A: Newman S P, Pitcairn G R, Hooper G, Knoch M: The nasal approach to delivering treatment for brain diseases: an anatomic, physiologic, and delivery technology overview. *Ther Deliv* 2014; 5: pp709-733.

² Gonçalves J, Bicker J, Gouveia F, Liberal J, Caetano Oliveira R, Alves G, Falcão A, Fortuna A: *Nose-to-brain delivery of levetiracetam after intranasal administration to mice*. *Int J Pharmaceut* 2019; 564: pp 329-339.

³ Schmolka, I R: Artificial skin I. *Preparation and properties of pluronic F-127 692 gels for treatment of burns*. *J. Biomed.Mater. Res.* 1972; 6, 571–582

⁴ Gonçalves J, Alves G, Bicker J, Falcão A, Fortuna A: *Development and full validation of an innovative HPLC-diode array detection technique to simultaneously*

quantify lacosamide, levetiracetam and zonisamide in human plasma. Bioanalysis 2018; 10: pp 541-557.

⁵ Dhuria SV, Hanson L R, Frey W H: *Intranasal delivery to the central nervous system: mechanisms and experimental considerations. J Pharm Sci* 2010; 99 pp 1654-1673.